REGULATION OF CARDIAC ELECTRICAL STABILITY BY INTRA- AND EXTRA-CARDIAC FACTORS:

Implications for Ventricular Arrhythomogenesis in the Chronic AV-Block Dog Model

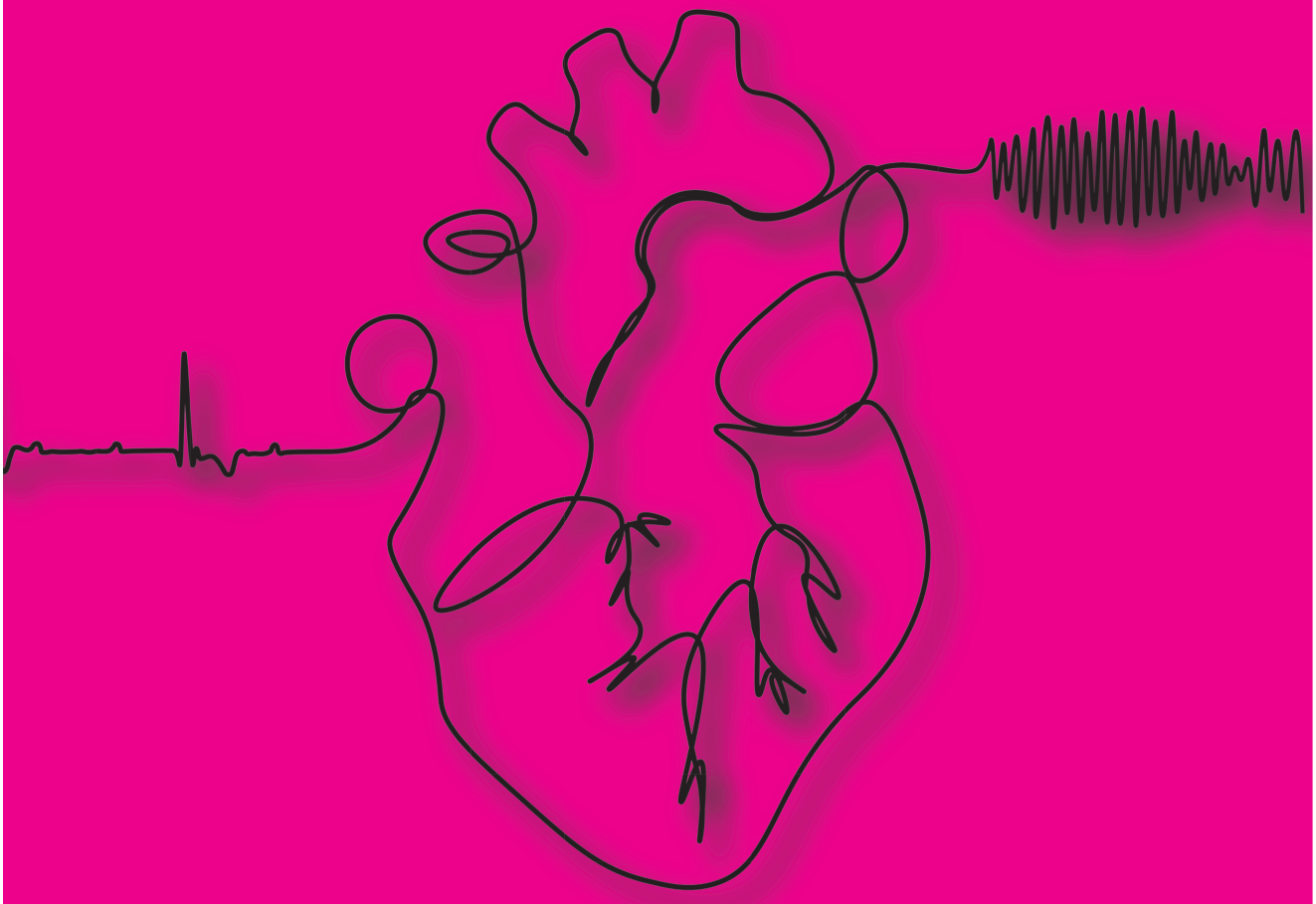

Valerie Yeh-Shing Hsieh van Weperen
謝月心

568622-L-bw-Weperen
Processed on: 3-11-2021

Regulation of cardiac electrical stability by intra- and extracardiac factors:
Implications for ventricular arrhythmogenesis in the chronic AV-block dog model.

ISBN: 9789039374276
Cover design: Valerie van Weperen
Layout: Valerie van Weperen
Printed by: Gildeprint

Regulation of Cardiac Electrical Stability by Intra- and Extra-Cardiac Factors:

Implications for Ventricular Arrhythmogenesis in the Chronic AV-block Dog Model

Regulatie van cardiale elektrische stabiliteit door intra- en extra-cardiale factoren:
Gevolgen voor het ontstaan van ventriculaire ritmestoornissen in het chronisch AV-blok hondenmodel

(met een samenvatting in het Nederlands)

Proefschrift

ter verkrijging van de graad van doctor aan de Universiteit Utrecht
op gezag van de rector magnificus, prof.dr. H.R.B.M. Kummeling,
ingevolge het besluit van het college voor promoties in het openbaar te verdedigen op

dinsdag 7 december 2021 des middags te 12.15 uur

door

Valerie Yeh-Shing Hsieh van Weperen

geboren op 5 mei 1996
te Riyadh, Saoedi-Arabië

Promotor:

Prof. dr. M.A. Vos

Copromotoren:

Dr. M.A.G. van der Heyden
Dr. O.A. Ajijola

Voor mama en papa...

...en natuurlijk ook Vivian

Table of Contents

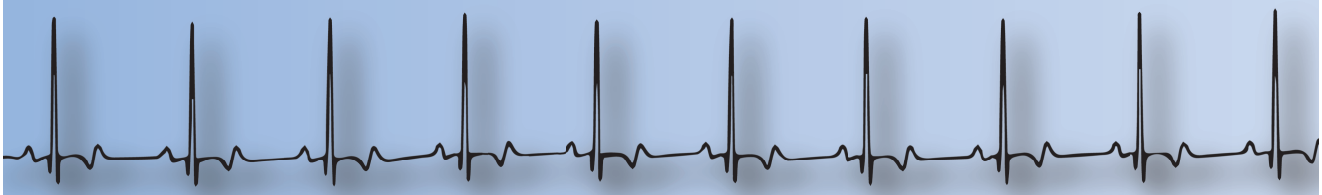

Valerie Y.H. van Weperen

CHAPTER 1

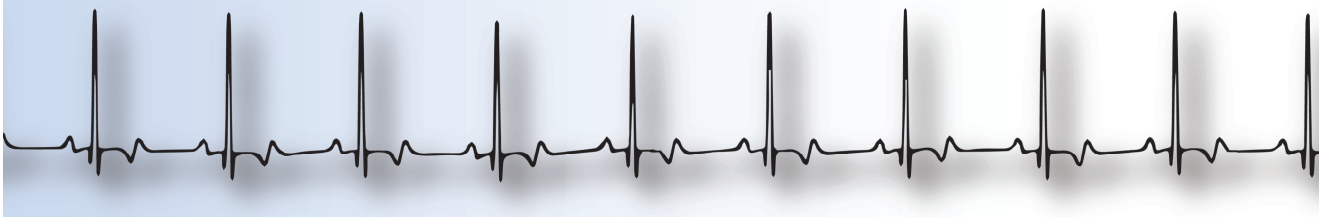

Introduction

The average heart beats more than 3 billion times in a lifetime,[1] rhythmically and continuously pumping blood throughout the entire body. Every beat is initiated by an electrical activation wave propagated through the entire heart. When this wave reaches the individual heart cells (myocytes), the electrical signal is transformed into a mechanical function, causing contraction of the myocytes. The sophisticated synchronization and harmonization of electrical activation and the subsequent electro-mechanical coupling culminates into the efficient ejection of blood from the heart.

However, when this complex elegance becomes disturbed, arrythmias can develop. Especially ventricular arrhythmias (VAs), which can deteriorate into ventricular fibrillation, imperil cardiac output (CO) and are responsible for most cases of sudden cardiac death (SCD).[2] Remarkably, even though the *prevalence* of SCD is highest in patients with severe pump failure, the *incidence* of SCD is higher in patients with no, or only mildly reduced cardiac function.[3,4] Hence, the susceptibility for VAs, and thus SCD, does not necessarily equate with the extent of cardiac dysfunction. Instead, ventricular remodelling, which is primarily initiated to compensate for a compromised or jeopardized cardiac function, appears to be a greater pro-arrhythmic factor. These structural, contractile and/or electrical remodelling processes of the heart can be induced by both congenital[5] (*i.e.* ion channel mutations) or acquired[6] (*i.e.* coronary artery disease) causes, but adversely increase the likelihood that VAs will develop. As such, it is of utmost importance to not only identify conditions and/or factors that predispose the heart to the development of VAs, but to also understand how they develop and how they affect arrhythmogenesis.

Normal cardiac electrophysiology

Electrical activity originates in the pacemaker cells in the sinoatrial node of the right atrium. The generated electrical wavefront activates and initiates contraction of the myocytes which it passes as it travels down the heart. First, both atria are activated, after which the electrical signal briefly slows in the atrioventricular node. Next, it is conducted over the proximal His-bundle and bundle branches, whereafter the Purkinje fibers disseminate the electrical activation wave to the ventricular myocytes in an apicobasal direction. This tight coordination of ventricular activation ensures appropriate and effective extrusion of ventricular blood (Figure 1A).

As the electrical wave propagates over the myocardium, action potentials are elicited in the individual myocytes through the harmonious synergy of various ion channels (Figure 1B). The action potential is prompted by the opening of voltage-gated sodium (Na^+) channels. The subsequent influx of positive ions establishes the depolarizing phase 0 of the action potential (Figure 1B). As these Na^+ channels rapidly inactivate whilst potassium (K^+) simultaneously effluxes through I_{to}, the early repolarization phase of the action potential is established (phase 1; Figure 1B). Next, during phase 2 of the action potential, intracellular calcium (Ca^{2+}) levels increase as (i) L-type Ca^{2+} channels open and (ii) Ca^{2+}-induced sarcoplasmic reticulum (SR) Ca^{2+} release is initiated through the activation of ryanodine receptors on the SR (Figure 1B). This cytosolic Ca^{2+} bridges the electrical and mechanical properties, as contraction results from the interaction of Ca^{2+} with the contractile elements of the myocyte (Figure 1B). Simultaneously, the delayed rectifying outward K^+ currents ($I_{K,r}$ and $I_{K,s}$) initiate K^+ efflux. However, when Ca^{2+} is sequestered back to the SR by the sarcoplasmic reticulum Ca^{2+}-ATPase (SERCA) or extruded by the sodium-calcium exchanger (NCX) the plateau phase transitions to phase 3 of the action potential and complete repolarization is accomplished. Lastly, in phase 4, a resting membrane potential of approximately -90 mV is mainly determined by $I_{K,1}$, whereas the Na^+/K^+-pump and the NCX maintain this resting potential as they compensate for the leakage of the associated ions (Figure 1B).

Even though the heart can thereby initiate and regulate its own function, it is also under the tight control of the autonomic nervous system (ANS). The sophisticated and dynamic interplay between the sympathetic and parasympathetic branches of the ANS ensures coordinated titration of CO on a beat-to-beat basis. This regulation is established through the integration of afferent information and calibrated efferent responses in a multi-tiered network of neurons that collectively compose the cardiac neuraxis (Figure 1C).

The central integration center of the sympathetic nervous system (SNS) resides in the spinal cord (level 3), where afferent cardiac information is integrated with signals from the higher centers. The formulated efferent outflow is relayed to the heart through the stellate ganglia, where this information can converge with and be further modulated by incoming cardiac afferents (level 2; figure 1C). Moreover, these afferent

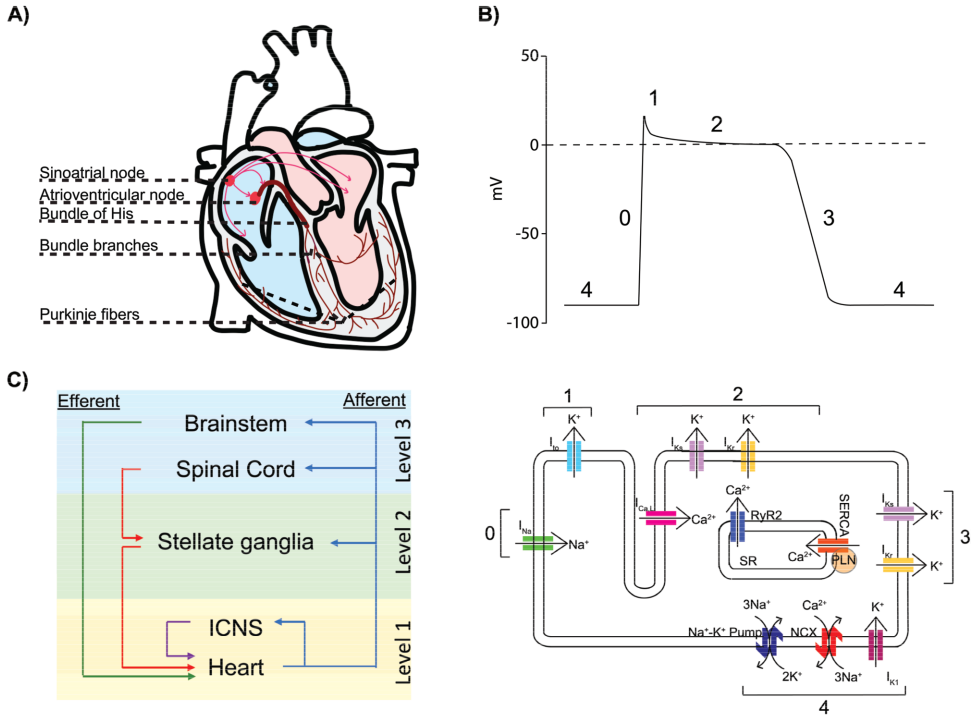

Figure 1. Overview of cardiac electrical activity and its modulation by the autonomic nervous system (ANS). A) Schematic representation of the cardiac conduction system. Electrical signals originate in the sinoatrial node from where they travel over the atria to the atrioventricular node. From there, the signals are conducted over the Bundle of His and the bundle branches to the apex of the heart, whereafter the Purkinje fibers spread the activation wave over the ventricles in an apicobasal direction. **B)** Action potential and the main currents involved in the various phases of the action potential. During phase 0, fast sodium current (I_{Na}) depolarizes the myocyte. As the sodium channels become inactivated, the slower activated transient potassium current (I_{to}) causes a small repolarizing current, constituting phase 1 of the action potential. In phase 2, also known as the plateau phase, depolarizing and repolarizing currents are more or less in an equilibrium. The depolarizing current is mainly established by the calcium influx through the LTCC which subsequently stimulates sarcoplasmic reticulum (SR) calcium release through the RyR2 channels. $I_{K,r}$ and $I_{K,s}$ constitute the main repolarizing currents. During phase 3, calcium influx is decreased and calcium is sequestered back to the SR by the sarcoplasmic reticulum Ca^{2+}-ATPase (SERCA) or extruded by the sodium-calcium exchanger (NCX) whereas $I_{K,r}$ and $I_{K,s}$ are maintained, resulting in repolarization. Phase 4 represents the resting potential. The I_{k1}, NCX, which exchanges one calcium from the intracellular environment for 3 sodium ions, and the sodium–potassium pump (Na^+-K^+ Pump), which actively imports 2 potassium ions and exports 3 sodium ions, maintain this potential. **C)** Schematic representation of the cardiac-neuraxis. Neural control is regulated through reflex loops originating from the intrinsic cardiac nervous system (ICNS) to the stellate ganglia (level 2) and the central nervous system (level 3). Blue arrows: afferent nerves. Red arrows: Sympathetic efferent nerves. Purple arrows: ICNS reflex loop.

that signal to the stellate ganglia can also provoke an efferent response at this level, thereby establishing a more local sympathetic reflex loop. In addition, within the stellate ganglia, this efferent information converges with cardiac afferents which *themselves* construct an extracardiac, intrathoracic reflex loop. The parasympathetic nervous system (PNS) has its central integration centers in the brainstem (level 3), from where preganglionic efferents travel towards the heart *via* the tenth cranial nerve, the *nervus vagus,* and release acetylcholine to modulate cardiac function. Moreover, neurons residing on the heart, composing the intrinsic cardiac nervous system, can both respond to these parasympathetic efferents as well as regulate cardiac function through local cardio-cardiac reflexes (level 1).

Through this elegant organization, the ANS modulates various cardiac physiological functions (*i.e.* chronotropy, dromotropy, inotropy and lusitropy); whereas the sympathetic nervous system (SNS) generally reinforces these functions through the release of (nor)epinephrine and sympathetic co-transmitters, the parasympathetic nervous system (PNS) generally establishes the opposite effect through its release of acetylcholine. The signalling pathways that are activated through this beta-adrenergic or muscarinic signalling, respectively, establish the physiological changes. For example, beta-adrenergic signalling increases myocardial contractility through increasing cytosolic Ca^{2+} concentrations,[7] whilst simultaneously promoting $I_{K,s}$ to counterbalance the possible prolongation of action potential duration caused by the increased cytosolic Ca^{2+} concentration (Figure 1B).[8]

It is clear that the rhythmic and adequate electrical activation of the heart relies heavily on the orchestrated ion channel dynamics and coordinated cardiac activation. Hence, perturbances of this electrical system of considerable elegance can predispose the heart to arrhythmias.

Origin of ventricular arrhythmias

Ventricular arrhythmogenesis is a complex process, reflecting a general state of cardiac electrical instability. There are many underlying causes of this instability, including intracardiac electrical derangements at the cellular and tissue level, as well as extra-cardiac factors that can influence and alter cardiac electrical properties. Nevertheless, this complex process, and the many factors involved, become much

more comprehendible in light of one of the fundamental paradigms laid down by the famous cardiologist Philippe Coumel (1987), who stated that *"there are always three main ingredients required for the production of a clinical arrhythmia, the arrhythmogenic substrate, the trigger factor and the modulation factors of which the most common is the autonomic nervous system"* (Figure 2A).[9,10]

The *trigger* is generated by a focal aberrancy in ion current dynamics, causing either an early- or late afterdepolarization (EAD or DAD, respectively; Figure 2B). Both types of afterdepolarizations can, in the presence of a susceptible substrate (described below), give rise to arrhythmic events.[11,12] EADs can result from the reactivation of L-type Ca^{2+} channels or the reverse mode of the NCX during early phase 3 of the action potential.[12,13] Hence, such EADs are especially likely to occur under conditions of prolonged repolarization duration. Similarly, DADs are also caused by the reverse mode of the NCX, but in this case during phase 4 of the action potential, and induced by the erroneous release of Ca^{2+} from (an overloaded) SR.[11] The likelihood that EADs or DADs will develop thus heavily relies on the (in)stability of the interplay between ionic currents. When unstable, this increases the beat-to-beat variation in action potential duration or repolarization. *Temporal dispersion of repolarization* quantifies this instability as short-term variability of repolarization (STV). STV is calculated using the difference of two consecutive repolarization times and averaging the deviation of this difference from the line of identity over x number of beats (Figure 2B). As such, the higher the temporal dispersion of repolarization, the higher the STV.[14]

The *substrate* on the other hand, refers to the receptiveness of the myocardium to arrhythmic events. As most arrhythmias depend on the spreading of an erroneous ventricular activation over the myocardium *via* non-conventional activation patterns, heterogeneity in repolarization dynamics is important as to maintain these aberrant activation pathways. This variation in repolarization duration is known as *spatial dispersion of repolarization* (Figure 2C).[15]

Lastly, as the ANS *modulates* the electrical properties of the myocardium, it also affects *temporal* and *spatial* dispersion of repolarization. This modulatory role can become pathological when the cardiac sympathetic innervation becomes overactive as it undergoes extensive anatomical and functional remodelling as a result of and in response to cardiac diseases.[16] This chronically increased activity of the SNS, coupled

with parasympathetic withdrawal, creates a condition of cardiac autonomic imbalance which can promote pro-arrhythmic conditions through various mechanisms.[16] For example, local sympathetic overexcitation stimulates calcium mishandling and can thereby increase *temporal dispersion.*[17]

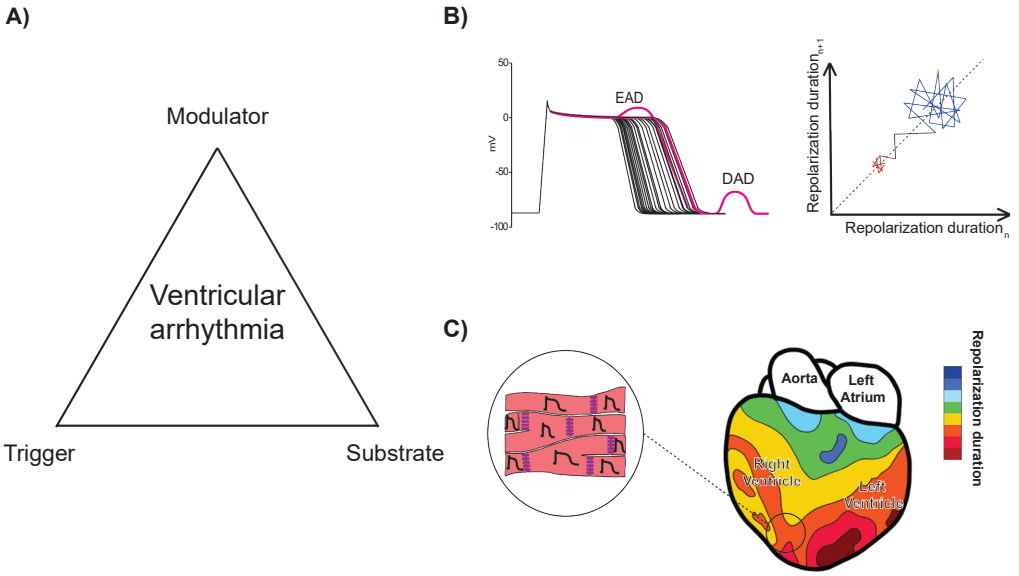

Figure 2.Schematic representation of ventricular arrhythmogenesis and the effects of temporal and spatial dispersion of repolarization. A) Ventricular arrhythmogenesis as explained by Coumel's triangle. According to this paradigm, ventricular arrhythmias results from the interplay between an arrhythmic trigger, an arrhythmia-susceptible substrate and a modulatory factor (most often the autonomic nervous system). **B)** Temporal dispersion is the beat-to-beat variability in repolarization duration. On a cellular level, this translates to variability in action potential duration. Especially in conditions with prolonged repolarization durations, increases in temporal dispersion and the associated erroneous handling of ions can result in EADs or DADs (during phase 3 and 4 of the action potential, respectively; pink traces). The likelihood that EADs or DADs will develop can be quantified by the short-term variability (STV) in repolarization, which calculates the differences in repolarization time of two consecutive beats and averages the deviation of these differences from the line of identity in a Poincaré plot. Hence, the greater the beat-to-beat variability in repolarization, the greater the distance of the points to the line of identity and thus the higher the STV. **B)** Schematic representation of spatial dispersion in repolarization. Local differences in ion handling result in spatial heterogeneity in repolarization duration. This dispersion exists on a cellular level (intercellular dispersion) but can also be visualized on the whole organ level with differences in repolarization times represented by different colours.

This effect becomes even more pronounced in the setting of prolonged increases in sympathetic tone, as this can induce the downregulation of potassium channels and thus lengthen repolarization duration.[18] Moreover, *spatial dispersion* can also become increased due to the aforementioned local sympathoexcitation and/or heterogeneity in nerve sprouting.[17] As such, blocking these pathological effects of sympathetic stimulation through administration of beta-blockers have become one of the cornerstones of current anti-arrhythmic therapies and (bilateral) stellectomies have demonstrated to be a highly effective strategy for refractory arrhythmias.[19–21]

Chronic atrioventricular block dog model

The chronic atrioventricular block (CAVB) dog model was first created in 1906 and 1907 to study Stokes-Adams disease. It wasn't until much later, in 1955 to be exact, that the first reports came that employed the CAVB dog as an animal model to study heart failure. Now, many years later, the CAVB dog has been established as an excellent model to study (factors playing into) the process of arrhythmogenesis and to establish pro- or anti-arrhythmic properties of drugs.[22,23] In this model of compensated hypertrophy and heart failure, extensive remodelling processes cause the heart to become prone to the development of Torsade de Pointes arrhythmias (TdP), which can then be studied under controlled conditions.

This ventricular remodelling is induced by (radiofrequency) ablation of the proximal His bundle. The acute interruption in atrio-ventricular signal transmission and consequential shift to idioventricular rhythm (IVR) results in (i) chronic bradycardia and (ii) mechanical dysfunction.[24] Moreover, the bradycardic conditions (~ 40 - 50 beats/minute under IVR *vs* ~ 110 - 120 beats/minute under sinus rhythm) induce a condition of volume-overload. In addition, the uncontrolled and often inconsistent origin of ventricular activation[24] introduces mechanical dysfunction, which creates inadequate extrusion of blood. Collectively, the bradycardic conditions and mechanical dysfunction cause a drop in CO, which acutely activate the neurohumoral system in an effort to improve contractility (Figure 3; green trace).[25] However, this mechanism compensates insufficiently for the depressed CO (Figure 2; black trace), thereby initiating long-term ventricular adaptational processes in electrical, contractile and structural properties. Notably, these three processes develop simultaneously, but asynchronously: whereas

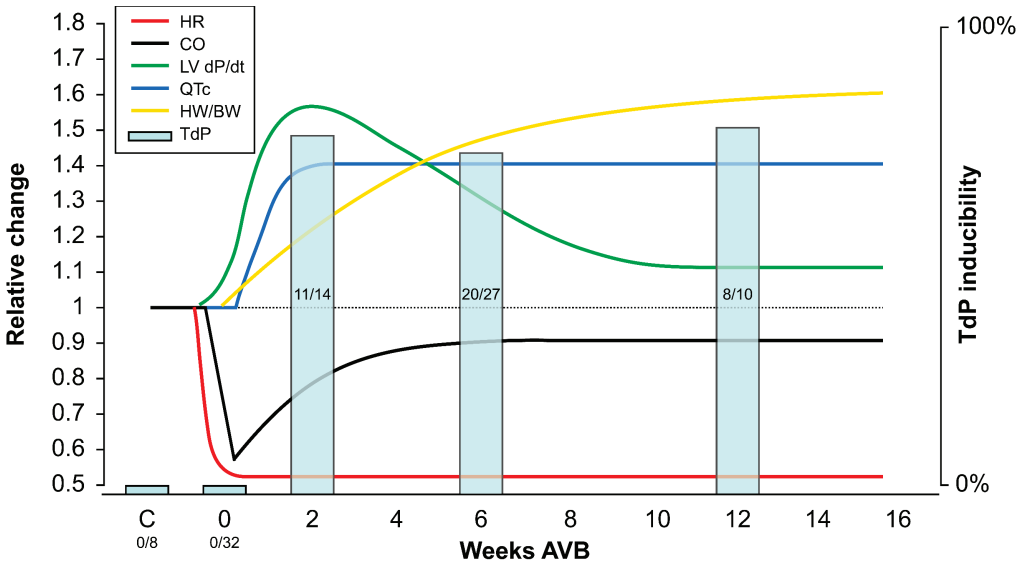

Figure 3. Overview of different ventricular remodelling processes and their consequences for Torsade de Pointes arrhythmia (TdP) inducibility in the complete and chronic AV-block (CAVB) dog model. The relative change in cardiac parameters (left y-axis) compared to control (sinus rhythm; C) conditions over the time course of 16 weeks (x-axis) following creation of complete AV-block (0). Complete AV-block induces an acute drop in heart rate (HR; red trace) as it shifts to idioventricular rhythm (IVR). Consequentially, CO (black trace) decreases and remodelling processes are initiated. Contractile remodelling (LV dP/dt; green trace) and electrical remodelling (QTc; blue trace) increase contractility and prolong repolarization duration, respectively. Both processes are completed within two weeks following AV-block. Structural remodelling (biventricular hypertrophy) on the contrary, takes approximately 6 weeks to be completed. Collectively, these remodelling processes restore CO, but simultaneously and adversely increase the inducibility of dofetilide-induced TdP, as depicted by the blue bars (right y-axis). Whereas no animals were inducible under control or acute AV-block conditions, approximately 75% of animals became reproducibly inducible after 2, 6 and 12 weeks of remodelling. (From Bourgonje et al.,[28] with permission of the authors).

structural remodelling (resulting in biventricular hypertrophy) progressively develops up until the 6th week after AV-block (Figure 3, yellow trace),[26,27] contractile and electrical remodelling are completed after two weeks of AV-block (Figure 3, green and blue trace, respectively).

Contractile adaptations are associated with a prolonged calcium window,[29] increased sarcoplasmic reticulum Ca^{2+} storage and increased systolic Ca^{2+} concentrations.[30] These alterations in Ca^{2+} handling, which are mainly the result of the downregulation of SERCA and the upregulation of (forward and reverse) NCX activity,[30]

strengthen the contractile force as reflected by an increased left ventricular dP/dt_{max} (Figure 3; green curve).

Electrical adaptations include the downregulation of $I_{K,r}$ and $I_{K,s}$,[31] which is reflected by a prolonged QT-interval on the surface electrogram (Figure 3, blue trace). This downregulation of potassium channels reduces the repolarization reserve and thereby increases the vulnerability for VAs. Moreover, this downregulation does not only create an instability of the repolarization machinery that is reflected in an increased *temporal dispersion of repolarization,* the spatial variation in extent of electrical remodelling also creates *spatial dispersion of repolarization.* When this intrinsically increased susceptibility for VAs[32] is further challenged with additional repolarization impeding factors, such as anesthesia[33] and pro-arrhythmic drugs, such as the $I_{K,r}$-blocker dofetilide,[34] TdP are provoked in up to 75% of the animals (Figure 3; blue bars).[34]

Even though these remodelling processes thus improve cardiac *function,* cardiac *electrophysiology* is imperilled and TdP susceptibility is created. Nonetheless, the process of arrhythmogenesis is much more complex than a result of ventricular remodelling alone. Instead, both acute and chronic, intra- and extracardiac factors contribute to ventricular arrhythmogenesis. However, many of the factors contributing to arrhythmogenesis remain to be identified and how these factors promote arrhythmogenesis is yet to be explored.

Thesis outline

In the present thesis, the first chapters explicate and study various chronic and acute factors influencing the arrhythmogenic outcome in the CAVB dog model. Thereafter, there will be a more detailed look into autonomic remodelling in the CAVB dog model and lastly a possible role of satellite glial cells in modulating cardiac neural output is studied.

Chapter two compares electrical parameters in the assessment of TdP inducibility in the CAVB dog model and highlights the importance of spatial dispersion of repolarization for the process of arrhythmogenesis. **Chapter three** establishes the role and importance of experimentally-induced severe bradycardia to induce arrhythmias and shows that the electrophysiological effects of severe bradycardia are

mainly caused by an increase in spatial dispersion of repolarization and to a lesser extent in temporal dispersion of repolarization. **Chapter four** studies how ventricular activation patterns and the consequential extent of mechanical dyssynchrony correlates with the arrhythmogenic phenotype following ventricular remodelling in the CAVB model and shows that the extent of mechanical dyssynchrony corresponds to the arrhythmogenic phenotype. **Chapter five** demonstrates that sympathetic activity contributes to ventricular arrhythmogenesis in the CAVB dog model. Even though pharmacological blockade of the complete autonomic nervous system or its sympathetic branch was insufficient to suppress TdP, bilateral stellectomies were a highly effective anti-arrhythmic strategy. The molecular characteristics and *in vivo* functional consequences of neural remodelling underlying these arrhythmogenic effects are studied in **chapter six.** Next, **chapter seven** explores the transcriptomic profile of satellite glial cells in the stellate ganglia and demonstrates that the subpopulations have distinct biochemical properties that might suggest dynamic adaptation of these glial cells in modulating neuronal function. **Chapter eight** reviews the recent developments in modulating sympathetic activity as a therapy for cardiac diseases and discusses their clinical implications. Lastly, **chapter nine** discusses the findings of this thesis and provides a prospective look on clinical implications and experimental studies regarding arrhythmogenesis.

REFERENCES

1. Zhang GQ & Zhang W. Heart rate, lifespan, and mortality risk. *Ageing Res. Rev.* **8,** 52–60 (2009).
2. Huikuri H V, Castellanos A & Myerburg RJ. Sudden Death Due to Cardiac Arrhythmias. *N. Engl. J. Med.* **345,** 1473–1482 (2001).
3. Allen LA, Stevenson LW, Grady KL, Goldstein NE, Matlock DD, Arnold RM, Cook NR, Felker GM, Francis GS, Hauptman PJ, Havranek EP, Krumholz HM, Mancini D, Riegel B & Spertus JA. Decision Making in Advanced Heart Failure. *Circulation* **125,** 1928 LP – 1952 (2012).
4. Stecker EC, Vickers C, Waltz J, Socoteanu C, John BT, Mariani R, McAnulty JH, Gunson K, Jui J & Chugh SS. Population-based analysis of sudden cardiac death with and without left ventricular systolic dysfunction: Two-year findings from the Oregon sudden unexpected death study. *J. Am. Coll. Cardiol.* **47,** 1161–1166 (2006).
5. Ahmad F, Seidman JG & Seidman CE. The genetic basis for cardiac remodeling. *Annu. Rev. Genomics Hum. Genet.* **6,** 185–216 (2005).
6. Shenasa M, Shenasa H & El-Sherif N. Left Ventricular Hypertrophy and Arrhythmogenesis. *Card. Electrophysiol. Clin.* **7,** 207–220 (2015).
7. Bers DM. Calcium cycling and signaling in cardiac myocytes. *Annu. Rev. Physiol.* **70,** 23–49 (2008).
8. Banyasz T, Jian Z, Horvath B, Khabbaz S, Izu LT & Chen-Izu Y. Beta-adrenergic stimulation reverses the I Kr–I Ks dominant pattern during cardiac action potential. *Pflugers Arch. Eur. J. Physiol.* **466,** 2067–2076 (2014).
9. Coumel P. The management of clinical arrhythmias. An overview on invasive versus non-invasive electrophysiology. *Eur. Heart J.* **8,** 92–99 (1987).
10. Farré J & Wellens HJ. Philippe Coumel: a founding father of modern arrhythmology. *Europace* **6,** 464–465 (2004).
11. Priori SG & Corr PB. Mechanisms underlying early and delayed afterdepolarizations induced by catecholamines. *Am. J. Physiol. - Heart Circ. Physiol.* **258,** (1990).
12. Weiss JN, Garfinkel A, Karagueuzian HS, Chen PS & Qu Z. Early afterdepolarizations and cardiac arrhythmias. *Heart Rhythm* **7,** 1891–1899

568622-L-bw-Weperen
Processed on: 3-11-2021

(2010).

13. Volders PGA, Kulcsár A, Vos MA, Sipido KR, Wellens HJJ, Lazzara R & Szabo B. Similarities between early and delayed afterdepolarizations induced by isoproterenol in canine ventricular myocytes. *Cardiovasc. Res.* **34,** 348–359 (1997).
14. Thomsen MB, Verduyn SC, Stengl M, Beekman JDM, de Pater G, van Opstal J, Volders PGA & Vos MA. Increased Short-Term Variability of Repolarization Predicts Sotalol–Induced Torsades de Pointes in Dogs. *Circulation* **110,** 2453–2459 (2004).
15. Dunnink A, Stams TRG, Bossu A, Meijborg VMF, Beekman JDM, Wijers SC, De Bakker JMT & Vos MA. Torsade de pointes arrhythmias arise at the site of maximal heterogeneity of repolarization in the chronic complete atrioventricular block dog. *Europace* **19,** 858–865 (2017).
16. Gardner RT, Ripplinger CM, Myles RC & Habecker BA. Molecular Mechanisms of Sympathetic Remodelling and Arrhythmias. *Circ. Arrhythmia Electrophysiol.* **9,** (2016).
17. Myles RC, Wang L, Kang C, Bers DM & Ripplinger CM. Local β-adrenergic stimulation overcomes source-sink mismatch to generate focal arrhythmia. *Circ. Res.* **110,** 1454–1464 (2012).
18. Aflaki M, Qi XY, Xiao L, Ordog B, Tadevosyan A, Luo X, Maguy A, Shi Y, Tardif JC & Nattel S. Exchange protein directly activated by cAMP mediates slow delayed-rectifier current remodelling by sustained β-adrenergic activation in guinea pig hearts. *Circ. Res.* **114,** 993–1003 (2014).
19. Dusi V, De Ferrari GM, Pugliese L & Schwartz PJ. Cardiac Sympathetic Denervation in Channelopathies. *Front. Cardiovasc. Med.* **6,** 27 (2019).
20. Ajijola OA, Lellouche N, Bourke T, Tung R, Ahn S, Mahajan A & Shivkumar K. Bilateral cardiac sympathetic denervation for the management of electrical storm. *J. Am. Coll. Cardiol.* **59,** 91–92 (2012).
21. Vaseghi M, Gima J, Kanaan C, Ajijola OA, Marmureanu A, Mahajan A & Shivkumar K. Cardiac sympathetic denervation in patients with refractory ventricular arrhythmias or electrical storm: Intermediate and long-term follow-up. *Heart Rhythm* **11,** 360–366 (2014).

22. Varkevisser R, Wijers SC, van der Heyden MAG, Beekman JDM, Meine M & Vos MA. Beat-to-beat variability of repolarization as a new biomarker for proarrhythmia in vivo. *Heart Rhythm* **9,** 1718–1726 (2012).
23. Bossu A, Varkevisser R, Beekman HDM, Houtman MJC, van der Heyden MAG & Vos MA. Short-term Variability of Repolarization Is Superior to Other Repolarization Parameters in the Evaluation of Diverse Antiarrhythmic Interventions in the Chronic Atrioventricular Block Dog. *J. Cardiovasc. Pharmacol.* **69,** 398–407 (2017).
24. Hope RR, Scherlag BJ, El-Sherif N & Lazzara R. Hierarchy of ventricular pacemakers. *Circ. Res.* **39,** 883–888 (1976).
25. Donker DW, Volders PGA, Arts T, Bekkers BCAM, Hofstra L, Spätjens RLHMG, Beekman JDM, Borgers M, Crijns HJGM & Vos MA. End-diastolic myofiber stress and ejection strain increase with ventricular volume overload: Serial in-vivo analyses in dogs with complete atrioventricular. *Basic Res. Cardiol.* **100,** 372–382 (2005).
26. Verduyn SC, Ramakers C, Snoep G, Leunissen JDM, Wellens HJJ & Vos MA. Time course of structural adaptations in chronic AV block dogs: evidence for differential ventricular remodeling. *Am. J. Physiol. Circ. Physiol.* **280,** 2882–2890 (2001).
27. Peschar M, Vernooy K, Vanagt WYR, Reneman RS, Vos MA & Prinzen FW. Absence of reverse electrical remodelling during regression of volume overload hypertrophy in canine ventricles. *Cardiovasc. Res.* **58,** 510–517 (2003).
28. Bourgonje VJA, van Veen TAB & Vos MA. Ventricular Electrical Remodelling in Compensated Cardiac Hypertrophy BT - Electrical Diseases of the Heart: Volume 1: Basic Foundations and Primary Electrical Diseases. in (eds. Gussak, I. & Antzelevitch, C.) 387–398 (2013). doi:10.1007/978-1-4471-4881-4_23
29. Antoons G, Volders PGA, Stankovicova T, Bito V, Stengl M, Vos MA & Sipido KR. Window Ca(2+) current and its modulation by Ca(2+) release in hypertrophied cardiac myocytes from dogs with chronic atrioventricular block. *J. Physiol.* **579,** 147–160 (2007).
30. Sipido KR, Volders PGA, de Groot SHM, Verdonck F, Van de Werf F, Wellens HJJ & Vos MA. Enhanced Ca(2+) Release and Na/Ca Exchange Activity in

Hypertrophied Canine Ventricular Myocytes. *Circulation* **102,** 2137–2144 (2000).

31. Volders PGA, Sipido KR, Vos MA, Spätjens RL, Leunissen JDM, Carmeliet E & Wellens HJJ. Downregulation of Delayed Rectifier K+ Currents in Dogs With Chronic Complete Atrioventricular Block and Acquired Torsades de Pointes. *Circulation* **100,** 2455–2461 (1999).
32. Dunnink A, van Opstal JM, Oosterhoff P, Winckels SKG, Beekman JDM, van der Nagel R, Cora Verduyn S & Vos MA. Ventricular remodelling is a prerequisite for the induction of dofetilide-induced torsade de pointes arrhythmias in the anaesthetized, complete atrio-ventricular-block dog. *Europace* **14,** 431–436 (2012).
33. Dunnink A, Sharif S, Oosterhoff P, Winckels S, Montagne D, Beekman J, van der Nagel R, van der Heyden MAG & Vos MA. Anesthesia and Arrhythmogenesis in the Chronic Atrioventricular Block Dog Model. *J. Cardiovasc. Pharmacol.* **55,** 601–608 (2010).
34. Oros A, Beekman JDM & Vos MA. The canine model with chronic, complete atrio-ventricular block. *Pharmacol. Ther.* **119,** 168–178 (2008).

Valerie Y. H. van Weperen, Alexandre Bossu & Marc A. Vos

Journal of cardiovascular pharmacology. 2019. **74**: 499 - 507. doi: 10.1097/FJC.0000000000000748.

CHAPTER 2

Point of View: Electrophysiological Endpoints Differ When Comparing the Mode of Action of Highly Successful Anti-arrhythmic Drugs in the CAVB Dog Model With TdP

ABSTRACT

In the anaesthetized, chronic atrioventricular block (CAVB) dog, ventricular ectopic beats and Torsade de pointes arrhythmias (TdP) are believed to ensue from an abrupt prolongation of ventricular repolarization and increased temporal dispersion of repolarization, quantified as short-term variability (STV). These TdP stop spontaneously or, when supported by substantial spatial dispersion of repolarization (SDR), degenerate into ventricular fibrillation. However, most studies involving ventricular arrhythmias do not quantify SDR by means of an electrophysiological parameter. Therefore, we reviewed the effects of 4 highly effective anti-arrhythmic drugs (flunarizine, verapamil, SEA-0400, and GS-458967) on the repolarization duration and associated STV. All drugs were tested as anti-arrhythmic strategies against TdP in CAVB dogs, their high anti-arrhythmic efficacy was defined as suppressing drug-induced TdP in 100% of the experiments. This comparison demonstrates that even though the anti-arrhythmic outcome was similar for all drugs, distinct responses of repolarization duration and associated STV were observed. Moreover, the aforementioned and commonly adopted electrophysiological parameters were not always sufficient in predicting TdP susceptibility, and additional quantification of the SDR proved to be of added value in these studies. The variability in electrophysiological responses to the different anti-arrhythmic drugs and their inconsistent adequacy in reflecting TdP susceptibility, can be explained by distinct modes of interference with TdP development. As such, this overview establishes the separate involvement of temporal and spatial dispersion in ventricular arrhythmogenesis in the CAVB dog model and proposes SDR as an additional parameter to be included in future fundamental and/or pharmaceutical studies regarding TdP arrhythmogenesis.

INTRODUCTION

Easy to recognize, yet hard to prevent - Torsade de Pointes arrhythmias (TdP) can either terminate spontaneously or progress to an episode of possibly catastrophic ventricular fibrillation. Since Dessertenne[1] named them after their characteristic morphology, TdP have been classified as a distinct type of ventricular arrhythmias. However, the fundamental questions of what processes are involved in TdP arrhythmogenesis and how these processes are incorporated to establish an episode of TdP, remain unanswered.

Numerous studies have aimed to decipher TdP by experimentally or computationally analyzing arrhythmogenesis or by assessing the electrophysiological effects of (un)successful anti-arrhythmic drugs. In the last two decades, many of such studies have been conducted in the anaesthetized, chronic atrioventricular block (CAVB) dog model. In this model, a collective of remodeling processes result in a predisposition to TdP development.[2] Exposing the remodeled animals to additional repolarization challenges results in the repetitive induction of TdP in up to 75% of the dogs.[3] Therefore, this model has proven to be of paramount value in studies aiming to understand, prevent, and/or suppress TdP.[3,4]

Nevertheless, as TdP arrhythmogenesis remains an enigmatic and indecipherable process; one could wonder whether we are studying and focusing on the right electrophysiological parameters to reflect a TdP-susceptible heart and/or an imminent episode of TdP. Repolarization duration is most commonly used as a representation of cardiac electrical (in)stability. This parameter can be obtained from the surface electrocardiogram [ECG; *i.e.,* corrected QT-interval (QTc)] and/or from endocardial catheters [*i.e.,* left ventricular (LV) monophasic action potential duration (MAPD)]. Previous studies have already demonstrated that its derivative, the short-term variability (STV) of repolarization, gives a more adequate reflection of the pro-arrhythmic susceptibility of an individual or the pro-arrhythmic character of drugs.[4] Nevertheless, both parameters still seem to be insufficiently accurate in predicting and/or explaining arrhythmogenesis.

A possible explanation for the inadequacy of these parameters is that they only disclose absolute changes in repolarization time and the local beat-to-beat variability herein. Most often, the adopted electrophysiological parameters do thus not represent

or assess spatial heterogeneity of repolarization, even though this heterogeneity has been demonstrated to be of importance in both the initiation and perpetuation of TdP.[5,6]

Therefore, we combined knowledge on arrhythmogenic mechanisms involved in the initiation and perpetuation of ventricular arrhythmias with electrophysiological parameters reflecting repolarization duration (QTc and MAPD), temporal dispersion of repolarization (STV), and/or spatial dispersion of repolarization (SDR). In this manner, we were able to determine the mode of action of four highly effective anti-arrhythmic drugs, all of which had been previously tested in the CAVB dog model. Also, we demonstrate that the commonly used electrophysiological parameters (QTc, MAPD, and STV) incompletely reflect the susceptibility for TdP arrhythmogenesis. We establish that this insufficiency results from their deficiency in reflecting SDR, which is shown to be a fundamental step in arrhythmogenesis. Therefore, we recommend including SDR as an additional parameter in future fundamental and/or pharmaceutical studies regarding TdP arrhythmogenesis.

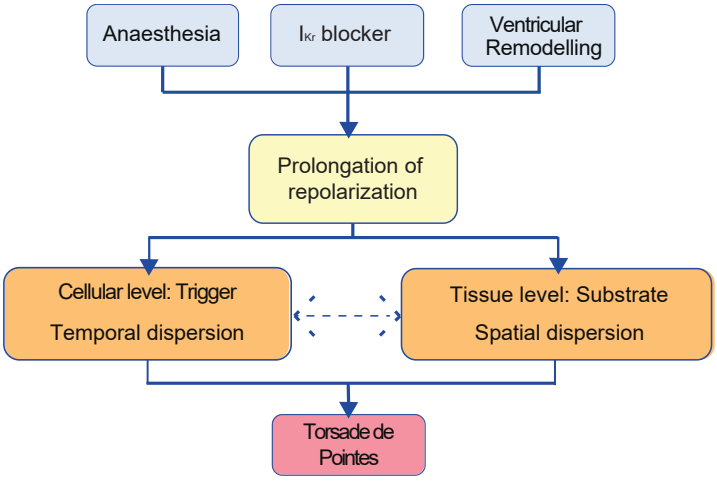

Figure 1. Schematic representation of the current paradigm of arrhythmogenesis in the CAVB dog model. Different factors, such as the use of anesthesia, ventricular remodeling, and the challenge with an I_{Kr}-blocker impair repolarization reserve, causing a prolongation in ventricular repolarization. This prolonged process of repolarization weakens the cellular electrophysiology, reflected in an increased temporal dispersion of repolarization. This cellular instability is believed to induce a susceptibility for the development of early and/or late afterdepolarizations, leading to triggered activity. Simultaneously, inhomogeneous prolongation of repolarization also causes an increase in the spatial dispersion of repolarization. This spatial variance in repolarization dynamics is thought to form the substrate of longer-lasting episodes of ventricular arrhythmias, because it allows for the maintenance and perpetuation of the aberrant stimulus. Though they presumably do reinforce each other, the two processes are believed to be separate pathways that cumulatively *trigger* and *perpetuate* episodes of Torsade de Pointes arrhythmias.

ARRHYTHMOGENESIS IN THE CAVB DOG MODEL

In the CAVB dog model, ablation of the atrioventricular node causes an acute drop in the cardiac output. The ensuing initiation of extensive structural, contractile and electrical remodeling processes restore this impaired cardiac output.[3,7–9] Simultaneously, TdP-susceptibility arises from the same adaptive processes, primarily from the electrical remodeling, which encompasses the downregulation of potassium channels[8] and an altered calcium handeling.[9] Regarding the downregulation of potassium channels, the overcapacity of the repolarization process, known as repolarization reserve becomes reduced. The repolarization reserve, first introduced by Roden,[10] refers to an overall redundancy of the factors involved in ventricular repolarization. Collectively, these factors are capable of preserving an intact repolarization process when the action potential cycle is challenged.[11] Hence, electrical remodeling causes the repolarization process to become more vulnerable for additional repolarization impediments. Moreover, the extent of potassium channel downregulation is believed to be heterogeneously dispersed over the myocardium. As such, this results in increased spatial differences in repolarization, which become further amplified when repolarization is challenged.[5] Alterations in calcium handling stimulate the intracellular calcium storage and release as this benefits the contractional force of the heart. An important adaptation of the calcium handling is the increased reverse activity of the sodium-calcium exchanger (NCX), leading to the transport of three sodium ions out of the cell in the exchange for one calcium ion.

The current paradigm of TdP development in the CAVB dog model is mainly centered around the permanently decreased repolarization reserve, which destabilizes the electrical activity of the heart (Fig. 1).[12] As schematically depicted in figure 2A, the action potential is constituted by multiple ion channels. During phase 0, sodium influx (I_{Na}) results in fast depolarization of the myocyte. Subsequent activation of the transient potassium channels (I_{to}) produces some repolarization, which results in the characteristic spike of the action potential. Next, calcium enters the cell through the L-type calcium channels (LTCC) which subsequently stimulate sarcoplasmic reticulum (SR) calcium release through the RyR2 channels. Simultaneously, this depolarizing current is counteracted by repolarizing currents I_{Kr} and I_{Ks}, causing a plateau in potential during phase 2. Subsequent decrements in depolarizing currents cause I_{Kr} and I_{Ks} to

prevail and to thereby establish repolarization during phase 3. In phase 4, the resting potential is maintained and restored by the NCX and the sodium-potassium pump.

Electrical remodeling in the CAVB dog does not affect the action potential morphology under baseline conditions (Fig. 2B). However, when the repolarization

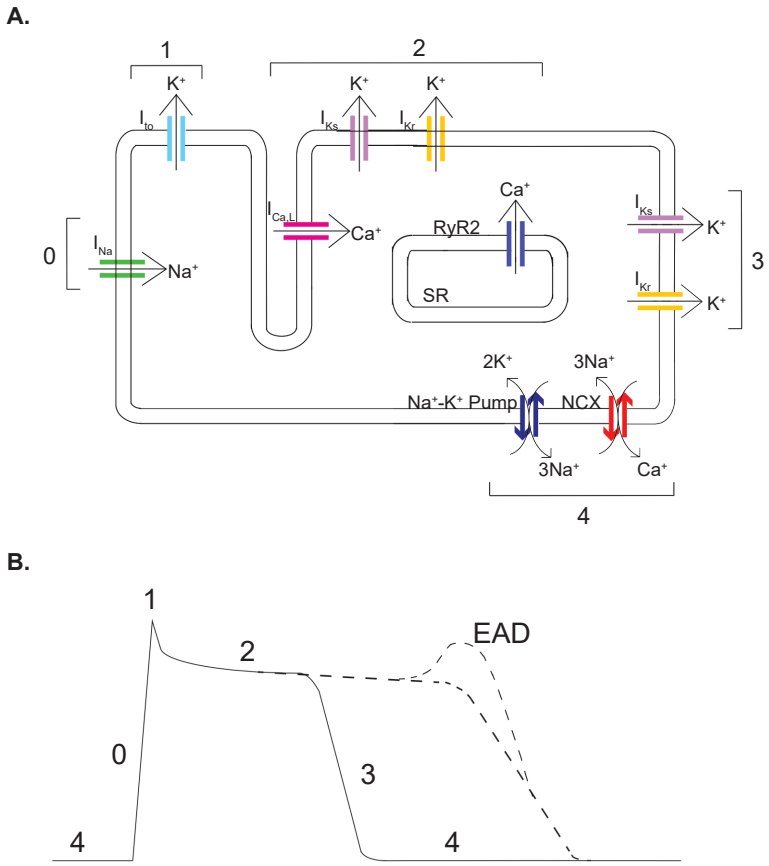

Figure 2. Schematic representation of the major ion currents involved in the establishment of a cardiac action potential and the development of an early after depolarization (EAD). A) The action potential can be divided into five different phases. During phase 0, fast sodium current (I_{Na}) depolarizes the myocyte. As the sodium channels become inactivated, the slower activated transient potassium current (I_{to}) causes a small repolarizing current, constituting phase 1 of the action potential. In phase 2, also known as the plateau phase, depolarizing and repolarizing currents are more or less in an equilibrium. The depolarizing current is mainly established by the calcium influx through the L-type calcium channels (LTCC) which subsequently stimulate sarcoplasmic reticulum (SR) calcium release through the RyR2 channels. I_{Kr} and I_{Ks} constitute the main repolarizing currents. During phase 3, the calcium influx is decreased whereas I_{Kr} and I_{Ks} are maintained, resulting in repolarization. Phase 4 represents the resting potential. The sodium-calcium exchanger, which exchanges one calcium from the intracellular environment for three sodium ions, and the sodium-potassium pump, which actively imports two potassium ions and exports three sodium ions, maintain and restore this potential. **B)** Schematic representation of the different phases of the action potential duration (APD) under baseline (solid line) conditions and following additional I_{Kr}-block (dashed line). When repolarization becomes prolonged, EADs can develop during phase 3 of the APD.

reserve is additionally challenged by infusion of an I_{Kr}- or I_{Ks}-blocker, such as the I_{Kr}-blocker dofetilide, the process of repolarization becomes excessively impeded. This causes the action potential duration (APD) to prolong extensively (Fig. 2B), which subsequently increases dispersion of repolarization in both the temporal[13] *and* spatial[5] dimension. At a cellular level, this prolongation of APD results in increased cytoplasmatic calcium concentrations. In combination with the aforementioned alterations in calcium handling, this can lead to excessively increased levels of SR calcium storage and systolic calcium release. This increase in intracellular calcium concentrations becomes a self-propagating cycle as it further prolongs APD, which influences the calcium cycling of the next APD. Consequently, APD becomes unstable and inconsistent. At a macroscopic level, this cellular instability in calcium handling is observed as temporal dispersion of repolarization, reflected by the beat-to-beat variability of repolarization, quantified as the STV (Figs. 1 and 3A).[4,14,15] If calcium release becomes suprathreshold, this can cause activation of the forward mode of the NCX during phase 3 of the APD, and thereby establish a sodium influx, which could reverse the process of repolarization and trigger an early afterdepolarization (Figs. 1 and 2B). The likelihood that these abnormal afterdepolarizations will develop can be deduced from the increase in temporal dispersion (Figs. 1 and 4).[11]

Simultaneously, the aforementioned heterogeneity of electrical remodelling results in an increased SDR as I_{Kr} blockade causes spatially heterogeneous prolongations in repolarization (Figs. 1, 3B, and 4).[6] This gradient of repolarization duration aids the development of triggered activity, because it establishes a gradient for the ectopic beat to emerge from.[5,11] In addition, this SDR also constitutes the required substrate for longer lasting arrhythmic events,[16,17] because these local differences in electrophysiological kinetics allow for the perpetuation of aberrant ectopic activity. As a gradual progression from single to multiple ectopic beats to TdP is observed in most experiments, SDR is believed to progress more slowly and/or to have a relatively higher critical threshold than temporal dispersion of repolarization (Figs. 1 and 4). Moreover, the extent of dofetilide-induced SDR is thus also a main determinant of the pro-arrhythmic phenotype of CAVB dogs.

Hence, these two processes synchronously, and presumably reciprocally, result in a *trigger* and a *substrate* for TdP.[6]

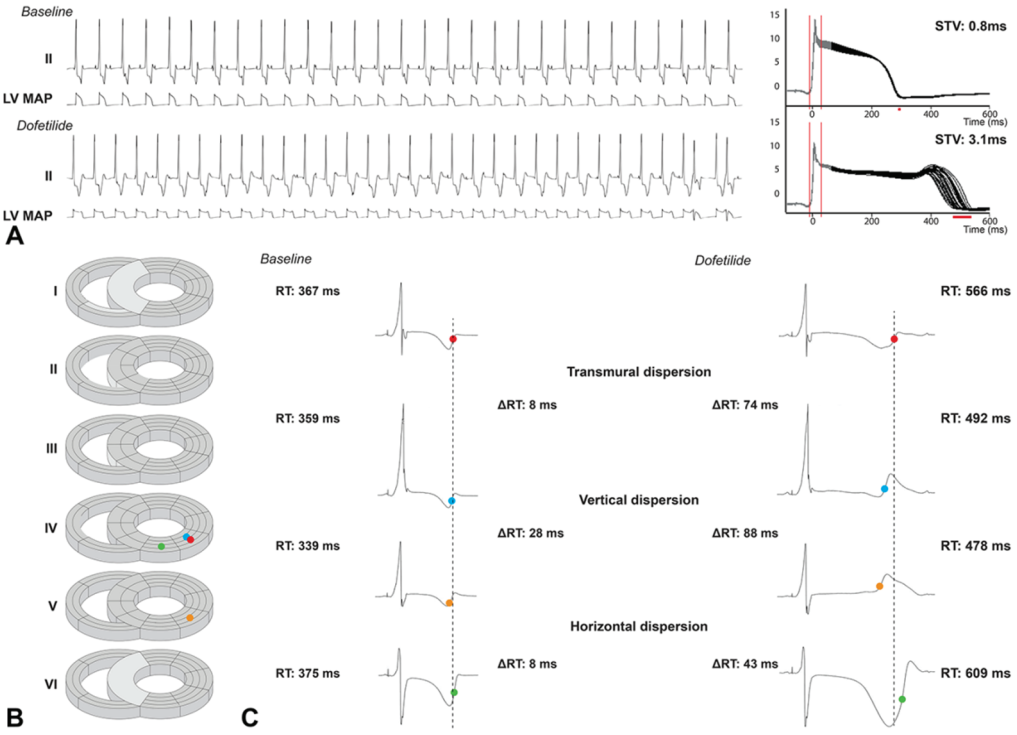

Figure 3. Representation of the quantification of temporal and spatial dispersion of repolarization. **A)** Temporal dispersion of repolarization represents the beat-to-beat variability in repolarization. Under baseline conditions, consecutive beats are mostly alike, resulting in low variation in action potential duration when the beats are stacked upon each other (variation depicted by the red bar under the x-axis). This corresponds to a low short-term variability (STV). After dofetilide administration, repolarization prolongs, and consecutive beats start to differ more (depicted by the red bar under the x-axis). This is reflected in the increase in repolarization duration and higher LV STV. **B)** Spatial dispersion of repolarization (SDR) is the difference in repolarization duration from one location to another. Transverse sections through the myocardium from base (I) to apex (VI) allow for the assessment of SDR in the vertical (red *vs.* orange), horizontal (red *vs.* green) and transmural (red *vs.* blue) orientation. Together, these three orientations form the cubic orientation. **C)** Under baseline conditions, SDR is low, but becomes increased in all orientations upon infusion of dofetilide. Repolarization times (RT) were measured as the interval between the pacing spike and the steepest upslope of the T-wave (colored dots); the colors correspond with the location of the electrodes as depicted in part B.

ANTI-ARRHYTHMIC TESTING IN THE CAVB DOG MODEL

This overview compares the previously published arrhythmic and electrophysiological outcome of four drugs (flunarizine, verapamil, SEA-0400, and GS-458967) in the CAVB dog model.[18–20] All drugs were investigated between 2010 and 2018 as potential anti-arrhythmic strategies. These four drugs were selected for their high anti-arrhythmic effect, defined as the capability of suppressing dofetilide-induced

568622-L-bw-Weperen
Processed on: 3-11-2021

TdP in 100% of the experiments.[4] All experiments described in this overview were performed in a total of 31 adult purpose-bred mongrel dogs (22 female, 23 ± 4 kg; Marshall, NY).

Evaluation of anti-arrhythmic efficacy

All drugs were tested in suppression experiments.[4] In this setting, ten minutes of baseline recordings were followed by the administration of dofetilide to induce reproducible TdP. According to this protocol, TdP were defined as a polymorphic ventricular tachycardia, characterized by the "twisting of the points" around the isoelectric line and consisting of ≥5 ectopic beats.[21] An animal was considered to be inducible when ≥3 TdP developed during the according stage. If the animal was inducible for TdP following dofetilide infusion, one of the following anti-arrhythmic drugs was given: flunarizine (2mg/kg/2 minutes; n = 10),[18] verapamil (0.4 mg/kg/3 minutes; n = 7),[18] SEA-0400 (0.8mg/kg/5 minutes; n = 4),[19] or GS-458967 (0.1mg/kg/5 minutes; n = 10).[20]

Anti-arrhythmic efficacy was primarily assessed as percentage of animals that remained inducible after infusion of the anti-arrhythmic drug and further specified with the arrhythmia score (AS).[21] This score awards points to arrhythmic events according to the *n + 1* formula*; n* being the number of ectopic beats. Ectopic beats were defined as premature ventricular contractions, characterized by the “R on T” phenomenon. Electrical cardioversions were scored according to the number of defibrillations needed to terminate the event (50, 75, or 100 points for 1, 2, or ≥3 cardioversions, respectively). Finally, the AS was determined by taking the average of the three most severe arrhythmic events within the respective stage.[21] TdP-inducibility was statistically analyzed using the McNemar’s test, whereas the nonparametric Friedman test and Whitney *U* test were used to compare AS and number of TdP, respectively.

Electrophysiological Parameters

All of the experiments presented in this overview included a surface ECG from which the QTc was measured and could be compared. Furthermore, except for SEA-0400, an LV MAPD from an LV endocardial catheter had been measured in all experiments. LV STV was calculated from 30 consecutive beats of the corresponding timepoint using

the formula: $\sum|Dn+1 - Dn|/(30 \times \sqrt{2})$; D being the LV MAPD or, in case of the SEA-0400 experiments, the QTc.[13]

As previously described by Dunnink *et al.* (2017),[5] high resolution electrical mapping experiments were performed in five CAVB dogs to investigate the effects of GS-458967 on the spatial dispersion.[20] Statistical analysis of all electrophysiological parameters was performed with a one-way repeated measurement analysis of variance (ANOVA) followed by a post-hoc Bonferroni test or (un)paired Student's *t*-test. All data included in this overview are presented as mean ± standard deviation (SD). Results were considered to be statistically significant if $P<0.05$.

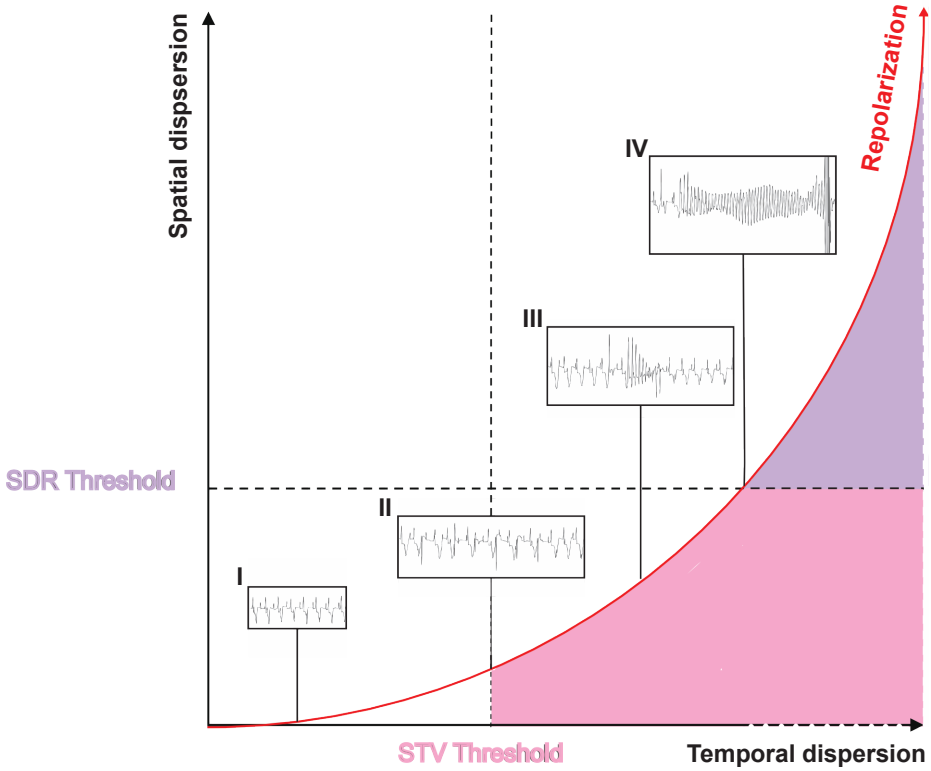

Figure 4. Schematic representation of the contribution of temporal and spatial dispersion of repolarization in arrhythmogenesis. Prolongation of repolarization (red arrow) underlies the simultaneous increases in temporal and SDR, the latter developing slower and/or having a higher threshold before it becomes pathological. If both dispersions are insufficiently increased, no arrhythmic events will develop (reflected in ECG recording I). As, temporal, but not spatial, dispersion of repolarization (quantified by the STV) reaches its critical threshold, triggered activity is induced (ECG recording II). Further increments in STV are associated with the subsequent development of short runs of Torsade de Pointes arrhythmias (ECG recording III), completely founded by focal activity. However, when in the additional presence of sufficient SDR, longer lasting arrhythmic episodes and the degeneration to ventricular fibrillation can be established (depicted in ECG recording IV). All ECG recordings are traces of lead II.

ANTI-ARRHYTHMIC EFFICACY

In all experiments, administration of dofetilide induced TdP in all animals, which was accompanied by a significant increase in the AS. Upon infusion of the anti-arrhythmic drugs, animals were no longer inducible and the AS and number of TdP were greatly decreased (Table 1). The anti-arrhythmic effects of verapamil and flunarizine were most pronounced, as they also significantly reduced the incidence of single and multiple ectopic beats (Fig. 5).

Repolarization Duration

Dofetilide prolonged QTc in all experiments, which was paralleled by significant increases in the LV MAPD. After the administration of the anti-arrhythmic drugs, the following three different responses were observed. First, LV MAPD was fully reversed to baseline values by flunarizine (from 355 ± 35 ms in baseline, to 492 ± 53 ms after dofetilide to 367 ± 42 ms following flunarizine, $P < 0.05$ *vs.* dofetilide) (Fig. 5). Second, in response to verapamil and GS-458967, LV MAPD, despite being shortened, remained prolonged in comparison to baseline values (Verapamil: 349 ± 88 ms under baseline to 466 ± 95 after verapamil; GS-458967: 263 ± 27 under baseline to 392 ± 65 ms after GS-458967, both $P < 0.05$ *vs.* baseline) (Fig. 5) . Third, administration of SEA-0400 did not shorten QTc (from 549 ± 95 ms after dofetilide to 702 ± 45 ms after SEA-0400, $P > 0.05$*)* (Table 1 and Fig. 5).

Short-Term Variability of Repolarization

Corresponding to the dofetilide-induced arrhythmic activity, STV was substantially increased in all experiments. Infusion of the anti-arrhythmic drugs induced two different responses in STV: following flunarizine, verapamil, and SEA-0400, STV was comparable to, or even lower than, baseline values (from 1.8 ± 0.5, 1.7 ± 0.4 and 6.2 ± 3.7 under baseline, to 1.5 ± 0.6, 1.5 ± 0.7 and 7.3 ± 3.2 ms after flunarizine, verapamil, and SEA-0400, respectively; all $P > 0.05$ *vs.* baseline) (Fig. 5). In contrast, the LV STV following GS-458967 remained more than 200% higher than under baseline conditions (1.1 ± 0.4 under baseline to 2.7 ± 0.9 ms following GS-458967, $P < 0.05$ *vs.* baseline) (Table 1 and Fig. 5).

568622-L-bw-Weperen
Processed on: 3-11-2021

Table 1. Electrophysiological Effects of Dofetilide and the Subsequent Infusion of the Different Anti-arrhythmic Drugs.

	Flunarizine[18]	**Verapamil**[18]	**GS-458967**[20]	**SEA-0400**[19] [&]
	2 mg/kg/2'	0.4 mg/kg/3'	0.1 mg/kg/5'	0.8 mg/kg/5'
	n = 10	n = 7	n = 7	n = 4
Baseline				
RR (ms)	1181 ± 87	1361 ± 190	1000 ± 0	1787 ± 164
QTc (ms)	421 ± 49	424 ± 62	406 ± 25	408 ± 51
LV MAPD	355 ± 35	349 ± 88	263 ± 27	-
(ms)	1.8 ± 0.5	1.7 ± 0.4	1.1 ± 0.4	6.2 ± 3.7
STV (ms)	0 / 10	0 / 7	0 / 7	0 / 4
n Inducible	0 ± 0	0 ± 0	0 ± 0	0 ± 0
# TdP	1.2 ± 0.7	1.1 ± 0.4	1.3 ± 0.5	1.0 ± 0.0
AS				
Dofetilide				
RR (ms)	1291 ± 140	1520 ± 210 [#]	1000 ± 0	2044 ± 106 [#]
QTc (ms)	553 ± 40 [#]	566 ± 87 [#]	609 ± 44 [#]	549 ± 95
LV MAPD	492 ± 53 [#]	505± 110 [#]	410 ± 70 [#]	-
(ms)	4.5 ± 1.5 [#]	3.2 ± 1.1 [#]	4.2 ± 2.5 [#]	12.0 ± 6.4
STV (ms)	10 / 10 [#]	7 / 7 [#]	7 / 7 [#]	4 / 4
n Inducible	10 ± 10 [#]	6 ± 4 [#]	7 ± 8 [#]	6 ± 2 [#]
# TdP	50.8 ± 13.9 [#]	71.2 ± 13.4 [#]	46.7 ± 27.9 [#]	63.9 ± 6.8 [#]
AS				
Drug				
RR (ms)	1219 ± 251	1476 ± 166	1000 ± 0	2112 ± 297
QTc (ms)	425 ± 38 *	516 ± 90 [#]	551 ± 77 [#]*	702 ± 45
LV MAPD	367 ± 42 *	466 ± 95 [#]	392 ± 65 [#]	-
(ms)	1.5 ± 0.6 *	1.5 ± 0.7 *	2.7 ± 0.9 [#]	7.3 ± 3.2
STV (ms)	0 / 10 *	0 / 7 *	0 / 7 *	0 / 4
n Inducible	0 ± 0 *	0 ± 0 *	0 ± 0 *	1 ± 1
# TdP	1.4 ± 0.8 *	1.9 ± 0.8 *	2.3 ± 1.4	7.2 ± 10.2
AS				

[#] $p<0.05$ vs Baseline

* $p<0.05$ vs Dofetilide

[&] STV was derived from QT

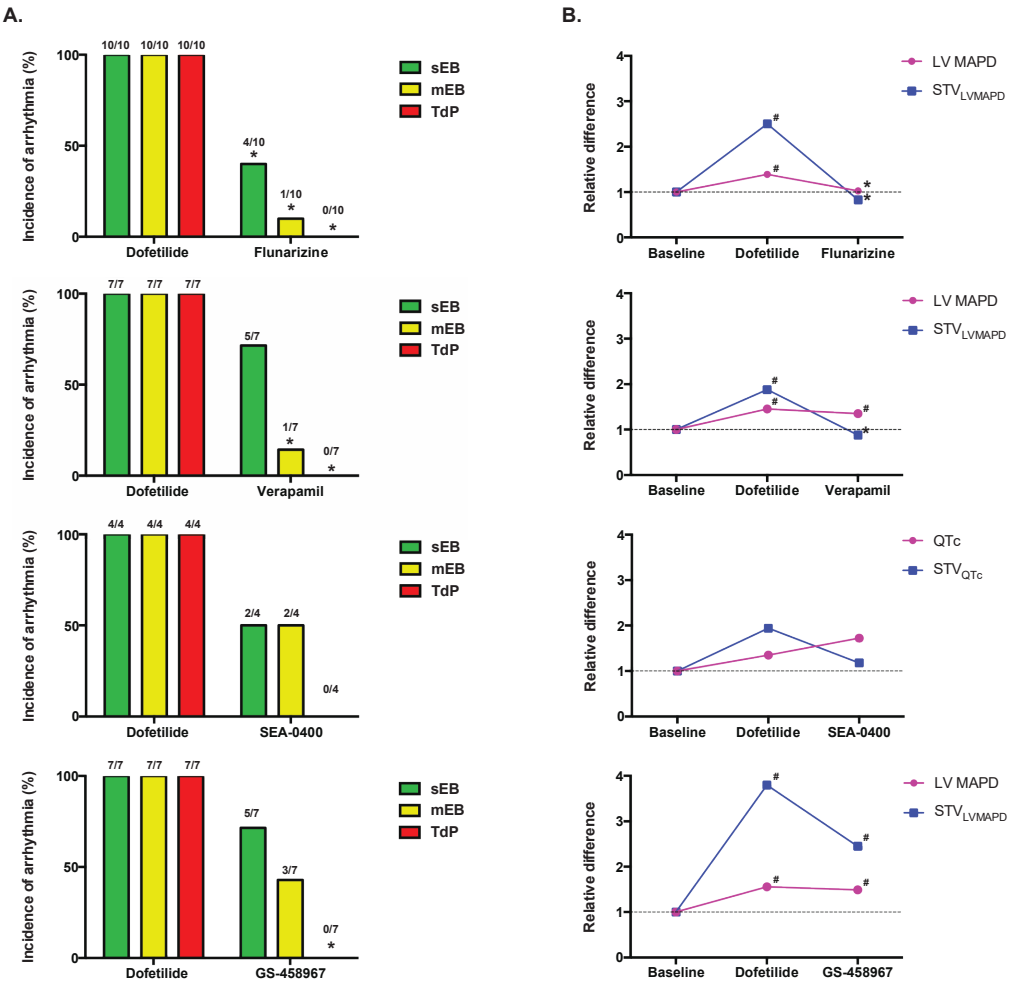

Figure 5. Arrhythmogenic and electrophysiological responses to dofetilide and the subsequent infusion of the different drugs. A) The administration of dofetilide caused single ectopic beats (sEB), multiple ectopic beats (mEB) and Torsade de Pointes arrhythmias (TdP) in all animals. Following infusion of the anti-arrhythmic drugs, the incidence of the different arrhythmic events was decreased. **B)** Dofetilide caused prolongation of repolarization (LV MAPD; QTc for SEA-0400) and increased the associated short-term variability (STV) in all animals. Subsequent infusion of flunarizine caused a full reversal of both LV MAPD and LV STV. In case of verapamil and SEA-0400 repolarization duration was incompletely reversed or even further prolonged, whereas the anti-arrhythmic efficacy of the drugs was reflected by the full reversal of the STV. However, the efficacy of GS-458967 was not portrayed by its effects on LV MAPD, nor by its actions on LV STV. LV = Left Ventricular; MAPD = Monophasic Action Potential Duration. # $P < 0.05$ *versus* baseline; * $P < 0.05$ *versus* dofetilide.

Spatial Dispersion of Repolarization

In the five additional mapping experiments involving GS-458967, administration of dofetilide induced TdP in three of the five animals and increased repolarization

parameters similarly to the aforementioned experiments.[20] In addition, dofetilide increased the SDR significantly (maximal cubic dispersion: from 68 ± 14 ms to 237 ± 54 ms after dofetilide, $P < 0.05$). Subsequent infusion of GS-458967 decreased maximal cubic dispersion of repolarization to 123 ± 34 ms ($P < 0.05$ *vs.* dofetilide). The spatial dispersion was also significantly reduced in all other orientations, except for the vertical dispersion.

TEMPORAL AND SPATIAL DISPERSION ARE SEPARATELY INVOLVED IN ARRHYTHMOGENESIS

This overview explored the adequacy of the commonly adopted electrophysiological parameters QTc, LV MAPD, and LV STV to give an accurate indication of TdP-susceptibility of the CAVB dog model. It is demonstrated that these three parameters, that only disclose the temporal behavior of repolarization, are not always sufficient in representing the (in)stability of the cardiac electrophysiology. This does not only indicate that an SDR parameter is of additional value in the assessment of cardiac electrophysiology, but also implies that spatial and temporal dispersion of repolarization are separately involved in arrhythmogenesis.

Prolongation of Repolarization

In the CAVB dog model, several factors have been demonstrated to promote the inducibility for TdP, *i.e.,* ventricular remodeling,[2,22] anaesthesia,[23] acute bradycardia,[24] and the administration of an I_K-blocker.[3] All of these factors are believed to contribute to the development of TdP by reducing the already weakened repolarization reserve below a critical threshold. The subsequent functional impediment in repolarization is first observed through a prolongation in repolarization, commonly displayed by an increase in QTc and/or LV MAPD.

This prolongation is believed to precipitate the increases in both temporal and spatial dispersion of repolarization. Accordingly, targeting the prolonged repolarization would not only reverse the prolongation in QTc and/or LV MAPD, but would also reverse the increased temporal and spatial dispersion of repolarization and thereby yield highly effective anti-arrhythmic results. Of the drugs incorporated in this overview, the data on flunarizine support this hypothesis. Flunarizine diminished most of the dofetilide-induced arrhythmic activity, which was accompanied by a full reversal of all electrophysiological parameters measured (Table 1 and Fig. 5). The ability of

flunarizine to reverse the LV MAPD can be attributed to the fact that it simultaneously impedes multiple currents involved in depolarization: LTCC, T-type calcium channel, and the sodium current (I_{Na}).[18] Accordingly, flunarizine successfully reversed both temporal and spatial dispersion of repolarization (the latter was studied in one animal, data not published) back to baseline values. However, it is of course also probable that the decrease in LV STV results from a multi-targeted effect of flunarizine and was not merely the consequence of the complete reversal of the LV MAPD.

Temporal Dispersion of Repolarization

At the cellular level, prolongation of APD increases temporal dispersion of repolarization as the normal interplay between depolarizing and repolarizing currents becomes disturbed. This increases the cellular vulnerability for afterdepolarizations, which is reflected by a rise in beat-to-beat variability of repolarization.[13] Hence, STV reflects the remaining capabilities of the repolarization reserve to compensate for electrophysiological disturbances, and therefore gives an indication of the *probability* that triggered activity will occur. Drugs that would resolve this electrophysiological instability would thus be expected to *prevent* the development of the trigger, thereby reducing not only the incidence of single and multiple ectopic beats, but also of TdP (Fig. 4). This effect would be reflected in a reduction in LV STV, but to lesser or no extent in the QTc and/or LV MAPD (Fig. 1).

This pattern was indeed observed in the experiments with verapamil and SEA-0400, as both drugs demonstrated an *isolated* reversal of the dofetilide-induced increase in LV STV (Fig. 5). This decrease reflects the ability of these drugs to restore the repolarization reserve, in an APD-*independent* manner. This thus implies a different anti-arrhythmic mechanism in comparison to flunarizine, where STV is, at least in part, lowered in an APD-*dependent* manner. SEA-0400 and verapamil are known to be potent blockers of the NCX and/or LTCC, respectively.[18,19] Therefore, the primary anti-arrhythmic effect of both drugs seems to rely on their interference with the aforementioned remodeling-induced alterations in calcium handling. Blocking NXC and/or LTCC could counteract the abnormal calcium release and therefore hamper the development of afterdepolarization and thus result in a decrease in arrhythmic activity. However, as shown in Figure 5, arrhythmic activity was still observed following infusion of SEA-0400. Though not considered inducible (< 3 TdP), isolated TdP remained

present in two of four dogs. As SEA-0400 is an inhibitor of the NCX, and to lesser extent of the LTCC,[19] it could be hypothesized that the less extensive calcium-blocking effects of SEA-0400 allowed for the development of some remnant early afterdepolarization (EADs). Such ectopic activity could, in the presence of sufficient SDR, have evoked the TdP in the two animals. However, no additional experiments wherein LTCC-blockers were combined with SEA-0400 have been conducted to test for this hypothesis. Nevertheless, the drugs verapamil and SEA-0400 demonstrate that reversing STV prevents the development of both ectopic beats and TdP and that STV represents the electrophysiological (in)stability more adequately than the QTc and/or LV MAPD.

Spatial Dispersion of Repolarization

Prolongation of repolarization increases SDR. This is probably the result of inhomogeneous electrical remodeling of the heart, which causes the extent of prolongation, and thus also the consequential electrophysiological instability, to be heterogeneously dispersed. Previous studies have established that spatial dispersion is involved in both the initiation and perpetuation of TdP. For example, Dunnink *et al.* (2017)[5] demonstrated that TdP arise at the region with the greatest gradient in spatial dispersion. Other studies have shown the involvement of spatial dispersion (and re-entry) in the perpetuation of TdP in dog models,[6, 25] and in humans.[26] As such, it is believed that local differences in repolarization prolongation allow for ectopic activity of competing foci to emerge, as heterogeneities in repolarization duration would facilitate the conduction of these ectopic stimuli through the myocardium. Also, this spatial heterogeneity in repolarization duration is thought to induce a functional block in conduction, which subsequently enhances possibilities of re-entry circuits. Vandersickel *et al.* (2017)[6] demonstrated that these circuits were involved in the perpetuation of longer-lasting TdP episodes in the CAVB dog model.[6, 27] Drugs hindering arrhythmogenesis by reducing the dofetilide-induced increase in spatial dispersion would therefore be expected to prevent the development of re-entry loops and thus prevent the occurrence of long-lasting TdP. Moreover, it would also be expected that only short bursts of arrhythmic activity should still be present, because this homogenization of repolarization duration would impede the establishment of competing foci. If such drugs would exclusively target the SDR, LV MAPD and LV STV would be expected to demonstrate an insignificant response to the infusion of these

drugs (Figs. 1 and 4). Such results were obtained in the GS-458967 experiments, as the marginal reductions in LV MAPD and LV STV could not explain the objectified anti-arrhythmic effect of GS-458967. More specifically, they did not reflect the total abolishment of TdP, nor the decrease in single and multiple ectopic beats (Fig. 5). The hypothesis that GS-458967 exerts its anti-arrhythmic effects by opposing the dofetilide-induced increase in spatial dispersion was supported in additional mapping experiments. Thus, it seems that after infusion of GS-458967, temporal dispersion remained and *evoked* the ectopic beats, but that the length of these arrhythmic events was impeded by limited spatial dispersion. This hypothesis is in accordance with the moderate anti-arrhythmic effects of the late sodium current blocker ranolazine. Infusion of this drug in our CAVB dog model led to a significant decrease of TdP, whereas single and multiple ectopic beats and an elevated MAPD and STV persisted.[28] In addition, experiments in class III anti-arrhythmic drug-treated rabbits demonstrated that reduction of the SDR could, at least in part, explain the anti-arrhythmic effects of ranolazine.[29] Hence, it is becoming increasingly clear that SDR plays a pivotal role of in the process of arrhythmogenesis.

Regarding the partial restoration of LV MAPD and LV STV, it is suggested that the blocking of the late sodium current shortens MAPD, which consequently also reduces STV. In addition, STV could also be reduced, because blocking late I_{Na} decreases the influx of sodium. This would have resulted in a decreased activity of the NCX and consequently reduced intracellular calcium concentration. A reduction in intracellular calcium could have stabilized cellular APD and thereby impeded the development of afterdepolarizations and decreased STV.

Clinical Implications

This overview demonstrated the separate involvement of temporal and SDR in TdP arrhythmogenesis. As such, it is necessary to include electrophysiological parameters that represent both processes independently in experimental studies in the field of arrhythmogenesis. Furthermore, these observations also offer interesting and innovative prospects for future anti-arrhythmic pharmaceuticals. It has been demonstrated that an effective anti-arrhythmic outcome can be obtained by adequate interference with either of the three processes involved in arrhythmogenesis (Figs. 1 and 4). Because currently most anti-arrhythmic drugs target either the prolongation of

MAPD/QT or increased STV, it would be interesting to exploit SDR as a target for future anti-arrhythmic drugs.

Limitations

Because the first ectopic event is commonly followed by the continuous initiation of more ectopic beats and TdP, it is most often impossible to measure STV at later timepoints. As such, it is largely unknown how STV further develops after the initiation of the first ectopic event and how the spatial and temporal dispersion of repolarization interact. Also, mapping experiments were only conducted in five GS-458967 experiments and one flunarizine experiment. Therefore, there are insufficient data to substantiate the hypothesis that drugs reversing LV MAPD, such as flunarizine, cause a complete reduction in spatial dispersion. Moreover, no mapping experiments were performed with verapamil and SEA-0400. Hence, it remains hypothetical that these two drugs, that reversed LV STV but not QTc nor LV MAPD, do not affect SDR. Furthermore, SEA-0400 was only tested in four animals.[19] The smaller sample size and the absence of a LV MAPD measurement could have resulted in an incomplete representation of the anti-arrhythmic effects of the drug. Finally, the choice of dosage of each drug is arbitrary, because it is well known that higher dosages can be more effective. However, dose dependency has not been tested by us and the dosages described in this manuscript all resulted in a 100% anti-arrhythmic effect of the drugs.

CONCLUSIONS

The common parameters QTc, LV MAPD and LV STV, that do not disclose any information on SDR, only partially reflect TdP-susceptibility of the CAVB dog model. This implies that temporal and spatial dispersion of repolarization are separately involved in arrhythmogenesis. It is therefore recommended that spatial dispersion becomes included as an electrophysiological parameter in (experimental) studies concerning arrhythmogenesis. Moreover, SDR may be an effective and innovative target in future anti-arrhythmic therapies.

ACKNOWLEDGEMENTS

The authors thank Dr. M.A.G. van der Heyden (Department of Medical Physiology, UMC Utrecht, the Netherlands) for his critical evaluation of the manuscript.

REFERENCES

1. Dessertenne F. La tachycardie ventriculaire a deux foyers opposes variables. Arch Mal Coeur Vaiss. 1966 Feb; 59(2):263–72.
2. Dunnink A, van Opstal JM, Oosterhoff P, Winckels SKG, Beekman JDM, van der Nagel R, Cora Verduyn S, Vos MA. Ventricular remodelling is a prerequisite for the induction of dofetilide-induced torsade de pointes arrhythmias in the anaesthetized, complete atrio-ventricular-block dog. Europace. 2012 Feb; 14(3):431–6.
3. Oros A, Beekman JDM, Vos MA. The canine model with chronic, complete atrio-ventricular block. Pharmacol Ther. 2008 Aug; 119(2):168–78.
4. Bossu A, Varkevisser R, Beekman HDM, Houtman MJC, van der Heyden MAG, Vos MA. Short-term Variability of Repolarization Is Superior to Other Repolarization Parameters in the Evaluation of Diverse Antiarrhythmic Interventions in the Chronic Atrioventricular Block Dog. J Cardiovasc Pharmacol. 2017 Jun; 69(6):398–407.
5. Dunnink A, Stams TRG, Bossu A, Meijborg VMF, Beekman JDM, Wijers SC, De Bakker JMT, Vos MA. Torsade de pointes arrhythmias arise at the site of maximal heterogeneity of repolarization in the chronic complete atrioventricular block dog. Europace. 2017 May; 19(5):858–65.
6. Vandersickel N, Bossu A, De Neve J, Dunnink A, Meijborg VMF, van der Heyden MAG, Beekman JDM, De Bakker JMT, Vos MA, Panfilov A V. Short-Lasting Episodes of Torsade de Pointes in the Chronic Atrioventricular Block Dog Model Have a Focal Mechanism, While Longer-Lasting Episodes Are Maintained by Re-Entry. JACC Clin Electrophysiol. 2017 Dec; 3(13):1565–76.
7. Verduyn SC, Ramakers C, Snoep G, Leunissen JDM, Wellens HJJ, Vos MA. Time course of structural adaptations in chronic AV block dogs: evidence for differential ventricular remodeling. Am J Physiol Circ Physiol. 2001 Jun; 280(6):2882–90.
8. Volders PGA, Sipido KR, Vos MA, Spätjens RL, Leunissen JDM, Carmeliet E, Wellens HJJ. Downregulation of Delayed Rectifier K+ Currents in Dogs With Chronic Complete Atrioventricular Block and Acquired Torsades de Pointes. Circulation. 1999 Dec; 100(24):2455–61.

568622-L-bw-Weperen
Processed on: 3-11-2021

9. Sipido KR, Volders PG, de Groot SH, Verdonck F, Van de Werf F, Wellens HJ, Vos MA. Enhanced Ca(2+) release and Na/Ca exchange activity in hypertrophied canine ventricular myocytes: potential link between contractile adaptation and arrhythmogenesis. Circulation. 2000 Oct; 102(17):2137–44.
10. Roden DM. Taking the “Idio” out of “Idiosyncratic”: Predicting Torsades de Pointes. Pacing Clin Electrophysiol. 1998 May; 21(5):1029–34.
11. Varro A, Baczko I. Cardiac ventricular repolarization reserve: a principle for understanding drug-related proarrhythmic risk. Br J Pharmacol. 2011 Sep; 164(1):14–36.
12. Thomsen MB, Oros A, Schoenmakers M, van Opstal JM, Maas JN, Beekman JDM, Vos MA. Proarrhythmic electrical remodelling is associated with increased beat-to-beat variability of repolarisation. Cardiovasc Res. 2007 Feb; 73(3):521–30.
13. Thomsen MB, Verduyn SC, Stengl M, Beekman JDM, de Pater G, van Opstal J, Volders PGA, Vos MA. Increased Short-Term Variability of Repolarization Predicts Sotalol–Induced Torsades de Pointes in Dogs. Circulation. 2004 Oct; 110(16):2453–9.
14. Thomsen MB, Volders PGA, Beekman JDM, Matz J, Vos MA. Beat-to-Beat Variability of Repolarization Determines Proarrhythmic Outcome in Dogs Susceptible to Drug-Induced Torsades de Pointes. J Am Coll Cardiol. 2006 Sep; 48(6):1268–76.
15. Varkevisser R, Wijers SC, van der Heyden MAG, Beekman JDM, Meine M, Vos MA. Beat-to-beat variability of repolarization as a new biomarker for proarrhythmia in vivo. Heart Rhythm. 2012 Oct; 9(10):1718–26.
16. Antzelevitch C. Drug-induced spatial dispersion of repolarization. Cardiol J. 2008; 15(2):100–21.
17. Tse G. Mechanisms of cardiac arrhythmias. J arrhythmia. 2016 Apr; 32(2):75–81.
18. Oros A, Houtman MJ, Neco P, Gomez AM, Rajamani S, Oosterhoff P, Attevelt NJ, Beekman JD, van der Heyden MAG, Ver Donck L, Belardinelli L, Richard S, Antoons G, Vos MA, investigators for the C. Robust anti-arrhythmic efficacy of verapamil and flunarizine against dofetilide-induced TdP arrhythmias is based upon a shared and a different mode of action. Br J Pharmacol. 2010 Sep;

161(1):162–75.

19. Bourgonje VJA, Vos MA, Ozdemir S, Doisne N, Acsai K, Varro A, Sztojkov-Ivanov A, Zupko I, Rauch E, Kattner L, Bito V, Houtman M, van der Nagel R, Beekman JD, van Veen TAB, Sipido KR, Antoons G. Combined Na(+)/Ca(2+) exchanger and L-type calcium channel block as a potential strategy to suppress arrhythmias and maintain ventricular function. Circ Arrhythm Electrophysiol. 2013 Apr; 6(2):371–9.
20. Bossu A, Houtman MJC, Meijborg VMF, Varkevisser R, Beekman HDM, Dunnink A, de Bakker JMT, Mollova N, Rajamani S, Belardinelli L, van der Heyden MAG, Vos MA. Selective late sodium current inhibitor GS-458967 suppresses Torsades de Pointes by mostly affecting perpetuation but not initiation of the arrhythmia. Br J Pharmacol. 2018 Jun; 175(12):2470–82.
21. Stams TR, Oosterhoff P, Heijdel A, Dunnink A, Beekman JD, van der Nagel R, van Rijen HV, van der Heyden MA, Vos MA. Beat-to-Beat Variability in Preload Unmasks Latent Risk of Torsade de Pointes in Anesthetized Chronic Atrioventricular Block Dogs. Circ J. 2016 May; 80(6):1336–45.
22. Oosterhoff P, Thomsen MB, Maas JN, Atteveld NJM, Beekman JDM, Van Rijen HVM, van der Heyden MAG, Vos MA. High-Rate Pacing Reduces Variability of Repolarization and Prevents Repolarization-Dependent Arrhythmias in Dogs With Chronic AV Block. J Cardiovasc Electrophysiol. 2010 Dec; 21(12):1384–91.
23. Dunnink A, Sharif S, Oosterhoff P, Winckels S, Montagne D, Beekman J, van der Nagel R, van der Heyden MAG, Vos MA. Anesthesia and Arrhythmogenesis in the Chronic Atrioventricular Block Dog Model. J Cardiovasc Pharmacol. 2010 Jun; 55(6):601–8.
24. Van Weperen VYH, Dunnink A, Bossu A, Beekman HDM, Meijborg VMF, de Bakker JMT, Coronel R, Varkevisser R, Van Der Heyden MAG, Vos MA. Severe bradycardia increases the incidence and severity of Torsade de Pointes arrhythmias by augmenting preexistent spatial dispersion of repolarization in the CAVB dog model. Front Physiol. 2021 Apr; 12: 642083.
25. Kozhevnikov DO, Yamamoto K, Robotis D, Restivo M, El-Sherif N. Electrophysiological mechanism of enhanced susceptibility of hypertrophied heart to acquired torsade de pointes arrhythmias: tridimensional mapping of

activation and recovery patterns. Circulation. 2002 Apr; 105:1128–34.

26. Krummen DE, Hayase J, Morris DJ, Ho J, Smetak MR, Clopton P, Rappel W-J, Narayan SM. Rotor stability separates sustained ventricular fibrillation from self-terminating episodes in humans. J Am Coll Cardiol. 2014 Jun; 63(24):2712–21.
27. Restivo M, Caref EB, Kozhevnikov DO, El-Sherif N. Spatial Dispersion of Repolarization is a Key Factor in the Arrhythmogenicity of Long QT Syndrome. J Cardiovasc Electrophysiol. 2004 Mar; 15(3):323–31.
28. Antoons G, Volders PGA, Stankovicova T, Bito V, Stengl M, Vos MA, Sipido KR. Window Ca(2+) current and its modulation by Ca(2+) release in hypertrophied cardiac myocytes from dogs with chronic atrioventricular block. J Physiol. 2007 Feb; 579(Pt 1):147–60.
29. Frommeyer G, Kaiser D, Uphaus T, Kaese S, Osada N, Rajamani S, Belardinelli L, Breithardt G, Eckardt L, Milberg P. Effect of ranolazine on ventricular repolarization in class III antiarrhythmic drug-treated rabbits. Heart Rhythm. 2012 Dec; 9(12):2051–8.

Valerie Y.H. van Weperen*, Albert Dunnink*, Alexandre Bossu, Jet D.M. Beekman, Veronique M.F. Meijborg, Jacques M.T. de Bakker, Ruben Coronel, Rosanne Varkevisser, Marcel A.G. van der Heyden & Marc A. Vos

Frontiers in physiology. 2021. **12**: 642083.
doi: 10.3389/fphys.2021.642083.

CHAPTER 3

Severe bradycardia increases the incidence and severity of Torsade de Pointes arrhythmias by augmenting preexistent spatial dispersion of repolarization in the CAVB dog model

ABSTRACT

Introduction: Torsade de pointes arrhythmias (TdP) in the chronic atrioventricular block (CAVB) dog model result from proarrhythmic factors, which trigger TdP and/or reinforce the arrhythmic substrate. This study investigated electrophysiological and arrhythmogenic consequences of severe bradycardia for TdP.

Methods: Dofetilide (25 µg/kg per 5 min) was administered to eight anesthetized, idioventricular rhythm (IVR) remodeled CAVB dogs in two serial experiments: once under 60 beats per minute (bpm), right ventricular apex paced (RVA60) conditions, once under more bradycardic IVR conditions. Recordings included surface electrocardiogram and short-term variability (STV) of repolarization from endocardial unipolar electrograms. TdP-inducibility (three or more episodes within ten minutes after start of dofetilide) and arrhythmic activity scores (AS) were established. Mapping experiments in ten additional dogs determined the effect of lowering rate on STV and spatial dispersion of repolarization (SDR) in baseline.

Results: IVR-tested animals had longer baseline RR-interval (1,403 ± 271 ms) and repolarization intervals than RVA60-animals. Dofetilide increased STV similarly under both rhythm strategies. Nevertheless, TdP inducibility and AS were higher under IVR-conditions (6/8 and 37 ± 27 *vs.* 1/8 and 8 ± 12 in RVA60, respectively, both $p < 0.05$). Mapping: Pacing from high (128 ± 10 bpm) to middle (88 ± 10 bpm) to experimental rate (61 ± 3 bpm) increased all electrophysiological parameters, including *inter*ventricular dispersion, due to steeper left ventricular restitution curves, and *intra*ventricular SDR: maximal cubic dispersion from 60 ± 14 (high) to 69 ± 17 (middle) to 84 ± 22ms ($p < 0.05$ *vs.* high and middle rate).

Conclusion: In CAVB dogs, severe bradycardia increases the probability and severity of arrhythmic events by heterogeneously causing electrophysiological instability, which is mainly reflected in an increased spatial, and to a lesser extent temporal, dispersion of repolarization.

INTRODUCTION

Ventricular arrhythmias comprise a multitude of life-threatening conditions that often result in sudden cardiac death (SCD).[1] Much research is therefore dedicated to deciphering the complex processes that collectively result in the generation and perpetuation of ventricular arrhythmias, and the development of possible therapies to prevent such events.

The employment of the chronic atrioventricular block (CAVB) dog model has resulted in great advances in the research field of ventricular arrhythmias. The reproducibility of Torsade de Pointes arrhythmias (TdP) in this model results from complex ventricular adaptation processes, initiated by ablation of the proximal His bundle. The subsequent chronic drop in heart rate and thus cardiac output, combined with an altered ventricular activation pattern, initiate contractile, structural, and electrical remodeling processes. Cumulatively, these adaptations reestablish an adequate cardiac output but simultaneously, and adversely, also increase susceptibility for TdP.[2,3]

Arrhythmogenesis in the CAVB dog is stimulated by multiple factors that promote the development of *triggered activity* and/or modulate the arrhythmogenic *substrate*. Even though both mechanisms are essential for the generation of TdP, they serve different purposes herein. The *trigger* initiates ectopic activity and originates from early or late afterdepolarizations at the cellular level. Normally, a redundancy in the repolarization machinery, known as repolarization reserve, hinders the development of such erroneous afterdepolarizations as it allows myocytes to compensate for repolarization impeding or challenging circumstances.[4,5] However, in the CAVB dog model, electrical remodeling,[6,7] which includes down-regulation of repolarization currents I_{Kr} and I_{Ks}, causes this reserve to become chronically impaired. As such, electrical instability induced by additional debilitating factors, such as infusion of a pro-arrhythmic drug, is inadequately compensated for, resulting in the appearance of triggered activity and TdP.[2,3,8,9] Short-term variability (STV) of repolarization reflects the condition of the repolarization reserve; the more it is diminished, the higher the STV.[10,11] In addition, progression of these ectopic beats to more severe arrhythmic events also relies on the presence of sufficient spatial dispersion of repolarization (SDR).[12] This heterogeneity in repolarization duration has been demonstrated to be involved in the

propagation of ectopic events and to be of increasing importance for the evolution of ectopic events to TdP.[12]

Identification of factors that reduce repolarization reserve is of great importance for the complete understanding of ventricular arrhythmias and might have important clinical and experimental implications. In both the clinical and experimental setting, bradycardia has been acknowledged to be one of such repolarization reserve challenging factors. In fact, when Dessertenne first described TdP in 1966,[13] the mentioned episode also developed under bradycardic conditions. Moreover, tachypacing has been established to be an effective arrhythmia suppressor in both the clinical and experimental settings.[14–16] Despite this clear evidence on the antiarrhythmic properties of *increasing* heart rate, the exact arrhythmogenic and electrophysiological consequences of severely *decreasing* heart rate have been much less explored.

This study therefore specifically aimed to *in vivo* quantify and reaffirm the proarrhythmic character of severe bradycardia and to establish its electrophysiological effects on STV and SDR in three dimensions. As such, eight CAVB dogs were serially subjected to a proarrhythmic challenge with the specific $I_{K,r}$ blocker dofetilide. One experiment was conducted under idioventricular rhythm (IVR) conditions, anesthesia, and dofetilide inducing further slowing of IVR. In the other experiment, all animals were continuously paced at 60 beats per minute (bpm) from the right ventricular apex (RVA60). Additionally, detailed *in vivo* mapping experiments were conducted under different pacing frequencies to elucidate the effect of pacing frequency on SDR.

MATERIALS AND METHODS

All experiments were approved by the Committee for Experiments on Animals of Utrecht University, the Netherlands. Animal handling and care were in accordance with the European Directive for the Protection of Vertebrate Animals Used for Experimental and Scientific Purposes 2010/63/EU of the European Parliament and Council of September 22, 2010. This study included a total of 18 adult purpose-bred mongrel dogs (15 females, 3 males; average weight: 24 ±3 kg; Marshall, United States).

Animals were housed in conventional dog kennels enriched with wooden bedding and playing tools. If possible, dogs were housed in pairs and let out of the kennel at least once a day to go outside and play. The animals had *ad libitum* access

to water and were provided with dog food pellets twice a day. Daily checks on health and comfort were performed; weight was measured once a week.

Animal Preparation

Premedication consisted of 0.5 mg/kg methadone, 0.5 mg/kg acepromazine and 0.02 mg/kg atropine [intramuscular (i.m.)]. In addition, prophylactic antibiotic ampicillin (1,000 mg) was given before and after the experiment and perioperative analgesics consisted of meloxicam (Metacam) (0.2 mg/kg subcutaneously preoperatively) and buprenorphine (0.3 mg i.m., postoperatively). General anesthesia was induced using pentobarbital sodium [25 mg/kg intravenously (i.v.)] and maintained with mechanical ventilation of isoflurane (1.5%) in a mixture of O_2 and N_2O (1:2).

A pacemaker screw-in lead was introduced through the jugular vein and positioned in the RVA after which it was connected to an internal pacemaker (Medtronic, Maastricht, the Netherlands). Subsequent radiofrequency ablation of the proximal His-bundle induced complete AV block. All animals were allowed a minimum remodeling period of 3 weeks. All animals remodeled under continuous IVR conditions except for three dogs used in the mapping experiments, which remodeled under continuously RVA paced conditions at the lowest captured rate. Experiments included in the serial study were performed 5.6 ± 1.8 weeks after creation of AV block, whereas the mapping experiments were performed 14.1 ± 4.6 weeks after creation of AV block.

Electrophysiological recordings were continuously made during all experiments and consisted of a standard 6-leads electrocardiogram (ECG) with four additional precordial leads, right ventricular (RV) monophasic action potential (MAP) catheters (Hugo Sachs Elektronik GmbH, March, Germany; not in mapping experiments) and either a left ventricular (LV) MAP catheter or a duo-decapolar catheter (St Jude Medical, St Paul, MN, United States) recording unipolar electrograms (EGMs) from ten distinct endocardial regions in the LV. The measurements derived from a MAP or an EGM catheter are interchangeable.[17,18]

Experiments

Dofetilide Experiments

Eight animals were subjected to a dofetilide challenge twice; in one experiment, animals were in IVR, anesthesia, and dofetilide slowing heart rate, whereas the other experiment was performed under RVA60 conditions.

The dofetilide challenge was performed as previously described by Bossu *et al.* (2018).[19] In short, ten minutes of baseline electrophysiological recordings were followed by administration of dofetilide (0.025 mg/kg per 5 minutes; i.v.), a specific I_{Kr} blocker, to assess inducibility for TdP. Electrophysiological recordings were continued for a minimum of ten minutes following start of infusion. In experiments where TdP occurred within five minutes of dofetilide infusion, administration was immediately discontinued. In addition, persistent arrhythmias (> 10 s) were manually terminated by electrical cardioversion, applied *via* thoracic patches.

Mapping experiments

In vivo mapping experiments were performed in ten other animals to assess the effects of acute bradycardia on SDR under baseline conditions. In these experiments, 56 needles with each four recording electrodes (interelectrode distance 0.4 mm) were evenly inserted into the LV and RV walls [12]. All animals were continuously paced from the RVA, and SDR was assessed as pacing frequency was decreased from high (128 ± 10 bpm; similar to canine sinus rhythm) to middle (88 ± 10 bpm) to experimental (61 ± 3 bpm) rate.

Data analysis

Electrophysiological data obtained from the surface ECG (RR, QRS and QT intervals) were analyzed using EPTracer software (Cardiotek, Maastricht, The Netherlands). All intervals were determined from lead II of the surface ECG and measured manually from five consecutive beats during baseline and either prior to the first ectopic beat or at 5 minutes following start of dofetilide infusion. QT interval was corrected for heart rate (QTc) using the Van der Water formula.[20] Additionally, the interval between the peak of the T-wave and the end of the T-wave (Tp-e) and the interval between the J-point and the T-peak (JTp) were measured as parameters reflective of early and global SDR, respectively.[21,22]

Activation time (AT) was manually determined as the time difference between the start of the QRS complex (IVR) or pacing spike (RVA60) and the steepest upstroke of the MAP or the steepest downstroke of the QRS in the EGM (Figure 1A). The MAP durations (MAPDs) were determined at 80% repolarization using a custom-made MATLAB application (MathWorks, Natick, MA, United States) (Figure 1A).

The same software was used to measure LV activation recovery intervals (ARIs), which were obtained from a unipolar EGM from the most apical located electrode of the duo-decapolar catheter (Figure 1A). A duo-decapolar catheter was used in eight and six experiments of the serial comparison and mapping experiments, respectively.

STV of repolarization was calculated from 30 consecutive beats using the formula:

$$STV = \frac{\sum |D_{n+1} - D_n|}{30\ x\ \sqrt{2}}$$

with D being LV ARI or LV MAPD (LV ARI/MAPD) or RV MAPD.[10]

Interventricular dispersion of APD (ΔAPD) was calculated as LV ARI/MAPD – RV MAPD. Repolarization time (RT) was obtained by summation of the AT and

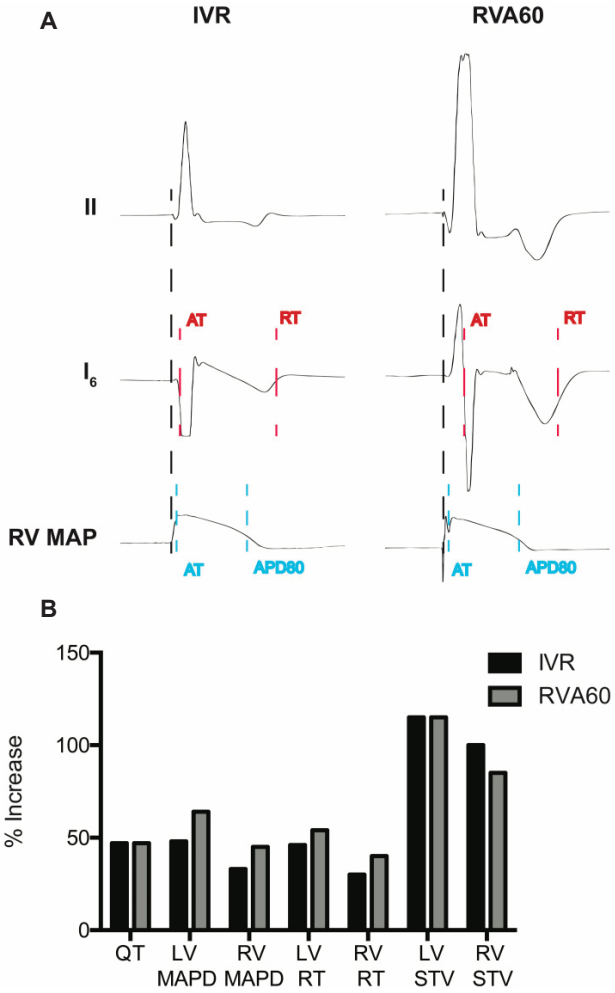

Figure 1. Measurement of electrophysiological parameters and the percentage (%) increases of electrophysiological parameters following infusion of dofetilide in the serially performed IVR and RVA60 experiments. (A) Representative beats from lead II, a left ventricular (LV) intraventricular electrogram (EGM) and a right ventricular (RV) monophasic action potential (MAP) in IVR and RVA experiments. Start of activation (black dashed line) was determined at the start of the QRS complex (IVR experiments) or pacing spike (RVA experiments) in lead II. LV activation time (AT) was measured as the time between start of ventricular activation and the steepest downslope of the EGM (red dashed line), whereas LV repolarization time (RT) was measured at the steepest upslope (red dashed line). LV activation recovery interval (ARI) was measured as LV RT - LV AT. RV AT was measured from the start of ventricular activation to the upstroke of the RV MAP (blue dashed line). Monophasic action potential duration (MAPD) was determined at 80% of repolarization (blue dashed line). **(B)** The percentage in electrophysiological parameters representing repolarization time and stability following infusion of dofetilide in the serially performed IVR and RVA60 experiments. IVR: Idioventricular rhythm; LV/RV MAPD: left/right ventricular monophasic action potential duration; LV/RV RT: left/right ventricular repolarization time; LV/RV STV: left/right ventricular short-term variability; RVA60: Right ventricular apex paced at 60 beats per minute.

MAPD, or ARI. Interventricular difference between AT (ΔAT) and RT (ΔRT) was calculated as LV-AT or -RT minus RV-AT or -RT, respectively.

The unipolar EGMs of the mapping experiments were analyzed using the custom-made analysis program Maplab (MATLAB R2016a, Mathworks).[23] For all timepoints, AT and RT of all 224 electrodes were averaged from five consecutive beats. AT and RT were similarly determined as described for the catheter-derived EGM signals. SDR was calculated as the average and maximal difference in RT between two adjacent electrodes in the horizontal, vertical, transmural, and cubic orientation.[12] The latter was the maximal difference in RT within four squared needles.[12] Repolarization restitution curves were created using the ARI (RT-AT) of the needle electrodes. Averaged LV and RV recordings were used to assess global ventricular RTs. Diastolic interval was calculated as cycle length minus QT.

Arrhythmia Quantification

Animals were defined to be inducible when three or more episodes of TdP occurred during the ten-minute period after the onset of dofetilide administration. TdP were defined as a polymorphic ventricular tachycardia of five beats or more, twisting around the isoelectric line.

During this ten-minute interval, an arrhythmia score (AS) was calculated to quantify the severity of the arrhythmic activity in the experiments. Ectopic events were scored according to the $n + 1$ rule, wherein n reflects the number of ectopic beats. Persistent TdP were scored according to the number of defibrillation shocks needed to terminate the TdP; one defibrillation was awarded 50 points, two cardioversions were given 75 points, and three or more shocks were given 100 points. AS was then calculated by averaging the scores of the three most severe arrhythmic episodes within the ten-minute interval.[24]

Statistical Analysis

All obtained data are expressed as mean ± standard deviation (SD). Statistical analyses and comparison of serial electrophysiological data were performed with (un)paired Student *t*-tests. Inducibility was analyzed using the McNemar test. AS was analyzed with the Wilcoxon signed rank test, and the Mann-Whitney *U* test was used for the number of TdP. $P < 0.05$ was considered statistically significant.

Table 1. Serial comparison of the electrophysiological effects of IVR and acute RVA60 conditions in baseline and following dofetilide administration (both groups n = 8).

	IVR			RVA60		
Parameters (ms)	**Baseline**	**Dofetilide**	**% Increase**	**Baseline**	**Dofetilide**	**% Increase**
PP	551 ± 75	748 ± 133**	36	573 ± 101	874 ± 187***	53
RR	1403 ± 271	1569 ± 392	12	1000 ± 0^{+}	1000 ± 0^{+}	0
QRS	95 ± 12	97 ± 11	2	115 ± 9^{+}	116 ± 7^{+}	0
QT	374 ± 51	549 ± 145**	47	384 ± 44	563 ± 76***	47
QTc	339 ± 50	500 ± 119**	47	384 ± 44	563 ± 76***	47
JT	244 ± 48	403 ± 112**	65	268 ± 44	448 ± 76***	67
JTp	195 ± 26	267 ± 58*	40	159 ± 25^{+}	231 ± 42***	46
Tp-e	84 ± 44	185 ± 90*	151	108 ± 33	215 ± 61***	108
LV-AT	20 ± 6	21 ± 5		53 ± 8^{+}	56 ± 9^{+}	
RV-AT	28 ± 7	29 ± 8		29 ± 7	31 ± 10	
∆AT	-11 ± 5	-9 ± 4		23 ± 10^{+}	25 ± 17^{+}	
LVMAPD/LVARI	313 ± 45	462 ± 108*	48	254 ± 28^{+}	417 ± 58***	64
RVMAPD	251 ± 29	335 ± 78*	33	228 ± 25^{+}	330 ± 47***	45
∆MAPD	40 ± 33	112 ± 53*	180	27 ± 18	107 ± 48**	296
LV-RT	332 ± 50	484 ± 107*	46	307 ± 30	473 ± 58***	54
RV-RT	280 ± 34	365 ± 80*	30	257 ± 27	361 ± 53**	40
∆RT	30 ± 38	102 ± 55*	240	50 ± 17	131 ± 58*	162
STV_LV	2.0 ± 1.1	4.3 ± 1.6***	115	1.3 ± 1.4	2.8 ± 2.2*	115
STV_RV	1.0 ± 1.1	2.0 ± 1.1*		1.3 ± 1.5	2.4 ± 2.4	
Inducibility, %		75	100		13^{+}	85
AS	1 ± 0	37 ± 27		1 ± 0	8 ± 12^{+}	
Average n TdP	0.0 ± 0.0	9.5 ± 12.3		0.0 ± 0.0	0.8 ± 1.8^{+}	

Values are represented as mean ± SD.

* p<0.05, ** p<0.01, *** p<0.001 *vs.* Baseline

Comparison IVR experiment – RVA60 experiment:

$^{+}$ p<0.05 *vs.* IVR experiment

AS: arrhythmia score; ∆AT: interventricular differences in activation time (calculated as ∆AT = LV-AT – RV-AT); ∆APD: interventricular dispersion of repolarization (calculated as ∆APD = LV MAPD/ARI – RV MAPD); ∆RT: Interventricular dispersion of repolarization time (calculated as ∆RT = LV-RT – RVRT); LV-AT left ventricular activation time; LVARI: left ventricular activation recovery interval; LVMAPD: left ventricular monophasic action potential duration (measured at 80% repolarization); LV-RT: left ventricular repolarization time (calculated as LV-RT = LV-AT + LVMAPD/ARI) RV-RV-AT: right ventricular activation time; RVMAPD: right ventricular monophasic action potential duration (measured at 80% repolarization); RV-RT: right ventricular repolarization time (calculated as RV-RT = RV-AT + RVMAPD); STV_LV: short-term variability of repolarization (from 30 consecutive LV MAPD/ARI); STV_RV: short-term variability of repolarization (from 30 consecutive RV MAPD)

RESULTS

Dofetilide Experiments

In the IVR experiments, a trend toward further prolongation in cycle length was observed following administration of dofetilide (RR from 1,403 ± 271 to 1,569 ± 392 ms, p = 0.07*)*, but this was not accompanied by changes in QRS-morphology. In comparison to the IVR experiments, pacing from the RVA (1,000 ± 0 ms) significantly delayed LV activation (53 ± 8 *vs.* 20 ± 6 ms in IVR experiments, $p < 0.05$) and shortened LV MAPD/ARI and RV MAPD from 313 ± 45 and 251 ± 29 ms to 254 ± 28 and 228 ± 25 ms, respectively (both p < 0.05 *vs.* IVR experiments). The differences in pacing rate did not affect temporal dispersion of repolarization, as baseline LV and RV STV did not differ between both rhythm strategies (Table 1).

Dofetilide administration caused a similar prolongation of the QTc from 330 ± 50 and 384 ± 44 ms to 500 ± 119 and 563 ± 76 ms in IVR and RVA60 experiments,

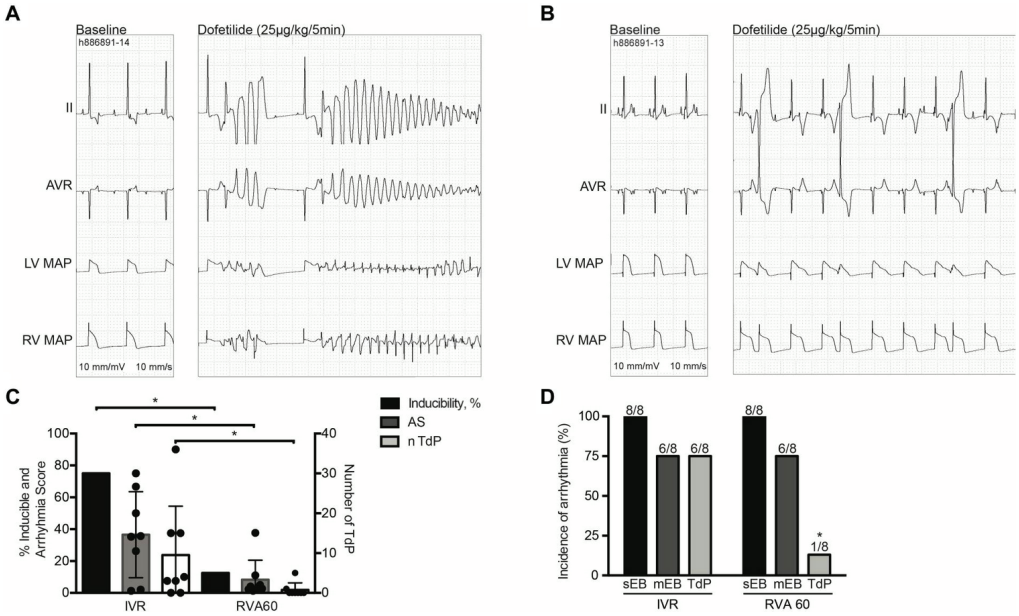

Figure 2. Dofetilide experiments performed under IVR or RVA60 conditions in chronic atrioventricular block dogs. Representative ECG traces (lead II and AVR) associated with MAPs recorded from the LV and RV at baseline and after dofetilide (25 µg/kg per 5 min) infusion in serial IVR **(A)** and RVA60 **(B)** experiments. Quantification of TdP-inducible CAVB dogs, AS and average number of TdP. The circular dots represent the different experiments **(C).** The incidence of sEB, mEB and TdP under IVR and RVA60 conditions **(D)**. Values are represented as mean ± SD. AS: arrhythmia score; CAVB: chronic atrioventricular block; ECG: electrocardiogram; IVR: Idioventricular rhythm; LV/RV MAP: left/right ventricular monophasic action potential; mEB: multiple ectopic beat; RVA60: Right ventricular apex paced at 60 beats per minute; sEB: single ectopic beat; TdP: Torsade de Pointes arrhythmia. *$p < 0.05$ *vs.* IVR

respectively (both $p < 0.05$). Moreover, dofetilide caused a substantial prolongation of LV MAPD/ARI, RV MAPD, and ΔMAPD under both rhythm strategies (Table 1). Even though no statistically significant differences herein were observed between IVR and RVA60 conditions, these dofetilide-induced prolongations did seem to be more pronounced in RVA60 experiments, as these values depicted a greater relative increase in duration (Figure 1B and Table 1). Nevertheless, absolute LV and RV STV values following dofetilide infusion, as well as their relative increases in comparison to baseline, did not differ between the two different experimental settings.

Nevertheless, TdP inducibility of 75% (6/8) in IVR experiments was significantly higher than the 13% (1/8) observed in the RVA60 experiments ($p < 0.05$) (Table 1 and Figures 2A - C). Moreover, the IVR experiments displayed more severe arrhythmic events (AS: 37 ± 27 vs 8 ± 12 in RVA60 experiments, $p < 0.05$; Table 1 and Figures 2C, D). Collectively, these results demonstrated and confirmed that the slowing of heart rate increased the incidence and severity of arrhythmic events in the CAVB dog.

Mapping Experiments

Detailed mapping experiments (n = 10) established the effects of stepwise lowering heart rate on spatial heterogeneity in repolarization. Lowering pacing rate from high to middle rate pacing prolonged repolarization as demonstrated by QTc and LV ARI from 344 ± 12 and 202 ± 15 to 365 ± 15 and 229 ± 17, respectively, both $p < 0.05$ (Table 2).

This effect was also reflected in the RT of the local EGMs (LV RT from 268 ± 19 to 295 ± 19 ms; RV RT from 244 ± 19 to 257 ± 14 ms; both $p < 0.05$). Subsequent

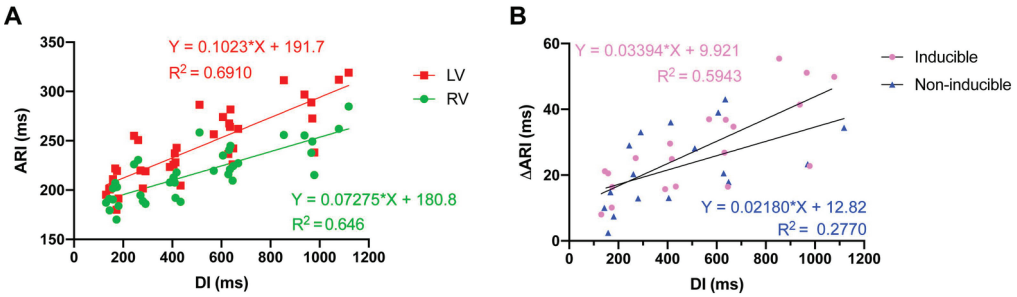

Figure 3. Action recovery interval (ARI) restitution curves. (A) Increasing cycle length, and thus diastolic interval (DI), caused *inter*ventricular dispersion of ARI as the repolarization duration of the left ventricle prolonged more than the right ventricle. **(B)** The *inter*ventricular dyssynchrony in ARI prolongation (ΔARI) was more pronounced in animals that were to become inducible (n = 5) when challenged with dofetilide, compared to noninducible animals (n = 5).

Table 2. Serial comparison of the electrophysiological effects of high, middle and experimental rate pacing (n = 10).

Parameters (ms)	High rate (128 ± 10 bpm)	Middle rate (88 ± 10 bpm)	Experimental rate (61 ± 3 bpm)
PP	582 ± 63	565 ± 67	552 ± 65
RR	471 ± 46	690 ± 77 *	986 ± 45 *+
QRS	112 ± 6	111 ± 7	109 ± 8
QT	298 ± 12	338 ± 14 *	368 ± 28 *+
QTc	344 ± 12	365 ± 15 *	369 ± 27 *
JT	186 ± 13	226 ± 17 *	259 ± 31 *+
JTp	128 ± 19	159 ± 23 *	184 ± 37*+
Tp-e	58 ± 11	68 ± 12 *	75 ± 19*+
LVMAPD/LVARI	202 ± 15	229 ± 17 *	260 ± 19 *+
STV_LV	0.9 ± 0.4	1.2 ± 0.5	1.4 ± 0.8
RV-AT	55 ± 15	51 ± 10	49 ± 9
LV-AT	65 ± 13	67 ± 10	66 ± 9
RV-RT	244 ± 19	257 ± 14 *	279 ± 15 *+
LV-RT	268 ± 19	295 ± 19 *	325 ± 20 *+
Transmural dispersion	14 ± 2	15 ± 2 *	20 ± 4 *+
Vertical dispersion	25 ± 4	28 ± 7	33 ± 7 *+
Horizontal dispersion	24 ± 4	27 ± 5 *	34 ± 8 *+
Cubic dispersion	33 ± 5	36 ± 6 *	46 ± 11 *+
Maximal dispersion			
Transmural dispersion	45 ± 9	50 ± 10	62 ± 12 *+
Vertical dispersion	53 ± 12	57 ± 14	71 ± 15 *+
Horizontal dispersion	55 ± 14	60 ± 16	76 ± 24 *+
Cubic dispersion	60 ± 14	69 ± 17	84 ± 22 *+

Values are represented as mean ± SD.

* $p<0.05$ *vs.* High Rate Pacing

+ $p<0.05$ *vs.* Middle Rate Pacing

LV-AT left ventricular activation time; LVARI: left ventricular activation recovery interval; LVMAPD: left ventricular monophasic action potential duration (measured at 80% repolarization); LV-RT: left ventricular repolarization time (calculated as LV-RT = LV-AT + LVMAPD/ARI) RV-RV-AT: right ventricular activation time; RVMAPD: right ventricular monophasic action potential duration (measured at 80% repolarization); RV-RT: right ventricular repolarization time (calculated as RV-RT = RV-AT + RVMAPD); STV_LV: short-term variability of repolarization (from 30 consecutive LV MAPD/ARI)

lowering to experimental rate caused a further prolongation of repolarization; LV ARI to 260 ± 19 ms ($p < 0.05$ *vs.* high and middle rate) and RT to 325 ± 20 ms (LV) and 279 ± 15 ms (RV) (both $p<0.05$ *vs* high and middle rate). Moreover, although insignificant, a modest trend toward increasing temporal dispersion seemed to appear as rate was decreased from high to middle rate (from 0.9 ± 0.4 to 1.2 ± 0.5 ms, $p = 0.31$).

ARI-restitution curves were dissimilar for the LV and the RV. The steeper slope of the LV curve reflected the greater prolongation of LV ARI in response to increasing cycle lengths (Figure 3A). A comparison of the animals that became inducible when challenged with dofetilide to the animals that were TdP resistant (non-inducible) showed that the interventricular difference in ARI-prolongation was greater in the inducible animals (Figure 3B).

Intraventricularly, SDR in the LV increased as pacing rate was stepwise decreased, starting from a rate similar to canine sinus rhythm. This increase was most

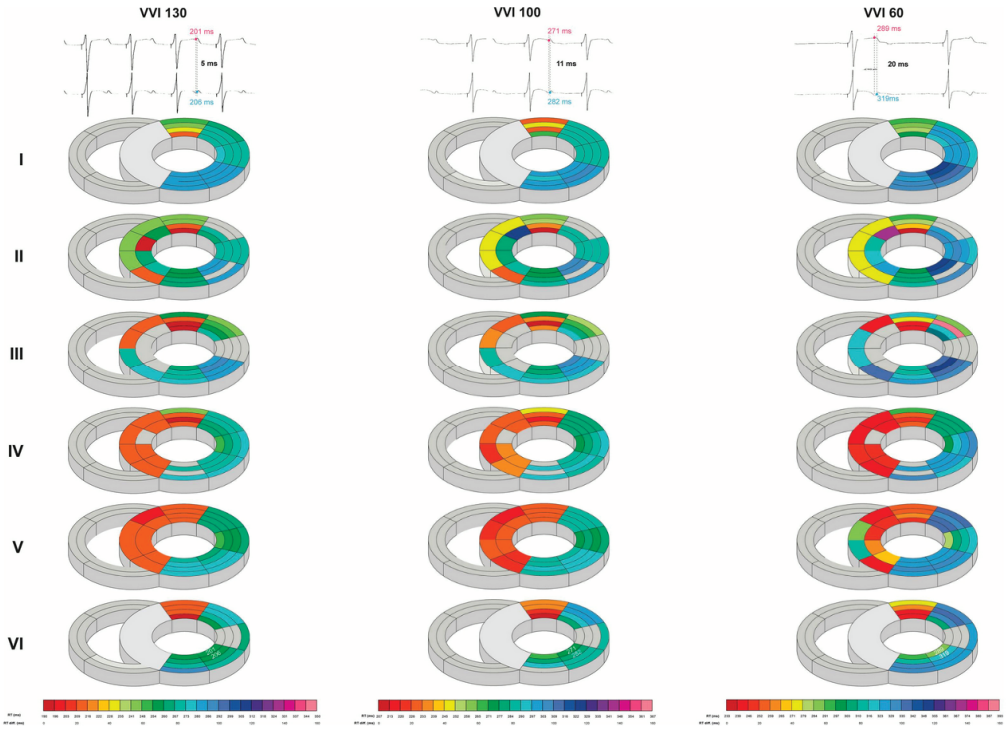

Figure 4. Bradycardia-induced increases in left ventricular intraventricular spatial dispersion of repolarization. Local repolarization times (RT) of one animal during high (130 beats/min), middle (100 beats/min) and experimental (60 beats/min) rate in the septum and LV from base (I) to apex (VI). Traces of two unipolar electrograms with their corresponding RT and their difference herein are depicted to illustrate the evolution of spatial dispersion. Colors and color gradients correspond to the absolute RT and ΔRT values, respectively, as depicted in the color bars below the cardiac maps.

prominent under the most bradycardic conditions, as average and maximal SDRs were significantly increased in all orientations compared to both high- and middle-rate pacing (Table 2 and Figure 4). This effect was most pronounced in the cubic orientation; decreasing pacing frequency from high to middle to experimental rate increased the maximal cubic dispersion from 60 ± 14 to 69 ± 17 ms to 84 ± 22 ms, respectively ($p < 0.05$ *vs.* high and middle rate).

DISCUSSION

This study established the contribution of severe bradycardia in arrhythmogenesis and correlated its proarrhythmic effects with changes in electrophysiological parameters. The results have confirmed that severe bradycardia increases (1) the likelihood of arrhythmia development and (2) the severity of arrhythmic events, and show for the first time *in vivo* that this can be explained by (3) bradycardia-induced increases in SDR in three dimensions, and (4) to a much lesser extent temporal dispersion of repolarization.

Bradycardia as a Modulator of Arrhythmogenesis in the CAVB Dog Model

The two main characteristics of the CAVB dog - the compensated heart failure combined with its increased susceptibility for TdP - which both result from ventricular remodeling, make this animal model unique in the research field of ventricular arrhythmias. Also in humans, cardiac remodeling that results in compensated heart failure is associated with an increased risk of SCD as the result of ventricular arrhythmias.

This disposition for ventricular arrhythmias arises from multiple electrical alterations that cumulatively augment the likelihood that ectopic stimuli are generated and enhance spatial differences that facilitate the spread and perpetuation of such stimuli. Hence, it creates a *substrate,* which facilitates the development of ectopic beats and TdP. However, an additional *trigger* is needed to provoke such events. These *triggers* initiate ectopic stimuli by destabilizing cellular electrophysiology to such extent that early or late after-depolarization is provoked; this increasing instability is reflected by the *temporal* dispersion of repolarization, quantified as the STV.[10] In most experiments, a gradual progression from single to multiple ectopic beats to TdP can be observed in the course of the experiment. This evolution of arrhythmic events has been

demonstrated to mainly rely on increases in *SDR*.[12] As such, in comparison to the first ectopic beat, STV is not further increased prior to the first TdP, whereas the SDR has become significantly higher.[25,26]

In the serial comparison, dofetilide induced ectopic events in all animals, regardless of rhythm strategy. Nevertheless, in RVA60 paced animals, these events were limited to single and multiple ectopic beats, whereas TdP were abundantly present in the IVR tested animals (Figure 2). This difference in severity of arrhythmic events was also reflected in the significantly higher AS in IVR experiments (Table 1).

However, the increased incidence and severity of arrhythmic events in IVR experiments were not reflected in the dofetilide-induced increases in repolarization duration and/or STV (Figure 1 and Table 1). This discrepancy complies with the aforementioned paradigm on arrhythmogenesis in the CAVB dog model, whereby temporal dispersion of repolarization is involved in the initiation of arrhythmic events, and SDR becomes of increasing importance in the perpetuation of progression of arrhythmic events. Hence, the results obtained in the serial comparison suggest that developing bradycardia encourages arrhythmogenesis through increasing SDR, which results in more severe TdP. Interestingly, although insignificantly different, dofetilide appeared to induce a greater increase in Tp-e in the IVR than in the RVA experiments.

Correspondingly, the additional mapping experiments that studied SDR under baseline conditions demonstrated that heterogeneities in interventricular and intraventricular repolarization durations increased as pacing frequency was gradually lowered. *Inter*ventricular dispersion of repolarization is known to be of importance in TdP arrhythmogenesis and to be a bradycardia-dependent phenomenon.[27,28] As ΔAPD reflects the dispersion of repolarization over a larger area, this parameter of heterogeneity might be less informative on arrhythmogenic consequences than *intra*ventricular SDR, as the arrhythmogenic potential mainly relies on the steepness of (local) repolarization gradients. Nevertheless, as we see a clear rate dependency of *inter*ventricular dispersion (Figure 3), this clearly indicates that the global (in)stability of repolarization is profoundly affected by changes in heart rate. In addition, the aforementioned local repolarization gradients were assessed in the mapping experiments. Dunnink *et al.* (2017)[12] have demonstrated the importance of this *intra*ventricular SDR in arrhythmogenesis, as they showed that dofetilide-induced TdP are associated with increases in intraventricular SDR and that dispersion becomes

higher in inducible animals than noninducible animals.[12] Furthermore, our results of the serial comparison show great similarities to a study by Bossu *et al.* (2018).[19] In their study, infusion of the anti-arrhythmic drug GS-458967 caused a reversal of dofetilide-induced increases in *intra*ventricular SDR, which was associated with the complete abolishment of TdP, but not of single and multiple ectopic beats.[19] Hence, severe bradycardia appears to cause heterogeneous electrical alterations that result in an increased incidence and severity of arrhythmic events. This effect is mainly reflected in an increased interventricular and intraventricular SDR, and to a lesser extent the temporal dispersion of repolarization.

These results correspond to prior studies reporting an increased SDR under bradycardic conditions. For example Kim *et al.* (2013),[29] showed that bradycardia altered calcium handling in their Langendorff-perfused rabbit hearts, and that this alteration augmented SDR, thereby facilitating ventricular ectopy. Moreover, multiple studies have identified bradycardia as a modulator of ventricular arrhythmogenesis in both acquired and congenital long-QT syndromes. Shimizu and Antzelevitch (1998)[30] demonstrated how bradycardia-induced prolongation of APD increased the transmural dispersion of repolarization in a perfused RV-wedge model, facilitating the development of TdP. Similarly, Restivo et al. (2004),[31] investigated the effects of bradycardia on SDR *in vivo* in a guinea pig model of long-QT syndrome three. They demonstrated that bradycardia augmented the baseline heterogeneities in APD, which promoted ventricular arrhythmogenesis. However, in contrast to the current study, these studies were limited in their assessment of repolarization to either a small number of RV sites or the epicardium, precluding the evaluation of global ventricular changes. Hence, while prior studies have underlined the importance of bradycardia as a modulator of arrhythmogenesis and demonstrated its effects on SDR, the current study is unique in its high-resolution, global, three-dimensional evaluation of these effects in an *in vivo* large animal model.

Nevertheless, even though the aforementioned studies and the current study demonstrate a clear correlation between heart rate and changes in dispersion of repolarization, instability of other electrical properties, for example, myocardial activation, might have also played into the observed episodes of arrhythmogenesis.

Interestingly, dofetilide tended to prolong the PP intervals more in the RVA experiments than in the IVR experiments. Hence, a heightened sympathetic tone in the

more bradycardic IVR experiments could have promoted the more arrhythmogenic outcome of these experiments.

Clinical and Experimental Implications

For the experimental setting, these results emphasize the importance of carefully considering rhythm control in studies in the field of arrhythmogenesis and antiarrhythmic interventions. For example in studies testing drugs, it is important that one is able to discriminate between arrhythmogenic effects related to the drug tested and experimental intrinsic effects, such as the administration of anesthetics.[32] The identification of acute bradycardia as an additional experimental design-related proarrhythmic factor thus encompasses multiple implications for future experiments one of which being that the presence of severe bradycardia might lead to an overestimation or underestimation of the proarrhythmic or antiarrhythmic efficacy of drugs and/or therapies, respectively.

In the clinical setting, it is important to understand how heart rate directly affects cardiac electrophysiology and how it can both contribute to and impede ventricular arrhythmogenesis. Especially the latter observation is of great clinical interest. The observation that arrhythmogenesis can be impeded by increasing pacing rate highlights the potential of pacemakers to treat chronic cardiac conditions wherein there is an increased risk of ventricular arrhythmogenesis.

Limitations

Inconsistent ventricular activation is known to cause electrophysiological instability, possibly evoking an electrical storm. In IVR experiments, the uncontrollability of ventricular activation focus might have been an additional proarrhythmic factor. However, no changes in QRS morphologies were observed in the serial comparisons, implying that instability of ventricular activation is unlikely to have caused the increased arrhythmic activity observed in the IVR experiments.

In addition, as dofetilide infusion is stopped prematurely when TdP occur within the five-minute window of infusion, less dofetilide was administered in IVR experiments. Therefore, the obtained result might still be an underestimation of the proarrhythmic effects of severe bradycardia.

Moreover, pacing the animals in the serial experiments could have been a confounding factor as eliciting an activation front may have interfered with

568622-L-bw-Weperen
Processed on: 3-11-2021

arrhythmogenesis. Nevertheless, as we see a similar increase in STV and observe a comparable initiation of ectopic events, we believe that the increased TdP incidence in IVR experiments is a result of the greater increase in SDR. As we show that the extent of SDR closely correlates to heart rate, we do not believe that cardiac pacing was responsible for the difference in arrhythmogenesis.

Lastly, the frequency-dependency of SDR was only studied under baseline conditions and not additionally tested following the administration of dofetilide. Hence these mapping experiments demonstrate that bradycardia induces proarrhythmic increases in SDR, but do not directly demonstrate its role in arrhythmogenesis.

CONCLUSION

Severe bradycardia in the CAVB dog increases the probability of arrhythmia development and the severity of arrhythmic events by heterogeneously causing cellular electrophysiological instability, which is mainly reflected in an increased spatial, and to a lesser extent temporal, dispersion of repolarization.

REFERENCES

1. Morin DP & Homoud MK. Prediction and Prevention of Sudden Cardiac Death. *Card. Electrophysiol. Clin.* **9,** 631–638 (2017).
2. Dunnink A, van Opstal JM, Oosterhoff P, Winckels SKG, Beekman JDM, van der Nagel R, Cora Verduyn S & Vos MA. Ventricular remodelling is a prerequisite for the induction of dofetilide-induced torsade de pointes arrhythmias in the anaesthetized, complete atrio-ventricular-block dog. *Europace* **14,** 431–436 (2012).
3. Oros A, Beekman JDM & Vos MA. The canine model with chronic, complete atrio-ventricular block. *Pharmacol. Ther.* **119,** 168–178 (2008).
4. Roden DM. Taking the "Idio" out of "Idiosyncratic": Predicting Torsades de Pointes. *Pacing Clin. Electrophysiol.* **21,** 1029–1034 (1998).
5. Varró A & Baczkó I. Cardiac ventricular repolarization reserve: A principle for understanding drug-related proarrhythmic risk. *British Journal of Pharmacology* **164,** 14–36 (2011).
6. Volders PGA, Sipido KR, Vos MA, Spätjens RL, Leunissen JDM, Carmeliet E & Wellens HJJ. Downregulation of Delayed Rectifier K+ Currents in Dogs With Chronic Complete Atrioventricular Block and Acquired Torsades de Pointes. *Circulation* **100,** 2455–2461 (1999).
7. Takahara A, Wagatsuma H, Aritomi S, Konda T, Akie Y, Nakamura Y & Sugiyama A. Measurements of cardiac ion channel subunits in the chronic atrioventricular block dog. *J. Pharmacol. Sci.* **116,** 132–135 (2011).
8. Schreiner KD, Voss F, Senges JC, Becker R, Kraft P, Bauer A, Kelemen K, Kuebler W, Vos MA & Schoels W. Tridimensional activation patterns of acquired torsade-de-pointes-tachycardias in dogs with chronic AV-block. *Basic Res. Cardiol.* **99,** 288–298 (2004).
9. Kozhevnikov DO, Yamamoto K, Robotis D, Restivo M & El-Sherif N. Electrophysiological mechanism of enhanced susceptibility of hypertrophied heart to acquired Torsade de Pointes arrhythmias: Tridimensional mapping of activation and recovery patterns. *Circulation* **105,** 1128–1134 (2002).
10. Thomsen MB, Verduyn SC, Stengl M, Beekman JDM, de Pater G, van Opstal

J, Volders PGA & Vos MA. Increased Short-Term Variability of Repolarization Predicts Sotalol–Induced Torsades de Pointes in Dogs. *Circulation* **110,** 2453–2459 (2004).

11. Antoons G, Johnson DM, Dries E, Santiago DJ, Ozdemir S, Lenaerts I, Beekman JDM, Houtman MJC, Sipido KR & Vos MA. Calcium release near l-type calcium channels promotes beat-to-beat variability in ventricular myocytes from the chronic AV block dog. *J. Mol. Cell. Cardiol.* **89,** 326–334 (2015).
12. Dunnink A, Stams TRG, Bossu A, Meijborg VMF, Beekman JDM, Wijers SC, De Bakker JMT & Vos MA. Torsade de pointes arrhythmias arise at the site of maximal heterogeneity of repolarization in the chronic complete atrioventricular block dog. *Europace* **19,** 858–865 (2017).
13. Dessertenne F. La tachycardie ventriculaire a deux foyers opposes variables. *Arch. Mal. Coeur Vaiss.* **59,** 263–272 (1966).
14. Wathen MS, Sweeney MO, DeGroot PJ, Stark AJ, Koehler JL, Chisner MB, Machado C, Adkisson WO & Investigators for the PR. Shock Reduction Using Antitachycardia Pacing for Spontaneous Rapid Ventricular Tachycardia in Patients With Coronary Artery Disease. *Circulation* **104,** 796–801 (2001).
15. Wijers SC, Bossu A, Dunnink A, Beekman JDM, Varkevisser R, Aranda Hernández A, Meine M & Vos MA. Electrophysiological measurements that can explain and guide temporary accelerated pacing to avert (re)occurrence of torsade de pointes arrhythmias in the canine chronic atrioventricular block model. *Heart Rhythm* **14,** 749–756 (2017).
16. Smoczyńska A, Loen V, Aranda A, Beekman HDM, Meine M & Vos MA. High-rate pacing guided by short-term variability of repolarization prevents imminent ventricular arrhythmias automatically by an implantable cardioverter-defibrillator in the chronic atrioventricular block dog model. *Heart Rhythm* (2020). doi:10.1016/j.hrthm.2020.07.023
17. Oosterhoff P, Thomsen MB, Maas JN, Atteveld NJM, Beekman JDM, Van Rijen HVM, van der Heyden MAG & Vos MA. High-Rate Pacing Reduces Variability of Repolarization and Prevents Repolarization-Dependent Arrhythmias in Dogs With Chronic AV Block. *J. Cardiovasc. Electrophysiol.* **21,** 1384–1391 (2010).
18. Wijers SC, Sprenkeler DJ, Bossu A, Dunnink A, Beekman JDM, Varkevisser R,

Hernández AA, Meine M & Vos MA. Beat-to-beat variations in activation-recovery interval derived from the right ventricular electrogram can monitor arrhythmic risk under anesthetic and awake conditions in the canine chronic atrioventricular block model. *Heart Rhythm* **15,** 442–448 (2018).

19. Bossu A, Houtman MJC, Meijborg VMF, Varkevisser R, Beekman HDM, Dunnink A, de Bakker JMT, Mollova N, Rajamani S, Belardinelli L, van der Heyden MAG & Vos MA. Selective late sodium current inhibitor GS-458967 suppresses Torsades de Pointes by mostly affecting perpetuation but not initiation of the arrhythmia. *Br. J. Pharmacol.* **175,** 2470–2482 (2018).
20. Van de Water A, Verheyen J, Xhonneux R & Reneman RS. An improved method to correct the QT interval of the electrocardiogram for changes in heart rate. *J. Pharmacol. Methods* **22,** 207–217 (1989).
21. Opthof T, Coronel R, Wilms-Schopman FJG, Plotnikov AN, Shlapakova IN, Danilo P, Rosen MR & Janse MJ. Dispersion of repolarization in canine ventricle and the electrocardiographic T wave: Tp-e interval does not reflect transmural dispersion. *Heart Rhythm* **4,** 341–348 (2007).
22. Johannesen L, Vicente J, Mason JW, Sanabria C, Waite-Labott K, Hong M, Guo P, Lin J, Sørensen JS, Galeotti L, Florian J, Ugander M, Stockbridge N & Strauss DG. Differentiating drug-induced multichannel block on the electrocardiogram: Randomized study of dofetilide, quinidine, ranolazine, and verapamil. *Clin. Pharmacol. Ther.* **96,** 549–558 (2014).
23. Potse M, Linnenbank AC & Grimbergen CA. Software design for analysis of multichannel intracardial and body surface electrocardiograms. *Comput. Methods Programs Biomed.* **69,** 225–236 (2002).
24. Stams TR, Oosterhoff P, Heijdel A, Dunnink A, Beekman JD, van der Nagel R, van Rijen HV, van der Heyden MA & Vos MA. Beat-to-Beat Variability in Preload Unmasks Latent Risk of Torsade de Pointes in Anesthetized Chronic Atrioventricular Block Dogs. *Circ. J.* **80,** 1336–1345 (2016).
25. Smoczynska A, Aarnink EW, Dunnink A, Bossu A, Van Weperen VYH, Meijborg VMF, Beekman HDM & Vos MA. Abstract 12257: Interplay Between Temporal and Spatial Dispersion of Repolarization in the Initiation and Perpetuation of Torsade De Pointes Arrhythmias. *Circulation* 140:A12257 (2019).
26. van Weperen VYH, Bossu A & Vos MA. Point of View: Electrophysiological

Endpoints Differ When Comparing the Mode of Action of Highly Successful Anti-arrhythmic Drugs in the CAVB Dog Model With TdP. *J. Cardiovasc. Pharmacol.* **74,** 499–507 (2019).

27. Verduyn SC, Vos MA, van der Zande J, van der Hulst FF & Wellens HJ. Role of interventricular dispersion of repolarization in acquired torsade-de-pointes arrhythmias: reversal by magnesium. *Cardiovasc. Res.* **34,** 453–463 (1997).
28. Meijborg VMF, Chauveau S, Janse MJ, Anyukhovsky EP, Danilo PR, Rosen MR, Opthof T & Coronel R. Interventricular dispersion in repolarization causes bifid T waves in dogs with dofetilide-induced long QT syndrome. *Heart Rhythm* **12,** 1343–1351 (2015).
29. Kim JJ, Nemec J, Papp R, Strongin R, Abramson JJ & Salama G. Bradycardia alters Ca(2+) dynamics enhancing dispersion of repolarization and arrhythmia risk. *Am. J. Physiol. Heart Circ. Physiol.* **304,** H848-60 (2013).
30. Shimizu W & Antzelevitch C. Cellular Basis for the ECG Features of the LQT1 Form of the Long-QT Syndrome. *Circulation* **98,** 2314–2322 (1998).
31. Restivo M, Caref EB, Kozhevnikov DO & El-Sherif N. Spatial Dispersion of Repolarization is a Key Factor in the Arrhythmogenicity of Long QT Syndrome. *J. Cardiovasc. Electrophysiol.* **15,** 323–331 (2004).
32. Dunnink A, Sharif S, Oosterhoff P, Winckels S, Montagne D, Beekman J, van der Nagel R, van der Heyden MAG & Vos MA. Anesthesia and Arrhythmogenesis in the Chronic Atrioventricular Block Dog Model. *J. Cardiovasc. Pharmacol.* **55,** 601–608 (2010).

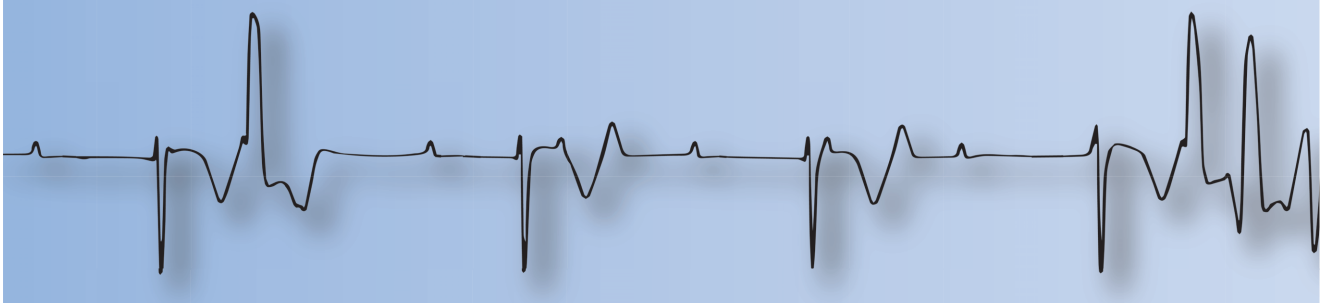

Valerie Y.H. van Weperen, Iris ter Horst, Albert Dunnink, Alexandre Bossu, Odette A. Salden, Henriette D.M. Beekman, Avram Oros, Vincent Bourgonje, Thom Stams, Mathias Meine & Marc A. Vos

Submitted

CHAPTER 4

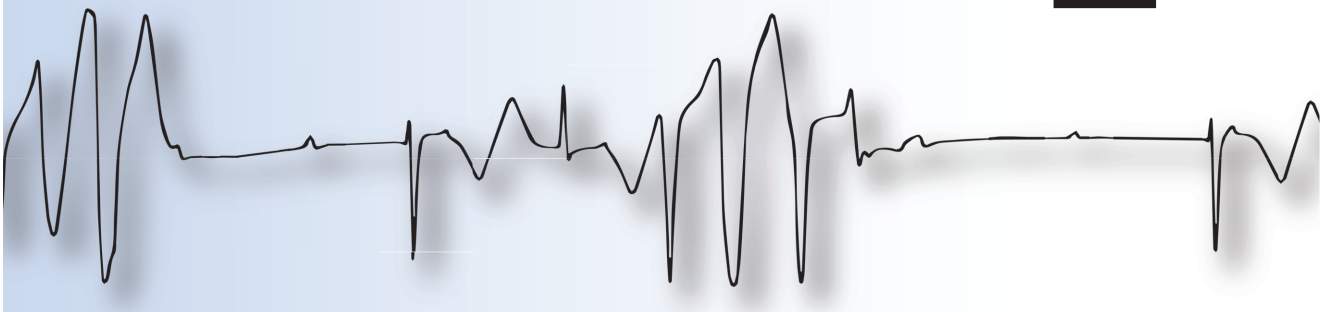

Chronically altered ventricular activation causes pro-arrhythmic cardiac electrical remodeling in the chronic AV-block dog model

ABSTRACT

Background: Altered ventricular activation (AVA) causes intraventricular mechanical dyssynchrony (MD) and impedes contraction, promoting proarrhythmic electrical remodeling in the chronic AV block (CAVB) dog. We aimed to study arrhythmogenic and electromechanical outcomes of different degrees of AVA.

Methods: Following atrioventricular-block, AVA was established through idioventricular rhythm (IVR; n=29), right ventricular apex pacing (RVA; n=12) or biventricular pacing (CRT; n=10). After ≥3 weeks of bradycardic remodeling, Torsade de Pointes arrhythmia (TdP) inducibility, defined as ≥3 TdP/10 minutes, was tested with specific I_{Kr}-blocker dofetilide (25 µg/kg/5 minutes). MD was assessed by echocardiography as time-to-peak (TTP) of LV free-wall minus septum (ΔTTP). Electrical intraventricular dyssynchrony was assessed as slope of regression line correlating intraventricular LV activation time (AT) and activation recovery interval (ARI).

Results: Under sinus rhythm, contraction occurred synchronously (ΔTTP: -8.6±28.9 ms), and latest activated regions seemingly had slightly longer repolarization (AT-ARI slope: -0.4). Acute AV-block increased MD in all groups, but following ≥3 weeks of remodeling IVR animals became significantly more TdP-inducible (19/29 IVR *vs* 5/12 RVA and 2/10 CRT, both $p<0.05$ *vs* IVR). After chronic AVA, intraventricular MD was lowest in CRT animals (ΔTTP: -8.5±31.2 *vs* 55.80±20.0 and 82.7±106.2ms in CRT, IVR and RVA, respectively, $p<0.05$ RVA *vs* CRT). Although dofetilide steepened negative AT-ARI slope in all groups, this heterogeneity in dofetilide-induced ARI prolongation seemed least pronounced in CRT animals (slope to -0.8, -3.2 and -4.5 in CRT, IVR and RVA, respectively).

Conclusion: Severity of intraventricular MD affects the extent of electrical remodeling and proarrhythmic outcome in the CAVB dog model.

NONSTANDARD ABRREVIATIONS AND ACRONYMS

AS: Arrhythmia Score

CAVB: Chronic AV-block dog model

CRT: Cardiac resynchronization therapy

ΔAT: Interventricular differences in activation time (calculated as LV_{AT} –RV_{AT})

ΔMAPD: Interventricular dispersion of repolarization (calculated as LV ARI – RV MAPD)

ΔOnset: Intraventricular difference in onset of radial contraction ($Onset_{free\text{-}wall}$ – $Onset_{septum}$)

ΔPS: Intraventricular difference in peak strain ($PS_{free\text{-}wall}$ – PS_{septum})

ΔTTP: Intraventricular difference in time-to-peak ($TTP_{free\text{-}wall}$ – TTP_{septum})

HF: Heart failure

IVR: Idioventricular rhythm

LV: Left ventricle

LV ARI: Left ventricular activation recovery interval

LV_{AT}: Left ventricular activation time

LV STV: Short-term variability of repolarization

Onset: Onset of radial strain

PS: Peak strain

RV: Right ventricle

RVA: Right ventricular apex paced

RV_{AT}: Right ventricular activation time

RVMAPD: Right ventricular monophasic action potential duration

RV STV: Short-term variability of repolarization

SR: Sinus Rhythm

Tp-e : Time between the peak and the end of the T-wave

TTP: Time-to-peak

568622-L-bw-Weperen
Processed on: 3-11-2021

INTRODUCTION

A prolonged QRS complex is associated with higher all-cause mortality and possibly fatal, ventricular arrhythmias in heart failure (HF) patients.[1,2] Therefore, an increasing number of HF patients are receiving cardiac resynchronization therapy (CRT),[3] also known as biventricular pacing. CRT aims to restore ventricular electromechanical synchrony and can reduce morbidity and mortality in HF patients.[4,5] Moreover, the BLOCK-HF study showed that CRT resulted in fewer deaths and less progression of HF than in right ventricular apex (RVA) paced patients,[6] suggesting the superiority of CRT over more conventional chronic RVA-pacing.

However, although almost one-third of CRT-recipients are refractory to this therapy,[7] the pathophysiology underlying CRT 'non-responders' and how this outcome can be *predicted* and *prevented* remains poorly understood. Moreover, a meta-analysis by Deif *et al.*[8] reported higher incidence of ventricular arrhythmias in non-responders compared to responders. Furthermore, Haugaa *et al.*[9] demonstrated significant correlation between incidence of ventricular arrhythmias and CRT-associated mechanical dyssynchrony. Collectively, these results suggest that pacing-induced altered ventricular activation, and consequential mechanical dyssynchrony, might initiate pro-arrhythmic cardiac remodeling. Simultaneously, this would also explain the superiority of CRT over RVA,[6] as CRT should cause less dyssynchrony than RVA and therefore induces less pro-arrhythmic remodeling. Moreover, it is known that altered activation pattern can change electrical properties of the heart, which is known as cardiac memory.[10] However, more research is needed into the electrical consequences of acute and chronic pacing, and the role of mechanical (dys)synchrony on promoting development of pro-arrhythmic conditions.

Studies on pacing-induced electrical remodeling can be performed in the chronic atrioventricular block (CAVB) dog, which has proven to be an outstanding paradigm to study 1) etiological factors that predisposition to ventricular arrhythmias and sudden cardiac deaths and 2) the electromechanical consequences of different pacing strategies.[11–13] In this model, ablation of the AV-node and subsequent drop in cardiac output initiate several remodeling processes that cumulatively restore cardiac output.[14] Adversely, electrical remodeling, which includes downregulation of potassium channels, results in susceptibility for Torsade de Pointes arrhythmias (TdP). Especially

in combination with additional (acute) impediments of cardiac repolarization such as anaesthetics[15], bradycardia[16] and/or administration of specific I_{Kr}-blocker dofetilide[17], TdP-inducibility is reached in ±75% of animals.[14]

In this study, we compared the electromechanical and arrhythmogenic consequences of different extents of altered ventricular activation, achieved through chronic exposure to either idioventricular (IVR), RVA or CRT conditions, in the CAVB dog model.

METHODS

All experiments were approved by 'the Committee for Experiments on Animals' of Utrecht University, the Netherlands. Animal handling and care was in accordance with the 'European Directive for the Protection of Vertebrate Animals used for Experimental and Scientific Purpose European Community Directive 86/609/CEE'. In total, 51 adult purpose-bred mongrel dogs (18 males, 24±3 kg, Marshall, USA) were included.

Animal preparation

Premedication was given ±30 minutes before induction of general anesthesia, and consisted of 0.5 mg/kg methadone (*i.m.*), 0.5 mg/kg acepromazine (*i.m.*), 0.02 mg/kg atropine (*i.m.*) and 0.1 mg/kg metacam (*s.c.*). Before the experiment, prophylactic antibiotic ampicillin (1000 mg) was injected (*i.v.*) and buprenorphine 0.3 mg (*i.m*) was administered after the experiments. Following the first experiment, temperature was monitored daily and amoxicillin-clavulanic acid (250 mg, *p.o.*) and metacam (0.1 mg/kg, *p.o.*) were administered for five consecutive days. General anesthesia was induced using pentobarbital (25 mg/kg, *i.v.*) and maintained with mechanical ventilation of isoflurane (1.5%) in a mixture of O_2 and N_2O (1:2). In CRT-paced animals (n=10), left ventricular leads of the CRT pacemaker were implanted through a right-sided thoracotomy (fourth intercostal space). All animals were implanted with leads and generators from Medtronic (Maastricht, Netherlands). In CRT-paced animals, the epicardial, left ventricular (LV) unipolar pacing lead (5071; 53 cm) was screwed on the basal, anterolateral wall of the LV. Correct pacing and absence of adverse phrenic nerve stimulation were confirmed.

Hereafter, the right ventricular (RV) bipolar pacing lead (5076; 85 cm) was introduced in CRT and RVA (n=12) paced animals *via* the jugular vein and, under

fluoroscopic guidance, screwed in the RVA. The RVA lead was tunneled to the thoracic device pocket and all leads were connected to the pacemaker (different models for RVA animals–CRT-P, Consulta, C3TR01; LV-RV delay: 0±8ms for CRT animals). Proper functioning was tested, impedance and pacing threshold determined, and the thorax closed. Next, radiofrequency ablation of the proximal His-bundle induced complete AV-block in all animals.

Following the acute experiment, rate was uncontrolled in idioventricular rhythm (IVR; n=29) animals, whereas RVA and CRT animals were paced at the lowest captured rate (55±7 beats/min for RVA animals; 54±5 beats/minute for CRT animals).

Experiments

Anaesthetized experiments including electrical and mechanical recordings were performed under sinus rhythm (SR), following acute IVR, RVA or CRT-pacing (aIVR, aRVA or aCRT, respectively) and after remodeling under IVR, RVA or CRT conditions had completed (cIVR, cRVA and cCRT, respectively; Figure 1A).[18] Mechanical recordings were made in four IVR, six RVA and all CRT animals. Under experimental conditions, RVA and CRT animals were continuously paced at 60 beats/minute. The cIVR, cRVA and cCRT experiments were conducted at 3.6±1.0, 3.1±0.4 and 2.9±0.2 weeks after creation of AV-block, and included additional assessment of TdP-inducibility in all animals. TdP-susceptibility was determined through administration of specific I_{Kr}-blocker dofetilide (0.025 mg/kg/5 minutes, *i.v.*; Figure 1A). Dofetilide infusion was discontinued if TdP occurred within five minutes after start of administration and persistent arrhythmias (>10s) were manually terminated by electrical cardioversion. Electrophysiological recordings consisted of 6-leads surface ECG, an endocardial RV monophasic action potential (MAP) catheter (Hugo Sachs Electronik, March-Hugstetten, Germany; not in cIVR experiments) and endocardial duo-decapolar catheter (St. Jude Medical, Veenendaal, the Netherlands), recording unipolar electrograms (EGM) from ten distinct LV regions (Figure 1B). In IVR experiments, the use of an LV EGM was limited to four animals. Catheters were introduced through the femoral artery or vein and positioned under fluoroscopic guidance. Electrophysiological recordings included a ten-minute baseline period, and twenty minutes following start of dofetilide infusion.

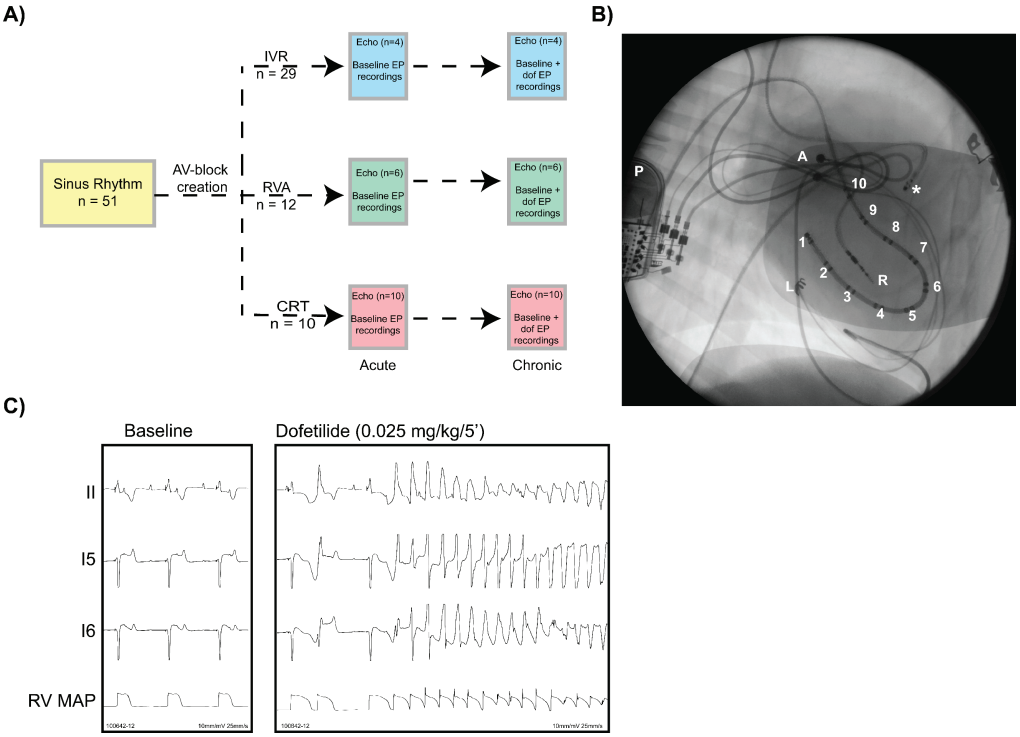

Figure 1. Overview of experimental methodology. A) Experimental design and setup. **B)** Positioning of the duo-decapolar catheter in the ventricle (1-10 depict the ten left ventricular (LV) electrodes measuring local electrograms). The asterisk (*) represents the monophasic action potential catheter in the right ventricle (RV MAP). The atrial lead (A), epicardial lead stimulating the LV (L), the right ventricular pacing lead (R) and the pacemaker (P), are also depicted. Animal in left-supine position. **C)** Representative tracings under baseline and following dofetilide infusion. Recordings from lead II, electrode 5 (I5) and 6 (I6) from the LV duo-decapolar catheter and RV MAP are shown.

Echocardiography

Echocardiography was performed under anesthesia using a Philips iE33 ultrasound machine (Philips, Best, the Netherlands). Animals (n=13 for SR, n=4 for IVR, n=6 for RVA and n=10 for CRT) were positioned in the right-sided supine position, except for aCRT conditions. LV parasternal short-axis views were made at papillary level and appropriate beats were selected based on PQ-interval duration. Radial myocardial peak strain (PS), onset of radial strain (Onset), and time-to-peak (TTP) of LV septal- and free-wall were analyzed with TomTec-Arena, 2D-Strain (TomTec, Unterschleissheim, Germany). LV septal- and free-wall regions were determined after division of the LV into six segments; regions were averages of the two adjoining segments best corresponding to the septal- and free-wall. The remaining segments,

located between the septal- and free-wall sections, were discarded. The ΔPS, ΔOnset and ΔTTP were calculated by subtracting the value of the septal-wall from the free-wall (free-wall – septum).

Electrophysiology

PP, RR, QRS, QT and T-wave peak-to-end (Tp-e) intervals were obtained from the surface ECG and analyzed offline using EPTracer (Cardiotek, Maastricht, the Netherlands). Duration of all intervals were manually measured and averaged over five consecutive beats. QT-interval was corrected for heart rate (QTc) using the Van der Water formula.[19] RV MAP durations (MAPD; determined at 80% repolarization) and LV activation recovery intervals (ARI) were determined by a custom-made Matlab application (Mathworks, Naticks, USA). Signals derived from the most distal and proximal electrode (1 and 10, respectively) of the duo-decapolar catheter were excluded from analysis because of P-wave interference. Short-term variability of repolarization (STV) was determined from 30 consecutive beats using the formula: $\sum|D_n+1 - D_n|/(30 \times \sqrt{2})$; D being RV MAPD or LV ARI.[20] Interventricular dispersion of repolarization (ΔMAPD) was calculated as LV ARI – RV MAPD; the average ARI of all LV electrograms was used for calculations. Activation times (AT) of the LV EGM electrodes were manually determined as time difference between pacing spike and minimum dV/dt of the EGM. LV_{AT} was calculated as average AT of all LV electrograms. RV_{AT} was measured as time difference between pacing spike and steepest upstroke of the MAP. Interventricular delay in activation (ΔAT) was calculated as LV_{AT} minus RV_{AT}. LV intraventricular heterogeneity in activation and repolarization were assessed by comparing ARI and AT of the duo-decapolar catheter. AT and ARI of EGM electrodes were used to establish AT-ARI slopes. All electrophysiological measurements were made under baseline conditions and either before the first ectopic beat or 5 minutes following start of dofetilide infusion.

Arrhythmia quantification

TdP were identified as polymorphic ventricular tachycardias of ≥5 beats twisting around the isoelectric line. TdP-inducibility was defined as ≥3 TdP within ten-minutes following start of dofetilide. Severity of arrhythmic activity was quantified as arrhythmia score (AS): all events were scored according to the *n*+1 rule (*n*=number of ectopic beats in

an arrhythmic event). Defibrillations were awarded 50, 75 or 100 points when single, double or ≥triple defibrillations were required, respectively. The score of the three most severe episodes during the ten minutes following start of dofetilide were averaged to obtain a final AS.

Statistical analysis

All results are displayed as mean ± standard deviation (SD). Repeated-measures ANOVA with post-hoc Bonferroni correction was used to determine the statistical significances of the electrophysiological and echocardiographic data. Inducibility and AS were analyzed by McNemar's and Wilcoxon signed rank tests, respectively. Results were considered statistically significant if $p<0.05$.

RESULTS

Sinus rhythm and acute AV-block

Average sinus rate of animals was 102±8 beats/minute and ventricular activation occurred rapidly (QRS interval: 66.5±5.3 ms) and synchronously (ΔAT: -1.6±2.6 ms; Table 1).

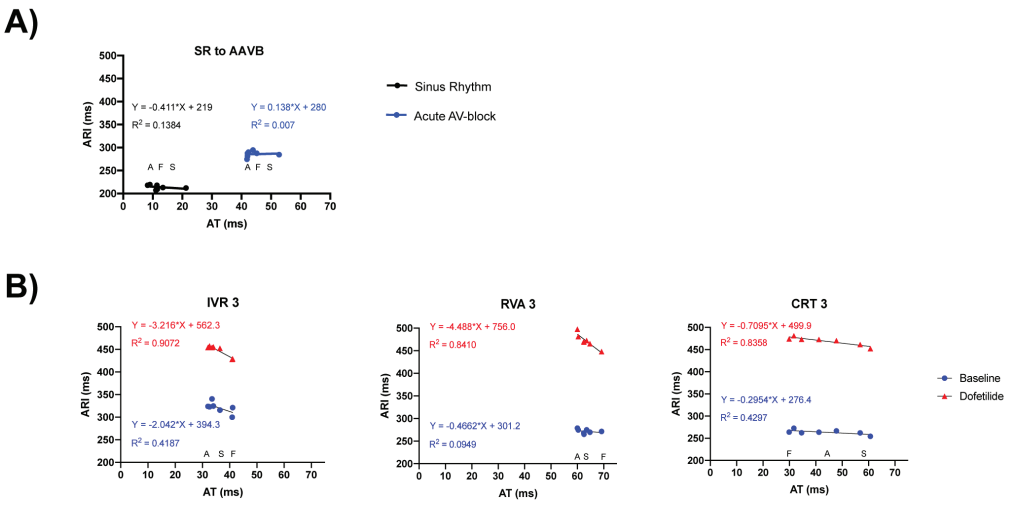

Figure 2. Left ventricular (LV) endocardial duo-decapolar catheter and the dynamical relationship between LV activation and repolarization over time. The relationship between local LV activation times (AT) and corresponding activation recovery intervals in **A)** SR and following acute AV-block and **B)** following three weeks of remodeling under the respective rate strategies. Order of left ventricular activation are represented by the letters A (Apex), F (Free-wall) and S (Septum). Baseline measurements are blue, dofetilide measurements are red.

Table 1: Electrical consequences of acute AV-block with different (pacing) strategies of rate control

	SR	AAVB
PP	589.8 ± 82.4	515.4 ± 102.0****
RR	587.1 ± 81.7	1084.0 ± 218.3****
QRS	66.5 ± 5.3	101.9 ± 13.1****
QT	262.3 ± 15.2	339.1 ± 38.5****
QTc	293.1 ± 20.5	333.2 ± 44.5****
JTc	232.0 ± 10.6	227.5 ± 34.3
Tp-e	34.5 ± 8.8	52.8 ± 17.6****
RV_{AT}	14.3 ± 2.0	36.1 ± 12.2****
LV_{AT}	12.3 ± 2.0	49.6 ± 17.8****
ΔAT	-1.6 ± 2.6	11.9 ± 22.7*
RV MAPD	192.8 ± 10.4	236.7 ± 27.8****
LV ARI	213.9 ± 14.6	278.1 ± 19.8****
ΔMAPD	21.1 ± 14.1	42.6 ± 21.6**
RV STV	0.4 ± 0.2	0.9 ± 0.6*
LV STV	0.6 ± 0.3	1.0 ± 0.9

Values are represented as mean ± SD.
* $p<0.05$ *vs.* Sinus Rhythm; ** $p<0.01$ *vs.* Sinus Rhythm; **** $p<0.001$ *vs.* Sinus Rhythm

Moreover, *intra*ventricular repolarization duration appeared homogenous and showed a slightly negative AT-ARI relationship (slope: -0.4; Figure 2A), suggestive of slightly earlier repolarization in the latest activated regions. Correspondingly, both ventricles contracted simultaneously and synchronously (ΔOnset: 2.4±8.5 and ΔTTP: 8.6±28.9 ms; Table 2).

Creation of AV-block acutely decreased heart rate, slowed conduction (QRS: 101.9±13.1 ms, $p<0.001$ *vs* SR) and induced interventricular dyssynchrony in activation (ΔAT: 11.9±22.7 ms, $p<0.05$ *vs* SR; Table 1; Supplementary Table 1). Moreover, the AT-ARI slope became slightly positive, suggesting that repolarization became longest in the latest activated regions (Figure 2A). These electrical changes were mirrored by changes in timing of ventricular contraction, ΔOnset increasing from 2.4±8.5 ms in SR to 76.8±75.9, 32.6±61.5 and -36.3±81.1 ms in IVR, RVA and CRT animals, respectively (all non-significant *vs* SR; Supplementary Table 2). Moreover, although synchrony of

Table 2: Mechanical effects of chronic RVA and CRT-pacing

		SR	*IVR*	*RVA*	*CRT*
TTP (ms)	*Free-wall*	263.4 ± 58.1	290.5 ± 13.2	380.3 ± 105.2*	307.9 ± 39.3
	Septum	272.0 ± 51.6	269.8 ± 54.5	297.6 ± 43.2	316.3 ± 39.3
	ΔTTP	-8.6 ± 28.9	55.8 ± 20.0	82.7 ± 106.2*	-8.5 ± 31.2†
PS (%)	*Free-wall*	24.2 ± 7.7	47.4 ± 13.3*	22.9 ± 8.6*	34.4 ± 7.5
	Septum	25.7 ± 7.2	37.4 ± 2.8	28.3 ± 8.5	36.0 ± 13.2
	ΔPS	-1.5 ± 7.7	10.0 ± 10.8	-5.4 ± 8.5	-1.6 ± 14.1
Onset (ms)	*Free-wall*	10.8 ± 13.1	61.8 ± 62.1	74.2 ± 61.2	37.6 ± 60.3
	Septum	8.4 ± 12.2	8.7 ± 10.2	7.3 ± 9.0	45.2 ± 52.3*
	ΔOnset	2.4 ± 8.5	53.1 ± 62.9	66.8 ± 61.0*	-7.6 ± 37.0†

Values are represented as mean ± SD.
* $p<0.05$ *vs.* SR; * $p<0.05$ *vs.* IVR3; † $p<0.05$ vs RVA3

contraction also seemed acutely affected by AVA, this effect appeared less in CRT animals (ΔTTP from -8.6±28.9 ms in SR to 20.0±10.0, 51.8±43.3 and 4.2±31.9 ms in IVR, RVA and CRT animals, respectively, *p<0.05* for RVA *vs* SR; Figure 3A, Supplementary Table 2).

Chronically altered ventricular activation

Chronically altered ventricular activation induced different extents of pro-arrhythmic remodeling in the three groups. With just 20%, TdP-inducibility was lowest in the cCRT group (2/10 animals). In cRVA animals, inducibility was more than twice as likely as cCRT animals, as 42% became TdP-inducible (5/12 animals). However, cIVR caused most TdP-inducibility as 66% of animals were inducible for TdP (19/29 animals; $p<0.05$ *vs* cRVA and cCRT; Figure 4; Table 3). Correspondingly, dofetilide caused less increase in AS in cCRT and cRVA groups (to 10.9±18.8 and 15.4±18.9, respectively) than in cIVR animals (to 42.8±33.0, $p<0.05$ *vs* cRVA and cCRT; Figure 4; Table 3).

Mechanically, each group exhibited different extents of mechanical dyssynchrony (Table 2). Most notably, this interventricular dyssynchrony in timing and force of contraction was lowest in cCRT animals (ΔTTP: -8.5±31.2 ms in cCRT *vs* 55.8±20.0 ms in cIVR and 82.7±106.2 ms in the cRVA animals; $p<0.05$ RVA *vs* CRT; Figure 3B; Table 2). Moreover, although contraction was delayed in cCRT animals, the synchrony and force of contraction appeared very similar to SR conditions (ΔTTP: -8.6±28.9 ms in SR; ΔPS: -1.5±7.7% and -1.6±14.1% in SR and cCRT animals, respectively, all *non-significant;* Table 2).

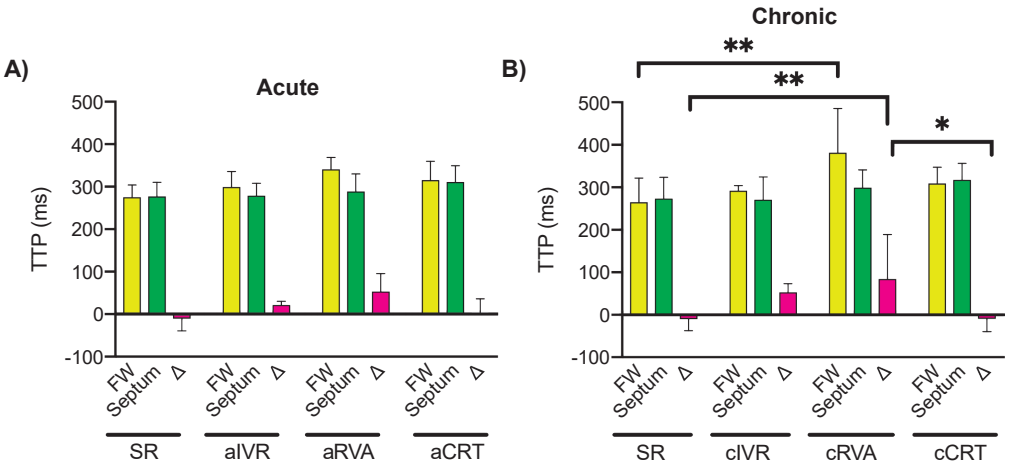

Figure 3. Time-to-peak (TTP) of LV radial strain under different conditions. Radial strain time-to-peak (TTP) of LV free-wall (FW; yellow), septal-wall (Septum; green), and the difference herein calculated as TTP FW – TTP septum (**Δ**; pink) following acute AV-block **(A)** and after chronic exposure to bradycardic idioventricular rhythm (cIVR), RV apex paced (cRVA) or biventricular paced (cCRT) conditions **(B)**.

Electrically, ventricular activation was significantly more synchronous in cCRT than in cRVA animals (ΔAT: -2.4±9.6 *vs* 37.6±8.1 ms, respectively, $p<0.05$). Moreover, all groups showed a negative AT-RT slope (as in SR), which became increasingly steeper from cCRT to cRVA to cIVR animals (Figure 2). Dofetilide further unmasked this *intra*ventricular heterogeneity in repolarization reserve, as regardless of rate strategy, repolarization prolonged most in the earliest activated regions. This steepening of the slope was least pronounced in the least-inducible group of cCRT animals (slope: -0.7) in comparison to cRVA and cIVR animals (slope: -4.5 and -3.2, respectively). Additionally, administration of dofetilide prolonged PP-intervals in all animals, but the extent of this prolongation also differed between each group; the prolongation becoming increasingly more pronounced going from cIVR to cRVA to cCRT animals (PP-interval following dofetilide to 713.8±120.3, 809.7±141.8 and 885.9±166.6 ms in cIVR, cRVA and cCRT animals, respectively; $p<0.05$ for cIVR *vs* cCRT; Table 3).

Table 3: Electrical consequences of chronic altered ventricular in idioventricular rhythm (IVR), right ventricular apex paced (RVA) or cardiac resynchronization therapy (CRT) conditions.

Baseline	*IVR*	*RVA*	*CRT*
PP	560.3 ± 68.8	516.3 ± 77.2	533.5 ± 53.8
RR	1338.0 ± 361.2	1000.0 ± 0.0*	1000.0 ± 0.0*
QRS	98.8 ± 4.6	118.8 ± 10.1*	95.6 ± 5.9†
QT	386.4 ± 67.0	379.6 ± 37.6	337.0 ± 24.6
QTc	357.0 ± 56.5	379.6 ± 37.6	337.0 ± 24.6
JTc	258.2 ± 56.2	260.8 ± 35.3	241.3 ± 24.6
Tp-e	82.6 ± 35.2	67.2 ± 15.0	61.9 ± 17.5
RV_{AT}		26.9 ± 4.6	46.0 ± 6.1*
LV_{AT}	35.8 ± 12.8	64.6 ± 8.3*	43.6 ± 8.3†
ΔAT		37.6 ± 8.1	-2.4 ± 9.6†
RV MAPD		242.1 ± 16.0	221.6 ± 15.7†
LV ARI	324.8 ± 51.0	271.2 ± 24.1*	266.0 ± 21.2*
ΔMAPD		30.0 ± 12.7	44.4 ± 14.7
RV STV		1.1 ± 0.3	1.4 ± 0.7
LV STV	3.2 ± 1.1	1.1 ± 0.7	0.7 ± 0.2*
Dofetilide			
PP	713.8 ± 120.3‡	809.7 ± 141.8‡	885.9 ± 166.6*‡
RR	1501.0 ± 333.2‡	1000.0 ± 0.0*	1000.0 ± 0.0*
QRS	100.9 ± 4.6‡	119.6 ± 9.8*	96.9 ± 6.0†‡
QT	579.7.3 ± 85.7‡	612.0 ± 84.4‡	565.6 ± 77.5‡
QTc	536.0 ± 81.7‡	612.0 ± 84.4*‡	565.6 ± 77.5‡
JTc	435.2 ± 81.8‡	492.5 ± 83.3‡	468.8 ± 76.7‡
Tp-e	177.2 ± 46.2‡	174.2 ± 52.3‡	172.8 ± 51.8‡
RV MAPD		359.0 ± 33.9‡	328.2 ± 53.2‡
LV ARI	448.0 ± 48.5‡	474.6 ± 59.0‡	455.7 ± 42.7‡
ΔMAPD		115.5 ± 45.5‡	127.5 ± 47.7†‡
RV STV		1.6 ± 0.6	1.8 ± 1.3
LV STV	4.7 ± 0.9	3.9 ± 1.4‡	4.2 ± 1.4‡
Inducibility (%)	66 (19/29)	42 (5/12)*	20 (2/10)*
AS	42.8 ± 33.0	15.4 ± 18.9*	10.9 ± 18.8*

Values are represented as mean ± SD.
* p<0.05 *vs.* IVR; † p<0.05 vs RVA; ‡ p<0.05 *vs.* Baseline

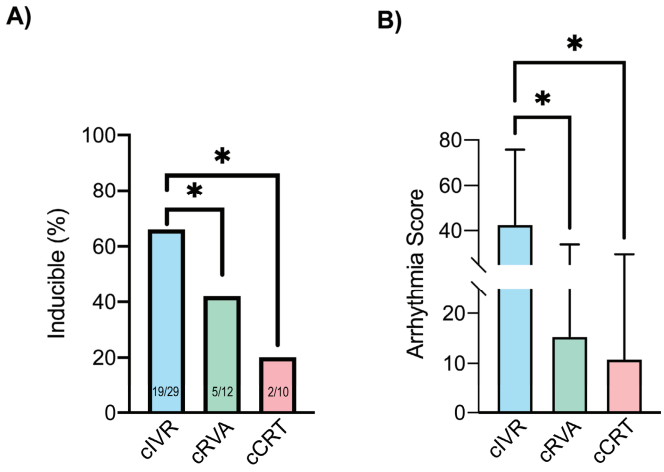

Figure 4. TdP-inducibility and Arrhythmia Score upon dofetilide administration following three weeks of remodeling. A) Following three weeks of remodeling, 66% of IVR animals became TdP-inducible, compared to 42% and 20% in the RVA and CRT-paced groups, respectively. **B)** In comparison to RVA and CRT, arrhythmic events were more severe in IVR animals. * $p<0.05$

DISCUSSION

In this study, we demonstrate that development of TdP-susceptibility in the CAVB dog model is correlated with extent of electromechanical dyssynchrony, which is induced by altered ventricular activation. We showed that TdP-susceptibility was lowest in cCRT animals, which were characterized by (1) less mechanical ventricular dyssynchrony and (2) less LV intraventricular dispersion of repolarization.

Arrhythmogenic vulnerability caused by mechanical discoordination

Multiple studies have suggested that chronic RVA-pacing progresses LV dysfunction as a result of electrical, and consequentially, mechanical dyssynchrony.[21,22] Correspondingly, biventricular pacing, which enhances synchrony of ventricular activation, is superior to RVA-pacing in preserving LV function.[7] As electrical remodeling is initiated to improve contractile function, the extent wherein this occurs seems to correlate with the severity of mechanical dyssynchrony. Electrical remodeling under chronic RVA-conditions is therefore more extensive than under chronic CRT-conditions, resulting in more dispersion of repolarization and increased arrhythmic susceptibility.[23] Also in CAVB dogs, three weeks of remodeling partially reverses RVA-pacing induced mechanical dyssynchrony, although TdP-susceptibility increases.[12] Hence, mechanical dyssynchrony appears to induce ventricular (electrical) remodeling,

which improves synchrony of contraction, but adversely increases TdP-susceptibility. Similarly, suboptimal CRT implantation could initiate mechanical dyssynchrony and thereby induce pro-arrhythmic remodeling in CRT non-responders.[8,9]

In this study, we exposed CAVB dogs to chronically unpaced (cIVR), cRVA or cCRT conditions, to compare arrhythmic outcomes of remodeling under different conditions of altered ventricular activation and thus extents of mechanical dyssynchrony. Notably, in IVR animals, focus of activation is uncontrolled, unstable and originates from three predilected sites.[24] While activation is controlled in RVA and CRT animals, this unnatural activation pattern naturally results in mechanical dyssynchrony, whilst its inconsistency is difficult to adapt to. Following chronically altered activation, several electrical parameters, including LV STV, were significantly different between the groups. However, these differences, reflective of different degrees of remodeling, became even clearer upon administration of dofetilide, and made most evident by TdP-susceptibility of each group. Whereas TdP-susceptibility was highest in IVR, CRT animals were significantly less vulnerable to TdP. CRT animals also displayed the most synchronous LV contraction on echocardiography, closely resembling SR conditions. Hence, although all groups were exposed to altered ventricular activation, the extent of continuous and chronic mechanical dyssynchrony that persists may determine the extent of ventricular pro-arrhythmic electromechanical remodeling. However, whether the electrical or mechanical changes are the primary drive of remodeling remains unclear.

Ventricular electrical remodeling

In the CAVB dog model, electrical remodeling induces changes in Ca^{2+}-handling and downregulation of potassium channels.[25,26] Consequently, administration of $I_{K,r}$-blocker dofetilide further impedes cardiac electrical stability by reducing repolarization reserve, which is quantified by STV.[14,20] This study showed that ventricular remodeling, initiated by chronically altered activation and bradycardia, reduces repolarization reserve and thereby increases TdP-susceptibility (Table 3).

This study also assessed electrical remodeling in the *spatial* dimension, using the AT-ARI slope.[12] Similar to previous studies, dofetilide steepened the negative AT-ARI slope, suggesting that repolarization reserve reduces most in early activated regions as they show relatively more dofetilide-induced ARI-prolongation.[12] This

steeper slope reflects more *intra*ventricular dispersion of repolarization, which is also inverted compared to acute AV-block, and has been implicated in both the development and perpetuation of longer-lasting TdP.[12,27,28] Additionally, this study showed that regardless of ventricular activation pattern, dofetilide causes the largest repolarization prolongation in early activated regions, indicating that electrical remodeling is driven by differences in AT and/or the consequential mechanical dyssynchrony.

Neural remodeling

Previous studies have demonstrated that sympathetic modulation promotes arrhythmogenesis in the CAVB dog model.[29] In this study, dofetilide-induced increases in PP-interval were significantly less in IVR animals compared to RVA and CRT animals. This suggests that AV-block induced neural responses could be proportional to the degree of mechanical dyssynchrony; a stronger neural response (as possibly present in IVR animals), resulting in more sympathetic activation and therefore more pro-arrhythmic conditions. However, this correlation remains hypothetical and the relationship between mechanical dysfunction and neural remodeling warrants further investigation.

Clinical relevance

This study showed that extent of electro-mechanical dyssynchrony relates to the development of arrhythmogenic vulnerability. It therefore highlights the importance of avoiding dyssynchrony in structurally remodeled hearts and potentially explains results of the Echocardiography Guided Cardiac Resynchronization Therapy (EchoCRT) study. This study, which was prematurely terminated due to futility,[30] reported a tendency towards increased mortality in HF patients without a prolonged QRS (≤130 ms) who underwent CRT therapy. Potentially, CRT induced electro-mechanical dyssynchrony, which resulted in pro-arrhythmic cardiac remodeling.[30] Hence, though CRT reduces morbidity and mortality in carefully selected HF patients,[4,5] inappropriate CRT implantation can be detrimental. Importantly, these findings are also relevant in the setting of left bundle-branch block pacing and His-bundle pacing.

Limitations

Due to arrhythmic activity, electrophysiological data following infusion of dofetilide in cIVR, cRVA and cCRT experiments are taken at different timepoints. As

less dofetilide was administered at earlier timepoints, this could have caused underestimation of the changes herein.

In IVR animals, dofetilide was administered under more bradycardic conditions. Bradycardia promotes arrhythmogenesis in the CAVB dog model[16] and might have contributed to the increased TdP-susceptibility.

Echocardiography and electrophysiological studies with an LV EGM were performed in only four IVR animals. Though limited, these results adequately represent mechanical and electrical dyssynchrony in these animals. Especially since in IVR, the focus is inconsistent and arising from three different predilected sites, reliable quantification of dyssynchrony is challenging.

CONCLUSION

In the CAVB dog model, altered ventricular activation contributes to pro-arrhythmic remodeling as the degree of electromechanical dyssynchrony correlates with the arrhythmogenic outcome.

REFERENCES

1. Kashani A, Barold SS. Significance of QRS complex duration in patients with heart failure. *J Am Coll Cardiol*. 2005;46(12):2183-2192. doi:10.1016/j.jacc.2005.01.071
2. Zimetbaum PJ, Buxton AE, Batsford W, et al. Electrocardiographic predictors of arrhythmic death and total mortality in the multicenter unsustained tachycardia trial. *Circulation*. 2004;110(7):766-769. doi:10.1161/01.CIR.0000139311.32278.32
3. Leyva F, Nisam S, Auricchio A. 20 Years of Cardiac Resynchronization Therapy. *J Am Coll Cardiol*. 2014;64(10):1047-1058. doi:https://doi.org/10.1016/j.jacc.2014.06.1178
4. Priori SG, Napolitano C, Memmi M, et al. Clinical and Molecular Characterization of Patients With Catecholaminergic Polymorphic Ventricular Tachycardia. *Circulation*. 2002;106(1):69-74. doi:10.1161/01.CIR.0000020013.73106.D8
5. Bristow MR, Saxon LA, Boehmer J, et al. Cardiac-resynchronization therapy with or without an implantable defibrillator in advanced chronic heart failure. *N Engl J Med*. 2004;350(21):2140-2150. doi:10.1056/NEJMoa032423
6. Curtis AB, Worley SJ, Adamson PB, et al. Biventricular Pacing for Atrioventricular Block and Systolic Dysfunction. *N Engl J Med*. 2013;368(17):1585-1593. doi:10.1056/NEJMoa1210356
7. Daubert C, Behar N, Martins RP, Mabo P, Leclercq C. Avoiding non-responders to cardiac resynchronization therapy: a practical guide. *Eur Heart J*. 2017;38(19):1463-1472. http://dx.doi.org/10.1093/eurheartj/ehw270.
8. Deif B, Ballantyne B, Almehmadi F, et al. Cardiac resynchronization is pro-arrhythmic in the absence of reverse ventricular remodelling: a systematic review and meta-analysis. *Cardiovasc Res*. 2018;114(11):1435-1444. doi:10.1093/cvr/cvy182
9. Haugaa KH, Marek JJ, Ahmed M, et al. Mechanical dyssynchrony after cardiac resynchronization therapy for severely symptomatic heart failure is associated with risk for ventricular arrhythmias. *J Am Soc Echocardiogr*. 2014;27(8):872-879. doi:10.1016/j.echo.2014.04.001

10. Shvilkin A, Huang HD, Josephson ME. Cardiac Memory. *Circ Arrhythmia Electrophysiol*. 2015;8(2):475-482. doi:10.1161/CIRCEP.115.002778
11. Dunnink A, van Opstal JM, Oosterhoff P, et al. Ventricular remodelling is a prerequisite for the induction of dofetilide-induced torsade de pointes arrhythmias in the anaesthetized, complete atrio-ventricular-block dog. *Europace*. 2012;14(3):431-436. doi:10.1093/europace/eur311
12. Stams TRG, Dunnink A, van Everdingen WM, et al. Deleterious acute and chronic effects of bradycardic right ventricular apex pacing: consequences for arrhythmic outcome. *Basic Res Cardiol*. 2017;112(4):46. doi:10.1007/s00395-017-0636-z
13. Thomsen MB, Oros A, Schoenmakers M, et al. Proarrhythmic electrical remodelling is associated with increased beat-to-beat variability of repolarisation. *Cardiovasc Res*. 2007;73(3):521-530. http://cardiovascres.oxfordjournals.org/content/73/3/521.abstract.
14. Oros A, Beekman JDM, Vos MA. The canine model with chronic, complete atrio-ventricular block. *Pharmacol Ther*. 2008;119(2):168-178. doi:10.1016/j.pharmthera.2008.03.006
15. Dunnink A, Sharif S, Oosterhoff P, et al. Anesthesia and Arrhythmogenesis in the Chronic Atrioventricular Block Dog Model. *J Cardiovasc Pharmacol*. 2010;55(6):601-608. doi:10.1097/FJC.0b013e3181da7768
16. van Weperen VYH, Dunnink A, Bossu A, et al. Severe Bradycardia Increases the Incidence and Severity of Torsade de Pointes Arrhythmias by Augmenting Preexistent Spatial Dispersion of Repolarization in the CAVB Dog Model. *Front Physiol*. 2021;12:642083. doi:10.3389/fphys.2021.642083
17. Champeroux P, Thireau J, Judé S, et al. Short-term variability in QT interval and ventricular arrhythmias induced by dofetilide are dependent on high-frequency autonomic oscillations. *Br J Pharmacol*. 2015;172(11):2878-2891. doi:10.1111/bph.13093
18. Bourgonje VJA, van Veen TAB, Vos MA. Ventricular Electrical Remodeling in Compensated Cardiac Hypertrophy BT - Electrical Diseases of the Heart: Volume 1: Basic Foundations and Primary Electrical Diseases. In: Gussak I, Antzelevitch C, eds. London; 2013:387-398. doi:10.1007/978-1-4471-4881-4_23

19. Van de Water A, Verheyen J, Xhonneux R, Reneman RS. An improved method to correct the QT interval of the electrocardiogram for changes in heart rate. *J Pharmacol Methods*. 1989;22(3):207-217. doi:10.1016/0160-5402(89)90015-6
20. Thomsen MB, Verduyn SC, Stengl M, et al. Increased Short-Term Variability of Repolarization Predicts Sotalol–Induced Torsades de Pointes in Dogs. *Circulation*.2004;110(16):2453-2459. doi:10.1161/01.CIR.0000145162.64183.C8
21. Lamas GA, Lee KL, Sweeney MO, et al. Ventricular Pacing or Dual-Chamber Pacing for Sinus-Node Dysfunction. *N Engl J Med*. 2002;346(24):1854-1862. doi:10.1056/nejmoa013040
22. Wilkoff BL, Cook JR, Epstein AE, et al. Dual-chamber pacing-or ventricular backup pacing in patients with an implantable defibrillator: The Dual Chamber and VVI Implantable Defibrillator (DAVID) Trial. *J Am Med Assoc*. 2002;288(24):3115-3123. doi:10.1001/jama.288.24.3115
23. Marrus SB, Andrews CM, Cooper DH, Faddis MN, Rudy Y. Repolarization changes underlying long-term cardiac memory due to right ventricular pacing: noninvasive mapping with electrocardiographic imaging. *Circ Arrhythm Electrophysiol*. 2012;5(4):773-781. doi:10.1161/CIRCEP.112.970491
24. Cardinal R, Scherlag BJ, Vermeulen M, Armour JA. Distinct Activation Patterns of Idioventricular Rhythms and Sympathetically-Induced Ventricular Tachycardias in Dogs with Atrioventricular Block. *Pacing Clin Electrophysiol*. 1992;15(9):1300-1316. doi:10.1111/j.1540-8159.1992.tb03141.x
25. Sipido KR, Volders PGA, de Groot SHM, et al. Enhanced Ca(2+) Release and Na/Ca Exchange Activity in Hypertrophied Canine Ventricular Myocytes. *Circulation*.2000;102(17):2137-2144. http://www.ncbi.nlm.nih.gov/pubmed/11044433. Accessed May 10, 2019.
26. Volders PGA, Sipido KR, Vos MA, et al. Downregulation of Delayed Rectifier K+ Currents in Dogs With Chronic Complete Atrioventricular Block and Acquired Torsades de Pointes. *Circulation*. 1999;100(24):2455-2461. doi:10.1161/01.CIR.100.24.2455
27. Vandersickel N, de Boer TP, Vos MA, Panfilov A V. Perpetuation of Torsade de Pointes in heterogeneous hearts: competing foci or re-entry? *J Physiol*. 2016;594(23):6865-6878. doi:10.1113/JP271728

28. Dunnink A, Stams TRG, Bossu A, et al. Torsade de pointes arrhythmias arise at the site of maximal heterogeneity of repolarization in the chronic complete atrioventricular block dog. *Europace*. 2017;19(5):858-865. doi:10.1093/europace/euw087

29. van Weperen VYH, Bossu A, Beekman JDM, van der Heyden MAG, Vos MA. ABSTRACT 19818: Local, but Not Systemic, Blockade of Autonomic Nervous System Activity is Antiarrhythmic in the Dog With Dofetilide Induced Torsade de Pointes Arrhythmias. *Circulation*. 2017;136(suppl_1):A19818-A19818. doi:10.1161/circ.136.suppl_1.19818

30. Ruschitzka F, Abraham WT, Singh JP, et al. Cardiac-Resynchronization Therapy in Heart Failure with a Narrow QRS Complex. *N Engl J Med*. 2013;369(15):1395-1405. doi:10.1056/NEJMoa1306687

SUPPLEMENTARY TABLES

Supplementary table 1: Electrical consequences of acute AV-block with different (pacing) strategies of rate control

Baseline		*SR*	*aIVR*	*aRVA*	*aCRT*
	PP	589.8 ± 82.4	514.6 ± 112.9*	509.0 ± 81.1*	525.4 ± 101.2
	RR	587.1 ± 81.7	1149.0 ± 276.3*	1000.0 ± 0.0*	1000.0 ± 0.0*
	QRS	66.5 ± 5.3	95.8 ± 6.9*	121.1 ± 8.1*†	95.8 ± 7.3*‡
	QT	262.3 ± 15.2	315.3 ± 30.2*	378.3 ± 25.1*†	358.6 ± 18.1*†‡
	QTc	293.1 ± 20.5	302.3 ± 27.5	378.3 ± 25.1*	358.6 ± 18.1*
	JTc	232.0 ± 10.6	206.5 ± 25.8*	257.2 ± 25.8*†	263.0 ± 16.0†
	Tp-e	34.5 ± 8.8	49.8 ± 21.6*	58.9 ± 10.8*†	54.2 ± 2.6*
RV AT		14.3 ± 2.0	40.0 ± 30.7*	27.4 ± 5.3*	47.1 ± 6.5*‡
LV AT	Mean	12.3 ± 2.0	28.9 ± 29.0	61.5 ± 9.6*†	43.6 ± 8.2*‡
	Apex	8.7 ± 4.3	27.2 ± 30.7*	56.4 ± 10.2*†	42.1 ± 8.8*†‡
	Free wall	12.3 ± 3.4	27.7 ± 29.9*	67.0 ± 13.1*†	35.4 ± 6.8*‡
	Septum	16.3 ± 11.1	31.3 ± 20.4	57.5 ± 12.8*†	56.5 ± 16.2*†
ΔAT		-1.6 ± 2.6	-11.1 ± 13.1	35.6 ± 8.7*†	-3.2 ± 5.7‡
RV MAPD		192.8 ± 10.4	252.5 ± 46.2*	240.2 ± 27.8*	228.9 ± 21.7*
LV ARI	Mean	213.9 ± 14.6	296.7 ± 27.6*	276.7 ± 18.3*	272.3 ± 15.2*
	Apex	219.5 ± 20.0	289.3 ± 17.9*	273.8 ± 22.2*	283.1 ± 16.0*
	Free wall	210.5 ± 15.5	292.3 ± 25.4*	281.5 ± 12.5*	276.1 ± 16.1*
	Septum	215.4 ± 16.2	299.3 ± 29.9*	285.7 ± 20.1*	268.6 ± 27.5*
ΔMAPD		21.1 ± 14.1	44.1 ± 33.9*	36.4 ± 16.7	43.5 ± 22.1*
RV STV		0.4 ± 0.2	0.9 ± 0.3	0.8 ± 0.4	0.8 ± 0.8
LV STV		0.6 ± 0.3	0.8 ± 0.4	1.3 ± 1.2	0.6 ± 0.2

Values are represented as mean ± SD.
* p<0.05 vs. Sinus Rhythm; † p<0.05 vs. IVR; ‡ p<0.05 vs. RVA
SR: Sinus rhythm; IVR: Idioventricular rhythm; RVA: Right ventricular apex paced; CRT: Biventricular paced; RV AT: Right ventricular activation time; LV AT: Left ventricular activation time; ΔAT: Interventricular differences in activation time (LV AT – RV AT); LV ARI: Left ventricular activation recovery interval; RV MAPD: Right ventricular monophasic action potential duration; ΔMAPD: Interventricular dispersion of repolarization (LV ARI – RV MAPD); RV STV: Right ventricular short-term variability of repolarization ; LV STV: Left ventricular short-term variability of repolarization

Supplementary table 2: Mechanical consequences of acute AV-block with different (pacing) strategies of rate control

		SR	*aIVR*	*aRVA*	*aCRT*
TTP (ms)	Free wall	263.4 ± 58.1	297.7 ± 37.9	339.1 ± 29.5*	314.1 ± 45.9
	Septum	272.0 ± 51.6	277.7 ± 30.6	287.3 ± 42.5	309.9 ± 39.1
	ΔTTP	-8.6 ± 28.9	20.0 ± 10.0	51.8 ± 43.3*	4.2 ± 31.9‡
PS (%)	Free wall	24.2 ± 7.7	36.9 ± 9.4	28.9 ± 5.1	24.8 ± 7.0
	Septum	25.7 ± 7.2	24.6 ± 10.9	25.9 ± 6.6	24.5 ± 7.0
	ΔPS	-1.5 ± 7.7	12.3 ± 6.5	3.0 ± 9.4	0.3 ± 10.8
Onset (ms)	Free wall	10.8 ± 13.1	103.5 ± 66.8	60.8 ± 59.5*	47.4 ± 49.4
	Septum	8.4 ± 12.2	26.7 ± 15.3	28.2 ± 13.0	83.7 ± 71.2*
	ΔOnset	2.4 ± 8.5	76.8 ± 75.9	32.6 ± 61.5	-36.3 ± 81.1†

Values are represented as mean ± SD.
* p<0.05 vs. Sinus Rhythm; † p<0.05 vs. IVR; ‡ p<0.05 vs. RVA
SR: Sinus rhythm; RVA: Right ventricular apex paced; CRT: Biventricular paced; TTP: Time to peak; PS: Peak strain; Onset: Onset of radial strain; ΔTTP: Intraventricular difference in time to peak (TTPfree wall – TTPseptum); ΔPS: Intraventricular difference in peak strain (PSfree wall – PSseptum); ΔOnset: Intraventricular difference in onset of radial contraction (Onsetfree wall – Onsetseptum)

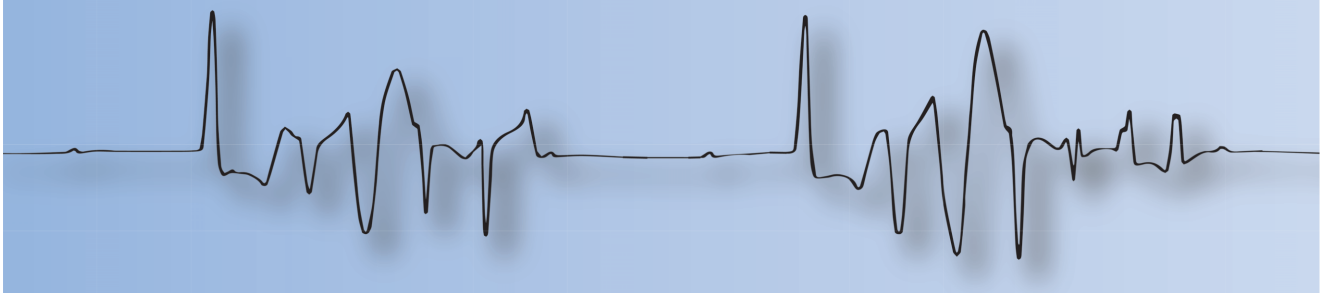

Valerie Y.H. van Weperen*, Alexandre Bossu*, Henriette D.M. Beekman, Veronique M.F. Meijborg, Ruben Coronel, Marcel A.G. van der Heyden & Marc A. Vos

Submitted

CHAPTER 5

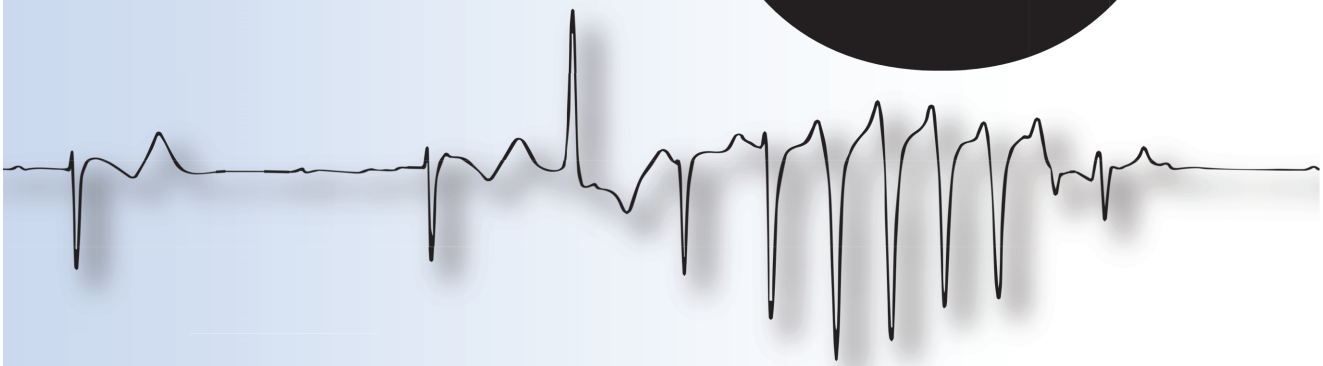

Local, but not systemic, blockade of autonomic nervous system activity is antiarrhythmic against dofetilide-induced Torsade de Pointes arrhythmias in the anesthetized chronic atrioventricular block dog

ABSTRACT

Aims: Autonomic nervous system (ANS) activity is a potent extracardiac trigger for ventricular arrhythmias. This study compared the antiarrhythmic efficacy of pharmacological autonomic modulation to bilateral stellectomy in the chronic atrioventricular block (CAVB) dog model.

Methods and Results: Twenty-six anesthetized CAVB dogs received dofetilide (25µg/kg/5min) to induce Torsade de Pointes arrhythmias (TdP) before (suppression) or after (prevention) ANS-modulation. ANS-modulations included hexamethonium (20mg/kg/5min, suppression and prevention), propranolol (0.3mg/kg/3min, suppression) and/or bilateral stellectomy (prevention). Surface electrocardiogram intervals and short-term variability of repolarization (STV) from endocardial unipolar electrogram were measured. Spatial dispersion of repolarization (SDR), through high-resolution in-vivo mapping experiments, and left ventricular contractility (dP/dt+), from intraventricular pressure catheter, were assessed in stellectomy experiments. Severity of arrhythmias was scored (AS) and TdP-inducibility was defined as ≥3 episodes within ten-minutes following start of dofetilide. Hexamethonium and propranolol failed to suppress arrhythmias: 3/7 and 4/5 dogs remained TdP-inducible, respectively. Hexamethonium could also not prevent TdP; all previously inducible-animals remained inducible. Correspondingly, these drugs did not shorten repolarization and/or lower STV. However, bilateral stellectomy decreased TdP-inducibility (from 17/17 to 2/17 dogs; $p<0.005$) and AS (from 47.3±13.3 to 10.1±18.5; $p<0.05$). This highly anti-arrhythmic effect was not established through decreased repolarization duration/prolongation, STV or SDR, but was associated with a decreased contractility (dP/dt+ both at baseline from 2327±553 to 1385±518 and following dofetilide from 2769±798 to 1993±658 mmHg/s, both $p<0.05$).

Conclusion: Pharmacological ANS-modulation using hexamethonium or propranolol exerted no antiarrhythmic effect in CAVB dogs. In contrast, bilateral stellectomy, presumably through decreasing contractility, was highly antiarrhythmic.

ABBREVIATIONS

ANS: autonomic nervous system

ARI: activation recovery interval

AS: arrhythmia score

CAVB: chronic atrioventricular block

ECG: electrocardiogram

EGM: endocardial unipolar electrogram

IVR: idioventricular rhythm

LV: left ventricle

MAP: monophasic action potential

MAPD: monophasic action potential duration

PNS: parasympathetic nervous system

RV: right ventricle

SNS: sympathetic nervous system

STV: short-term variability of repolarization

TdP: Torsade de Pointes arrhythmia

568622-L-bw-Weperen
Processed on: 3-11-2021

INTRODUCTION

Ventricular arrhythmias result from the complex interplay between trigger, substrate and (extra)cardiac modulation hereof.[1–5] The multi-layered complexity of the genesis, perpetuation and termination of life-threatening ventricular arrhythmias is incompletely understood.[6,7] Neuromodulation has emerged as a potent anti-arrhythmic strategy in both clinical and experimental settings, with beta-blockers serving as one of its therapeutic cornerstones.[8] Moreover, to date, beta-blockers are the only class of drugs that improve survival in primary or secondary prevention of sudden cardiac death.[9] The efficacy of neuromodulatory therapies resides in their ability to counteract the cardiac disease-induced sympathetic overexcitation.[10]

Under healthy conditions, the two divisions of the autonomic nervous system - the sympathetic (SNS) and the parasympathetic nervous system (PNS) - finely regulate the excitatory and inhibitory cardiac outputs, respectively.[10–12] The relative activity of both divisions optimizes cardiac chronotropy, inotropy, dromotropy, bathmotropy and lusitropy on a beat-to-beat basis.[13] Anatomically, these antagonizing effects originate from different regions in the central nervous system. The SNS originates in the spinal cord, from where preganglionic fibers travel towards the para- and prevertebral ganglia, including the stellate ganglia. Here preganglionic nerves synapse upon postganglionic nerves that directly innervate the heart.[14–16] The vagus nerve coming from the nucleus ambiguus composes the source of cardiac parasympathetic input[17] and synapses upon postganglionic nerves on the surface of the myocardium.[18,19] Of note, both divisions employ acetylcholine (Ach) binding on to nicotinic Ach-receptors as the primary neurotransmitter in the pre- to postganglionic nerve transmission. However, at the level of the heart, the SNS and PNS employ different neuro-transmitters and -peptides to achieve their antagonizing effects: the SNS primarily releases (nor)epinephrine binding to beta-receptors, whereas the PNS establishes its effects through Ach binding to muscarinic receptors.

Cardiac disease is often characterized by neural remodelling resulting in SNS overexcitation. This imbalance can initiate ventricular arrhythmias through promoting both arrhythmic trigger and substrate through modulation and destabilization of cardiomyocyte ion handling[20–22] and increasing spatial differences in electrical properties,[23–25] respectively. Although this causal relation between sympathetic activity

568622-L-bw-Weperen
Processed on: 3-11-2021

and ventricular arrhythmogenesis has been extensively demonstrated following myocardial infarction, characterized by well delineated scar tissue, the applicability and mechanism of action of neuromodulatory therapies are much less understood in the setting of non-ischemic cardiac injury. Moreover, multiple studies have reported more effective antiarrhythmic outcomes of mechanical approaches compared to pharmacological strategies modulating the ANS,[26–28] but no adequate comparison of these distinct strategies has yet been carried out in the same subject. Therefore, we aimed to compare the antiarrhythmic properties of three conventional approaches of autonomic modulation against dofetilide-induced Torsade de Pointes arrhythmias (TdP) in chronic atrioventricular block (CAVB) dogs. In this animal model, ablation of the AV node and consequent ventricular bradycardia, acutely results in a drop of cardiac output, which elicits contractile, electrical and structural remodelling processes.[29] Cumulatively, these cardiac adaptations restore the cardiac output, but simultaneously increase the susceptibility for TdP. The reproducibility of cardiac remodelling and associated TdP inducibility make this model reliable and adequate to determine the efficacy of antiarrhythmic strategies.[29,30]

We explored three therapeutic methods including pharmacological autonomic modulation using hexamethonium or propranolol and bilateral stellectomy. All ANS modulations were assessed in prevention and/or suppression experiments with dofetilide-induced TdP.

METHODS

All experiments, animal care and handling were in accordance with the Directive 2010/63/EU of the European Parliament and of the Council of 22 September on the protection of animals used for scientific purposes and the Dutch Law on animal experimentation and were approved by the Committee for Experiments on Animals of Utrecht University, the Netherlands. All experiments described in this study were performed in a total of 26 adult purpose-bred mongrel dogs (14 females; 25 ± 3 kg; Marshall, New York, USA).

1. Creation of chronic AV-block

All experiments were preceded by an overnight fast and premedication including methadone, acepromazine and atropine (0.5, 0.5 and 0.02 mg/kg i.m., respectively).

Perioperative care consisted of antibiotic prophylaxis using ampicillin (1000 mg, before (i.v.) and after (i.m.) experiment) and analgesia with metacam 0.1 mg/kg s.c. (before experiment) and buprenorphine (0.3 mg, i.m.; after experiment). General anaesthesia was then induced using pentobarbital sodium (Nembutal 25 mg/kg i.v.) and maintained with mechanical ventilation of isoflurane (1.5%) in a mixture of O_2 and N_2O (1:2). A pacemaker screw-in lead was introduced *via* the jugular vein, positioned in the right ventricular apex and connected to an internal pacemaker (Medtronic, Maastricht, the Netherlands). Complete AV-block was then established by radiofrequency ablation of the proximal His-bundle. A remodelling period of at least 3 weeks under idioventricular rhythm (IVR) was allowed before conduction of the following experiments.

2. Experiments

All experiments included the administration of the specific I_{Kr} blocker dofetilide (25 µg/kg/5min i.v.; Procter & Gamble Pharmaceuticals, Cincinnati, Ohio, USA) in an effort to induce repetitive TdP, defined as a polymorphic ventricular tachycardia of at least 5 ectopic beats characterized by the twisting shape of QRS complexes around the isoelectric line. Non-terminating arrhythmias (>10 s) were defibrillated by a direct-current shock applied through thoracic patches or internal paddles.

Electrophysiological recordings included a standard 6-leads surface electrocardiogram (ECG) and four precordial leads along with left ventricular (LV) endocardial signals derived from either a monophasic action potential (MAP) catheter (Hugo Sachs, Germany) or a duo-decapolar catheter (St. Jude Medical, St. Paul, MN, USA) recording unipolar electrograms (EGM) from distinct locations in the LV. Endocardial right ventricular (RV) MAP was also recorded.

2.1 Pharmacological blockade of the autonomic nervous system

To determine the antiarrhythmic effect of complete pharmacological blockade of the ANS, hexamethonium (20 mg/kg/5min; Sigma Chemical Co., St. Louis, Missouri) was administered intravenously to CAVB dogs after (n=7) or before (n=5) a dofetilide challenge, in suppression and prevention experiments, respectively (Figure 1A and B). In all animals a LV unipolar electrogram was recorded. In the suppression experiment, IVR was not hemodynamically tolerated in four experiments, therefore

these animals were temporarily paced at 60 beats/min. In the prevention and inducibility experiment, one animal had to be paced at 60 beats/min.

2.2 Pharmacological blockade of the sympathetic nervous system

To assess the cardiac effects of isolated sympathetic depression, propranolol (0.3 mg/kg/3min; Sigma Chemical Co., St. Louis, Missouri), a non-specific beta-blocker, was administered to 5 CAVB dogs in a similar fashion as the suppression experiment with hexamethonium (n=1 with LV EGM, n=4 with LV MAP; Figure 1C).

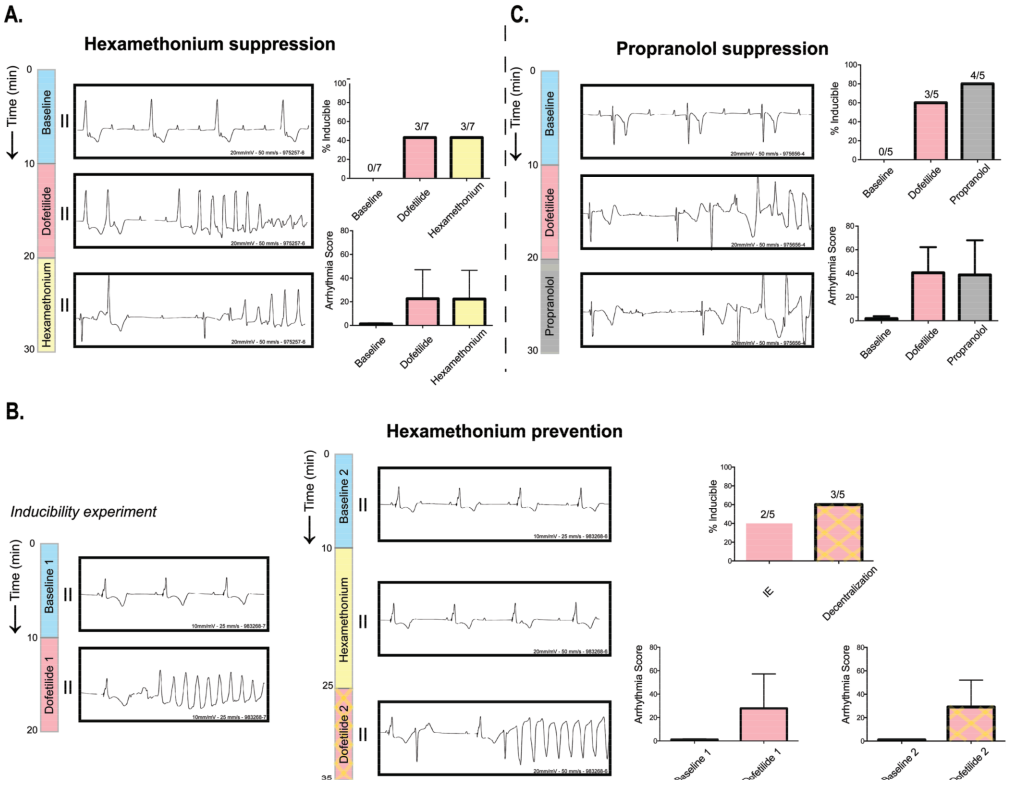

Figure 1: Overview of pharmacological approaches aimed at cardiac autonomic-nervous system modulation A. Hexamethonium suppression experiments (n = 7) involved the administration of Dofetilide (25µg/kg/5min) followed by administration of Hexamethonium (20 mg/kg/5min). **B.** Hexamethonium prevention experiments (n = 5) involved an inducibility experiment (IE) and a prevention experiment in which the administration of Hexamethonium (20 mg/kg/5min; follow-up for 15 minutes) was followed by administration of Dofetilide (25µg/kg/5min). **C.** Propranolol suppression experiments (n = 5) involved the administration of Dofetilide (25µg/kg/5min) followed by administration of Propranolol (0.3 mg/kg/3min). Representative traces of the surface electrogram lead II are shown next to the different stages. Inducibility percentages and arrhythmia score during the different experiments are also shown (statistical tests used: McNemar's test and non-parametric Friedman test, respectively).

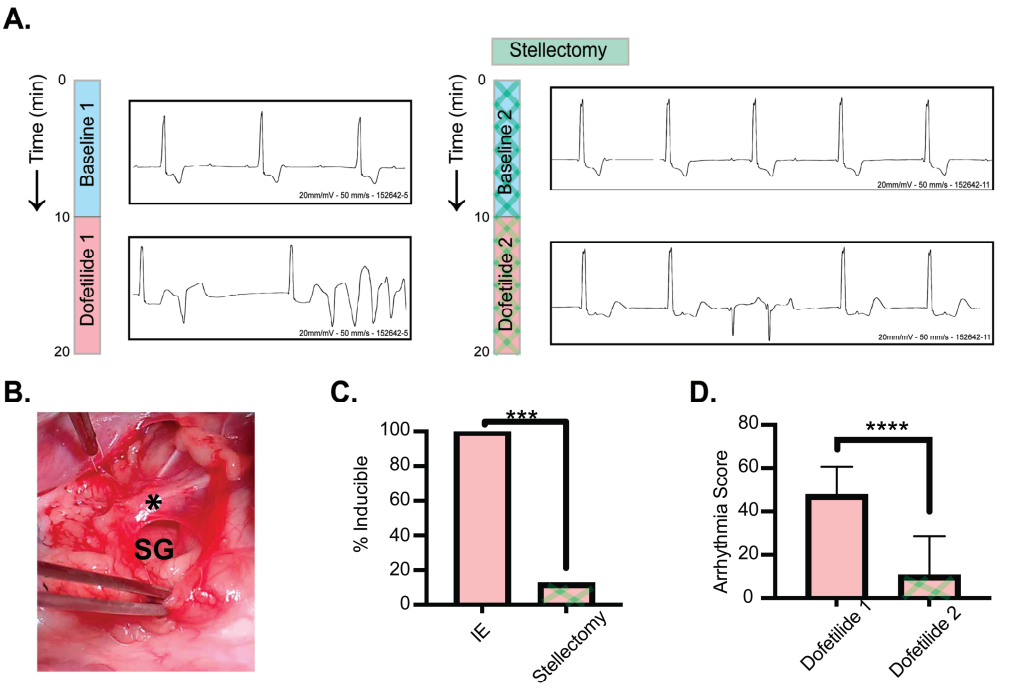

Figure 2: Overview of the inducibility percentage and arrhythmic outcome of bilateral stellectomy in CAVB dogs (n = 17) A. Schematic overview of the experimental protocol. Inducibility following stellectomy was compared to a prior inducibility experiment. **B.** Picture of a left stellate ganglion (SG, asterisk) in an CAVB dog prior to stellectomy. **C.** Inducibility percentage during the inducibility experiment (IE) and following bilateral stellectomy (statistical test: McNemar's test). **D.** Arrhythmia score during the inducibility experiment and following bilateral stellectomy (Statistical test: non-parametric Friedman test). *** p<0.001 *vs* IE; **** p<0.0001 *vs* dofetilide 1.

2.3 Isolated mechanical sympathetic blockade

In 17 TdP inducible CAVB dogs, bilateral stellectomy was carried out according to the protocol described by Wu *et al.*[31]Access to the left stellate ganglion was obtained by performing a thoracotomy through the third intercostal space. After correct identification, confirmed by the increase in arterial pressure upon stimulation, the ganglion was resected. Following the closure of the thorax, a right-sided thoracotomy was performed and the right stellate ganglion was identified. Correct identification was confirmed by a shortening of PP-interval upon stimulation. After resection of the right stellate ganglion and closure of the thorax, dofetilide was administered to determine TdP inducibility (Figure 2A and B; n = 14 with LV EGM). In five terminal bilateral stellectomy experiments, *in vivo* high-resolution mapping studies were performed as previously described by Dunnink *et al* (2017).[32] In short, 56 needles, each carrying four

recording electrodes, were evenly distributed over both ventricular walls and used for the assessment of spatial dispersion of repolarization (SDR). In five separate animals, continuous left ventricular pressure recordings were made using an intraventricular 7 Fr pig-tail catheter. In the inducibility experiments, one animal was paced at 45 beats/min. After denervation, nine animals were paced at 48 ± 8 beats/min.

3. Data analysis

Surface ECG intervals (PP, RR, QRS and QT) were measured manually from five consecutive beats during baseline, dofetilide, hexamethonium and/or propranolol conditions. Dofetilide measurements were made prior to the first ectopic beat or at the moment with the longest QT interval. In inducibility prevention experiments, dofetilide measurements were made at the time corresponding to the first ectopic event in the inducibility experiment. Hexamethonium and propranolol measurements were made 5 or 15 minutes after start of infusion, respectively. Recorded data were analysed using EPTracer software (Cardiotek, Maastricht, The Netherlands). QT interval was corrected for heart rate (QTc) using the Van der Water formula.[33] LV activation recovery intervals (LV ARI) were derived from high quality signals of the most apical located electrode of a unipolar EGM and were as the difference between the repolarization and the activation times.[34] Activation time (AT) was determined at the time of steepest negative slope of QRS, whereas repolarization time (RT) was measured at the point of steepest positive slope of the T-wave. The endocardial LV and RV MAP durations (MAPD) were determined as interval from steepest positive slope to at 80% repolarization using a custom made Matlab application (Mathworks, Naticks, USA). Short-term variability of repolarization (STV) was calculated from 30 consecutive beats according to the formula: $\sum|D_{n+1} - D_n|/(30 \times \sqrt{2})$ with D being LV ARI/MAPD or RV MAPD.[35] Interventricular dispersion of repolarization (Δ MAPD) was calculated as LV ARI/MAPD – RV MAPD.

LV pressure recordings were measured using the same custom made Matlab application (Mathworks, Naticks, USA).[36] Hemodynamic parameters included left ventricular end-systolic and end-diastolic pressures (ESP and EDP, respectively), as well as the maximal rise and decay in left ventricular pressure (dP/dt+ and dP/dt–, respectively). All measurements were averaged over five consecutive beats.

Mapping data was analysed offline using the custom-made analysis program Maplab (MATLAB R2016a; Mathworks). AT and RT (determined as previously described for the catheter-derived EGM signals) of the 224 needle electrodes were measured for all timepoints and averaged over five consecutive beats. SDR was quantified as the average and maximal difference in RT between two adjacent electrodes in the horizontal, vertical, transmural and cubic orientation.

4. Arrhythmia incidence

Ectopic activity over the course of an experiment was quantified within a 10-minute period during the different stages of the experiment. Early ectopic beats were identified as premature ventricular contraction, initiated before the end of the T wave of the previous beat. Furthermore, a dog was considered inducible when three or more TdP episodes occurred within the 10-minute interval following the onset of dofetilide administration.

The ectopic activity was expressed as an arrhythmia score (AS), calculated conform to the n+1 formula, n being the number of ectopic beats. Cardioversions were scored according to the number of interventions needed; 50, 75 or 100 points for 1, 2 or ≥3 cardioversions, respectively. For each period of the experiment, AS was calculated as the average of the three most severe arrhythmic events within the respective 10-minute intervals.[37,38]

5. Statistical analysis

Data are expressed as mean ± SD. Comparisons of serial data were performed with a one-way repeated measurement analysis of variance (ANOVA) followed by a post-hoc Bonferroni test or (un)paired Student's t-tests. Inducibility, AS and number of TdP/defibrillations were analysed with the McNemar's test, non-parametric Friedman test and Whitney U test, respectively. Results with $p<0.05$ were considered statistically significant.

Table 1. Electrophysiological effects of dofetilide and subsequent administration of hexamethonium in chronic atrioventricular block dogs (n=7).

Parameters (ms)	Baseline	Dofetilide 25 µg/kg/5min	Hexamethonium 20 mg/kg/5min
RR	1038 ± 183	1085 ± 215	1222 ± 498
PP	515 ± 87	731 ± 231	913 ± 145 **
QRS	107 ± 12	110 ± 8	108 ± 12
QTc	353 ± 32	599 ± 68 ***	590 ± 89 **
LV ARI	276 ± 47	491 ± 76 *	500 ± 102 *
RV MAPD	222 ± 17	383 ± 53 ***	395 ± 65 ***
Δ MAPD	41 ± 11	81 ± 54	84 ± 74
LV STV	2.0 ± 1.4	3.6 ± 1.6	3.3 ± 0.1
RV STV	1.6 ± 1.4	4.9 ± 1.2 *	4.6 ± 0.3 *
AS	1.3 ± 0.5	22.6 ± 24.5	22.3 ± 24.3

Values are represented as mean ± SD; Parametric (electrophysiology) and non-parametric (AS) repeated measurement ANOVA, post hoc Bonferroni comparison: * $p<0.05$, ** $p<0.01$, *** $p<0.001$ *vs.* Baseline

LV ARI: left ventricular activation recovery interval; RV MAPD: right ventricular monophasic action potential duration (measured at 80% repolarization); Δ MAPD: interventricular dispersion of repolarization (calculated as Δ MAPD = LV ARI – RV MAPD); LV STV: short-term variability of repolarization (from 30 consecutive LV MAPD/ARI); RV STV: short-term variability of repolarization (from 30 consecutive RV MAPD); AS: arrhythmia score

RESULTS

1. Pharmacological autonomic modulation

1.1 Hexamethonium: suppression experiment

Infusion of dofetilide at 25 µg/kg/5min resulted in a significant prolongation of repolarization, as reflected by the increase of QTc and LV ARI (Table 1). The reduction in repolarization reserve caused an increase in LV and RV STV (from 2.0 ± 1.4 and 1.6 ± 1.4 to 3.6 ± 1.6 (*non-significant*) and 4.9 ± 1.2 ms respectively, after *vs* before dofetilide; ($p<0.05$); Table 1). Dofetilide also induced TdP in 3/7 dogs (Figure 1A) and increased, although not statistically significant, AS (from 1.3 ± 0.5 to 22.6 ± 24.5; Figure 1A). Despite the subsequent administration of hexamethonium (20 mg/kg/5min), TdP remained present in inducible animals (Figure 1A), and AS remained unchanged (22.3 ± 24.3 after hexamethonium; Figure 1A). In addition, QTc, LV ARI, RV MAPD and RV STV were unaffected by hexamethonium administration (Table 1).

Table 2. Electrophysiological effects of dofetilide without (inducibility experiment) and with hexamethonium pre-treatment (prevention experiment) in chronic atrioventricular block dogs (n=5).

	Inducibility experiment			Prevention experiment	
Parameters (ms)	Baseline 1	Dofetilide 1 25 µg/kg/5min	Baseline 2	Hexamethonium 20 mg/kg/5min	Dofetilide 2 25 µg/kg/5min
RR	1197 ± 275	1281 ± 398	1184 ± 171	1240 ± 172	1507 ± 365
PP	580 ± 153	742 ± 203	573 ± 128	660 ±115	1018 ± 106 ‡ ** §
QRS	102 ± 19	102 ± 19	102 ± 20	103 ± 19	103 ± 20
QTc	386 ± 90	615 ± 55 ††	338 ± 68	383 ± 110	661 ± 102 ‡ **
LV MAPD/ARI	306 ± 102	460 ± 55	301 ± 96	296 ± 94	483 ± 130
RV MAPD	263 ± 72	341 ± 44 †	254 ± 49	265 ± 58	389 ± 30 ‡ *
Δ MAPD	42 ± 31	112 ± 22 †	29 ± 42	17 ± 32	79 ± 72
LV STV	2.1 ± 1.8	3.3 ± 1.3	2.2 ± 1.4	1.9 ± 1.3	3.5 ± 0.8
RV STV	1.8 ± 1.6	3.3 ± 1.9 ††	1.0 ± 0.4	0.9 ± 0.5	3.5 ± 2.1
AS	1.3 ± 0.5	27.9 ± 29.3	1.0 ± 0.0	1.3 ± 0.6	29.1 ± 23.0

Values are represented as mean ± SD
Inducibility experiment: Parametric (electrophysiology) or non-parametric (AS) paired *t*-test;
† $p<0.05$, †† $p<0.01$ *vs.* Baseline 1
Prevention experiment: Parametric (electrophysiology) or non-parametric (AS) repeated measurement ANOVA, post hoc Bonferroni comparison
* $p<0.05$, ** $p<0.01$ *vs.* Baseline 2; ‡ $p<0.05$ *vs.* Hexamethonium
Comparison inducibility experiment – prevention experiment:
Parametric (electrophysiology) or non-parametric (AS) repeated measurement ANOVA, post hoc Bonferroni comparison
§ $p<0.05$ *vs.* Dofetilide 1

LV MAPD: left ventricular monophasic action potential duration (measured at 80% repolarization); LV ARI: left ventricular activation recovery interval; RV MAPD: right ventricular monophasic action potential duration (measured at 80% repolarization); Δ MAPD: interventricular dispersion of repolarization (calculated as Δ MAPD = LV MAPD/ARI – RV MAPD); LV STV: short-term variability of repolarization (from 30 consecutive LV ARI); AS: arrhythmia score

1.2 Hexamethonium: prevention experiment

In 5 CAVB dogs, hexamethonium administration (20 mg/kg/5min) prolonged PP and RR intervals (although not significantly) as well as repolarization without affecting LV and RV STV or QRS duration (Table 2). Hexamethonium provoked no arrhythmias, but could also not prevent the incidence of dofetilide-induced arrhythmias (Figure 1B); 3/5 dogs demonstrated repeated episodes of TdP causing an increase of AS from 1.3 ± 0.6 after hexamethonium to 29.1 ± 23.0 after dofetilide (*non-significant,* Figure 1B). In addition, hexamethonium pre-treatment did not alleviate dofetilide-induced prolongation of ventricular repolarization as compared with the inducibility experiment: QTc, LV MAPD/ARI and LV STV increased similarly upon dofetilide administration

Table 3. Electrophysiological effects of dofetilide and subsequent administration of propranolol in chronic atrioventricular block dogs (n=5).

Parameters (ms)	Baseline	Dofetilide 25 µg/kg/5min	Propranolol 0.3 mg/kg/3min
RR	1494 ± 198	1700 ± 373	1793 ± 320
PP	636 ± 105	841 ± 84 *	1068 ± 80 **
QRS	92 ± 19	93 ± 20	97 ± 26
QTc	385 ± 95	614 ± 50 *	692 ± 161 *
LV MAPD/ARI	321 ± 92	457 ± 53	539 ± 173
RV MAPD	274 ± 61	331 ± 44 *	422 ± 107 *
Δ MAPD	47 ± 35	126 ± 33	117 ± 108
LV STV	1.0 ± 1.3	2.8 ± 1.3	1.7 ± 0.9
RV STV	0.9 ± 0.6	2.0 ± 0.6 *	0.8 ± 0.4
AS	1.9 ± 1.9	40.6 ± 21.6	38.8 ± 29.3

Values are represented as mean ± SD
Parametric (electrophysiology) or non-parametric (AS) repeated measurement ANOVA, post hoc Bonferroni comparison: * $p<0.05$ *vs.* Baseline

LV MAPD: left ventricular monophasic action potential duration (measured at 80% repolarization); LV ARI: left ventricular activation recovery interval; RV MAPD: right ventricular monophasic action potential duration (measured at 80% repolarization); Δ MAPD: interventricular dispersion of repolarization (calculated as Δ MAPD = LV MAPD/ARI – RV MAPD); LV STV: short-term variability of repolarization (from 30 consecutive LV MAPD/ARI); RV STV: short-term variability of repolarization (from 30 consecutive RV MAPD)
AS: arrhythmia score

(Table 2). Thus, pre-treatment with hexamethonium did not prevent TdP, nor did it impede dofetilide-induced prolongation of repolarization.

1.3 Propranolol: suppression experiment

Administration of dofetilide (25 µg/kg/5min) resulted in a comparable increase of repolarization parameters (Table 3) as observed in the hexamethonium-experiments and induced TdP in 3/5 dogs (Figure 1C). After the subsequent infusion of propranolol 0.3 mg/kg/3min, TdP remained present in the 3 initially dofetilide-inducible dogs, and AS remained high (from 40.6 ± 21.6 after dofetilide to 38.8 ± 29.3 after propranolol; Figure 1C). Nevertheless, propranolol further prolonged PP-interval and repolarization parameters (although not significantly; Table 3), suggestive of sympathetic blockade.

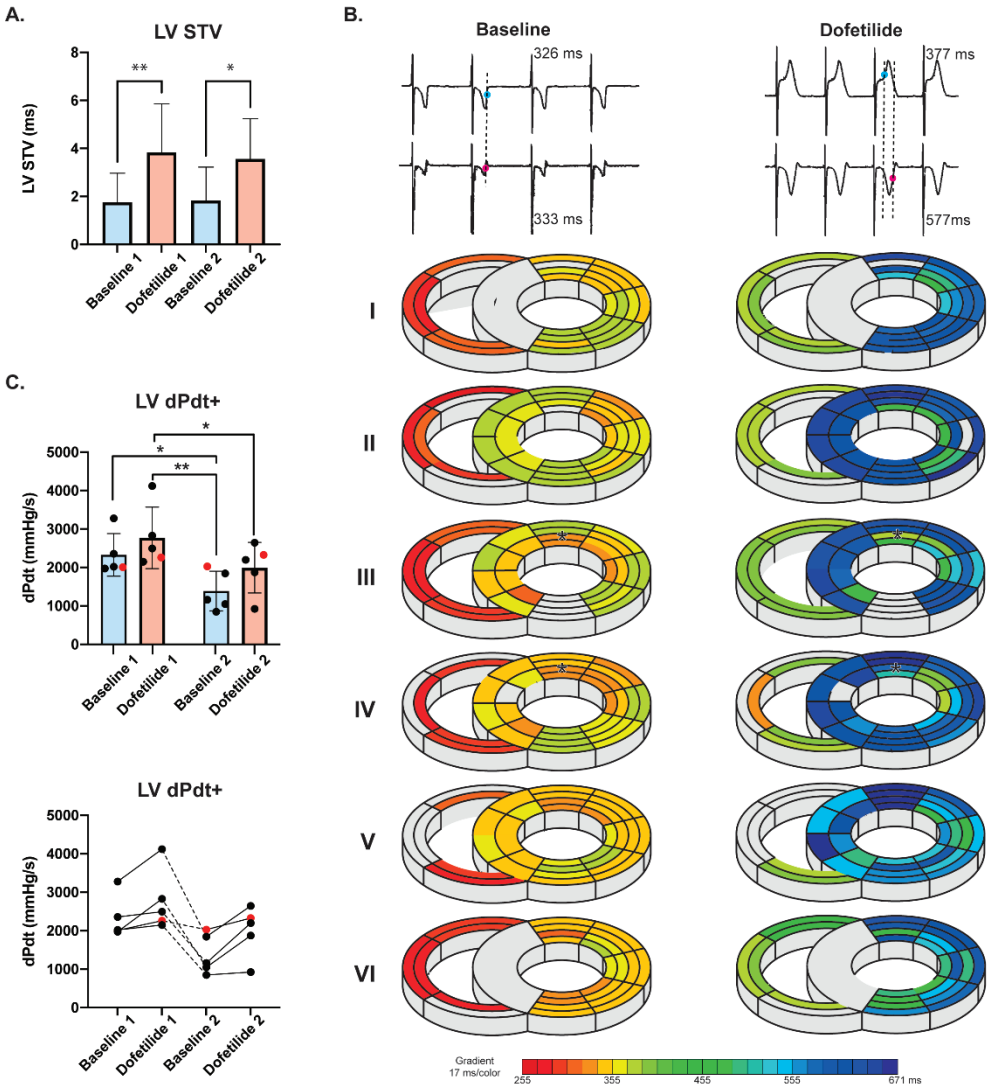

Figure 3: Overview of electrical and hemodynamic effects of bilateral stellectomy in CAVB dogs A. Left ventricular short-term variability similarly increases upon administration of dofetilide in the inducibility experiment and following bilateral stellectomy (n = 17; paired t-test). **B.** Following bilateral stellectomy, dofetilide still increases spatial dispersion of repolarization (n = 5). Local repolarization times (RT) of one animal during baseline and following dofetilide-infusion in the stellectomy experiment from base (I) to apex (VI). Traces of representative unipolar electrograms depicted by the asterisks show the increase in spatial dispersion of repolarization. Colours correspond to absolute RT values as depicted in the colour scale. **C.** Maximal rise in left ventricular pressure in the inducibility experiment (baseline 1 and dofetilide 1) and following bilateral stellectomy (baseline 2 and dofetilide 2) (n = 5; parametric two-way ANOVA). The animal that remained inducible after bilateral stellectomy is represented by the red dot. * $p<0.05$; ** $p<0.01$

Table 4. Electrophysiological effects of dofetilide before (Inducibility experiment) and following bilateral stellectomy (Sympathetic decentralization experiment) in chronic atrioventricular block dogs (n=17).

	Inducibility experiment		Decentralization experiment	
Parameters (ms)	Baseline 1	Dofetilide 1 25 µg/kg/5min	Baseline 2	Dofetilide 2 25 µg/kg/5min
RR	1300 ± 215	1444 ± 240 †††	1421 ± 231	1579 ± 395 *
PP	517 ± 45	643 ± 121 †††	732 ± 77 ||	1000 ± 260 ** §§
QRS	98 ± 13	97 ± 13	108 ± 16 ||	111 ± 17 §§
QTc	399 ± 61	560 ± 45 †††	405 ± 81	630 ± 115 ***
LV MAPD/ARI	323 ± 53	493 ± 96 †††	313 ± 67	491 ± 146 ***
RV MAPD	253 ± 29	356 ± 89 ††	279 ± 38	490 ± 142
Δ MAPD	46 ± 27	132 ± 64 ††	16 ± 9	55 ± 41
LV STV	1.8 ± 1.2	3.8 ± 2.0 ††	1.8 ± 1.4	3.6 ± 1.7 *
RV STV	0.9 ± 0.5	1.8 ± 0.9 †	0.8 ± 0.7	1.5 ± 1.2
AS	1.0 ± 0.0	47.3 ± 13.3 †	1.0 ± 0.0	10.1 ± 18.5 §

Values are represented as mean ± SD
Inducibility experiment: paired *t*-test;
† $p<0.05$, †† $p<0.01$, ††† $p<0.001$ *vs.* Baseline 1
Decentralization experiment: paired *t*-test;
* $p<0.05$, *** $p<0.001$ *vs.* Baseline 2
Comparison inducibility experiment – Decentralization experiment:
Parametric (electrophysiology) or non-parametric (AS) repeated measurement ANOVA, post hoc Bonferroni comparison
§ $p<0.05$, §§ $p<0.01$ *vs.* Dofetilide 1

LV MAPD: left ventricular monophasic action potential duration (measured at 80% repolarization); LV ARI: left ventricular activation recovery interval; RV MAPD: right ventricular monophasic action potential duration (measured at 80% repolarization); Δ MAPD: interventricular dispersion of repolarization (calculated as Δ MAPD = LV MAPD/ARI – RV MAPD); LV STV: short-term variability of repolarization (from 30 consecutive LV ARI); AS: arrhythmia score

2. Sympathetic decentralization through bilateral stellectomy

Acute bilateral stellectomy prolonged baseline PP interval (from 517 ± 45 to 732 ± 77 ms, before and after stellectomy, respectively, $p<0.05$; Table 4) and QRS duration, but had no effect on ventricular repolarization (Table 4). In the inducibility experiment, all 17 animals were TdP-inducible upon administration of dofetilide administration, which was associated with a significant increase of AS to 47.3 ± 13.3 ($p<0.05$ *vs* baseline). In the same animals, dofetilide administration after bilateral stellectomy only resulted in TdP-inducibility in 2/17 animals (Figure 2C), and AS was merely increased to 10.1 ±

18.5 (both $p<0.05$ *vs.* dofetilide in inducibility experiment; Figure 2D). However, ventricular repolarization parameters (QTc, LV MAPD/ARI, RV MAPD) were similarly increased as in the inducibility experiments, and dofetilide-induced increases in LV and RV STV were not significantly different between both experiments (Figure 3A; Table 4). High-resolution mapping experiments further demonstrated that upon administration of dofetilide, spatial dispersion of repolarization remained high in all orientations (Cubic from 118 ± 50 to 255 ± 50 ms; Figure 3B; Table 5).

Hemodynamically, bilateral stellectomy significantly decreased baseline dPdt+ from 2327 ± 553 to 1385 ± 518 mmHg/s. Upon administration of dofetilide, contractility parameters increased in both experiments, but absolute values remained significantly different (to 2769 ± 798 and 1993 ± 658, without and with stellectomy, respectively, $p<0.05$; Table 6; Figure 3C).

Table 5. Effects of dofetilide on spatial dispersion of repolarization following bilateral stellectomy in chronic atrioventricular block dogs (n=5).

	Baseline 2			Dofetilide 2		
LV-AT	73.7	±	7.4	74.1	±	7.4
RV-AT	36.9	±	4.8	37.1	±	3.9
LV- ARI	288.4	±	27.0	405.2	±	100.2
RV- ARI	265.5	±	19.8	352.4	±	56.9 *
LV-RT	362.1	±	28.7	479.3	±	98.7
RV-RT	302.4	±	15.8	389.5	±	58.9 *
Transmural dispersion	28.1	±	6.0	68.5	±	28.5 *
Vertical dispersion	53.2	±	25.8	102.8	±	28.7 *
Horizontal dispersion	44.8	±	14.9	107.1	±	39.9 *
Cubic dispersion	59.8	±	19.0	138.4	±	47.2 *
Maximal dispersion						
Transmural dispersion	86.1	±	36.0	211.2	±	66.4 *
Max Vertical dispersion	110.5	±	53.3	233.1	±	70.6 *
Max Horizontal dispersion	97.6	±	36.5	225.8	±	73.0 *
Max Cubic dispersion	117.9	±	50.2	254.5	±	50.0 *

Values are represented as mean ± SD
paired *t*-test: * $p<0.05$ *vs.* Baseline 2

LV-AT: left ventricular activation time; RV-AT: right ventricular activation time; LV ARI: left ventricular activation recovery interval; RV ARI: right ventricular activation recovery interval; LV-RT: left ventricular repolarization time; RV-RT: right ventricular repolarization time.

Table 6. Effects of dofetilide on left ventricular pressure and contractility before (Inducibility experiment) and following bilateral stellectomy (Sympathetic decentralization experiment) in chronic atrioventricular block dogs (n=5).

	Inducibility experiment		Decentralization experiment	
Parameters	Baseline 1	Dofetilide 1 25 µg/kg/5min	Baseline 2	Dofetilide 2 25 µg/kg/5min
ESP	104 ± 9	108 ± 15	91 ± 13 II §	102 ± 16 *
EDP	6 ± 1	7 ± 3	6 ± 3	6 ± 3
dPdt+	2327 ± 553	2769 ± 798	1385 ± 518 II §§	1993 ± 658 §
dPdt-	-2365 ± 305	-2175 ± 562	-1260 ± 526 II §§	-1253 ± 382 II §§

Values are represented as mean ± SD
Inducibility experiment: paired *t*-test; † $p<0.05$ *vs.* Baseline 1
Decentralization experiment: paired *t*-test;
* $p<0.05$ *vs.* Baseline 2
Comparison inducibility experiment – Decentralization experiment:
Parametric (electrophysiology) or non-parametric (AS) repeated measurement ANOVA, post hoc Bonferroni comparison
II $p<0.05$ *vs.* Baseline 1; § $p<0.05$, §§ $p<0.01$ *vs.* Dofetilide 1

ESP: end systolic pressure (mmHg); EDP: end diastolic pressure (mmHg); dPdt+: maximal rise in left ventricular pressure (mmHg/ms). dPdt-: minimal decay in left ventricular pressure (mmHg/ms).

DISCUSSION

This study explored the efficacy of various cardiac autonomic modulatory methods as antiarrhythmic strategies in the CAVB dog model. While pharmacological blockade of parasympathetic and/or sympathetic cardiac innervation did not show antiarrhythmic properties, bilateral stellectomy efficiently prevented the development of TdP in CAVB dogs. This anti-arrhythmic effect was not reflected in electrophysiological parameters, but was associated with decreased cardiac contractility and left ventricular pressure.

1. Hexamethonium

Blocking the pre- to postganglionic nerve transmission of both autonomic divisions reduced sinus and ventricular rates in prevention experiments (although non-significant). However, it did not reverse or prevent (1) dofetilide-induced prolongation of repolarization, (2) increase in beat-to-beat variability in repolarization and importantly (3) incidence of TdP. Nevertheless, the changes in rate indicate that administration of hexamethonium interfered with the autonomic input to the heart. However, this effect

appeared insufficient to reverse / prevent pro-arrhythmic conditions. Interestingly, the lack of anti-arrhythmic efficacy of hexamethonium contradicts various earlier studies. For example, De La Coussaye *et al.* (1994)[39] reported that in their study pre-treatment with hexamethonium could reduce bupivacaine-induced QTc in anesthetized dogs, and Champeroux *et al.* (2015)[40] reported that hexamethonium could alleviate dofetilide-induced increase in STV_{QTc}, and thereby limited premature ectopic beats and completely prevented incidence of TdP in 6 cynomolgous monkeys. Our study on the other hand, did not observe an anti-arrhythmic effect of hexamethonium, nor a tendency towards less pro-arrhythmic electrophysiological parameters. Possibly, these differences can be explained by methodological differences, including the awake experiments of Champeroux *et al.* (2015)[40] in contrast to the anaesthetized experiments in this study, or the use of bupivacaine (a sodium channel that also blocks neuronal activity) by De La Coussaye *et al.* (1994)[39] in contrast to dofetilide in our study. Most importantly, both abovementioned studies were performed in healthy animals. CAVB dogs on the other hand, have undergone extensive mechanical, structural and electrical adaptations that contribute to the proarrhythmic vulnerability of this model.[41] In addition, although unexplored, neural remodelling is most likely to also occur during this remodelling period. Hence, remodelling-induced autonomic imbalance in the CAVB dog, could explain the inefficacy of hexamethonium as this drug blocks the entire cardiac autonomic input and will thus not alter autonomic balance. Hence, whilst a steady, balanced, autonomic state was present in the previously mentioned studies, our model possibly suffered from autonomic imbalance due to cardiac remodelling, which could not be restored by hexamethonium.

2. Propranolol

Pharmacological sympathetic blockade by propranolol reduced sinus rates, but did not reverse dofetilide-induced increases in STV. In addition, propranolol administration reduced neither the number nor the severity of dofetilide-induced arrhythmias. This absence of antiarrhythmic effects suggests that sympatholytic effects of propranolol could not sufficiently antagonize the pro-arrhythmic effects of dofetilide sufficiently to stabilize cardiac electrophysiology to such extents that arrhythmogenesis was impeded; repolarization and STV even increased further upon administration of

propranolol, although not significantly. This lack of anti-arrhythmic effect of propranolol is in line with many human studies, which report inadequate cardioprotective effects of propranolol[42,43] and other beta-blockers.[44] Possibly the incomplete blocking of all adrenergic receptors and/or pharmacokinetic characteristics of propranolol resulted in inadequate sympatholytic effects, rendering it insufficient in overriding the proarrhythmic effects of dofetilide. Moreover, beta-blockers do not affect additional co-transmitters that are released at the level of the myocyte. For example, Neuropeptide Y (NPY) has been demonstrated to be released upon stimulation of sympathetic postganglionic nerves and to be able to modulate myocardial electrophysiology on its own.[45,46] As such, Kalla *et al.* (2020)[47] showed that in isolated Langendorff perfused rat hearts, NPY is being released upon high-level stellate stimulation. The consequential calcium mishandling could not be reverted by the β_1-blocker metoprolol alone, but was nullified by adjuvant therapy with BIBO 3304, a NPY Y1-receptor antagonist. Moreover, Hoang *et al.* (2020)[46] showed that in their *in vivo* porcine model, propranolol could not abolish sympathetic stimulation-induced changes in electrophysiology. However, adjuvant therapy with BIBO 3304 fully stabilized cardiac electrophysiology.

Hence, both pharmacological ANS-modulating approaches failed to prevent and/or suppress dofetilide-induced ventricular arrhythmias in the CAVB dog model.

3. Mechanical sympathetic decentralization of the heart

Bilateral stellectomy effectively and significantly lowered TdP-inducibility in CAVB dogs. Surprisingly, this effect was associated with 1) a similar dofetilide-induced prolongation of repolarization in stellectomized and control animals 2) similar increases in LV and RV STV as in non-stellectomized animals (Figure 3A). Moreover, the additional high-resolution *in vivo* mapping studies also demonstrated that the reduction in arrhythmogenesis was not due to an abolishment of spatial dispersion of repolarization (Figure 3B). This was surprising as stellate ganglia stimulation has repeatedly been demonstrated to increase spatial dispersion of repolarization in other animal models.[24,48–50] However, upon dofetilide infusion, spatial dispersion of repolarization increased to similar values as in CAVB dogs that had not undergone this intervention (historical data).[32] Therefore, in our study, the dofetilide-induced increase in spatial dispersion of repolarization appears to mainly result from

(ventricular remodelling-induced) intrinsic heterogeneity in electrical properties, rather than from ANS modulation.

Hemodynamically, stellectomy did cause significant changes in contractile parameters. Comparing both baseline and dofetilide conditions, dPdt+ was significantly decreased in comparison to the inducibility experiment. Hence, sympathetic decentralization depressed the inotropic capacity of the heart, causing the pressure to never exceed the levels that it was in the inducibility experiment. As altered calcium handling underlies arrhythmogenesis in the CAVB dog model and higher contractile force has been associated with a more pro-arrhythmic phenotype, it seems reasonable that the depressed effects on inotropy might reflect a stabilization of calcium handling which translated in non-inducibility of the affected animals. This corresponds to the observation that one of the animals that remained inducible after stellectomy did not show this reduction in inotropy after stellectomy (Figure 3C, lower panel; Inducible animal in red). Our observations are consistent with the role of increased left ventricular pressure on arrhythmogenesis in isolated pig hearts.[51]

4. *Mechanical vs pharmacological autonomic modulation*

The conflicting antiarrhythmic efficacy of pharmacological and mechanical approaches could be explained by the extent to which the interventions modulate and impede autonomic activity. Whereas pharmacological blockade by hexamethonium and propranolol both target *efferent* signalling, bilateral stellectomy interferes with both *efferent* and *afferent* neurons traversing the stellate ganglia.[14] Consequently, the cardiac - stellate ganglia - cardiac reflex loop is also completely severed. Moreover, as previously mentioned, propranolol does not block all sympathetic co-transmitters. These additional effects are hindered with the more proximal sympathetic interference, including hexamethonium and bilateral stellectomy. However, as hexamethonium is also a pharmacological approach, it equally has the drawback that it depends on drug-receptor interactions and is thus less likely to establish a complete blockade of nerve transmission, whilst also, as previously mentioned, potentially not affecting the relative activity of both divisions. Hence, the more complete decentralization through bilateral sympathectomy appears to result in an additional anti-arrhythmic effect that cannot be replicated through (systemic) pharmacological approaches.

5. Contribution of autonomic nervous system in arrhythmogenesis

A number of studies have demonstrated the contribution of ANS in the process of arrhythmogenesis.[13,52–58] In addition, our own prior observations in the CAVB dog model, though unpublished, also suggest the involvement of ANS in the development of TdP. Examples hereof include the lack of dofetilide-induced TdP in Langendorff blood perfused hearts from *in vivo* TdP-inducible CAVB dogs. Furthermore, the administration of sympathomimetic drugs, such as adrenaline, to anesthetized CAVB dogs commonly results in ventricular tachycardia and fibrillation. As autonomic modulation is clearly involved in arrhythmogenesis in the CAVB dog model, the lack of antiarrhythmic effects following the aforementioned pharmacological neuromodulations could not be explained by an absence of autonomic influence on cardiac electrophysiology in the CAVB dog. Moreover, bilateral stellectomy was highly anti-arrhythmic. Interestingly, this efficacy of bilateral stellectomy also indicates that the pro-arrhythmic effects of sympathetic stimulation remain present under anesthetized conditions. The anaesthetics used (pentobarbital and isoflurane) facilitate arrhythmogenesis in our model[59] by inhibiting outward potassium currents (I_{Kr} and I_{Ks}). However, they simultaneously depress autonomic activity.[60] As bilateral stellectomy could impede arrhythmogenesis under conditions wherein autonomic activity was depressed, this only further highlights the powerful pro-arrhythmic effects of cardiac autonomic imbalance. Surprisingly, we observed that the detrimental effects of SNS stimulation are also present in unremodelled conditions (data not shown): in two unremodelled, acute AV-block animals, stimulation of the stellate ganglion and subsequent administration of dofetilide (with a recovery period of >1 hour in between) triggered the development of ventricular arrhythmias that could not be terminated by electrical defibrillation. However, a similar protocol does not cause TdP in *remodelled* animals wherein a bilateral stellectomy is performed following stellate stimulation and before dofetilide-challenge. Hence, persistent SNS activity in the stellate ganglia appears to be able to induce ventricular arrhythmias in unremodelled animals when additional pro-arrhythmic conditions are present.

Thus, our study provides evidence for a differential effect of ANS-modulation in remodelled and not remodelled heart, and points to an important anti-arrhythmic effect of pressure reduction. The latter has been observed clinically.[61] Thus our observations

can have farfetched effects on the development of novel neuromodulatory therapies and clinical implementation.

STUDY LIMITATIONS

Pacing conditions differed between various experiments. Eighteen experiments were necessarily conducted under pacing conditions, whereas the dogs of 38 experiments were studied in IVR. In general, an arrhythmic study is best conducted under IVR conditions, as bradycardia and the unstable origin of activity pose an additional proarrhythmic threat to the heart. Not all IVR rhythms can however be safely sustained when the dogs are anaesthetized. Furthermore, an acute change of the IVR focus can cause a morphologic change of the ECG, thereby causing difficulties for the subsequent examination and possibly rendering the recorded data unreliable for analysis. Ventricular pacing, because of the controlled rate and pattern of activation, allows the comparison of electrophysiological parameters within and between experiments, but may mask heart rate variability or the bradycardic effects of a drug.

Lastly, no direct measurements of the activity of the ANS were made. Therefore, the extent to which autonomic stimuli were suppressed was not addressed. The doses administered were however based on prior experiments of Champeroux and colleagues[40] that had demonstrated to cause a complete cardiac autonomic or sympathetic block, respectively. Also, the drug-induced changes in electrophysiological parameters observed in the prevention experiments validated proper pharmacodynamics of both drugs.

CONCLUSION

Bilateral stellectomy, but not pharmacological ANS-modulation, was highly antiarrhythmic in CAVB dogs. This anti-arrhythmic effect was associated with decreased cardiac contractility and left ventricular pressure.

REFERENCES

1. Akar FG, Spragg DD, Tunin RS, Kass DA, Tomaselli GF. Mechanisms Underlying Conduction Slowing and Arrhythmogenesis in Nonischemic Dilated Cardiomyopathy. *Circ Res* 2004;95:717–725.
2. Coumel P. The management of clinical arrhythmias. An overview on invasive versus non-invasive electrophysiology. *Eur Heart J* 1987;8:92–99.
3. Jalife J. Ventricular Fibrillation: Mechanisms of Initiation and Maintenance. *Annu Rev Physiol* 2000;62:25–50.
4. Rubart M, Zipes DP. Mechanisms of sudden cardiac death. *J Clin Invest* 2005;115:2305–2315.
5. Vandersickel N, Boer TP de, Vos MA, Panfilov A V. Perpetuation of Torsade de Pointes in heterogeneous hearts: competing foci or re-entry? *J Physiol* 2016;594:6865–6878.
6. Adabag AS, Luepker R V., Roger VL, Gersh BJ. Sudden cardiac death: Epidemiology and risk factors. *Nat Rev Cardiol* 2010;7:216–225.
7. Benjamin EJ, Muntner P, Alonso A, Bittencourt MS, Callaway CW, Carson AP, Chamberlain AM, Chang AR, Cheng S, Das SR, Delling FN, Djousse L, Elkind MSV, Ferguson JF, Fornage M, Jordan LC, Khan SS, Kissela BM, Knutson KL, Kwan TW, Lackland DT, Lewis TT, Lichtman JH, Longenecker CT, Loop MS, Lutsey PL, Martin SS, Matsushita K, Moran AE, Mussolino ME, et al. Heart Disease and Stroke Statistics-2019 Update: A Report From the American Heart Association. *Circulation* 2019;139:e56–e528.
8. Grandi E, Ripplinger CM. Antiarrhythmic mechanisms of beta blocker therapy. *Pharmacol Res* 2019;146:104274.
9. Al-Khatib SM, Stevenson WG, Ackerman MJ, Bryant WJ, Callans DJ, Curtis AB, Deal BJ, Dickfeld T, Field ME, Fonarow GC, Gillis AM, Granger CB, Hammill SC, Hlatky MA, Joglar JA, Kay GN, Matlock DD, Myerburg RJ, Page RL. 2017 AHA/ACC/HRS Guideline for Management of Patients With Ventricular Arrhythmias and the Prevention of Sudden Cardiac Death: Executive Summary: A Report of the American College of Cardiology/American Heart Association Task Force on Clinical Practice Gui. *Circulation* 2018;138:e210–e271.

10. Goldberger JJ, Arora R, Buckley U, Shivkumar K. Autonomic Nervous System Dysfunction: JACC Focus Seminar. *J Am Coll Cardiol* 2019;73:1189–1206.
11. Ardell JL, Armour JA. Neurocardiology: Structure-Based Function. *Comprehensive Physiology* Hoboken, NJ, USA: John Wiley & Sons, Inc.; 2016. p. 1635–1653.
12. Jänig W. Sympathetic nervous system and inflammation: A conceptual view. *Auton Neurosci Basic Clin* 2014;182:4–14.
13. Fukuda K, Kanazawa H, Aizawa Y, Ardell JL, Shivkumar K. Cardiac Innervation and Sudden Cardiac Death. *Circ Res* 2015;116:2005–2019.
14. Armour JA, Ardell JL. Basic and Clinical Neurocardiology. New York: Oxford University Press; 2004.
15. Jänig W. The integrative action of the autonomic nervous system: Neurobiology of homeostasis. Integr. Action Auton. Nerv. Syst. Neurobiol. Homeost. Cambridge, New York: Cambridge University Press; 2006.
16. Randall WC. "Efferent sympathetic innervation of the heart" in Neurocardiology. Armour JA, Ardell JL, eds. Oxford University Press, New York; 1994.
17. Hopkins DA, Bieger D, Vente J De, Steinbusch HWM. Vagal efferent projections: Viscerotopy, neurochemistry and effects of vagotomy. *Prog Brain Res* 1996;107:79–96.
18. Armour JA, Collier K, Kember G, Ardell JL. Differential selectivity of cardiac neurons in separate intrathoracic autonomic ganglia. *Am J Physiol - Regul Integr Comp Physiol* 1998;274.
19. Pauza DH, Rysevaite-Kyguoliene K, Vismantaite J, Brack KE, Inokaitis H, Pauza AG, Rimasauskaite-Petraitiene V, Pauzaite JI, Pauziene N. A combined acetylcholinesterase and immunohistochemical method for precise anatomical analysis of intrinsic cardiac neural structures. *Ann Anat* 2014;196:430–440.
20. Bers DM. Calcium cycling and signaling in cardiac myocytes. *Annu Rev Physiol* 2008;70:23–49.
21. Weiss JN, Garfinkel A, Karagueuzian HS, Chen PS, Qu Z. Early afterdepolarizations and cardiac arrhythmias. *Heart Rhythm* 2010;7:1891–1899.

22. Xie Y, Grandi E, Puglisi JL, Sato D, Bers DM. β-adrenergic stimulation activates early afterdepolarizations transiently via kinetic mismatch of PKA targets. *J Mol Cell Cardiol* 2013;58:153–161.
23. Jiang H, Lu Z, Yu Y, Zhao D, Yang B, Huang C. Relationship between sympathetic nerve sprouting and repolarization dispersion at peri-infarct zone after myocardial infarction. *Auton Neurosci Basic Clin* 2007;134:18–25.
24. Meijborg VMF, Boukens BJD, Janse MJ, Salavatian S, Dacey MJ, Yoshie K, Opthof T, Swid MA, Hoang JD, Hanna P, Ardell J, Shivkumar K, Coronel R. Stellate ganglion stimulation causes spatiotemporal changes in ventricular repolarization in pig. *Heart Rhythm* 2020;17:795–803.
25. Myles RC, Wang L, Kang C, Bers DM, Ripplinger CM. Local β-adrenergic stimulation overcomes source-sink mismatch to generate focal arrhythmia. *Circ Res* 2012;110:1454–1464.
26. Ajijola O, Vaseghi M, Mahajan A, Shivkumar K. Bilateral cardiac sympathetic denervation: why, who and when? *Expert Rev Cardiovasc Ther* 2012;10:947–949.
27. Vaseghi M, Gima J, Kanaan C, Ajijola OA, Marmureanu A, Mahajan A, Shivkumar K. Cardiac sympathetic denervation in patients with refractory ventricular arrhythmias or electrical storm: Intermediate and long-term follow-up. *Heart Rhythm* 2014;11:360–366.
28. Vaseghi M, Barwad P, Malavassi Corrales FJ, Tandri H, Mathuria N, Shah R, Sorg JM, Gima J, Mandal K, Sàenz Morales LC, Lokhandwala Y, Shivkumar K. Cardiac Sympathetic Denervation for Refractory Ventricular Arrhythmias. *J Am Coll Cardiol* 2017;69:3070–3080.
29. Oros A, Beekman JDM, Vos MA. The canine model with chronic, complete atrio-ventricular block. *Pharmacol Ther* 2008;119:168–178.
30. Bossu A, Varkevisser R, Beekman HDM, Houtman MJC, Heyden MAG van der, Vos MA. Short-term Variability of Repolarization Is Superior to Other Repolarization Parameters in the Evaluation of Diverse Antiarrhythmic Interventions in the Chronic Atrioventricular Block Dog. *J Cardiovasc Pharmacol* J 2017;69:398–407.

31. Wu G, DeSimone C V, Suddendorf SH, Asirvatham RS, Asirvatham SJ, Huang C, Chen P-S, Cha Y-M. Effects of stepwise denervation of the stellate ganglion: Novel insights from an acute canine study. *Heart Rhythm* 2016;13:1395–1401.
32. Dunnink A, Stams TRG, Bossu A, Meijborg VMF, Beekman JDM, Wijers SC, Bakker JMT De, Vos MA. Torsade de pointes arrhythmias arise at the site of maximal heterogeneity of repolarization in the chronic complete atrioventricular block dog. *Europace* 2017;19:858–865.
33. Water A Van de, Verheyen J, Xhonneux R, Reneman RS. An improved method to correct the QT interval of the electrocardiogram for changes in heart rate. *J Pharmacol Methods* 1989;22:207–217.
34. Coronel R, Bakker JM De, Wilms-Schopman FJ, Opthof T, Linnenbank AC, Belterman CN, Janse MJ. Monophasic action potentials and activation recovery intervals as measures of ventricular action potential duration: experimental evidence to resolve some controversies. *Heart Rhythm* 2006;3:1043–1050.
35. Thomsen MB, Verduyn SC, Stengl M, Beekman JDM, Pater G de, Opstal J van, Volders PGA, Vos MA. Increased Short-Term Variability of Repolarization Predicts Sotalol–Induced Torsades de Pointes in Dogs. *Circulation* 2004;110:2453–2459.
36. Potse M, Linnenbank AC, Grimbergen CA. Software design for analysis of multichannel intracardial and body surface electrocardiograms. *Comput Methods Programs Biomed* 2002;69:225–236.
37. Stams TRG, Winckels SKG, Oros A, Varkevisser R, Oosterhoff P, Nagel R van der, Beekman HDM, Vos MA. Novel Parameters to Improve Quantification of Repolarization Reserve and Arrhythmogenesis Using a Dofetilide Challenge. Abstract. *Heart Rhythm* 2013;10:1745–1746.
38. Smoczynska A, Beekman HDM, Vos MA. The increment of short-term variability of repolarisation determines the severity of the imminent arrhythmic outcome. *Arrhythmia Electrophysiol Rev* 2019;8:166–172.
39. La Coussaye JE de, Eledjam JJ, Bruelle P, Lefrant JY, Bassoul B, Peray PA, Desch G, Antoine S. Mechanisms of the Putative Cardioprotective Effect of

Hexamethonium in Anesthetized Dogs Given a Large Dose of Bupivacaine. *Anesthesiology* 1994;80:595–605.

40. Champeroux P, Thireau J, Judé S, Laigot-Barbé C, Maurin A, Sola ML, Fowler JSL, Richard S, Guennec JY Le. Short-term variability in QT interval and ventricular arrhythmias induced by dofetilide are dependent on high-frequency autonomic oscillations. *Br J Pharmacol* 2015;172:2878–2891.
41. Dunnink A, Opstal JM van, Oosterhoff P, Winckels SKG, Beekman JDM, Nagel R van der, Cora Verduyn S, Vos MA. Ventricular remodelling is a prerequisite for the induction of dofetilide-induced torsade de pointes arrhythmias in the anaesthetized, complete atrio-ventricular-block dog. *Europace* 2012;14:431–436.
42. Sumitomo N, Harada K, Nagashima M, Yasuda T, Nakamura Y, Aragaki Y, Saito A, Kurosaki K, Jouo K, Koujiro M, Konishi S, Matsuoka S, Oono T, Hayakawa S, Miura M, Ushinohama H, Shibata T, Niimura I. Catecholaminergic polymorphic ventricular tachycardia: electrocardiographic characteristics and optimal therapeutic strategies to prevent sudden death. *Heart* 2003;89:66–70.
43. Priori SG, Napolitano C, Memmi M, Colombi B, Drago F, Gasparini M, DeSimone L, Coltorti F, Bloise R, Keegan R, Cruz Filho FES, Vignati G, Benatar A, DeLogu A. Clinical and Molecular Characterization of Patients With Catecholaminergic Polymorphic Ventricular Tachycardia. *Circulation* 2002;106:69–74.
44. Chatzidou S, Kontogiannis C, Tsilimigras DI, Georgiopoulos G, Kosmopoulos M, Papadopoulou E, Vasilopoulos G, Rokas S. Propranolol Versus Metoprolol for Treatment of Electrical Storm in Patients With Implantable Cardioverter-Defibrillator. *J Am Coll Cardiol* 2018;71:1897–1906.
45. Heredia MDP, Delgado C, Pereira L, Perrier R, Richard S, Vassort G, Bénitah JP, Gómez AM. Neuropeptide Y rapidly enhances [Ca 2+] i transients and Ca 2+ sparks in adult rat ventricular myocytes through Y 1 receptor and PLC activation. *J Mol Cell Cardiol* 2005;38:205–212.

46. Hoang JD, Salavatian S, Yamaguchi N, Swid MA, Vaseghi M. Cardiac sympathetic activation circumvents high-dose beta blocker therapy in part through release of neuropeptide Y. *JCI Insight* 2020;5:e135519.

47. Kalla M, Hao G, Tapoulal N, Tomek J, Liu K, Woodward L, Dall'Armellina E, Banning AP, Choudhury RP, Neubauer S, Kharbanda RK, Channon KM, Ajijola OA, Shivkumar K, Paterson DJ, Herring N. The cardiac sympathetic co-transmitter neuropeptide Y is pro-arrhythmic following ST-elevation myocardial infarction despite beta-blockade. *Eur Heart J* 2020;41:2168–2179.

48. Ajijola OA, Yagishita D, Patel KJ, Vaseghi M, Zhou W, Yamakawa K, So E, Lux RL, Mahajan A, Shivkumar K. Focal myocardial infarction induces global remodeling of cardiac sympathetic innervation: neural remodeling in a spatial context. *Am J Physiol Hear Circ Physiol* 2013;305:1031–1040.

49. Vaseghi M, Yamakawa K, Sinha A, So EL, Zhou W, Ajijola OA, Lux RL, Laks M, Shivkumar K, Mahajan A. Modulation of regional dispersion of repolarization and T-peak to T-end interval by the right and left stellate ganglia. *Am J Physiol - Heart Circ Physiol* 2013;305:1020–1030.

50. Yagishita D, Chui RW, Yamakawa K, Rajendran PS, Ajijola OA, Nakamura K, So EL, Mahajan A, Shivkumar K, Vaseghi M. Sympathetic Nerve Stimulation, Not Circulating Norepinephrine, Modulates T-Peak to T-End Interval by Increasing Global Dispersion of Repolarization. *Circ Arrhythmia Electrophysiol* 2015;8:174–185.

51. Coronel R, Wilms-Schopman FJG, Degroot JR. Origin of ischemia-induced phase 1b ventricular arrhythmias in pig hearts. *J Am Coll Cardiol* 2002;39:166–176.

52. Cao J-M, Chen LS, KenKnight BH, Ohara T, Lee M-H, Tsai J, Lai WW, Karagueuzian HS, Wolf PL, Fishbein MC, Chen P-S. Nerve Sprouting and Sudden Cardiac Death. *Circ Res* 2000;86:816–821.

53. Chen LS, Zhou S, Fishbein MC, Chen P-S. New Perspectives on the Role of Autonomic Nervous System in the Genesis of Arrhythmias. *J Cardiovasc Electrophysiol* 2007;18:123–127.

54. Jiang Z, Zhao Y, Doytchinova A, Kamp NJ, Tsai W-C, Yuan Y, Adams D, Wagner D, Shen C, Chen LS, Everett TH, Lin S-F, Chen P-S. Using skin

sympathetic nerve activity to estimate stellate ganglion nerve activity in dogs. *Heart Rhythm* 2015;12:1324–1332.

55. Podrid PJ, Fuchs T, Candinas R. Role of the sympathetic nervous system in the genesis of ventricular arrhythmia. *Circulation* 1990;82:I103-13.
56. Schwartz PJ. The rationale and the role of left stellectomy for the prevention of malignant arrhythmias. *Ann N Y Acad Sci* 1984;427:199–221.
57. Shen MJ, Zipes DP. Role of the Autonomic Nervous System in Modulating Cardiac Arrhythmias This Review is in a thematic series on The Autonomic Nervous System and the Cardiovascular System, which includes the following articles: Role of the Autonomic Nervous System in Modula. *Circ Res* 2014;114:1004–1021.
58. Zhou S, Jung BC, Tan AY, Trang VQ, Gholmieh G, Han SW, Lin SF, Fishbein MC, Chen PS, Chen LS. Spontaneous stellate ganglion nerve activity and ventricular arrhythmia in a canine model of sudden death. *Heart Rhythm* 2008;5:131–139.
59. Dunnink A, Sharif S, Oosterhoff P, Winckels S, Montagne D, Beekman J, Nagel R van der, Heyden MAG van der, Vos MA. Anesthesia and Arrhythmogenesis in the Chronic Atrioventricular Block Dog Model. *J Cardiovasc Pharmacol* 2010;55:601–608.
60. Neukirchen M, Kienbaum P, Warner DS, Warner MA. Sympathetic Nervous SystemEvaluation and Importance for Clinical General Anesthesia. *Anesthesiology* 2008;109:1113–1131.
61. Mukherjee D, Feldman MS, Helfant RH. Nitroprusside Therapy: Treatment of Hypertensive Patients With Recurrent Resting Chest Pain, ST-Segment Elevation, and Ventricular Arrhythmias. *JAMA* 1976;235:2406–2409.

Valerie Y. H. van Weperen, Jet D. M. Beekman, Claire Mackaaij, Joanne J.A. van Bavel, Marcel G. J. Nederhoff, Toon A. B. van Veen & Marc A. Vos

In preparation

CHAPTER 6

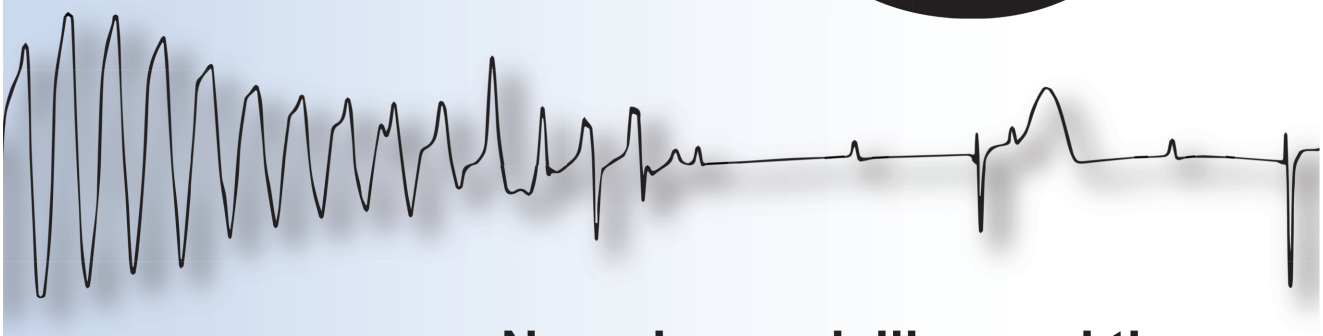

Neural remodelling and the development of cardiac sympathetic overdrive in the chronic AV-block dog

ABSTRACT

Background: Neural remodelling following non-ischemic cardiac injury is poorly understood. This study explored functional and cellular consequences of neural remodelling in the chronic atrioventricular-block (CAVB) dog model over time.

Methods: Awake surface electrogram recordings were made under sinus rhythm (SR; n=13), three ($CAVB_3$; n=9) five ($CAVB_5$; n=8) and eleven ($CAVB_{11}$; n=3) weeks after atrioventricular-block for heart rate variability analyses, including low-to-high frequency power (LF/HF). Anaesthetized experiments were performed at SR (n=5), $CAVB_5$ (n=8) and $CAVB_{11}$ (n=4) and continuously recorded surface electrograms, left ventricular (LV) pressure and intraventricular electrograms from a LV multipolar catheter. Baroreflex sensitivity (BRS), after injection of 1.5 µg/kg nitroprusside, was quantified as the relationship between beat-to-beat changes in PP-interval and LV pressure. Changes in dispersion of repolarization (∆DoR; quantified as repolarization time variance) upon left stellate ganglion (LSG) stimulation were compared over time. ∆DoR was also measured upon vagal nerve stimulation (VNS; n=4). LSG from CAVB and SR dogs (n=4 each, age-matched) were histologically examined.

Results: Following AV-block LF/HF seemed to increase progressively, whilst BRS decreased from 2.6±2.0 (SR) to 0.3±0.15 ms/mmHg ($CAVB_{11}$; $p<0.05$ *vs* SR). Over time, effects of LSG on DoR were augmented (from +1.0±0.1% (SR) to +3.0±1.0% ($CAVB_{11}$; $p<0.05$ *vs* SR)). In contrast, VNS tended to decrease DoR (∆DoR: 0.75±0.40%, *non*-significant). LSG neuronal size was significantly increased in CAVB animals (1055±313 *vs* 789±235µm^2 in SR; $p<0.05$).

Conclusion: CAVB induces sympatho-excitation, characterized by LSG neuronal hypertrophy, depressed BRS and seemingly elevated LF/HF. Over time, LSG stimulation increases DoR more, whereas VNS might achieve the opposite.

INTRODUCTION

Cardiovascular death remains the leading cause of mortality worldwide.[1] Sudden cardiac death (SCD), most often resulting from ventricular arrhythmias (VAs), constitutes approximately 60% of these deaths.[2] Thus far, beta-blockers are the only drugs that significantly lower mortality when used in primary or secondary prevention of SCD. The efficacy of these drugs lies in their ability to impede cardiac sympathetic overdrive, which often is one of the consequences of cardiac disease. Correspondingly, neuromodulatory therapies that aim to restore these autonomic imbalances are highly effective and rapidly becoming a compelling anti-arrhythmic avenue for patients refractory to more traditional therapies.

In response to cardiac injury, various remodelling processes are initiated that culminate in sympathetic activation and parasympathetic dysfunction. Amongst other changes, sympathetic overactivity is characterized by neuronal hypertrophy, glial activation, and inflammation in stellate ganglia.[3] Cardiac function benefits from this sympathetic stimulation in the short term, but chronic, excessive sympatho-excitation progresses heart failure and increases the risk of VAs and thus SCD.[4] In addition, lower heart rate variability (HRV) and depressed baroreflex sensitivity, physiological indices of increased cardiac sympathetic tone, have repetitively been shown to be negative prognostic factors for all-cause mortality, VAs and SCD in heart failure patients.[5]

The mechanisms by which overt sympathetic activation is induced and how it promotes arrhythmogenesis have most extensively been studied in the setting of ischemic injury. Under those conditions, an acute ischemic event induces neural remodelling, predominantly in the dense scar and infarct border zone. Accordingly, this region has been well-established to be most vulnerable to sympathetically-induced arrhythmic triggers and increases in spatial dispersion of repolarization (SDR), thereby reinforcing the arrhythmic substrate.[6] Similarly, neuromodulatory techniques that restore the sympatho-vagal balance have mostly been examined in experimental and clinical studies of ischemic heart disease.[4,7]

Nevertheless, excessive sympathetic activation is also intricately involved in the pathophysiology of non-ischemic cardiomyopathies. Accordingly, the efficacy of beta-blocking drugs have long been demonstrated in these patients,[8] and novel neuromodulatory strategies such as cardiac sympathetic denervation, have been

shown to effectively impede ventricular arrhythmogenesis in this population.[9–11] Moreover, ablation of the arrhythmic substrate in the setting of non-ischemic injury is associated with worse outcomes than in ischemic cardiomyopathy patients.[12–14] This further suggests that there is a highly functional aetiology underlying arrhythmias in non-ischemic cardiomyopathy which is likely driven by autonomic dysfunction. However, neural remodelling in the setting of non-ischemic cardiac injury is largely uncharacterized. Moreover, translating the knowledge on neural remodelling in ischemic cardiomyopathy patients to the non-ischemic cardiomyopathy setting is difficult as the initiating event and arrhythmic substrates differ vastly.

Therefore, we aimed to combine histological and functional techniques to characterize neural remodelling in the chronic AV-block (CAVB) dog model, a non-ischemic animal model that has been validated extensively and proven to be an excellent representation of compensated heart failure.[15–17] In this model, intra-cardiac remodelling processes (contractile, structural and electrical)[15,17–20] in conjunction with neural remodelling restore cardiac output after AV-node ablation, but simultaneously promote TdP-susceptibility.[21] The role of sympathetic activation as a fundamental contributor to ventricular arrhythmogenesis in the CAVB model has already been established in a previous study, in which the high anti-arrhythmic efficacy of bilateral sympathetic denervation was reported.[22]

The current study demonstrates that in the CAVB dog model, non-ischemic injury induces a condition characterized by relative sympathetic hyperactivity. This autonomic dysfunction is reflected in a decreased HRV, depressed baroreflex sensitivity and increased spatial dispersion of repolarization upon sympathetic activation. Histologically, remodelling of the stellate ganglia results in neuronal hypertrophy.

METHODS

All experiments were approved by 'the Committee for Experiments on Animals' of Utrecht University, the Netherlands. Animal handling and care was in accordance with the Directive 2010/63/EU of the European Parliament and of the Council of 22 September 2010 on the protection of animals used for scientific purposes and the Dutch Law on animal experimentation.

This study included serial testing of 13, adult purpose-bred mongrel dogs (7 males, 27 ± 2 kg, Marshall, USA). Additionally, four inducible CAVB animals (11 ± 1 weeks CAVB) and four sinus rhythm control animals were used for immunohistochemical purposes.

Awake ECGs

Awake 6-leads surface electrocardiogram (ECG) recordings were made for a duration of five minutes at 3 weeks after CAVB ($CAVB_3$), 5 weeks after CAVB ($CAVB_5$), and 11 weeks after CAVB ($CAVB_{11}$). To promote animal familiarity with the procedure around these awake recordings, dogs were transferred to the ECG room and connected to the ECG leads on a weekly basis. Prior to all recordings, dogs were given some time to further acclimatize to the room. During the recording, animals were manually held in a seated position and exposed to minimal external stimuli. As animals were not yet accustomed to the ECG room and recording procedure at sinus rhythm, these recordings were shortened to <1 minute.

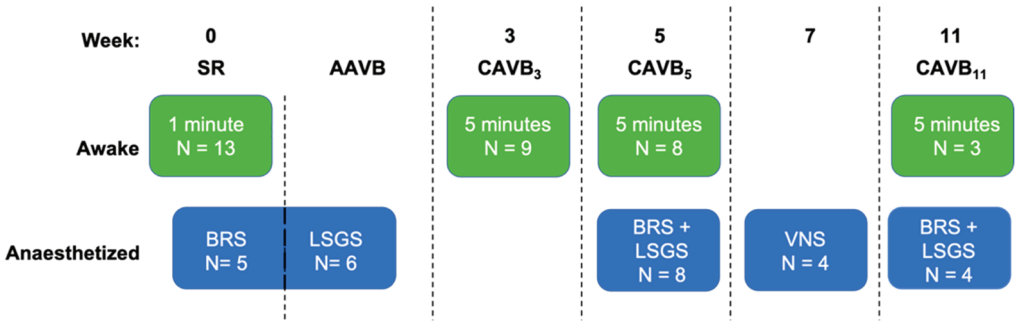

Figure 1. Schematic overview of the experimental setup. Awake and anaesthetized experiments were performed at different timepoints. Duration of awake electrogram recordings and autonomic tests of the anaesthetized experiments are shown. Number of animals included at the different stages are also shown. SR: Sinus Rhythm. AAVB: Acute AV-Block. CAVB: Chronic AV-block, BRS: Baroreflex sensitivity. LSGS: Left stellate ganglion stimulation. VNS: Vagal nerve stimulation.

Animal preparation

Animals were subjected to multiple serial experiments (Figure 1), in which autonomic tone and/or cardiac response to sympathetic or parasympathetic stimulation were assessed. These experiments were performed and compared between sinus rhythm (week 0), $CAVB_5$ and $CAVB_{11}$.

All experiments were performed under general anaesthesia. Animals were premedicated 30 minutes prior to the induction of anaesthesia. Premedication included methadone (0.5 mg/kg, *i.m.*), acepromazine (0.5 mg/kg, *i.m.*), atropine (0.02 mg/kg, *i.m.*) and metacam (0.1 mg/kg, *s.c.*). Anaesthesia was induced with pentobarbital sodium (25 mg/kg, *i.v.*) and maintained by isoflurane (1.5%, *inh*) mixed with O_2 and N_2O (1:2 ratio). Following the experiment, animals were given buprenorphine (0.3 mg, *i.m.*), and metacam (0.1 mg/kg, *p.o.*) was administered for five consecutive days. Antibiotics were given before (ampicillin 1000 mg, *i.v.*) and for five days after the experiments (amoxicillin-clavulanic acid 250 mg, *p.o.*). During the first experiment, complete atrio-ventricular block was induced by radiofrequency ablation of the proximal His-bundle. Animals were allowed a minimum of 3 weeks of recovery before subsequent experiments were performed. In 2 animals, idioventricular rhythm was too slow to sustain sufficient cardiac output. Therefore, a right ventricular pacing lead (Medtronic, Maastricht, the Netherlands) was introduced *via* the femoral vein, connected to a pacemaker, and set to pace the animals at a frequency of 40 beats/minute.

Experiments

All anaesthetized experiments (Figure 1) included the continuous recording of a 6-leads surface ECG, four precordial leads, a left ventricular (LV) 7 Fr pig-tail pressure catheter and an LV duo-decapolar catheter (Medtronic, Minneapolis, MN, USA).

Stellate ganglion stimulation

The left stellate ganglion was isolated through a left-sided thoracotomy between intercostal 1-2 or 2-3. Upon identification, the left stellate ganglion was minimally dissected. Custom-made bipolar needle electrodes, connected to a Grass stimulator, were used to stimulate the left stellate ganglion at 4Hz, 4ms (square wave), at 2 times

the threshold (determined as the voltage which caused a 10% increase in arterial blood pressure).[23] After left stellate ganglion stimulation (LSGS), needle electrodes were carefully removed, lungs were inflated to minimize the iatrogenic pneumothorax and the thorax was closed in layers.

Vagus nerve stimulation

The right-sided vagus nerve was exposed by a lateral neck cutdown, identified within the carotid sheath, and carefully dissected from surrounding structures. Custom-made bipolar hook electrodes, connected to a Grass Stimulator, stimulated the vagus nerve at 4Hz, 4ms duration (square wave), and at 1.2 times the threshold (defined as the voltage that caused a 10% increase in PP-interval).[24] Stimulation was maintained with a 100% duty cycle for 10 minutes.

Baroreflex sensitivity

Baseline values for heart rate, PP-interval, and LV pressure were recorded for at least five minutes. Nitroprusside (Sigma Chemical Co., Saint Louis, MO, USA) was dissolved in 0.9% NaCl and administered as an *i.v.* bolus injection (1.5 µg/kg) to evoke a 10-20 mmHg decrease in arterial blood pressure (Figure 2A). Hemodynamic and electrical parameters were given approximately 20 minutes to recover before subsequent interventions were continued.

Data analysis

For awake and anaesthetized experiments, PP-, RR-, QRS- and QT-intervals were derived from the surface ECG and manually measured using EPTracer software (Cardiotek, Maastricht, The Netherlands). All intervals were averaged over five (anaesthetized) or ten (awake) consecutive beats. QT-interval was corrected for heart rate (QTc) using the Van der Water formula.[25]

HRV analyses were performed using Lead II from the awake surface ECG recordings. First, RR-intervals were measured using a custom-made Matlab application (Mathworks, Naticks, USA).[26] All RR-intervals related to ectopic beats, as well as the five intervals following such an event, were manually removed. Next, RR-intervals were uploaded in R and analysed using the R package 'Heart Rate Variability Analysis of

ECG Data' (RHRV; v4.2.6).[27] As such, all signals were first interpolated at a sampling frequency of 4Hz. Next, 120 second segments with 50% overlap were generated for temporal and frequency analyses. For the temporal analyses, *interval* was set at the default of 7.1825 ms. For frequency analyses, Fourier transformation was performed and default values for power bands were used (VLF [0.03 - 0.04] Hz; LF [0.05 - 0.15] Hz; HF [0.15 - 0.4] Hz).

Intraventricular recordings were analysed using the aforementioned custom-made Matlab application[26] and averaged over five beats. Hemodynamic parameters were manually measured and included LV end-systolic pressure (ESP), end-diastolic pressure (EDP), maximal rise and maximal decay in LV pressure (dPdt+ and dPdt-, respectively).

Right ventricular (RV) electrical function was assessed by an endocardial monophasic action potential catheter. LV activation recovery intervals (ARI) were retrieved from eight out of ten electrodes of the duo-decapolar catheter, the most basal electrodes (verified by fluoroscopy) were not included due to P-wave interference. Short-term variability of repolarization (STV) was calculated from 30 consecutive beats using the formula: $\sum|D_{n}+1 - D_{n}|/(30 \times \sqrt{2})$; D being RV MAPD or the most apical LV ARI.[28] Interventricular dispersion of repolarization (ΔMAPD) was calculated as LV ARI – RV MAPD; LV ARI was derived from the most apical electrode. Intraventricular dispersion of repolarization (DoR) was calculated as the variance within the eight ARIs derived from the LV duo-decapolar catheter. In experiments involving stellate ganglion or vagal nerve stimulation, DoR was quantified under baseline and at 15% increase in LVP or 10% increase in PP-interval, respectively.

Baroreflex sensitivity (BRS) was quantified as the slope of the regression line representing the relationship between PP-interval and LV pressure (ms/mmHg; Figure 2A and B). Values were obtained in the period after administration in which both parameters were decreasing, indicative of effective vasodilatation inducing a reflexive increase in sympathetic tone. BRS measurements made after AV-block correlated PP-intervals to LVP-measurements belonging to the contraction that was closest in time.

Histological analyses

Left stellate ganglia from another series of inducible $CAVB_{11}$ animals (n = 4; 11 ± 1 week) and sinus rhythm controls (n = 4; weight-matched) were collected during the

terminal experiment as described by Wu *et al.* (2016).[29] Animals were defined inducible when infusion of dofetilide resulted in ≥3 Torsade de Pointes arrhythmias within 10-minutes following start of infusion during the terminal experiment. Stellate ganglia were rapidly excised and immediately fixed in 4% paraformaldehyde (dissolved in PBS) for 24 hours. Ganglia were washed in phosphate buffered saline (3 x 1 hour) and stored in 70% ethanol at 4 °C. Stellates were embedded in paraffin and sectioned at 5 µm in the cranial-caudal axis. Next, sections were placed on charged slides and stained with haematoxylin and eosin. Images were taken at 40x magnification and analysed with ImageJ. Per animal, 6 sections were imaged and size of 120 neurons were measured.

Statistical analyses

Data are presented as mean ± SD. Data was compared using a one-way analysis of variance (ANOVA) with post-hoc Bonferroni correction or unpaired *t*-test. In case of serial measurements, ANOVA was performed as repeated measures and the *t*-test was paired. Histological analyses were performed using linear mixed effects model testing with Bonferroni correction.[30] $p<0.05$ was considered statistically significant.

RESULTS

Awake rate changes

At $CAVB_3$, ventricular rate was significantly decreased in comparison to sinus rhythm (from 109 ± 22 beats/min to 44 ± 9 beats/min; $p<0.05$; Table 1). Over time, sinus and ventricular rates remained fairly constant (Table 1). HRV analyses tended to shift towards a relatively higher sympathetic tone. All temporal HRV parameters, which mostly reflect integrity of cardiac parasympathetic innervation, showed the same trend in continuous decline as remodelling advanced, suggestive of parasympathetic withdrawal. RMSSD for example, decreased from 63 ± 53 ms at $CAVB_3$ to 40 ± 36 ms at $CAVB_5$, to 30 ± 12 ms at $CAVB_{11}$ (*non-significant*; Table 1). In contrast, LF/HF which reflects the relative activity of the sympathetic-to-parasympathetic nervous system, seemed to increase in the period between $CAVB_3$ and $CAVB_{11}$ (from 13 ± 10 to 21 ± 27, respectively, *non-significant*; Table 1), which would correspond to a relatively higher cardiac sympathetic tone.

Table 1: Effects of remodelling on sinus rate, ventricular rate and heart rate variability

	SR (n = 13)	**$CAVB_3$ (n = 9)**	**$CAVB_5$ (n = 8)**	**$CAVB_{11}$ (n = 3)**
Rates				
PP (ms)	598 ± 72	428 ± 78*	478 ± 93	463 ± 41
RR (ms)	598 ± 72	1435 ± 145*	1434 ± 35*	1239 ± 118
Time-domain				
SDNN (ms)		87 ± 60	73 ± 56	53 ± 26
SDANN (ms)		32 ± 25	30 ± 26	10 ± 2
pNN50 (%)		15 ± 14	24 ± 20	4 ± 5
SDSD (ms)		63 ± 53	40 ± 37	31 ± 12
RMSSD (ms)		63 ± 53	40 ± 36	30 ± 12
Frequency-domain				
Total Power ($ms^{2)}$		7282 ± 9876	4449 ± 6823	1569 ± 1711
VLF (ms^2)		2040 ± 2286	2041 ± 4197	453 ± 599
LF (ms^2)		2417 ± 4714	1039 ± 1568	519 ± 671
HF (ms^2)		284 ± 524	94 ± 123	24 ± 3
LF/HF		13 ± 10	10 ± 11	21 ± 27

* $p<0.05$ *vs* SR

SR: Sinus rhythm; SDNN: Standard deviation of all RR-intervals; SDANN: Standard deviation of all RR-intervals, averaged per 120 second window; pNN50: Percentage of successive RR-intervals that differed by >50 ms; RMSSD: Root mean square of the successive RR-interval difference. VLF: Ultra low frequency [0.03 - 0.04] Hz; LF: Low frequency [0.05 - 0.15] Hz; HF: High frequency [0.15 - 0.4] Hz; LF/HF: LF-to-HF ratio

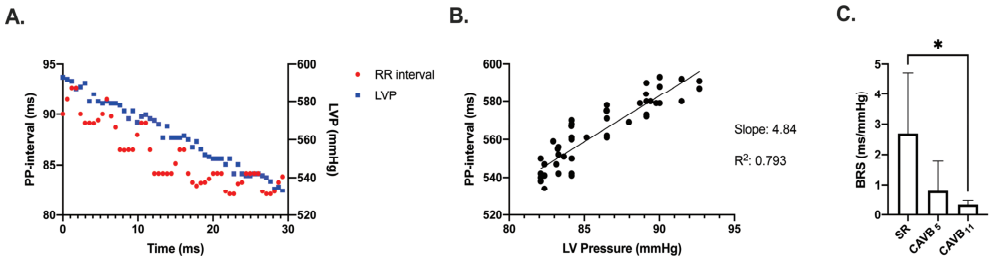

Figure 2. Baroreflex sensitivity. A) Representative traces of the period wherein nitroprusside simultaneously induced decreases in RR-interval and left ventricular pressure (LVP). **B)** The regression line that signifies the beat-to-beat change in RR-interval *vs* LVP quantifies the baroreflex sensitivity (BRS). **C)** Remodelling-induced changes in BRS over time in the CAVB dog model.

Baroreflex sensitivity

Nitroprusside consistently and adequately induced a 10-20 mmHg decrease in blood pressure and LVP. No adverse effects were induced by nitroprusside infusion. Of the different timepoints measured, BRS was highest under SR (2.6 ± 2.0 ms/mmHg), indicating that the sympathetic reflex was strongest under circumstances where remodelling was absent. With remodelling, this reflex weakened as BRS significantly decreased to 0.32 ± 0.15 ms/mmHg at $CAVB_{11}$ (p<0.05 *vs* SR; Figure 2C). Interestingly, BRS was already decreased to 0.8 ± 1.0 ms/mmHg at $CAVB_5$, (non-significant *vs* SR or $CAVB_{11}$), indicating that neural remodelling was progressively affecting cardiac autonomic tone and innervation.

Left stellate ganglion stimulation

In all experiments, LSGS reproducibly increased arterial and LV pressure (Table 2), whilst simultaneously shortening PP- and RR-intervals (Table 2). Moreover, LSGS also seemed to increase LV STV consistently from 1.4 ± 0.6 ms, 3.2 ± 1.1 ms, and 1.3 ± 0.6 ms under baseline, to 6.5 ± 2.2 ms, 9.1 ± 1.9 ms and 7.1 ± 4.0 ms during LSGS at SR, $CAVB_5$, and $CAVB_{11}$, respectively (p<0.05 for SR and $CAVB_5$).

In addition, LSGS-induced increases in spatial dispersion of repolarization were augmented by CAVB. This effect was especially clear at $CAVB_5$, as LV DoR increased from 809 ± 1096 ms^2 to 1281 ± 1526 ms^2 (p<0.05). Though insignificantly increased at $CAVB_{11}$, the effect of LSGS on DoR was significantly larger at $CAVB_{11}$ (+3.0 ± 1.0%) compared to SR (+1.0 ± 0.1 %, p<0.05; Figure 3A and B). Moreover, whereas in AAVB the septum showed most ARI-shortening upon sympathetic

568622-L-bw-Weperen
Processed on: 3-11-2021

Table 2: Electrical and hemodynamical effects of LSGS at acute AV-block, $CAVB_5$ and $CAVB_{11}$

	AAVB (n = 6)	$CAVB_{mid}$ (n = 8)	$CAVB_{end}$ (n = 4)
Baseline			
PP	385 ± 30	554 ± 66	593 ± 132
RR	1446 ± 396	1328 ± 121	1462 ± 297
QRS	98 ± 6	102 ± 13	116 ± 10
QT	338 ± 35	473 ± 55	442 ± 120
QTc	324 ± 48	445 ± 48	415 ± 91
JTc	236 ± 56	342 ± 49	322 ± 100
LV ARI	303 ± 30	355 ± 34	300 ± 85
LV STV	1.4 ± 0.6	3.2 ± 1.1	1.3 ± 0.6
LV DoR	133 ± 84	809 ± 1096	462 ± 713
ESP	88 ± 66	96 ± 6	90 ± 12
EDP	6 ± 2	5 ± 2	5 ± 2
dPdt+	1450 ± 302	2010 ± 227	1384 ± 500
dPdt-	-1521 ± 405	-1840 ± 196	-1214 ± 312
LSGS			
PP	374 ± 25*	503 ± 93*	609 ± 77
RR	1195 ± 181	1217 ± 135*	1189 ± 216
QRS	89 ± 14	97 ± 11*	114 ± 10
QT	317 ± 46	424 ± 50*	425 ± 101
QTc	313 ± 53	404 ± 44*	416 ± 101
JTc	232 ± 45	311 ± 42	302 ± 92
LV ARI	288 ± 52	330 ± 26*	270 ± 115
LV STV	6.5 ± 2.2*	9.1 ± 1.9*	7.1 ± 4.0
LV DoR	137 ± 82	1281 ± 1526*	931 ± 1217
ESP	103 ± 8*	110 ± 8*	103 ± 13*
EDP	7 ± 3	5 ± 1	5 ± 2
dPdt+	2040 ± 607	2712 ± 499*	2045 ± 1117
dPdt-	-1850 ± 397	-2285 ± 578*	-1542 ± 583

* $p<0.05$ *vs* Baseline

LSGS: Left stellate ganglion stimulation; LV: Left ventricular; ARI: Activation recovery interval; STV: Short term variability in repolarization; DoR: Dispersion of repolarization; ESP: End systolic pressure; EDP: End diastolic pressure; dPdt+: maximal rise in left ventricular pressure; dPdt-: minimal decay in left ventricular pressure

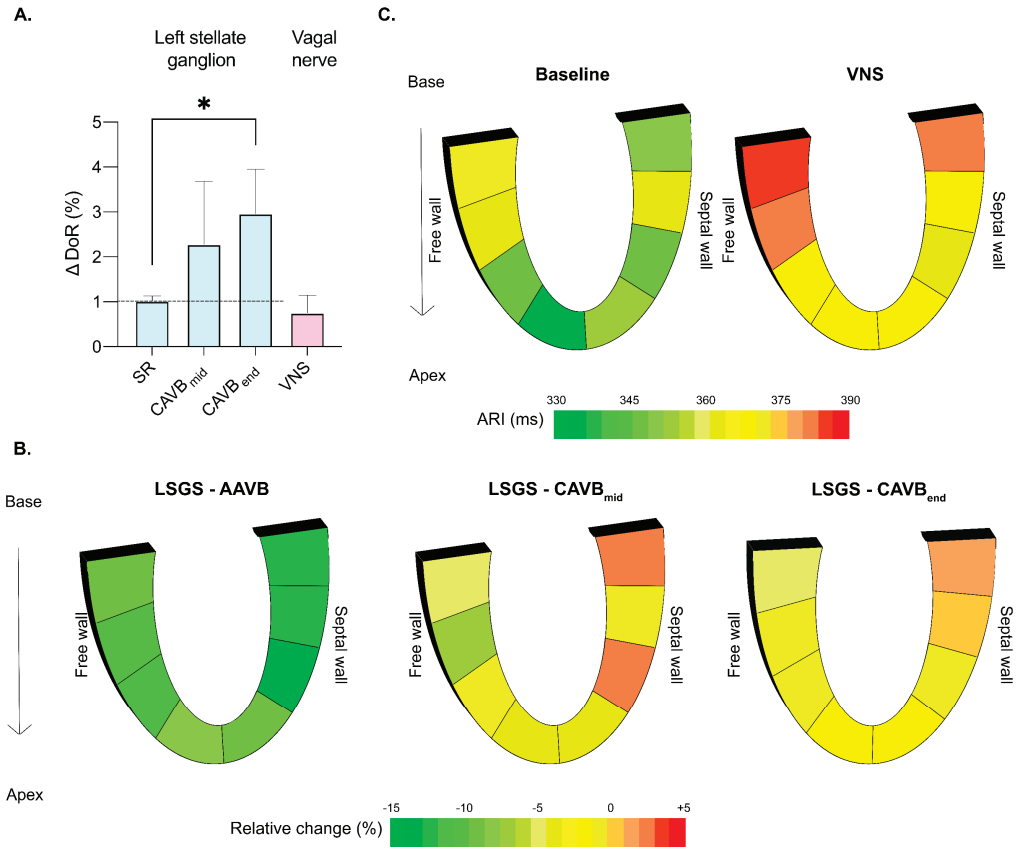

Figure 3. Electrophysiological effects of left stellate ganglion and vagal nerve stimulation. A) Relative change in left ventricular dispersion of repolarization (Δ DoR) upon stimulation of the left stellate ganglion (blue, left) or vagal nerve (right, pink). **B)** Schematic effects of left stellate ganglion stimulation (LSGS) on relative change (%) in activation recovery interval (ARI) are shown. **C**) Schematic effects of vagal nerve stimulation (VNS) on ARI are shown.

stimulation (Figure 3B; left panel), LSGS at $CAVB_5$ and $CAVB_{11}$ caused most shortening in repolarization duration at the LV free wall (Figure 3B; middle and right panel).

Vagus nerve stimulation

Vagus nerve stimulation decreased sinus rate from 109 ± 16 beats/min to 96 ± 15 beats/min. However, ventricular rate and repolarization duration were not significantly altered (Table 3). Similarly, temporal dispersion of repolarization was not affected by vagus nerve stimulation. However, DoR decreased from 914 ± 726 ms^2 under baseline

Table 3: Electrical and hemodynamical effects of vagal nerve stimulation (n= 4)

	Baseline	Vagal nerve stimulation	Relative change (%)
PP	559 ± 78	634 ± 94*	13 ± 6
RR	1449 ± 202	1417 ± 188	-2 ± 3
QRS	109 ± 11	104 ± 6	-4 ± 10
QT	464 ± 77	461 ± 74	-1 ± 2
QTc	425 ± 64	424 ± 66	0 ± 2
JTc	316 ± 58	320 ± 68	1 ± 4
LV ARI	362 ± 85	369 ± 97	1 ± 5
LV STV	5.6 ± 3.2	5.3 ± 3.6	-10 ± 17
LV DoR	914 ± 726	568 ± 611	-25 ± 39
ESP	94 ± 8	95 ± 8	1 ± 1
EDP	7 ± 2	6 ± 2	-2 ± 11
dPdt+	1390 ± 255	1423 ± 238	1 ± 4
dPdt-	-1381 ± 114	-1423 ± 139	1 ± 4

* $p<0.05$ *vs* Baseline

LV: Left ventricular; ARI: Activation recovery interval; STV: Short term variability in repolarization; DoR: Dispersion of repolarization; ESP: End systolic pressure; EDP: End diastolic pressure; dPdt+: maximal rise in left ventricular pressure; dPdt-: minimal decay in left ventricular pressure.

to 568 ± 611 ms^2 after stimulation (*non-significant*; Figure 3A and C; Table 3). Hemodynamically, vagal nerve stimulation did not affect dPdt+, dPdt-, ESP or EDP (Table 3), suggesting proper maintenance of left ventricular function.

Histology

Mean neuronal size was significantly larger in CAVB animals with an inducible phenotype (963 ± 123 μm^2 *vs* 757 ± 110 μm^2 in SR animals, $p<0.05$; Figure 4A). Correspondingly, mean neuronal diameter was also significantly increased in CAVB animals (38 ± 3 µm *vs* 34 ± 3 µm in SR animals, $p<0.05$; Figure 4B). A representative example is shown in Figure 4C.

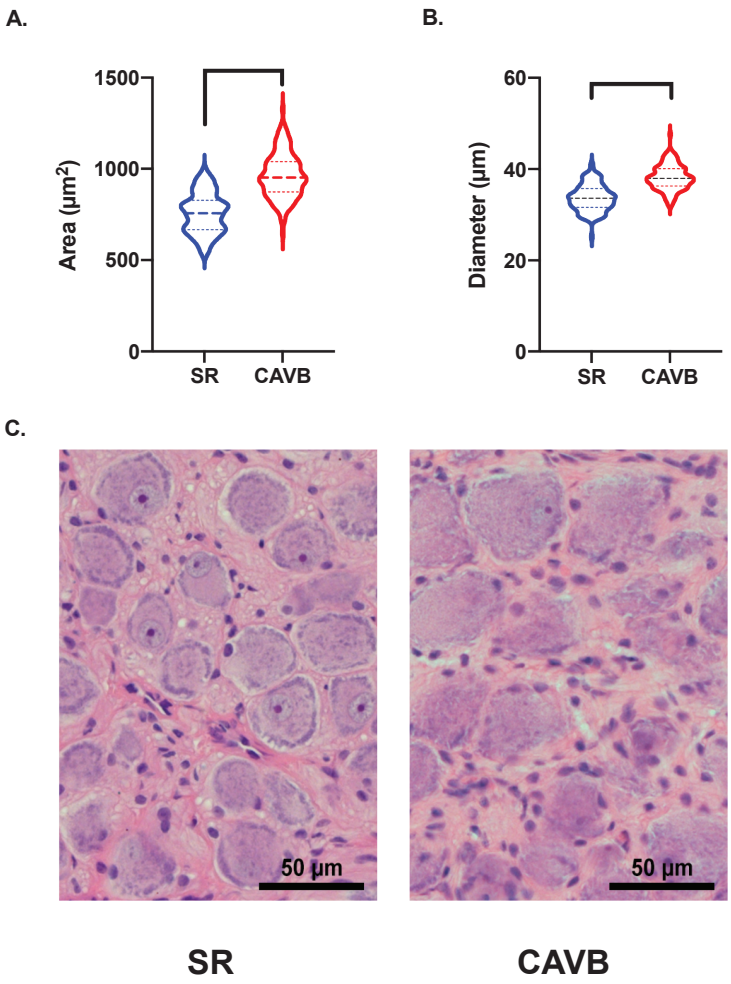

Figure 4. Neural remodelling-induced cellular changes in left stellate ganglia of chronic AV-block (CAVB) dogs. Neuronal remodeling in CAVB dogs caused neural area **(A)** and diameter **(B)** to become significantly greater. Representative figures of left stellate ganglion changes in sinus rhythm (SR) *vs* CAVB dogs **(C)**.

DISCUSSION

Neural remodelling in non-ischemic cardiomyopathies

In the present study, we explored neural remodeling in the CAVB dog model. We showed that non-ischemic cardiac injury initiates a neural remodeling resulting in progressive sympatho-excitation. HRV indices seem to reflect parasympathetic withdrawal and relative sympathetic overactivity, which was further corroborated by a decreased baroreflex sensitivity and an augmented response of spatial dispersion of

repolarization to sympathetic activation. In contrast, vagal nerve stimulation appeared to stabilize cardiac electrophysiology. On a cellular level, these functional changes were associated with neuronal hypertrophy in the left stellate ganglion.

The preponderance of research characterizing the functional and cellular effects of neural remodeling in cardiovascular disease and consequent sympatho-excitation has focused on ischemic cardiac disease. This research is, to the best of our knowledge, the first to serially assess the electrical, hemodynamical and histological characteristics of neural remodeling in an animal model of non-ischemic cardiac injury.

Neural remodeling in non-ischemic cardiomyopathies

Cardiac injury simultaneously initiates sympathetic overdrive and parasympathetic withdrawal as a means to acutely preserve adequate cardiac output. However, chronic cardiac exposure to excessive sympathetic excitation causes pathological circumstances wherein the susceptibility for VAs is greatly augmented. Correspondingly, beta-blockers are the cornerstone of current pharmacological anti-arrhythmic treatment,[24] whilst other neuromodulatory modalities, *i.e.* stellectomies, are revolutionizing the current therapeutic field. However, most mechanistic insights on the development and progression of neural remodeling are derived from experimental studies employing animal models of ischemic cardiac injury, or clinical studies wherein patients with ischemic cardiomyopathies are overrepresented.[5,25–27] Hence, the pathophysiology of neural remodeling in the setting of non-ischemic cardiac injury has been greatly overlooked and remains largely unknown. Nevertheless, the efficacy of beta-blocking therapies and the focal activity-driven character of VAs in this cohort of patients[28] suggest a perhaps even more intricate involvement of autonomic modulation in the pathophysiology of ventricular arrhythmogenesis. Accordingly, (bilateral) stellectomies are highly effective in patients suffering from non-ischemic cardiomyopathies, indicating that sympathetic overdrive is fundamental to ventricular arrhythmogenesis in these patients.[9,31–34] Moreover, a prior study by Ajijola *et al.* (2012)[30] demonstrated that neuronal hypertrophy is even more pronounced in patients suffering from non-ischemic cardiomyopathies, than in patients with ischemic substrates. Collectively, these findings indicate that neural remodeling is an active process initiated by non-ischemic cardiac injury, but how this phenotype of sympathetic

overdrive develops over time and how this change in autonomic balance could promote ventricular arrhythmogenesis remains unclear.

Neural remodelling induces sympathetic overdrive

In this study, the CAVB dog model was employed to assess alterations in cardiac autonomic tone in the setting of non-ischemic cardiac injury. Previous studies had already suggested that neural remodelling is involved in the development of Torsade de Pointes susceptibility in this model. For example, non-sustained VAs in the CAVB dog model are caused by triggered activity,[35] as is also the case in non-ischemic cardiomyopathy patients, indicating a modulatory role of the sympathetic nervous system. Moreover, interrupting sympathetic innervation to the heart through bilateral cardiac sympathetic denervation was a highly effective anti-arrhythmic intervention in this model.[22]

To explore temporal changes in autonomic tone we recorded awake ECGs, analysed sinus and ventricular rates, and evaluated multiple parameters of HRV. We did not observe any significant changes in PP- or RR-intervals as remodelling progressed, though there was a noticeable trend in HRV measurements. Whereas the time-domain indices, assessing the beat-to-beat variation in RR-interval, are mainly indicative of parasympathetic innervation, the frequency-domain parameters reflect both parasympathetic and sympathetic activity. Time-domain indices, corresponding to parasympathetic tone, tended to decrease in parallel with progressive cardiac remodelling. Similarly, all frequency-domain measures, except for LF/HF, decreased as well. Interestingly, this decrease also affected LF power, which is associated with cardiac sympathetic innervation. Hence, in a condition characterized by sympathetic overactivity, one would expect this parameter to increase instead. Nevertheless, this paradoxical decrease can be explained by a dulling of myocardial responsiveness to autonomic stimuli, which has been well-reported to develop in heart failure.[36] Thus, as these analyses measure the frequency by which myocardial function *responds* to autonomic innervation, and not the frequency by which autonomic nerves *innervate* the heart, a loss of total power could reflect a decreased responsiveness. Additionally, prior studies have shown that a decreased total power was associated with a higher incidence of adverse cardiac events, including VAs.[37]

Moreover, the LF/HF ratio, reflecting the sympathetic-to-parasympathetic tone increased, which further suggests that neural remodelling in the CAVB dog models induces a condition of sympathetic dominance. Similarly, Tan *et al.* (2020)[38] explored changes in autonomic tone in their premature ventricular contraction canine model of non-ischemic cardiomyopathy. In their study, 12 weeks of pacing-induced bigeminy (coupling interval: 200 ms) caused a significant reduction in HRV, suggestive of parasympathetic withdrawal and an overall shift towards more sympathetic conditions.

Additionally, this study also assessed baroreflex sensitivity under anaesthetized conditions to further explore changes in cardiac autonomic tone over time. In health, blood pressure is tightly regulated by mechanoreceptors in the aortic arch and carotid sinus.[39] Blood pressure homeostasis is continuously maintained, and when necessary, restored through the activation of baroreceptive-afferents and consequent stimulation sympathetic or parasympathetic efferents. This interplay between reflex restoration and basal autonomic tone can be assessed by the administration of blood pressure increasing (*i.e.* phenylephrine) or decreasing (*i.e.* nitroprusside) drugs. Hence, baroreflex sensitivity evaluates the prolongation or shortening in RR-interval that is induced by increases or decreases in arterial pressure, respectively. In general, a higher slope indicates adequate cardiac autonomic function, as sympathetic or parasympathetic reflexes can effectively restore blood pressure in a background of constant autonomic tone. A flattening of this slope on the contrary, is suggestive of reduced reflex responses caused by increased basal sympathetic tone.[40] In our series of experiments, BRS seemed to decline progressively, becoming significantly lower at $CAVB_{11}$ compared to SR (Figure 2). These results further strengthened the hypothesis that non-ischemic cardiac injury and subsequent neural remodelling result in a condition characterized by elevated sympathetic tone.

Electrical effects of sympathetic and parasympathetic stimulation

Aberrant sympathetic activation increases the risk of VAs in patients and animals models with either ischemic or non-ischemic cardiac injury.[41–44] Also in the CAVB dog model, autonomic imbalance promotes ventricular arrhythmogenesis, as bilateral denervation impeded arrhythmogenesis in 15 out of 17 (~ 90%) previously inducible animals.[22] However, the electrophysiological mechanisms by which sympathetic

stimulation of the non-ischemic substrate results in ventricular arrythmias remains unclear.

In the current study, we showed that left stellate ganglion stimulation increases temporal and spatial dispersion of repolarization at all timepoints. Especially LV STV seemed to be largely increased upon LSGS. As LV STV is derived from the beat-to-beat change in repolarization duration, a higher STV reflects instability in repolarization. This temporal dispersion in repolarization adequately reflects the propensity for afterdepolarizations[45–48] that could *trigger* an arrhythmic event. Hence, sympathetic stimulation appears to promote both the arrhythmic trigger and substrate regardless of the presence and extent of cardiac remodelling. However, the extent wherein sympathetic stimulation affected the electrical properties of the heart appeared to change over time.

Firstly, sympathetic-induced ARI-shortening was less pronounced at later timepoints, even though the effects of stimulation on LV pressure did not differ significantly (Table 2). This can be explained by remodelling-induced downregulation of $I_{K,s}$ conducting potassium channels in the CAVB dog model,[49] whereas sympathetic stimulation increases the conductance of these channels.[50] When the density of $I_{K,s}$ reduces, the capacity of LSGS to shorten repolarization, as it did at the earlier timepoints, is lost.

Secondly, Δ DoR (the difference in DoR between baseline and during LSGS) increased more as remodelling progressed. DoR is a parameter of the arrhythmic *substrate*, on which ectopic events, but also arrhythmias, can develop.[35, 48,51] Hence, with remodelling, potentiation of the arrhythmic substrate by LSGS was increased. Interestingly, the local effects of LSGS also appeared to change over time: whereas in AAVB the septal wall showed most ARI-shortening, this effect became reversed at later timepoints when the left ventricular free wall became most sensitive to sympathetic-induced ARI-shortening (Figure 3B). This relatively greater shortening of the LV free wall, suggests that nerve sprouting is centred around the LV free wall. This corresponds to the observation that in patients with idiopathic dilated cardiomyopathy, nerve sprouting follows the path of the coronary arteries,[52] which would also result in nerve sprouting at the basal LV free wall. Excitingly, previous studies have shown that VAs in the CAVB dog model mainly arise from the LV posterior free wall. Hence, the

observation that LSGS exerts its most pronounced effects at the LV free wall could translate to this increased tendency of arrhythmias to arise from this site.

Vagal nerve stimulation on the other hand, appeared to *stabilize* cardiac electrophysiology through decreasing DoR (Figure 3A). Correspondingly, vagal nerve stimulation did not trigger any arrhythmic events in all of the animals (data not shown). This suggests that vagal nerve stimulation could be an effective anti-arrhythmic therapy in the setting of non-ischemic cardiac injury. Similarly, the ANTHEM-HF study, which explored the benefits of vagal nerve stimulation in heart failure, showed that chronic vagal nerve stimulation stabilized cardiac electrophysiology and suppressed the occurrence of ventricular tachycardia.[53,54] However, non-ischemic cardiomyopathy patients were underrepresented in these follow-up studies (28%).[53,54]

Histological characteristics of neural remodelling

Chronic sympatho-excitation is likely initiated and propagated by pathological remodelling of autonomic neurons throughout the cardiac neuraxis. Most notably, stellate ganglia of cardiomyopathy patients suffering from recurrent VAs undergo profound cellular remodelling processes that culminate in neuronal hypertrophy, glial activation and inflammation.[3]

Likewise, we showed that in the CAVB dog model, neural remodelling results in a significant increase in neuronal size and diameter (Figure 4). This further corroborates the development of neuronal changes in response to cardiac injury and offers some mechanistic insights into the development of the sympathetic overdrive. Surprisingly, glial size was not significantly different (Figure 4C).

Limitations

Most animals underwent only a selection of the experiments to minimize animal discomfort and to prevent the possible confounding effects of repetitive nerve stimulations. Also, no HRV measurements could be made under SR, as animals were insufficiently familiarized to awake ECG recordings in those early weeks.

All CAVB animals included in the manuscript were inducible for VAs. Therefore, extent of neural remodelling and/or disbalance in cardiac autonomic tone could not be correlated to arrhythmic susceptibility.

Additionally, as complete AV-block uncouples atrio-ventricular activity, a modified BRS quantification was performed to achieve temporal correlation between LV pressure and PP-interval dynamics. Similarly, P-wave interference in QRS-complexes impeded HRV-analyses using PP-intervals. As such, HRV analyses were performed using RR-intervals, which might have underestimated the effects of remodelling on HRV.

Lastly, autonomic control of canine hearts might incompletely translate to human cardiac innervation.[55] Nevertheless, the characterization of changes in cardiac autonomic tone in response to non-ischemic cardiomyopathy might still be readily translatable to the human setting.

ACKNOWLEDGEMENTS

The authors thank K. Vardar for her help conducting experiments.

REFERENCES

1. Benjamin EJ, Muntner P, Alonso A, Bittencourt MS, Callaway CW, Carson AP, Chamberlain AM, Chang AR, Cheng S, Das SR, Delling FN, Djousse L, Elkind MSV, Ferguson JF, Fornage M, Jordan LC, Khan SS, Kissela BM, Knutson KL, Kwan TW, Lackland DT, Lewis TT, Lichtman JH, Longenecker CT, Loop MS, Lutsey PL, Martin SS, Matsushita K, Moran AE, Mussolino ME, O'Flaherty M, Pandey A, Perak AM, Rosamond WD, Roth GA, Sampson UKA, Satou GM, Schroeder EB, Shah SH, Spartano NL, Stokes A, Tirschwell DL, Tsao CW, Turakhia MP, VanWagner LB, Wilkins JT, Wong SS & Virani SS. Heart Disease and Stroke Statistics-2019 Update: A Report From the American Heart Association. *Circulation* **139,** e56–e528 (2019).
2. Adabag AS, Luepker R V., Roger VL & Gersh BJ. Sudden cardiac death: Epidemiology and risk factors. *Nat. Rev. Cardiol.* **7,** 216–225 (2010).
3. Ajijola OA, Hoover DB, Simerly TM, Brown TC, Yanagawa J, Biniwale RM, Lee JM, Sadeghi A, Khanlou N, Ardell JL & Shivkumar K. Inflammation, oxidative stress, and glial cell activation characterize stellate ganglia from humans with electrical storm. *JCI insight* **2,** e94715 (2017).
4. Goldberger JJ, Arora R, Buckley U & Shivkumar K. Autonomic Nervous System Dysfunction: JACC Focus Seminar. *J. Am. Coll. Cardiol.* **73,** 1189–1206 (2019).
5. La Rovere M, Bigger J, Marcus F, Mortara A & Schwartz P. Baroreflex sensitivity and heart-rate variability in prediction of total cardiac mortality after myocardial infarction. ATRAMI (Autonomic Tone and Reflexes After Myocardial Infarction) Investigators. *Lancet* **351,** 478–484 (1998).
6. Vaseghi M, Lux RL, Mahajan A & Shivkumar K. Sympathetic stimulation increases dispersion of repolarization in humans with myocardial infarction. *Am. J. Physiol. - Heart Circ. Physiol.* **302,** H1838-1846 (2012).
7. Sobowale C, Hori Y & Ajijola O. Neuromodulation Therapy in Heart Failure: Combined Use of Drugs and Devices. *J. Innov. Card. Rhythm Manag.* **11,** 4151–4159 (2020).
8. Heidenreich PA, Lee TT & Massie BM. Effect of beta-blockade on mortality in patients with heart failure: A meta-analysis of randomized clinical trials. *J. Am. Coll. Cardiol.* **30,** 27–34 (1997).

9. Dusi V, De Ferrari GM, Pugliese L & Schwartz PJ. Cardiac Sympathetic Denervation in Channelopathies. *Front. Cardiovasc. Med.* **6,** 27 (2019).
10. Vaseghi M, Gima J, Kanaan C, Ajijola OA, Marmureanu A, Mahajan A & Shivkumar K. Cardiac sympathetic denervation in patients with refractory ventricular arrhythmias or electrical storm: Intermediate and long-term follow-up. *Heart Rhythm* **11,** 360–366 (2014).
11. Vaseghi M, Barwad P, Malavassi Corrales FJ, Tandri H, Mathuria N, Shah R, Sorg JM, Gima J, Mandal K, Sàenz Morales LC, Lokhandwala Y & Shivkumar K. Cardiac Sympathetic Denervation for Refractory Ventricular Arrhythmias. *J. Am. Coll. Cardiol.* **69,** 3070–3080 (2017).
12. Liang JJ, Santangeli P & Callans DJ. Long-term outcomes of ventricular tachycardia ablation in different types of structural heart disease. *Arrhythmia Electrophysiol. Rev.* **4,** 177–183 (2015).
13. Dinov B, Fiedler L, Schönbauer R, Bollmann A, Rolf S, Piorkowski C, Hindricks G & Arya A. Outcomes in catheter ablation of ventricular tachycardia in dilated nonischemic cardiomyopathy compared with ischemic cardiomyopathy: Results from the prospective heart centre of leipzig vt. *Circulation* **129,** 728–736 (2014).
14. Gökoğlan Y, Mohanty S, Gianni C, Santangeli P, Trivedi C, Güneş MF, Bai R, Al-Ahmad A, Gallinghouse GJ, Horton R, Hranitzky PM, Sanchez JE, Beheiry S, Hongo R, Lakkireddy D, Reddy M, Schweikert RA, Dello Russo A, Casella M, Tondo C, Burkhardt JD, Themistoclakis S, Di Biase L & Natale A. Scar Homogenization Versus Limited-Substrate Ablation in Patients With Nonischemic Cardiomyopathy and Ventricular Tachycardia. *J. Am. Coll. Cardiol.* **68,** 1990–1998 (2016).
15. Oros A, Beekman JDM & Vos MA. The canine model with chronic, complete atrio-ventricular block. *Pharmacol. Ther.* **119,** 168–178 (2008).
16. Van Opstal JM, Verduyn SC, Leunissen HDM, De Groot SHM, Wellens HJJ & Vos MA. Electrophysiological parameters indicative of sudden cardiac death in the dog with chronic complete AV-block. *Cardiovasc. Res.* **50,** 354–361 (2001).
17. Loen V, Vos MA & Heyden MAG. The canine chronic atrio-ventricular block model in cardiovascular preclinical drug research. *Br. J. Pharmacol.* bph.15436 (2021). doi:10.1111/bph.15436

18. Verduyn SC, Ramakers C, Snoep G, Leunissen JDM, Wellens HJJ & Vos MA. Time course of structural adaptations in chronic AV block dogs: evidence for differential ventricular remodeling. *Am. J. Physiol. Circ. Physiol.* **280,** 2882–2890 (2001).
19. Volders PGA, Sipido KR, Vos MA, Spätjens RL, Leunissen JDM, Carmeliet E & Wellens HJJ. Downregulation of Delayed Rectifier K+ Currents in Dogs With Chronic Complete Atrioventricular Block and Acquired Torsades de Pointes. *Circulation* **100,** 2455–2461 (1999).
20. Sipido KR, Volders PGA, de Groot SHM, Verdonck F, Van de Werf F, Wellens HJJ & Vos MA. Enhanced Ca(2+) Release and Na/Ca Exchange Activity in Hypertrophied Canine Ventricular Myocytes. *Circulation* **102,** 2137–2144 (2000).
21. Dunnink A, van Opstal JM, Oosterhoff P, Winckels SKG, Beekman JDM, van der Nagel R, Cora Verduyn S & Vos MA. Ventricular remodelling is a prerequisite for the induction of dofetilide-induced torsade de pointes arrhythmias in the anaesthetized, complete atrio-ventricular-block dog. *Europace* **14,** 431–436 (2012).
22. van Weperen VYH, Bossu A, Beekman JDM, van der Heyden MAG & Vos MA. ABSTRACT 19818: Local, but Not Systemic, Blockade of Autonomic Nervous System Activity is Antiarrhythmic in the Dog With Dofetilide Induced Torsade de Pointes Arrhythmias. *Circulation* **136,** A19818–A19818 (2017).
23. Hoang JD, Salavatian S, Yamaguchi N, Swid MA & Vaseghi M. Cardiac sympathetic activation circumvents high-dose beta blocker therapy in part through release of neuropeptide Y. *JCI Insight* **5,** e135519 (2020).
24. Vaseghi M, Salavatian S, Rajendran PS, Yagishita D, Woodward WR, Hamon D, Yamakawa K, Irie T, Habecker BA & Shivkumar K. Parasympathetic dysfunction and antiarrhythmic effect of vagal nerve stimulation following myocardial infarction. *JCI insight* **2,** e86715 (2017).
25. Van de Water A, Verheyen J, Xhonneux R & Reneman RS. An improved method to correct the QT interval of the electrocardiogram for changes in heart rate. *J. Pharmacol. Methods* **22,** 207–217 (1989).
26. Potse M, Linnenbank AC & Grimbergen CA. Software design for analysis of

multichannel intracardial and body surface electrocardiograms. *Comput. Methods Programs Biomed.* **69,** 225–236 (2002).

27. Antonio C, Martínez G, Otero A, Xosé Q, Vila A, José M, Touriño L, Rodríguez-Liñares L, María J, Presedo R, José A & Penín M. *Heart Rate Variability Analysis with the R package RHRV*. (Springer International Publishing AG, 2017).
28. Thomsen MB, Verduyn SC, Stengl M, Beekman JDM, de Pater G, van Opstal J, Volders PGA & Vos MA. Increased Short-Term Variability of Repolarization Predicts Sotalol–Induced Torsades de Pointes in Dogs. *Circulation* **110,** 2453–2459 (2004).
29. Wu G, DeSimone C V, Suddendorf SH, Asirvatham RS, Asirvatham SJ, Huang C, Chen P-S & Cha Y-M. Effects of stepwise denervation of the stellate ganglion: Novel insights from an acute canine study. *Heart Rhythm* **13,** 1395–1401 (2016).
30. Sikkel MB, Francis DP, Howard J, Gordon F, Rowlands C, Peters NS, Lyon AR, Harding SE & Macleod KT. Hierarchical statistical techniques are necessary to draw reliable conclusions from analysis of isolated cardiomyocyte studies. *Cardiovasc. Res.* **113,** 1743–1752 (2017).
31. Vaseghi M, Gima J, Kanaan C, Ajijola OA, Marmureanu A, Mahajan A & Shivkumar K. Cardiac sympathetic denervation in patients with refractory ventricular arrhythmias or electrical storm: Intermediate and long-term follow-up. *Heart Rhythm* **11,** 360–366 (2014).
32. Schwartz PJ. Cardiac sympathetic denervation to prevent life-threatening arrhythmias. *Nature Reviews Cardiology* **11,** 346–353 (2014).
33. Ajijola OA, Lellouche N, Bourke T, Tung R, Ahn S, Mahajan A & Shivkumar K. Bilateral cardiac sympathetic denervation for the management of electrical storm. *J. Am. Coll. Cardiol.* **59,** 91–92 (2012).
34. Vaseghi M, Barwad P, Malavassi Corrales FJ, Tandri H, Mathuria N, Shah R, Sorg JM, Gima J, Mandal K, Sàenz Morales LC, Lokhandwala Y & Shivkumar K. Cardiac Sympathetic Denervation for Refractory Ventricular Arrhythmias. *J. Am. Coll. Cardiol.* **69,** 3070–3080 (2017).
35. Vandersickel N, Bossu A, De Neve J, Dunnink A, Meijborg VMF, van der

Heyden MAG, Beekman JDM, De Bakker JMT, Vos MA & Panfilov A V. Short-Lasting Episodes of Torsade de Pointes in the Chronic Atrioventricular Block Dog Model Have a Focal Mechanism, While Longer-Lasting Episodes Are Maintained by Re-Entry. *JACC Clin. Electrophysiol.* **3,** 1565–1576 (2017).

36. Florea VG & Cohn JN. The Autonomic Nervous System and Heart Failure. *Circ. Res.* **114,** 1815–1826 (2014).
37. Tsuji H, Larson MG, Venditti FJ, Manders ES, Evans JC, Feldman CL & Levy D. Impact of reduced heart rate variability on risk for cardiac events: The Framingham Heart Study. *Circulation* **94,** 2850–2855 (1996).
38. Tan AY, Elharrif K, Cardona-Guarache R, Mankad P, Ayers O, Joslyn M, Das A, Kaszala K, Lin SF, Ellenbogen KA, Minisi AJ & Huizar JF. Persistent Proarrhythmic Neural Remodeling Despite Recovery From Premature Ventricular Contraction-Induced Cardiomyopathy. *J. Am. Coll. Cardiol.* **75,** 1–13 (2020).
39. Walgenbach SC & Shepherd JT. Role of Arterial and Cardiopulmonary Mechanoreceptors in the Regulation of Arterial Pressure During Rest and Exercise in Conscious Dogs. *Mayo Clin. Proc.* **59,** 467–475 (1984).
40. La Rovere MT, Pinna GD & Raczak G. Baroreflex sensitivity: Measurement and clinical implications. *Annals of Noninvasive Electrocardiology* **13,** 191–207 (2008).
41. Ogawa M, Zhou S, Tan AY, Song J, Gholmieh G, Fishbein MC, Luo H, Siegel RJ, Karagueuzian HS, Chen LS, Lin SF & Chen PS. Left Stellate Ganglion and Vagal Nerve Activity and Cardiac Arrhythmias in Ambulatory Dogs With Pacing-Induced Congestive Heart Failure. *J. Am. Coll. Cardiol.* **50,** 335–343 (2007).
42. Cao J-M, Chen LS, KenKnight BH, Ohara T, Lee M-H, Tsai J, Lai WW, Karagueuzian HS, Wolf PL, Fishbein MC & Chen P-S. Nerve Sprouting and Sudden Cardiac Death. *Circ. Res.* **86,** 816–821 (2000).
43. Tan AY, Elharrif K, Cardona-Guarache R, Mankad P, Ayers O, Joslyn M, Das A, Kaszala K, Lin SF, Ellenbogen KA, Minisi AJ & Huizar JF. Persistent Proarrhythmic Neural Remodeling Despite Recovery From Premature Ventricular Contraction-Induced Cardiomyopathy. *J. Am. Coll. Cardiol.* **75,** 1–13 (2020).

44. Zhou S, Jung BC, Tan AY, Trang VQ, Gholmieh G, Han SW, Lin SF, Fishbein MC, Chen PS & Chen LS. Spontaneous stellate ganglion nerve activity and ventricular arrhythmia in a canine model of sudden death. *Heart Rhythm* **5,** 131–139 (2008).
45. Varró A & Baczkó I. Cardiac ventricular repolarization reserve: A principle for understanding drug-related proarrhythmic risk. *British Journal of Pharmacology* **164,** 14–36 (2011).
46. Bossu A, Varkevisser R, Beekman HDM, Houtman MJC, van der Heyden MAG & Vos MA. Short-term Variability of Repolarization Is Superior to Other Repolarization Parameters in the Evaluation of Diverse Antiarrhythmic Interventions in the Chronic Atrioventricular Block Dog. *J. Cardiovasc. Pharmacol.* **69,** 398–407 (2017).
47. Thomsen MB, Volders PGA, Beekman JDM, Matz J & Vos MA. Beat-to-Beat Variability of Repolarization Determines Proarrhythmic Outcome in Dogs Susceptible to Drug-Induced Torsades de Pointes. *J. Am. Coll. Cardiol.* **48,** 1268–1276 (2006).
48. van Weperen VYH, Bossu A & Vos MA. Point of View: Electrophysiological Endpoints Differ When Comparing the Mode of Action of Highly Successful Anti-arrhythmic Drugs in the CAVB Dog Model With TdP. *J. Cardiovasc. Pharmacol.* **74,** 499–507 (2019).
49. Oros A, Houtman MJ, Neco P, Gomez AM, Rajamani S, Oosterhoff P, Attevelt NJ, Beekman JD, van der Heyden MAG, Ver Donck L, Belardinelli L, Richard S, Antoons G, Vos MA & investigators for the C. Robust anti-arrhythmic efficacy of verapamil and flunarizine against dofetilide-induced TdP arrhythmias is based upon a shared and a different mode of action. *Br. J. Pharmacol.* **161,** 162–175 (2010).
50. Grandi E & Ripplinger CM. Antiarrhythmic mechanisms of beta blocker therapy. *Pharmacol. Res.* **146,** 104274 (2019).
51. Dunnink A, Stams TRG, Bossu A, Meijborg VMF, Beekman JDM, Wijers SC, De Bakker JMT & Vos MA. Torsade de pointes arrhythmias arise at the site of maximal heterogeneity of repolarization in the chronic complete atrioventricular block dog. *Europace* **19,** 858–865 (2017).

52. Cao JM, Fishbein MC, Han JB, Lai WW, Lai AC, Wu TJ, Czer L, Wolf PL, Denton TA, Shintaku IP, Chen PS & Chen LS. Relationship between regional cardiac hyperinnervation and ventricular arrhythmia. *Circulation* **101,** 1960–1969 (2000).

53. Libbus I, Nearing BD, Amurthur B, KenKnight BH & Verrier RL. Autonomic regulation therapy suppresses quantitative T-wave alternans and improves baroreflex sensitivity in patients with heart failure enrolled in the ANTHEM-HF study. *Heart Rhythm* **13,** 721–728 (2016).

54. Nearing BD, Anand IS, Libbus I, Dicarlo LA, Kenknight BH & Verrier RL. Vagus Nerve Stimulation Provides Multiyear Improvements in Autonomic Function and Cardiac Electrical Stability in the ANTHEM-HF Study. *J. Card. Fail.* **27,** 208–216 (2021).

55. Moïse NS, Flanders WH & Pariaut R. Beat-to-Beat Patterning of Sinus Rhythm Reveals Non-linear Rhythm in the Dog Compared to the Human. *Front. Physiol.* **10,** 1548 (2020).

Valerie Y.H. van Weperen, Russell J. Littman, Douglas V. Arneson,
Jaime Contreras, Xia Yang & Olujima A. Ajijola

Glia. 2021; **69**: 1281 - 1291
doi: 10.1002/glia.23965.

CHAPTER 7

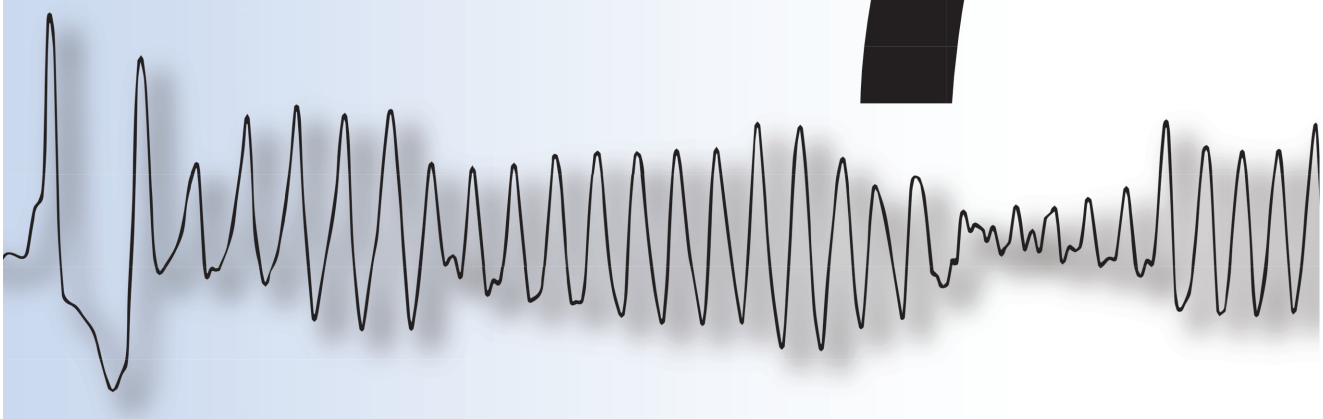

Single-cell transcriptomic profiling of satellite glial cells in stellate ganglia reveals developmental and functional axial dynamics

ABSTRACT

Stellate ganglion neurons, important mediators of cardiopulmonary neurotransmission, are surrounded by satellite glial cells (SGCs), which are essential for the function, maintenance, and development of neurons. However, it remains unknown whether SGCs in adult sympathetic ganglia exhibit any functional diversity, and what role this plays in modulating neurotransmission. We performed single-cell RNA sequencing (scRNAseq) of mouse stellate ganglia (n = 8 animals), focusing on SGCs (n = 11,595 cells). SGCs were identified by high expression of glial-specific transcripts, *S100b* and *Fabp7*. Microglia and Schwann cells were identified by expression of *C1qa/C1qb/C1qc* and *Ncmap/Drp2*, respectively, and excluded from further analysis. Dimensionality reduction and clustering of SGCs revealed six distinct transcriptomic subtypes, one of which was characterized the expression of pro-inflammatory markers and excluded from further analyses. The transcriptomic profiles and corresponding biochemical pathways of the remaining subtypes were analyzed and compared with published astrocytic transcriptomes. This revealed gradual shifts of developmental and functional pathways across the subtypes, originating from an immature and pluripotent subpopulation into two mature populations of SGCs, characterized by upregulated functional pathways such as cholesterol metabolism. As SGCs aged, these functional pathways were downregulated while genes and pathways associated with cellular stress responses were upregulated. These findings were confirmed and furthered by an unbiased pseudo-time analysis, which revealed two distinct trajectories involving the five subtypes that were studied. These findings demonstrate that SGCs in mouse stellate ganglia exhibit transcriptomic heterogeneity along maturation or differentiation axes. These subpopulations and their unique biochemical properties suggest dynamic physiological adaptations that modulate neuronal function.

INTRODUCTION

Glia are nonneuronal cells that are present throughout the entire nervous system. In the central nervous system (CNS), glial cells have been demonstrated to play important roles in both health and disease.[1] Astrocytes, the most abundant glial type in the CNS, are of particular importance in the development and functioning of the CNS but can become pathologically activated in response to injury.[1,2] Even though astrocytes are widely studied, much less is known about their peripheral counterpart, satellite glial cells (SGCs). These cells are found in sensory, parasympathetic, and sympathetic ganglia of the peripheral nervous system (PNS), where they envelope the neurons.[3] SGCs and neurons have been demonstrated to reciprocally modulate each other's activity *via* gap junctions as well as through the release of signaling molecules, such as adenosine triphosphate (ATP) and gamma aminobutyric acid (GABA).[3–6] Furthermore, SGCs have been described to become reactive in response to neuronal injury, which is reflected by an increase in size[7] and number[8] and is accompanied by changes in modulatory activity.[9,10] This reactivity is often objectified by the upregulation of glial fibrillary acidic protein (GFAP).[11,12] Despite this clear evidence that SGCs play a dynamic and important role in the PNS, studies into SGC biology are limited. Furthermore, most studies of SGCs have focused on their role in the sensory nervous system.

Nevertheless, it has been shown that SGCs in the sympathetic ganglia are able to modulate efferent sympathetic cardiac outflow.[13,14] Moreover, Ajijola *et al.* (2017)[15] demonstrated that GFAP was upregulated in the stellate ganglia SGCs of humans with heart failure (HF) and arrhythmias. As sympathetic outflow from the stellate ganglia is known to be increased in HF, these observations indicated a potential role for SGC activation in the development and/or progression of HF.

As much remains unknown about the molecular background of SGCs and their role in health and disease, we used single-cell RNA sequencing (scRNAseq) to study SGCs from healthy adult murine stellate ganglia to characterize their transcriptomic diversity. We demonstrate that SGCs in murine stellate ganglia can be divided into subpopulations that reflect different stages of maturation and activation, similar to astrocytes in the CNS. Moreover, we highlight the various developmental trajectories within the subtypes.

568622-L-bw-Weperen
Processed on: 3-11-2021
PDF page: 159

METHODS

Animals

Eight C57BL/6J male mice (Jackson Laboratory, Bar Harbor, ME), 10-12 weeks of age, were used for scRNAseq. Animals were sedated in an induction chamber (3%-5% isoflurane) and sacrificed by decapitation. All experiments were performed in accordance with guidelines set forth by the University of California Institutional Animal Care and Use Committee (IACUC) and The National Institutes of Health Guide for the Care and Use of Laboratory Animals. Data from study animals were also used for neuronal scRNAseq, and cardiac/paw neurons were identified by retrograde labeling using adeno-associated viruses (AAV, subtype 2). Those data are being reported elsewhere. AAVs are known to trigger very low immune responses and are thus unlikely to have caused much reactive response in the stellate ganglia.[15,16]

Cellular dissociation

Bilateral stellate ganglia were identified, isolated and collected in artificial cerebrospinal fluid (ACSF; Figure 1a). Next, ganglia were incubated for an hour at 37°C in a digestion solution prepared with 500 µl TrypLE Express (ThermoFisher Scientific, Waltham, MA), 2000 µl Papain solution (Worthington Biochemical Corporation, Lakewood, NJ; 25 units/ml in ACSF), 100 µl Collagenase-Dispase (Millipore Sigma, Burlington, MA; 20 mg/ml in ACSF) and 270 µl DNAse I (Worthington Biochemical Corporation; 200 units/ml in ACSF). Following this first hour, the cells were carefully triturated with fire-blown Pasteur pipettes every 30 minutes. After the second trituration, 100 µl fresh Collagenase-Dispase (20 mg/ml in ACSF) was added to the solution and cells were incubated for another hour at 37°C, triturating every 30 minutes. Next, the suspension was filtered through a 40 mm filter (ThermoFisher Scientific. Waltham, Massachusetts) and ACSF was added to stop the enzymatic digestions. The suspension was spun down at 100*g* for 4 minutes at room temperature, and the pellet was collected and resuspended in 500 µl ACSF and 500 µl supplemented Neurobasal-A medium (ThermoFisher Scientific. Waltham, Massachusetts; 250 µl B27, 250 µl Penicillin-streptomycin, 31.3 µl l-Glutamine). The cell suspension was transferred onto a density gradient (Millipore Sigma. Burlington, Massachusetts) and centrifuged at 100*g* for 10 minutes at room temperature. The supernatant was carefully removed until the solution was concentrated to 500 µl.

Single-cell RNA sequencing

Single-cell RNAseq was performed by microfluidic capture-based encapsulation, barcoding, and library preparation (10× Genomics Chromium scRNAseq system (10× Genomics, Pleasanton, CA). Cells were loaded into a Chromium Chip B along with partitioning oil, reverse transcription reagents, and a mix of hydrogel beads containing 3,500,000 unique 10× Barcodes. Paired-end sequencing was performed on a Novaseq S4 system, using the v3 Illumina platform. Coverage depth was 20K per cell, and the read length was 2 × 50. Analysis including demultiplexing, reference-based mapping (GRCm38.98), and UMI identification, was performed according to the 10× Cell Ranger pipeline.

scRNAseq data quality control, normalization, and integration

To eliminate lowly expressed genes, a gene was required to be expressed in at least five cells per sample or was removed. Cells with more than 20,000 UMIs, 6,000 expressed genes, or less than 500 expressed genes were considered outliers and removed. Cells were removed with more than 15% mitochondrial gene content. All of the following processing steps were performed in the R package Seurat (v3.0.0).[17] Each sample was normalized separately, scaling the total UMI count to 10,000 per cell and log-transformed. A total of 2,000 variable genes were identified among each sample with *FindVariableFeatures* function. The samples were integrated with Canonical correlation analysis[18] and mutual nearest neighbors with *FindIntegrationAnchors* and *IntegrateData* functions.

scRNA processing and clustering

The integrated scRNAseq data were scaled, regressing out the total number of genes and percent mitochondrial content in each cell. Principal component analysis was performed reducing the dimensionality to 30 dimensions. A graph of cell neighbors was created with the first 20 principal components (PCs), and Louvain clustering[19] was used to find cell clusters. We performed Uniform Manifold Approximation and Projection (UMAP)[20] on the first 20 PCs to visualize the clustering in two dimensions.

Identification of cell clusters and marker genes

SGCs were identified by the expression of SGC markers *S100B* and *Fabp7* (Figure 1a; Figure S1).[22,23] The feature counts of individual cells were divided by the total number of counts for that cell, multiplied by 10,000 and natural-log transformed. Fifty PCs were used for *Louvain* clustering, which was visualized using T-distributed stochastic neighbor embedding (t-SNE) dimensionality reduction analysis from the Seurat R Package (version 3.6.2) (Figure 1a). Differentially expressed genes (DEGs) were defined as genes that (a) were expressed in ≥30% of the cells from the cluster of interest and (b) if there was a ≥0.25 log fold change in gene expression between this cluster and the other groups and (c) adjusted *p*-value <0.05 using the Benjamini–Hochberg method to correct for multiple testing.

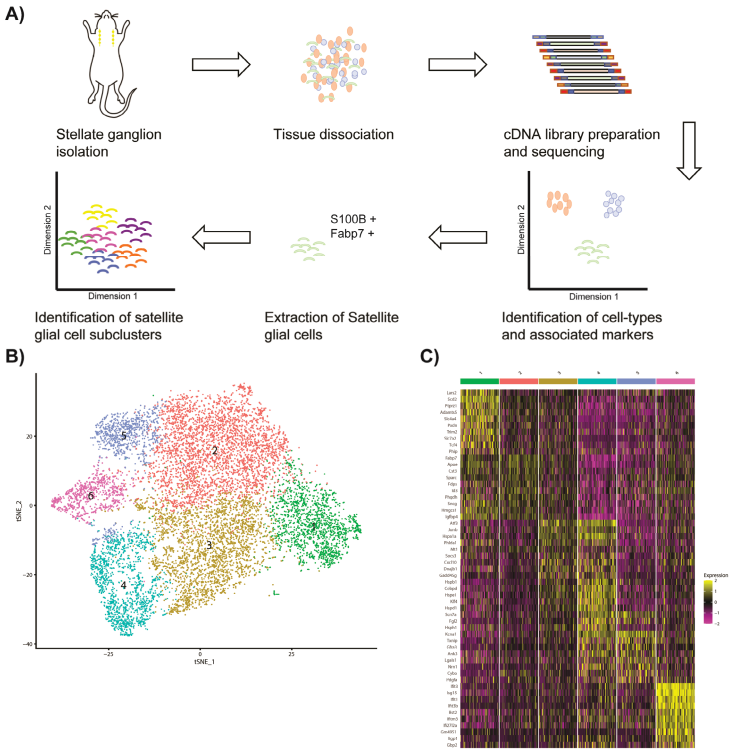

Figure 1. Single-cell RNA sequencing of murine stellate ganglia shows six subpopulations. **(a)** Pipeline depicting the derivation of stellate ganglion cells which were used for single cell RNA sequencing. Cell types within the stellate ganglia were identified and satellite glial cells (SGCs) were identified by the expression of genetic markers S100B and Fabp7. SGCs were distinguished from other cell types and used for subclustering. **(b)** Unsupervised clustering of SGC resulted in the identification of six SGC subclusters **(c)** Heatmap of the most differentially expressed genes, displayed as scaled expression levels, of the different SGC clusters.

568622-L-bw-Weperen
Processed on: 3-11-2021

Resolving cell identities of the different clusters

We determined cell identities by (a) manual assessment of the cellular function of the proteins encoded by the DEGs, (b) comparing DEGs of each cluster with expression patterns of astrocytes in different stages of maturation and (c) in-depth analysis of canonical pathways associated with DEGs of the clusters. Astrocyte-specific markers were retrieved from multiple studies that have previously published the transcriptome of astrocytes in different stages of development.[24–31]

Cell lineage trajectory analysis

Trajectory analysis was performed using the Slingshot R package.[31] This method first identifies lineages based on the minimum spanning tree between nodes, which are cell clusters here. Using a user defined root node, Slingshot subsequently computes individual cell pseudotimes for each inferred trajectory. We used cluster 1 as the root node, because it expressed genes suggestive of astrocyte progenitor cells such as *Slc12a2*, *Ptprz1* and *Itgb8* (Figure S2).[23,25] To identify trajectory associated genes for each predicted trajectory, we trained a random forest model (parsnip R package) on the top 1,000 highly variable genes to predict cell pseudotimes. We used 1,400 trees, 200 predictors sampled per split, and 15 as the minimum number of data points per node to be split again. This trained random forest model was used to identify the pseudotime-associated genes based on their regression coefficients. A different random forest model was trained for each trajectory.

Pathway annotation of cluster marker genes

Ingenuity Pathway Analysis (IPA; QIAGEN's Ingenuity Pathway Analysis, Qiagen, Redwood City, Build and content version: 49932394) was used to annotate the enriched ingenuity pathways among cluster marker genes. Lists containing the normalized average expression of the 500 highest expressed genes or cluster-specific DEGs were used to establish associated canonical pathways. All analyses were performed with the following settings: “Reference set: Ingenuity Knowledge Base (Genes only), Relationship to include: Direct and Indirect, Networks: Interaction and causal, Data sources: All, Species: All, Tissues and Cell lines: Nervous system, Consider only relationships where confidence = Experimentally Observed.” Multiple testing was corrected for using the Benjamini–Hochberg method. Pathways were

considered to be significantly associated with a cluster when -log(BH-adjusted *p*-value) ≥ 1.3.

RESULTS

Identification of SGC clusters in the mouse SG

Using acutely dissociated stellate ganglion preparations from eight mice, we performed scRNAseq using the 10× Genomics scRNAseq platform. In total, 11,595 single SGCs were captured, expressing 5,538 ± 2,486 genes on average. Using the bidimensional t-distributed stochastic neighbor embedding (t-SNE) algorithm, we transformed the multidimensional data and visualized the relationships between the cells in a two-dimensional t-SNE plot. Louvain clustering produced six subclusters of SGCs (Figure 1b; File S1). All clusters were similarly represented in the stellate ganglia of the eight mice (File S2; Figure S3). The top 10 differentially expressed genes (DEGs) per cluster with the highest discriminatory power in terms of p-value are depicted in the heatmap in Figure 1c. The sixth cluster was excluded from further analyses due to relatively high expression of reactive markers, including interferon-related genes which may be related to an endogenous low-level reactive subtype, or transient exposure to AAVs.

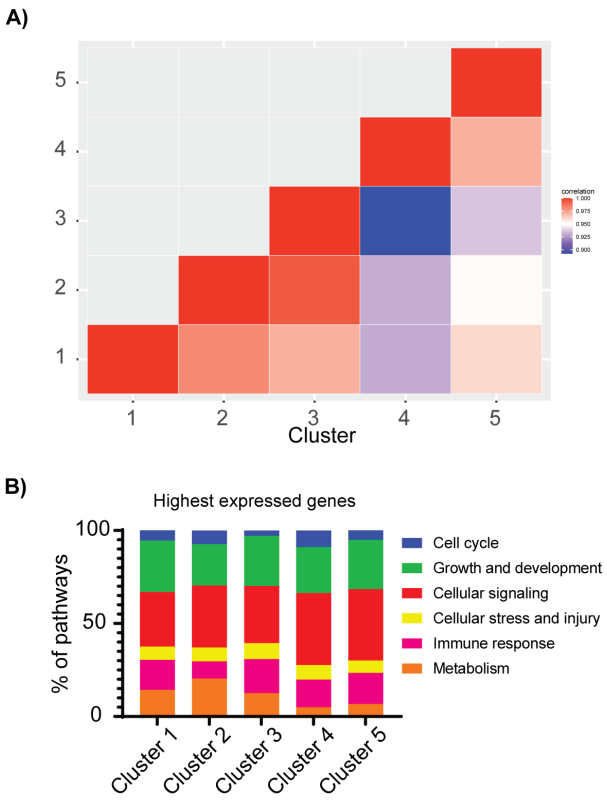

Figure 2. Average gene expression and highest expressed pathways show many similarities between the different subclusters of satellite glial cells. (a) Correlation map of the average gene expression of the five clusters. The extent of similarity is depicted by color; the blue and red colors corresponding with a continuous progression from lower to higher levels of similarities, respectively **(b)** Classification of the pathways corresponding to the 500 highest expressed genes of the different clusters to different biological functions.

568622-L-bw-Weperen
Processed on: 3-11-2021

Similarities between SGC clusters in the mouse SG

We began by examining similarities across the subclusters in their gene expression. A correlation map showing the similarities in average gene expression demonstrated a high level of correlation between all clusters (Figure 2a; File S3). Biochemical pathways associated with the 500 highest expressed genes for each cluster are listed in File S4. As shown in Figure 2b, 36 ± 14% of the pathways were similar across clusters, representing cellular signaling, growth and development, metabolism, immune response, cell cycle, and cellular stress and injury. These pathways, corresponding to glia-glia and glia-neuron communication, indicate that these functions were important for cell types across all clusters.

Determination of SGC identities in the mouse SG

Next, we investigated the cellular heterogeneity among the subclusters by examining DEGs. In-depth analysis of the DEGs in each cluster suggested that the cell populations were distinct from each other based on the state of maturation or functionality (Figure 3a; Figure S4).

Cluster 1, representing 14.57% of all SGCs, was identified as immature SGCs. This population was enriched in genetic cell cycle and pluripotency markers, corresponding to developing astrocytes in the CNS (Figure 3b).[24,27–31] This corresponded with the, though insignificant, upregulation of the pluripotency pathway in this cluster (Figure 3c). Cluster 2 and 3 were the two largest populations representing 25.27 and 32.00% of all SGCs, respectively. Both clusters had high expression of genes associated with mature astrocytes (Figure 3a, b).[24–27] Consistent with this, functional pathways, such as cholesterol synthesis, were enriched in clusters 2 and 3 (Figure 3c). These clusters were therefore identified as mature SGCs.

In contrast, clusters 4 and 5, containing 13.00 and 8.20% of the SGCs population, respectively, were characterized by downregulation of the functional pathways (Figure 3c) and showed activated stress response pathways. As such, both clusters were classified as aged SGCs since cellular stress responses and downregulation of metabolism pathways are indicative of aging.[32] However, this upregulation of cellular stress response pathways was less clear in cluster 5 (Figure 3c). Moreover, whereas the NRF2-mediated stress response seemed to be slightly upregulated, the production of nitric oxide and reactive oxygen species was

downregulated (Figure 3c). Therefore, we identified cluster 5 as a quiescent, aged group of SGCs.

File S5 lists the pathways associated with the DEGs of each cluster. DEGs of the different clusters were also compared to external transcriptomic datasets of astrocytes in the CNS (Figure 3b).[23,24] Combined, these results led to the grouping of the clusters in different states of maturation and activation (Figure 3a).

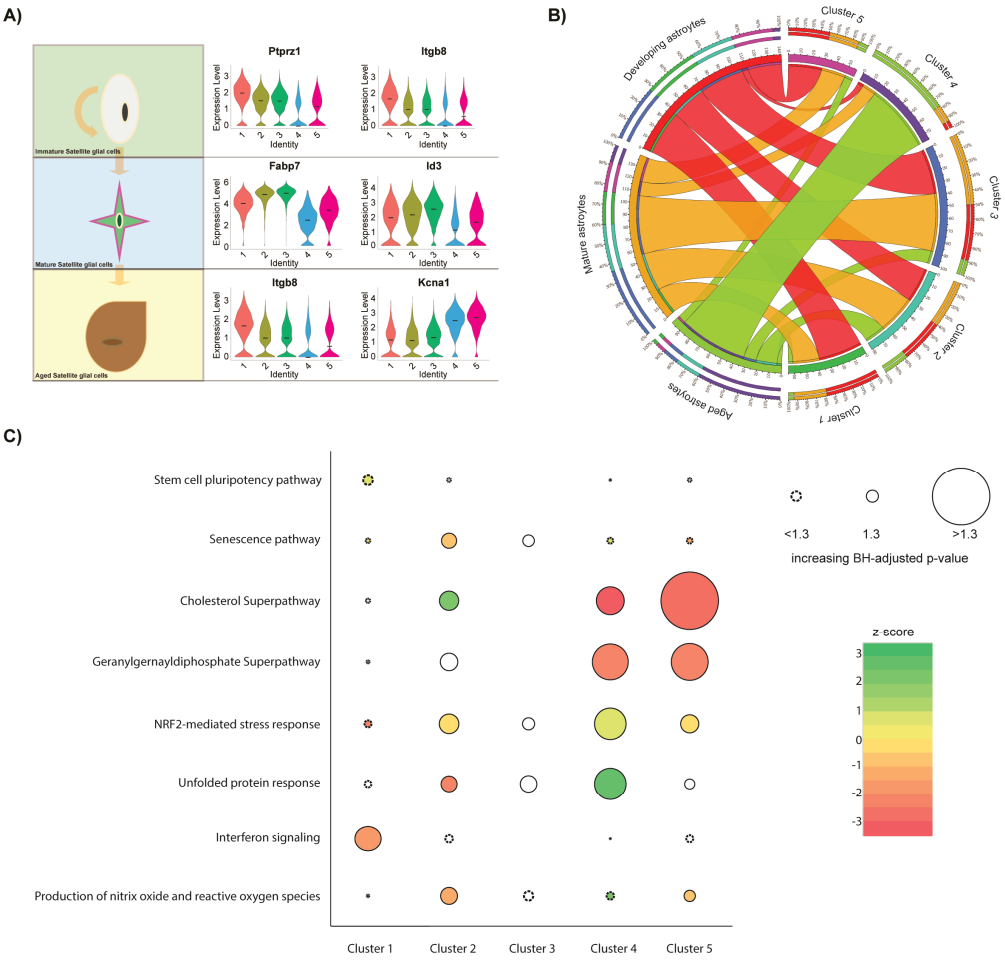

Figure 3. Satellite glial cell (SGC) subcluster identification. (a) The clusters were identified as SGCs in different stages of maturation or activation. As such, immature SGC are believed to either proliferate or progress to mature and aged SGC. The violin plots depict marker genes associated with the different states of SGC. **(b)** Comparison of the differentially expressed genes (DEGs) of the different clusters with marker genes of astrocytes in different stages of maturation. Extend of overlap between the different clusters of SGCs and developing astrocytes (red), mature astrocytes (orange), and aged astrocytes (yellow) corresponds with the thickness of the bands. **(c)** Pathways associated with the DEGs of the different clusters. *p*-value correlates with dot size, a dashed line indicating insignificance. Colors of the dots represent the *z*-score of the pathway in the respective cluster, when white, *z*-score could not be established.

Maturation and activation trajectories revealed by pseudo-time analysis

To test our hypothesis that the different clusters compose developmental and functional trajectories, we performed pseudotime analysis on the SGC clusters. Using cluster 1 as the starting cluster, three different trajectories were obtained (Figure 4a-c; Figure S5). Similar to the aforementioned developmental progression, cluster 1 seemed to evolve to cluster 2 (and 3), which were identified as the mature SGCs. From there, SGCs were observed to progress to cluster 4 or 5 which were identified as the (quiescent) aged SGCs (Figure 4a, b). Genes that trace these trajectories include *Adamts5* which was progressively downregulated as SGCs matured to subsequent clusters. Adamts5 is a metalloproteinase involved in cellular development and cell migration,[33] causing it to be upregulated in developing astrocytes,[23] which corresponds to the developmental function associated with cluster 1. Moreover, Txnip and Hspb1, which are both involved in cellular stress responses[34,35] and associated with aging astrocytes,[23] were traced in the trajectories leading up to the aged clusters 4 and 5.

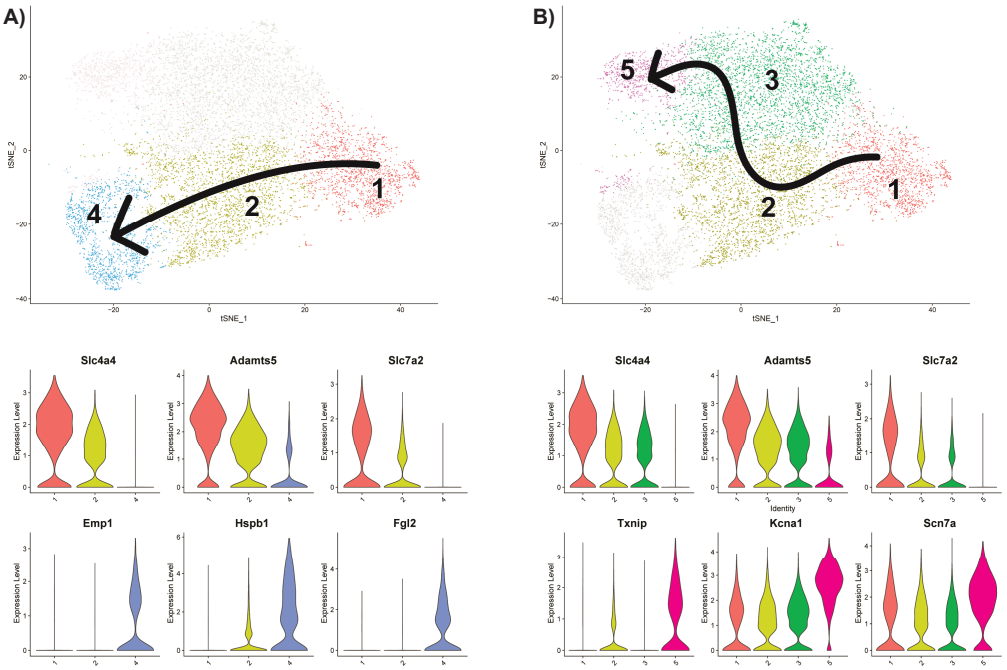

Figure 4. Pseudotime analysis of satellite glial cells (SGCs) results in three separate trajectories. The first trajectory comprised the progression of SGCs from cluster 1 to 2, to 3, and finally to 5 **(a)**. The second trajectory described the progression from cluster 1, to 3, to 4 **(b)**. Violin plots of the expression patterns of the genes associated with these trajectories across the clusters are depicted underneath their respective tSNE plots.

Signaling

Biochemical pathways associated with cell junction signaling, such as adherens and gap junctions signaling, were identified in all clusters, indicating the importance of direct cell-cell adhesion and communication pathways in fundamental functions of SGCs. In addition, the mature SGCs in cluster 3 were enriched for genes involved in aldosterone, endothelial nitric oxide synthase (eNOS), purinergic and gap junction signaling (Figure 5a, b; bold).

However, as the SGCs mature and age, distinct signaling pathways are employed. In general, signaling pathways associated with proliferation and metabolism, such as the aldosterone[36] (Figure 5a; blue) and mTOR signaling pathways[37] (Figure 5a, b; blue), and pathways associated with cell proliferation and neuronal guidance, such as 14-3-3 mediated signaling[38] and Reelin signaling,[39] were decreased (Figure 5b; blue). Also, adherens junction signaling seemed most important in the immature SGCs (Figure 5b; bold).

Moreover, aging (Figure 5a; arrows) was associated with the gradual upregulation of signaling pathways involved in cell death and cellular stress, for example, androgen[40] and BAG2 signaling pathways.[41]

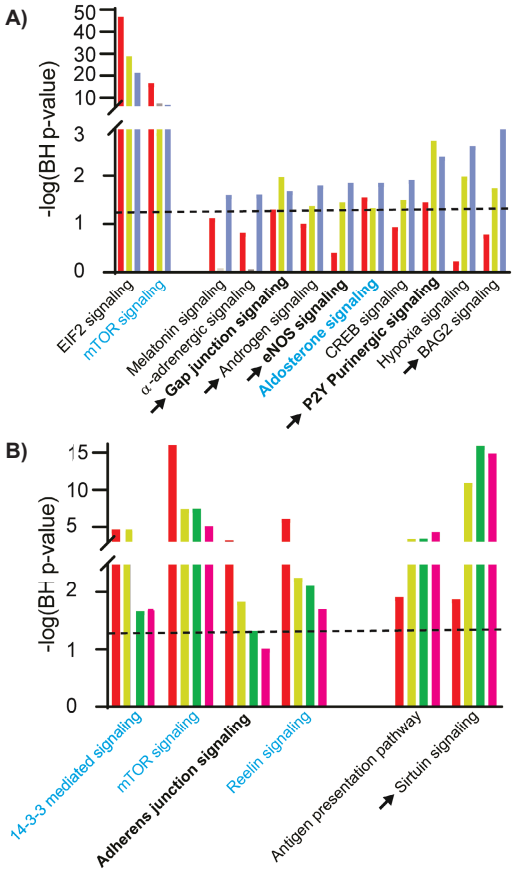

Figure 5. Active signaling pathways of the different trajectories in murine satellite glial cells (SGCs) in the stellate ganglia. a) Signaling pathways that are down- (left) or upregulated (right) as SGCs progress from immature SGCs (cluster 1; red) to mature (cluster 2; gold) to aged SGCs (Cluster 4; light blue). **b)** Signaling pathways that are down- (left) or upregulated (right) as SGCs progress from immature SGCs (cluster 1; red) to mature (cluster 2 [gold] and 3; green) to aged, quiescent SGCs (cluster 5; pink).

Furthermore, as the SGCs transitioned to a more quiescent state (Figure 5b; arrow), the Sirtuin signaling pathway was upregulated, which is involved in aging and stress resistance.[42]

DISCUSSION

Major findings

In the present study, we assessed the transcriptomic profiles of SGCs in the stellate ganglia at single-cell resolution. We show that the SGCs in the murine stellate ganglia are a) a fairly heterogeneous population of cells, that can be separated into five subpopulations of SGCs based on their state of maturation or activation, and b) that these subpopulations result from two nonlinear trajectories. In addition, we show that c) signaling pathways change as SGCs progress through the different trajectories, indicating different functions of the subclusters.

SGC subpopulations in the murine stellate ganglia

To our knowledge, this is the first study to elucidate the complexity of SGCs in the stellate ganglia based on transcriptomic profiles. We observed that the population of SGCs comprised five subpopulations that shared many characteristics, including signaling and metabolism pathways (Figure 2a). However, in-depth evaluation of cluster-specific DEGs and pathways revealed that the clusters represented SGCs in different states of maturation and/or states of functionality. This corresponds with the CNS, where astrocytes are known to coexist in different states of maturation.[43] Moreover, our results also corroborate studies by Pannese *et al.* (1960)[45] and Zhang *et al.* (2019)[46] which suggested subclustering within the SGCs based on microscopic imaging and immunohistochemical experiments, respectively. Using scRNAseq, we were able to validate the existence of SGC subpopulations and indicate that these cells can assume different states of activation that presumably change over time. We defined five subclusters and provided transcriptomic markers that allude to a functional identity.

We found that SGCs go through developmental progression within the stellate ganglia and identified cluster 1 as the most immature cluster. As pluripotency markers such as *Ptprz1* and *Itgb8* were enriched in these cells (Figure 3a), we suspect that this subpopulation remains undifferentiated and serves to locally replenish the SGC population in the stellate ganglia. Moreover, *NG2* was upregulated in cluster 1. In the CNS, *NG2* positive glia have been established to generate astrocytes as well as oligodendrocytes, strengthening the identification of cluster 1 as a pluripotent population of SGCs (Zhu et al., 2008).[47]

As the SGCs progress to more mature states, represented by the progression from cluster 2 to 3 in our data, metabolic functions such as cholesterol syntheses become increased (Figure 3c). Starting from cluster 3 and up, cells become increasingly enriched in cellular stress pathways, such as the unfolded protein response. Therefore, we established an aging trajectory as the cluster numbers go up. Moreover, though insignificant, the senescence pathway became upregulated as SGCs progress from cluster 2 to cluster 4 (Figure 3c). In addition, cholesterol-associated pathways that were upregulated in the mature SGCs became increasingly downregulated in the aged SGCs.

With regard to the highest expressed genes, cluster 5 was highly similar to cluster 4 (Figure 2a) and was also classified as aged SGCs. However, the enrichment in cellular stress pathways in cluster 4 was one of the main characteristics that distinguished the two clusters. The lesser inflammatory response combined with the low activity of functional metabolic and cell division pathways led to the identification of cluster 5 as quiescent, aged SGCs. However, it could also indicate that this cluster comprises recovering reactive SGCs and/or a mid-state in between the aging SGCs of clusters 3 and 4.

Signaling

As glia-glia and glia-neuron communication is of fundamental importance to the functioning of SGCs, we performed a more detailed evaluation of the signaling pathways that were active and evolving in the SGCs.

We demonstrated that signaling pathways associated with the cell cycle and neuronal guidance seemed to be enriched in the immature SGCs in cluster 1, and progressively downregulated as SGCs progressed to a more mature or activated state (Figure 5; left columns). Moreover, compared to all other clusters, cell junction signaling seemed to be increased in these immature SGCs (Figure 5b; bold). As cell-cell adhesion and communication have been shown to be important in stem cell behavior, the increased correlation of these pathways and cluster 1 further corroborate its pluripotent identity.[44,45]

With maturation, SGCs increased their aldosterone, eNOS, purinergic and gap junction signaling (Figure 5a; bold). These pathways correspond with experimental data on SGC communication in the trigeminal and dorsal root ganglia.[3] Aldosterone

signaling has been demonstrated to result in astrocyte proliferation,[36] but can also alter astrocyte function and activity,[46] which might cause neuronal death.[47] Comparison of these studies indicate a dose-dependent effect of aldosterone, the higher aldosterone levels causing neurotoxic effects. As aldosterone levels are also increased in HF, this could possibly indicate a (direct) connection between (neurohumoral) changes during the development and progression of HF and SGC function and activity.[48]

As astrocytes aged, (oxidative) stress signaling pathways, such as through the BAG2 protein pathway,[41] became progressively enriched (Figure 5a). Androgen signaling, which has been demonstrated to promote death in primary cortical astrocytes,[40] and α-adrenergic signaling were also increased (Figure 5A). Although the exact meaning of the latter pathway remains to be elucidated, Paukert *et al.* (2014)[52] showed that norepinephrine enhanced the reactivity of astrocytes to neuronal activity in the CNS. Surprisingly, melatonin signaling was also increased as SGCs aged (Figure 5a). Signaling through melatonin has been shown to protect astrocytes from oxidative-stress induced stress responses,[50] and might therefore reflect a compensatory reaction of aging SGCs.

Clinical relevance

SGCs have been demonstrated to modulate efferent sympathetic outflow to the heart and to be more activated in the stellate ganglia of cardiomyopathy patients.[48] Using scRNAseq, we offer unique insights into SGC biology and diversity. Especially the knowledge on glial communication, its dynamic response to injury, and how this injury-response translates to modulation of sympathetic outflow might be an interesting target for future HF therapies.

Future directions

The present study is the first to identify the coexistence of SGC subtypes in murine stellate ganglia and to describe their (functional) characteristics. Hence, the field of SGC behavior in stellate ganglia is wide open. The change in SGC characteristics and populations over time remains to be fully disseminated. Understanding how SGC adapt to aging and changing conditions would give more insight on the biological functions of SGCs and their modulatory and supportive roles in the stellate ganglia. Moreover, the current study only included male mice to exclude the possible effects of female sex

568622-L-bw-Weperen
Processed on: 3-11-2021

hormones. Nevertheless, the degree to which sex differences affect SGC behavior would be an interesting direction for future studies.

Limitations

While we have presented comprehensive transcriptomic analyses, we have not demonstrated physiological distinctions across the transcriptomes as this is beyond the scope of this report. The mice included in the study had received AAVs through paw and intracardiac injections, which were retrogradely transported to the stellate ganglia. Nevertheless, it is unlikely that these AAVs have disrupted normal SGC dynamics in the stellate ganglia as AAVs are known to trigger very low immune responses and to be rapidly cleared.[15,16] Moreover, the AAVs in this study were injected locally with minimal systemic exposure, and studies were performed 3 weeks after injection, which is well beyond the half-life and functional clearance of the viruses.[50,51] Even though it is unlikely to have disturbed SGC dynamics by AAV exposure, the sixth cluster, which was characterized by increased expression of pro-inflammatory markers, was excluded from further analyses.

CONCLUSION

SGCs are a heterogeneous population of neuronal modulatory cells in the stellate ganglia. Their diversity is based on the state of maturation or differentiation, which might be dynamically responding to environmental changes in health and disease. Functional studies in control and pathologic conditions are warranted to validate these findings.

DATA AVAILABILITY STATEMENT:

Glial transcriptomic data and code used to generate data in this manuscript are freely available to investigators, and can be obtained by an email to the corresponding author.

REFERENCES

1. Allen NJ & Lyons DA. Glia as architects of central nervous system formation and function. *Science.* **362,** 181–185 (2018).
2. Allen NJ & Eroglu C. Cell Biology of Astrocyte-Synapse Interactions. *Neuron* **96,** 697–708 (2017).
3. Hanani M. Satellite glial cells: More than just rings around the neuron. *Neuron Glia Biol.* **6,** 1–2 (2010).
4. Hanani M. Satellite glial cells in sympathetic and parasympathetic ganglia: In search of function. *Brain Res. Rev.* **64,** 304–327 (2010).
5. Huang LYM, Gu Y & Chen Y. Communication between neuronal somata and satellite glial cells in sensory ganglia. *Glia* **61,** 1571–1581 (2013).
6. Pannese E. *The Satellite Cells of the Sensory Ganglia*. *Advances in anatomy, embryology, and cell biology* **65** (1981).
7. Donegan M, Kernisant M, Cua C, Jasmin L & Ohara PT. Satellite glial cell proliferation in the trigeminal ganglia after chronic constriction injury of the infraorbital nerve. *Glia* **61,** 2000–2008 (2013).
8. Shinder V, Govrin-Lippmann R, Cohen S, Belenky M, Ilin P, Fried K, Wilkinson HA & Devor M. Structural basis of sympathetic-sensory coupling in rat and human dorsal root ganglia following peripheral nerve injury. *J. Neurocytol.* **28,** 743–761 (1999).
9. Pannese E, Ledda M, Cherkas PS, Huang TY & Hanani M. Satellite cell reactions to axon injury of sensory ganglion neurons: Increase in number of gap junctions and formation of bridges connecting previously separate perineuronal sheaths. *Anat. Embryol.* **206,** 337–347 (2003).
10. Pannese E. The structure of the perineuronal sheath of satellite glial cells (SGCs) in sensory ganglia. *Neuron Glia Biology* **6,** 3–10 (2010).
11. Woodham P, Anderson PN, Nadim W & Turmaine M. Satellite cells surrounding axotomised rat dorsal root ganglion cells increase expression of a GFAP-like protein. *Neurosci. Lett.* **98,** 8–12 (1989).
12. Blum E, Procacci P, Conte V, Sartori P & Hanani M. Long term effects of lipopolysaccharide on satellite glial cells in mouse dorsal root ganglia. *Exp. Cell Res.* **350,** 236–241 (2017).
13. Agulhon C, Boyt KM, Xie AX, Friocourt F, Roth BL & McCarthy KD. Modulation

of the autonomic nervous system and behaviour by acute glial cell G_q protein-coupled receptor activation *in vivo*. *J. Physiol.* **591,** 5599–5609 (2013).

14. Xie AX, Lee JJ & McCarthy KD. Ganglionic GFAP+ glial Gq-GPCR signaling enhances heart functions in vivo. *JCI Insight* **2,** e90565 (2017).
15. Ajijola OA, Hoover DB, Simerly TM, Brown TC, Yanagawa J, Biniwale RM, Lee JM, Sadeghi A, Khanlou N, Ardell JL & Shivkumar K. Inflammation, oxidative stress, and glial cell activation characterize stellate ganglia from humans with electrical storm. *JCI insight* **2,** e94715 (2017).
16. Basner-Tschakarjan E & Mingozzi F. Cell-mediated immunity to AAV vectors, evolving concepts and potential solutions. *Front. Immunol.* **5,** (2014).
17. Mays LE, Wang L, Lin J, Bell P, Crawford A, Wherry EJ & Wilson JM. AAV8 induces tolerance in murine muscle as a result of poor APC transduction, T cell exhaustion, and minimal MHCI upregulation on target cells. *Mol. Ther.* **22,** 28–41 (2014).
18. Stuart T, Butler A, Hoffman P, Hafemeister C, Papalexi E, Mauck WM, Hao Y, Stoeckius M, Smibert P & Satija R. Comprehensive Integration of Single-Cell Data. *Cell* **177,** 1888-1902.e21 (2019).
19. Canonical Correlation Analysis. in *Applied Multivariate Statistical Analysis* 321–330 (2007). doi:10.1007/978-3-540-72244-1_14
20. Blondel VD, Guillaume JL, Lambiotte R & Lefebvre E. Fast unfolding of communities in large networks. *J. Stat. Mech. Theory Exp.* **2008,** P10008 (2008).
21. McInnes L, Healy J & Melville J. UMAP: Uniform Manifold Approximation and Projection for Dimension Reduction. *Arxiv* (2018).
22. Wang X Bin, Ma W, Luo T, Yang JW, Wang XP, Dai YF, Guo JH & Li LY. A novel primary culture method for high-purity satellite glial cells derived from rat dorsal root ganglion. *Neural Regen. Res.* **14,** 339–345 (2019).
23. Weider M, Wegener A, Schmitt C, Küspert M, Hillgärtner S, Bösl MR, Hermans-Borgmeyer I, Nait-Oumesmar B & Wegner M. Elevated In Vivo Levels of a Single Transcription Factor Directly Convert Satellite Glia into Oligodendrocyte-like Cells. *PLoS Genet.* **11,** 1–21 (2015).
24. Cahoy JD, Emery B, Kaushal A, Foo LC, Zamanian JL, Christopherson KS, Xing Y, Lubischer JL, Krieg PA, Krupenko SA, Thompson WJ & Barres BA. A transcriptome database for astrocytes, neurons, and oligodendrocytes: A new

resource for understanding brain development and function. *J. Neurosci.* **28,** 264–278 (2008).

25. Boisvert MM, Erikson GA, Shokhirev MN & Allen NJ. The Aging Astrocyte Transcriptome from Multiple Regions of the Mouse Brain. *Cell Rep.* **22,** 269–285 (2018).
26. Magistri M, Khoury N, Mazza EMC, Velmeshev D, Lee JK, Bicciato S, Tsoulfas P & Faghihi MA. A comparative transcriptomic analysis of astrocytes differentiation from human neural progenitor cells. *Eur. J. Neurosci.* **44,** 2858–2870 (2016).
27. Zhang Y, Chen K, Sloan SA, Bennett ML, Scholze AR, O'Keeffe S, Phatnani HP, Guarnieri P, Caneda C, Ruderisch N, Deng S, Liddelow SA, Zhang C, Daneman R, Maniatis T, Barres BA & Wu JQ. An RNA-sequencing transcriptome and splicing database of glia, neurons, and vascular cells of the cerebral cortex. *J. Neurosci.* **34,** 11929–11947 (2014).
28. Jacob C. Transcriptional control of neural crest specification into peripheral glia. *Glia* **63,** 1883–1896 (2015).
29. Johnson MB, Wang PP, Atabay KD, Murphy EA, Doan RN, Hecht JL & Walsh CA. Single-cell analysis reveals transcriptional heterogeneity of neural progenitors in human cortex. *Nat. Neurosci.* **18,** 637–646 (2015).
30. Pollen AA, Nowakowski TJ, Chen J, Retallack H, Sandoval-Espinosa C, Nicholas CR, Shuga J, Liu SJ, Oldham MC, Diaz A, Lim DA, Leyrat AA, West JA & Kriegstein AR. Molecular Identity of Human Outer Radial Glia during Cortical Development. *Cell* **163,** 55–67 (2015).
31. Penisson M, Ladewig J, Belvindrah R & Francis F. Genes and Mechanisms Involved in the Generation and Amplification of Basal Radial Glial Cells. *Front. Cell. Neurosci.* **13,** 381 (2019).
32. Street K, Risso D, Fletcher RB, Das D, Ngai J, Yosef N, Purdom E & Dudoit S. Slingshot: Cell lineage and pseudotime inference for single-cell transcriptomics. *BMC Genomics* **19,** (2018).
33. Palmer AL & Ousman SS. Astrocytes and aging. *Front. Aging Neurosci.* **10,** 337 (2018).
34. Gottschall PE & Howell MD. ADAMTS expression and function in central nervous system injury and disorders. *Matrix Biol.* **44–46,** 70–76 (2015).

35. Oberacker T, Bajorat J, Ziola S, Schroeder A, Röth D, Kastl L, Edgar BA, Wagner W, Gülow K & Krammer PH. Enhanced expression of thioredoxin-interacting-protein regulates oxidative DNA damage and aging. *FEBS Lett.* **592,** 2297–2307 (2018).
36. Miller DJ & Fort PE. Heat shock proteins regulatory role in neurodevelopment. *Front. Neurosci.* **12,** 821 (2018).
37. Clark MA, Guillaume G & Pierre-Louis HC. Angiotensin II induces proliferation of cultured rat astrocytes through c-Jun N-terminal kinase. *Brain Res. Bull.* **75,** 101–106 (2008).
38. Latacz A, Russell JA, Ocloń E, Zubel-Lojek J & Pierzchala-Koziec K. mTOR pathway - novel modulator of astrocyte activity. *Folia Biol. (Praha).* **63,** 95–105 (2015).
39. Cornell B & Toyo-oka K. 14-3-3 proteins in brain development: Neurogenesis, neuronal migration and neuromorphogenesis. *Front. Mol. Neurosci.* **10,** 318 (2017).
40. Brunkhorst R, Bock H & Derouiche A. Reelin induces process growth in cultured astrocytes: Implication for Glia-synaptic plasticity. *Arch. Ital. Biol.* **153,** 249–254 (2015).
41. Gatson JW & Singh M. Activation of a membrane-associated androgen receptor promotes cell death in primary cortical astrocytes. *Endocrinology* **148,** 2458–2464 (2007).
42. Qin L, Guo J, Zheng Q & Zhang H. BAG2 structure, function and involvement in disease. *Cell. Mol. Biol. Lett.* **21,** 18 (2016).
43. Cheng Y, Takeuchi H, Sonobe Y, Jin S, Wang Y, Horiuchi H, Parajuli B, Kawanokuchi J, Mizuno T & Suzumura A. Sirtuin 1 attenuates oxidative stress via upregulation of superoxide dismutase 2 and catalase in astrocytes. *J. Neuroimmunol.* **269,** 38–43 (2014).
44. Brunne B, Zhao S, Derouiche A, Herz J, Petra M, Frotscher M & Bock HH. Origin, maturation, and astroglial transformation of secondary radial glial cells in the developing dentate gyrus. *Glia* **58,** 1553–1569 (2010).
45. Pannese E. Observations on the morphology, submicroscopic structure and biological properties of satellite cells (S.C.) in sensory ganglia of mammals. *Zeitschrift für Zellforsch. und Mikroskopische Anat.* **52,** 567–597 (1960).

46. Zhang L, Xie R, Yang J, Zhao Y, Qi C, Bian G, Wang M, Shan J, Wang C, Wang D, Luo C, Wang Y & Wu S. Chronic pain induces nociceptive neurogenesis in dorsal root ganglia from Sox2-positive satellite cells. *Glia* **67,** 1062–1075 (2019).
47. Zhu X, Hill RA & Nishiyama A. NG2 cells generate oligodendrocytes and gray matter astrocytes in the spinal cord. *Neuron Glia Biol.* **4,** 19–26 (2008).
48. Lechler T. Adherens junctions and stem cells. *Subcell. Biochem.* **60,** 359–377 (2012).
49. Pieters T & van Roy F. Role of cell-cell adhesion complexes in embryonic stem cell biology. *J. Cell Sci.* **127,** 2603–2613 (2014).
50. Zschocke J, Bayatti N, Clement AM, Witan H, Figiel M, Engele J & Behl C. Differential promotion of glutamate transporter expression and function by glucocorticoids in astrocytes from various brain regions. *J. Biol. Chem.* **280,** 34924–34932 (2005).
51. Min LJ, Mogi M, Iwanami J, Sakata A, Jing F, Tsukuda K, Ohshima K & Horiuchi M. Angiotensin II and aldosterone-induced neuronal damage in neurons through an astrocyte-dependent mechanism. *Hypertens. Res.* **34,** 773–778 (2011).
52. Ajijola OA, Hoover DB, Simerly TM, Brown TC, Yanagawa J, Biniwale RM, Lee JM, Sadeghi A, Khanlou N, Ardell JL & Shivkumar K. Inflammation, oxidative stress, and glial cell activation characterize stellate ganglia from humans with electrical storm. *JCI insight* **2,** e94715 (2017).
53. Paukert M, Agarwal A, Cha J, Doze VA, Kang JU & Bergles DE. Norepinephrine controls astroglial responsiveness to local circuit activity. *Neuron* **82,** 1263–1270 (2014).
54. Chen X, Xi Z, Liang H, Sun Y, Zhong Z, Wang B, Bian L & Sun Q. Melatonin Prevents Mice Cortical Astrocytes From Hemin-Induced Toxicity Through Activating PKCα/Nrf2/HO-1 Signaling in vitro. *Front. Neurosci.* **13,** 760 (2019).
55. van Gestel MA, Boender AJ, de Vrind VAJ, Garner KM, Luijendijk MCM & Adan RAH. Recombinant Adeno-Associated Virus: Efficient Transduction of the Rat VMH and Clearance from Blood. *PLoS One* **9,** e97639 (2014).
56. Mason MRJ, Ehlert EME, Eggers R, Pool CW, Hermening S, Huseinovic A, Timmermans E, Blits B & Verhaagen J. Comparison of AAV serotypes for gene delivery to dorsal root ganglion neurons. *Mol. Ther.* **18,** 715–724 (2010).

SUPPLEMENTARY MATERIAL

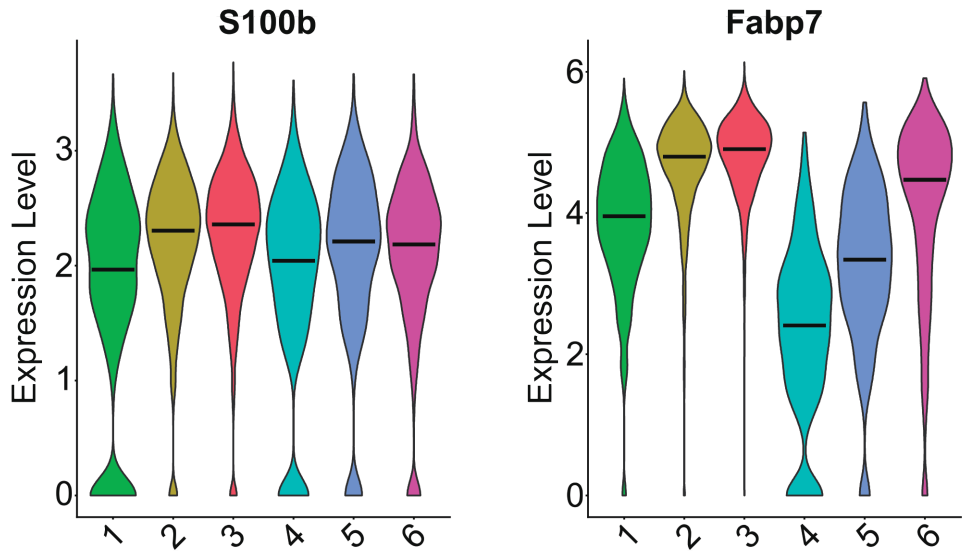

Figure S1: **Violin plots showing the expression of the known SGC markers *S100B* and *Fabp7* in the different clusters.**

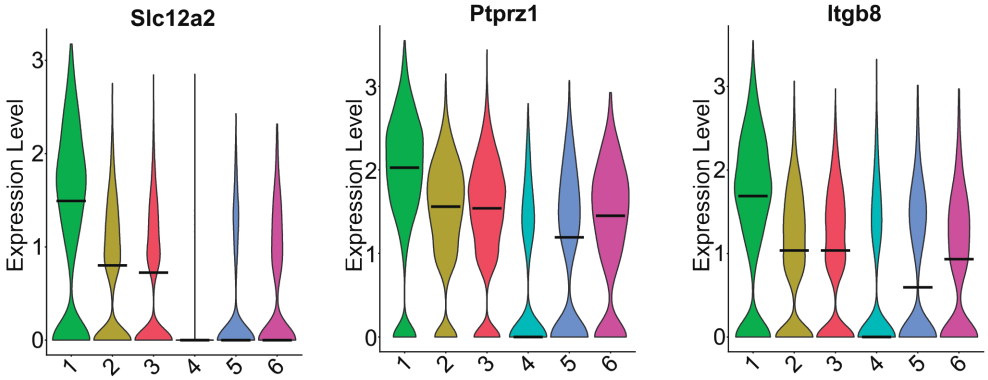

Figure S2: **Expression levels of astrocyte immaturity markers in the satellite glial cell clusters.** Violin plots depicting the relative expression levels of genetic markers *Slc12a2*, *Ptprz1* and *Itgb8,* which are highly expressed in astrocyte progenitor cells. As all three markers were highest expressed in cluster 1, this cluster was chosen as the root node for subsequent trajectory analysis.

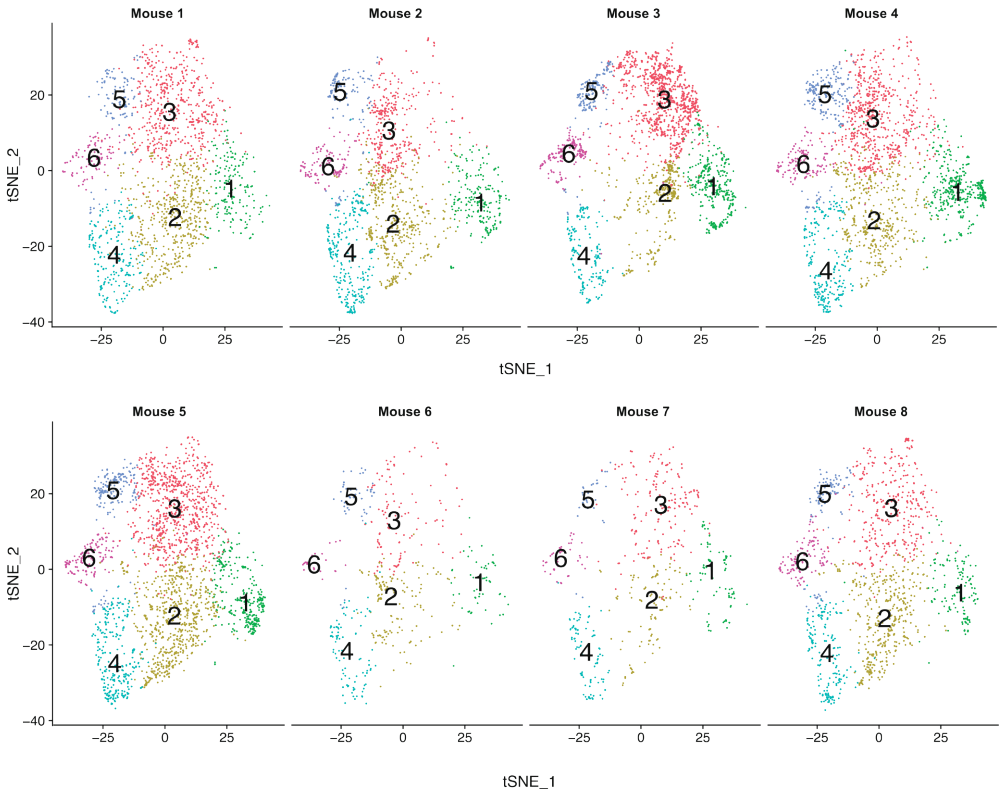

Figure S3: **t-SNE plots showing that all clusters were present and similarly represented in all eight mice.**

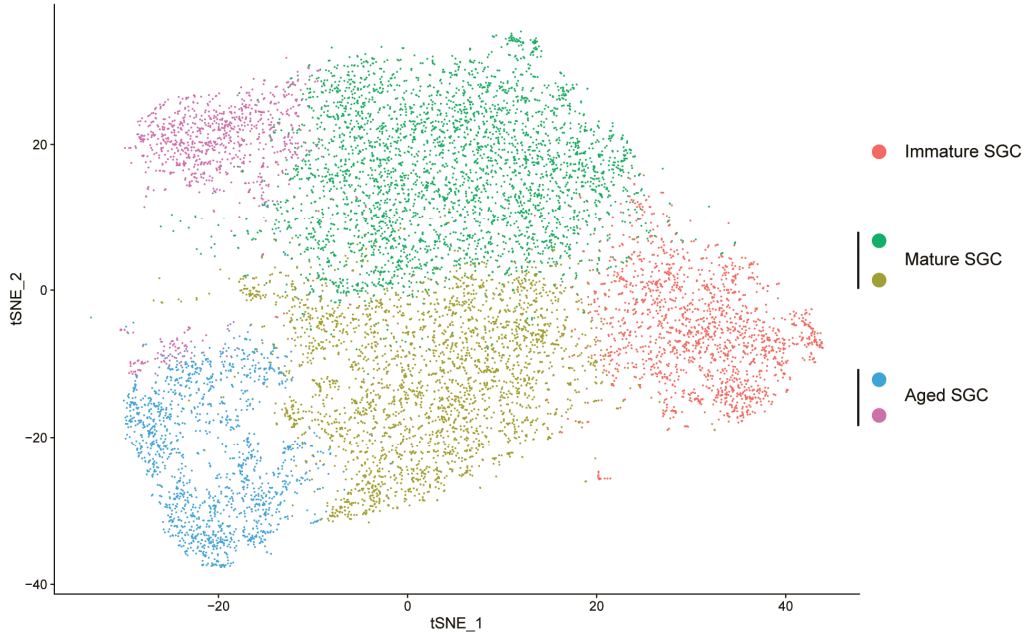

Figure S4: **t-SNE plot of the different clusters with their corresponding state of maturation or reactivity.**

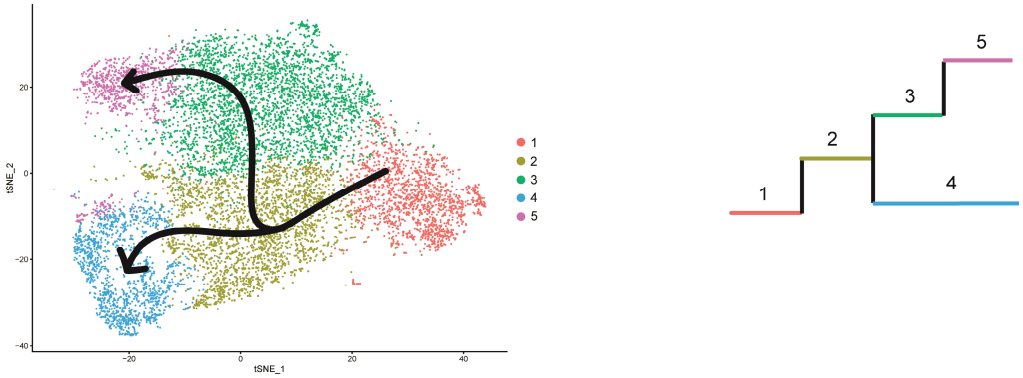

Figure S5: **Pseudo-time analysis on the satellite glial cell (SGC) clusters resulted in three different trajectories.** Cluster 1, identified as the immature SGC, initially matured to cluster 2. From there, SGC development branched, progressing to either cluster 3 or 4, which were identified as mature and aged SGCs, respectively. SGCs in cluster 3 subsequently progressed to aged SGC in cluster 5.

SUPPLEMENTARY FILE LEGENDS

File S1: **The differentially up- and down-regulated genes of the six satellite glial cell clusters.** P-values (p_val), adjusted p-values (p_val_adj) and the relative expression ratio in comparison to all other clusters (avg_logFC) are given.

File S2: **Absolute and relative size of the different clusters in the individual mice.** The upper table depicts the absolute number of cells in the different mice that were grouped in each of the different clusters. The lower table shows the percentage of satellite glial cells in each of the different clusters, separated per mouse.

File S3: **A ranking of the 500 highest expressed genes of the five satellite glial cell clusters.** The similarities in highest expressed genes suggested a great level of correlation between all clusters.

File S4: **Biochemical pathways associated with the 500 highest expressed genes of the different clusters.** Ingenuity canonical pathway names and cluster-specific expressed molecules that were associated with these pathways are given. Significance level of the correlation between the pathway and the cluster is given as *p*-value, -log(*p*-value) and Bonferroni-Hochberg corrected *p*-value (-log(B-H-p-value). The ratio of differential expression is expressed as *ratio*. Where applicable, the *z*-scores quantifying extent of activation or inhibition of the associated pathway are also listed. Multiple pathways were similar across clusters (see tab: highest expressed in all). The correlation level of these common pathways with the five clusters is compared using their -log(B-H-p-values).

File S5: **An overview of the pathways that were associated with the differentially expressed genes of the five clusters.** Ingenuity canonical pathway names and cluster-specific molecules associated with these pathways are listed, as are p-value, -log(p-value), and Bonferroni-Hochberg corrected p-value (-log(B-H-p-value). *Z*-score, if applicable, represents a measure of activation or inhibition of the associated pathway.

568622-L-bw-Weperen
Processed on: 3-11-2021

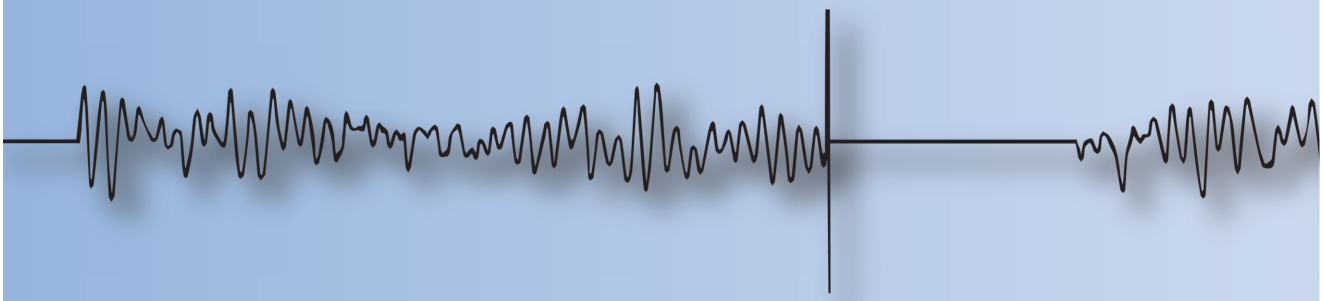

Valerie Y.H. van Weperen, Marc A. Vos & Olujimi A. Ajijola

Clinical Autonomic Research. 2021.
doi: 10.1007/s10286-021-00823-4.

CHAPTER 8

Autonomic modulation of ventricular electrical activity: recent developments and clinical implications

ABSTRACT

Purpose: This review aimed to provide a complete overview of the current stance and recent developments in antiarrhythmic neuromodulatory interventions, focusing on life-threatening ventricular arrhythmias.

Methods: Both preclinical studies and clinical studies were assessed to highlight the gaps in knowledge that remain to be answered and the necessary steps required to properly translate these strategies to the clinical setting.

Results: Cardiac autonomic imbalance, characterized by chronic sympathoexcitation and parasympathetic withdrawal, destabilizes cardiac electrophysiology and promotes ventricular arrhythmogenesis. Therefore, neuromodulatory interventions that target the sympatho-vagal imbalance have emerged as promising antiarrhythmic strategies. These strategies are aimed at different parts of the cardiac neuraxis and directly or indirectly restore cardiac autonomic tone. These interventions include pharmacological blockade of sympathetic neurotransmitters and neuropeptides, cardiac sympathetic denervation, thoracic epidural anesthesia, and spinal cord and vagal nerve stimulation.

Conclusion: Neuromodulatory strategies have repeatedly been demonstrated to be highly effective and very promising anti-arrhythmic therapies. Nevertheless, there is still much room to gain in our understanding of neurocardiac physiology, refining the current neuromodulatory strategic options and elucidating the chronic effects of many of these strategic options.

INTRODUCTION

With every beat, cardiovascular afferent nerves convey sensory information to various centers of the cardiac autonomic nervous system. The subsequent multi-tiered integration of this information results in the meticulous titration of sympathetic (excitatory) and parasympathetic (inhibitory) efferent outflow, modulating cardiac physiology on a beat-to-beat basis.[1–3] While this system has evolved to primarily protect and preserve cardiovascular homeostasis, derangement of this system is an elemental characteristic of a plethora of cardiac diseases.[2,4–6] The derangement-induced autonomic imbalance, which is commonly characterized by sympathetic overactivity and parasympathetic withdrawal, induces electrical instability and thereby greatly enhances the risk of tachycardic ventricular arrhythmias (VAs), both monomorphic and polymorphic, and thus sudden cardiac death.[1] Correspondingly, β-blockers that impede the sympathetic effects on the myocardium are one of the cornerstones of current anti-arrhythmic treatments.[7] However, not all patients benefit from treatment with β-blockers, and their systemic effects cause side-effects.[8,9] It is therefore unsurprising that much research has aimed to decipher the complex interplay between the autonomic nervous system and ventricular arrhythmogenesis, in order to develop innovative, effective and more targeted antiarrhythmic therapies.[10–13] Whereas much of this research remains in the preclinical phase, some neuromodulatory strategies are already implemented in the clinical setting. For that purpose, this review assesses both preclinical studies and clinical studies, thereby providing an overview of recent developments in the field of sympathetic modulation of ventricular electrical activity.

ANIMAL MODELS IN PRECLINICAL STUDIES

As this review assesses both preclinical studies and clinical studies, it is crucial to recognize the main differences in anatomy, neurophysiology and electrophysiology between different animal models and humans and to realize that no animal model is a precise replica of human cardiac anatomy and physiology. In order to describe and interpret preclinical data in the right context and to appreciate the limitations that are inherent to translating preclinical results to clinical practice, this review will briefly discuss the limitations of murine, canine and porcine models.

568622-L-bw-Weperen
Processed on: 3-11-2021

Murine models are widely used in preclinical studies, as they are easy to handle, a relatively cheap experimental model, and genetically manipulable, with many of such strains commercially available.[14] However, the main limitation to using mice in arrhythmia research is that their electrophysiological properties are substantially different from those of humans. For example, their resting heart rate is much higher (±600 beats/min)[15] and ionic currents contribute differently to the action potential (*e.g.* the calcium current is less dominant, and murine repolarization relies heavily on the transient outward current (I_{to}), which also causes their action potential to look greatly different from those of humans.[14,16] Moreover, with regard to the cardiac autonomic nervous system, autonomic tone is dominated by the sympathetic nervous system,[17] in contrast to the parasympathetic predominance in humans (and also dogs and pigs). Hence, these fundamental differences in cardiac physiology, in combination with the smaller size of the murine heart, make it less susceptible to spontaneous ventricular arrhythmias,[18] indicating that these differences significantly affect the process of ventricular arrhythmogenesis. Therefore, one should consider these limitations of murine arrhythmia models when interpreting results on neural remodeling and the effects of cardiac autonomic innervation on ventricular electrophysiology and be aware that most results cannot be directly extrapolated to humans.

Secondly, canine models have been of great value to the field of ventricular arrhythmogenesis, a significant advantage being that all major currents that are present in human myocytes are also found in dogs, resulting in a very similar action potential morphology.[19,20] Moreover, the social nature of dogs allows for awake experiments, which might be especially beneficial when studying the autonomic nervous system, as anesthesia can pose a confounding factor in such experiments.[21] However, canine models also come with various disadvantages and limitations. For example, dogs have a shorter action potential duration and a higher resting heart rate and respiratory rate.[20] Moreover, though parasympathetic tone is dominant in resting humans, the resting autonomic tone in dogs is even more heavily influenced by the parasympathetic nervous system, which is also reflected in their more pronounced respiratory sinus arrhythmia and increased heart rate variability.[22] This difference in autonomic tone must thus be carefully considered in the setting of preclinical studies in

neurocardiology. Lastly, dogs are a costly, time-consuming and labor-intensive animal model, which greatly limits their use.[20]

Pigs are another well-established animal model in the research areas of ventricular arrhythmias and neural remodeling. A great advantage of the pig model is that its coronary circulation is highly similar to that of humans.[23] As a result, the pathophysiology of coronary ligation closely mimics the effects a myocardial infarction has in humans.[23] Moreover, the pig's heart size, heart-to-body weight and inflammatory response are also all very similar to those of humans.[23] However, in comparison to humans, there are some differences in electrophysiology. For example, Purkinje fibers are richly distributed throughout the ventricular walls of pigs.[23] Consequently, the activation wave spreads faster, but the Purkinje fibers might also facilitate the development of sustained ventricular tachycardias.[23] The latter corresponds to the observation that pigs are much more susceptible to ventricular fibrillation then humans, which presents a limitation when it comes to translating results on arrhythmic inducibility and sudden cardiac death to humans. Moreover, one must keep in mind that many experimental groups use pigs that are less than a year old (corresponding to 18 human years).[24] Therefore, the relatively young age of these animals should be kept in mind when extrapolating the effects of neural and/or cardiac remodeling to the human setting, as aging affects the ability and extent to which organs can adapt to a diseased state.

CARDIAC NEURAXIS

Anatomically, the cardiac neuraxis can be divided into three main levels (Figure 1). On the surface of the heart the local *intrinsic cardiac nervous system* (ICNS) represents level 1 of cardiac-neural interplay. This "little brain on the heart" comprises multiple clusters of ganglia, called ganglionated plexi, that are located in epicardial fat pads on the myocardium.[2] The second anatomical level is established by the *intrathoracic extracardiac components*, which amongst other structures, comprises the cervicothoracic ganglia. Thirdly, the *extrathoracic extracardiac components* include nodose ganglia, dorsal root ganglia and various areas within the spinal cord and brainstem that are involved in cardiovascular regulation (Figure 1).[2,25]

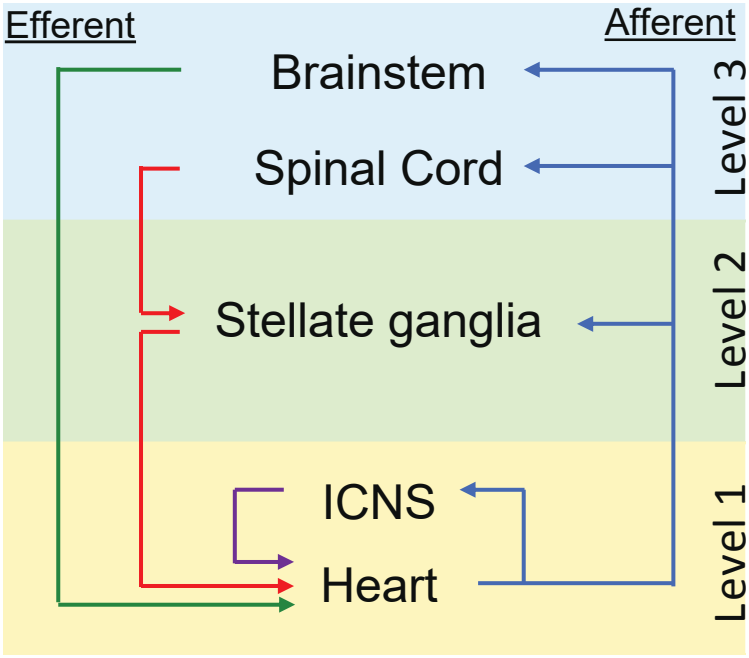

Figure 1. Simplified, schematic overview of the cardiac neuraxis. Neural control is effectuated through reflex loops at different levels of the cardiac neuraxis. ICNS: Intrinsic cardiac nervous system. Blue arrows: afferent nerves. Green arrows: parasympathetic nerves. Red arrows: sympathetic nerves. Purple arrows: ICNS reflex loop.

Functionally, there are multiple characteristics based on which the cardiac neuraxis can be further organized. For example, neurons can be classified as (1) afferent, (2) efferent or (3) local circuit neurons (Figure 1). Collectively, these neurons work in concert to establish feedback loops that convey afferent (sensory) information to integration centers from where efferent (motor) signals are transmitted to the myocardium.[2] Of note, efferent and afferent pathways often comprise series of multiple neurons. In the case of efferent signals, transmission between two such neurons generally occurs within a ganglion, such as the stellate ganglion. Here, *preganglionic neurons* synapse upon *postganglionic* neurons, and additional (afferent) information can be integrated, which might modulate the efferent signal. In this manner, multiple feedback loops between the heart and different levels of the cardiac neuraxis are established (Figure 1).[2,4]

Another, parallel categorization method allocates neural pathways to the sympathetic or parasympathetic branch of the autonomic nervous system. In the case of the sympathetic nervous system, efferents originate in the intermediolateral cell

column of the cervical and thoracic spinal cord (C7-T6). These postganglionic neurons project to the superior, middle, cervicothoracic and stellate ganglia, where they synapse upon postganglionic nerves that travel towards the myocardium.[26–28] Similarly, parasympathetic efferents originate in the dorsal motor nucleus and nucleus ambiguus of the medulla.[29] These pre-ganglionic nerves mainly run through the vagus nerve and its dorsal root ganglion. However, parasympathetic pre- to postganglionic transmission occurs at the level of the heart, as its post-ganglionic nerves constitute the majority of the ICNS.[30,31]

Nevertheless, even though anatomical structures can be roughly assigned to the sympathetic or parasympathetic division, it is important to keep in mind that many of these structures comprise a combination of both divisions; for example the ICNS also contains sympathetic nerves.[32] In contrast, separate neurons are *either* sympathetic *or* parasympathetic and exert their antagonizing effects through different neurotransmitters: whereas norepinephrine (NE), binding to β-adrenergic receptors on myocytes, is the main neurotransmitter of sympathetic nerves, the parasympathetic nerves release acetylcholine (ACh), which interacts with muscarinic receptors on the heart. Of note, ACh, binding onto nicotinic receptors is the primary neurotransmitter in pre- to postganglionic neural transmission for both divisions.

Collectively, this complex yet elegant network allows for continuous feedback between the myocardium and the different levels of the cardiac neuraxis, which results in the beat-to-beat regulation and modulation of all facets of cardiac function, including cardiac electrophysiology.[4] The release of NE and other co-transmitters, such as neuropeptide Y (NPY), from sympathetic cardiac nerve terminals and secretion of epinephrine from adrenal glands initiates various signaling pathways that collectively establish the sympathetic effects on cardiac electrophysiology.[33] For example, both NE and epinephrine can bind to β-adrenergic receptors on myocytes, which initiates a phosphorylation cascade through cAMP-dependent activation of protein kinase A (PKA).[34] As such, PKA-mediated phosphorylation of the L-type calcium channels increases the systolic intracellular calcium concentration and thereby enhances contractional force.[34] Simultaneously, cAMP-dependent PKA phosphorylates ryanodine receptors on the sarcoplasmic reticulum, thereby enhancing the calcium-induced calcium release. This sarcoplasmic release of calcium is especially important

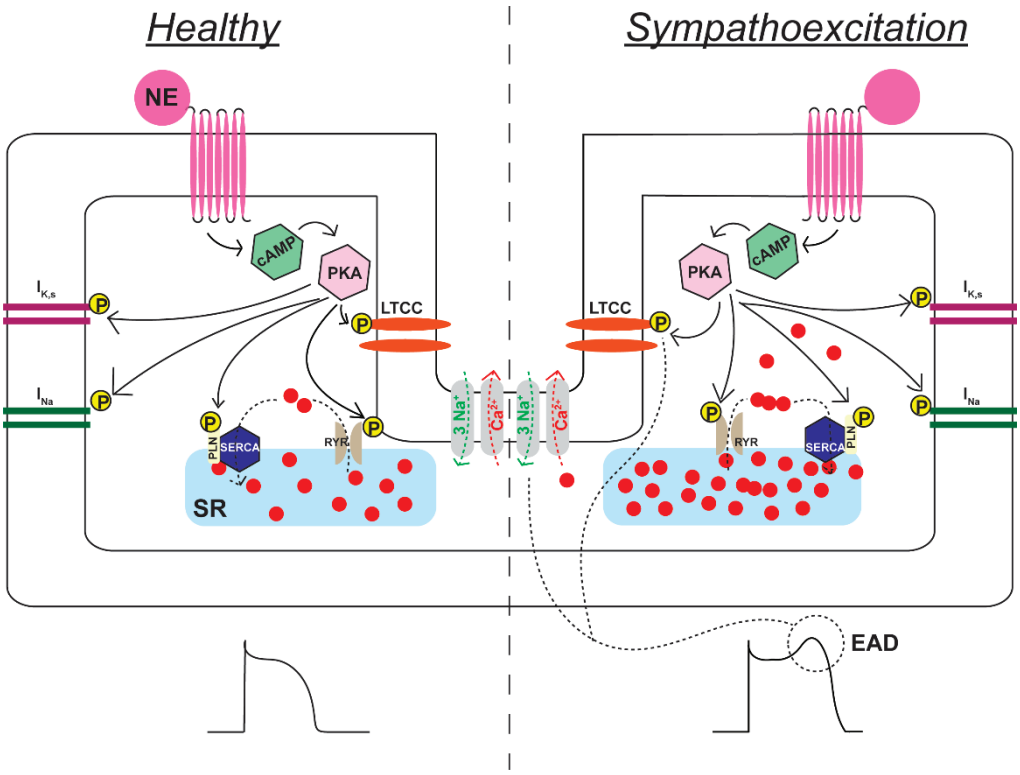

Figure 2. Schematic representation of the electrical effects of sympathetic stimulation under health conditions and in the setting of sympathoexcitation. Healthy: The binding of norepinephrine (NE) or epinephrine to the β-receptor results in cAMP-mediated activation of protein kinase A (PKA). Next, PKA phosphorylates the L-type calcium channel (LTCC), promoting the influx of calcium. Simultaneously, the calcium-induced calcium release from the sarcoplasmic reticulum (SR) is also enhanced by the phosphorylation of the ryanodine receptor (RYR). Simultaneously, phospholamban is also phosphorylated, which enhances the calcium re-uptake through the sarco/endoplasmic reticulum calcium ATPase (SERCA). Lastly, PKA also phosphorylates I_{Na} and $I_{K,s}$, which accommodate the faster heart rate by increasing conduction velocity and shortening repolarization, respectively. Sympathoexcitation: At the cellular level, sympathetic excitation results in the same effects as under healthy conditions. However, the increased calcium influx through LTCC and the increased SR calcium release (due to increased calcium loading) improve contractile force, but also predispose to the development of early- (EAD) or delayed afterdepolarization (DAD; an EAD is shown, a normal action potential is depicted under "healthy" for reference). These afterdepolarizations are caused by the reactivation of the LTCC during the prolonged plateau phase of the action potential or by sodium-calcium exchanger (NCX)-medicated depolarization due to spontaneous calcium release. This predisposition to the development of an early afterdepolarization is further enhanced by the stimulation of I_{Na}, and by the slower effect of sympathetic stimulation on $I_{K,s}$ activation, both of which cause a prolongation in action potential duration.

for increasing systolic calcium concentrations. However, PKA also phosphorylates phospholamban, which stimulates the sarcoplasmic re-uptake of calcium and thereby speeds relaxation.[34] Moreover, the slowly activating potassium channels ($I_{K,s}$) also

become phosphorylated and thereby increased in activity,[35,36] which shortens repolarization to counterbalance calcium-induced prolongation of action potential duration and facilitates an increase in heart rate by shortening the effective refractory period.[37,38] Lastly, phosphorylation of I_{Na} increases ventricular conduction velocities which also accommodates the increased heart rate (Figure 2).[39–41]

Parasympathetic effects, on the other hand, caused by the interaction between ACh and muscarinic receptors, generally counterbalance these sympathetic effects and, amongst other effects, result in a slower heart rate, decrease the L-type calcium channel current and activate the acetylcholine-activated potassium current ($I_{K,Ach}$).[42]

NEURAL REMODELING

In the setting of cardiac injury and impaired cardiac function, the autonomic nervous system remodels to preserve adequate systemic circulation. Consequently, a condition with chronic sympathetic overexcitation and parasympathetic withdrawal is established.

Moreover, these functional changes are mirrored by structural adaptations in the ICNS and stellate and nodose ganglia. For example, in the stellate ganglia, neuronal and glial hypertrophy and increased inflammatory processes have been reported,[43] and in post-infarct murine models, sympathetic nerves in stellate ganglia have been demonstrated to undergo cholinergic transdifferentiation.[44,45] Similarly, neurons in nodose ganglia and ICNS also enlarge, but show an increased sympathetic or decreased cholinergic phenotype, respectively.[46–48] Lastly, parasympathetic withdrawal is also characterized by abnormal activity of vagal neurons[49] and structural and functional changes in the dorsal motor nucleus of the vagus nerve.[48]

At the level of the heart, cardiac injury, especially a myocardial infarction, can result in degeneration of nerve fibers in both the scar and surrounding viable tissue.[50–53] Even though these nerves can regenerate, the extent to which this process develops, occurs in a spatially heterogeneous manner, thereby inducing a condition wherein sympathetic hyperinnervation and denervation co-exist.[50–53]

In animal and human studies, myocardial infarction results in structural and phenotypic changes in ICNS characteristics.[46,47] Moreover, these phenotypic changes most likely reflect functional adaptations, as also observed in a porcine model of myocardial infarction.[47] In this model, myocardial infarction changed the activity pattern of afferent,

processing and efferent neurons of the ICNS. Heterogeneous activation of the ICNS has also been shown to be pro-arrhythmic ,[54,55] whereas blunting of this effect was antiarrhythmic.[56–58] Additionally, in the presence of extracardiac remodeling, heterogeneous nerve sprouting and local autonomic denervation,[51] heterogenous activity of the ICNS is most likely only further amplified. Hence, ICNS remodeling seems to significantly contribute to the establishment of an arrhythmia-susceptible condition.

SYMPATHETIC MODULATION OF MYOCARDIAL ELECTRICAL ACTIVITY IN THE DISEASED HEART

As mentioned, the autonomic nervous system modulates cardiac electrophysiology. It is thus unsurprising that neural remodeling, especially in the presence of diseased or injured myocardium, can adversely impact the electrical stability of the heart. In this way, overt sympathetic innervation can promote the development of arrhythmic *triggers* and/or increase the arrhythmic *susceptibility* of the myocardial substrate.[59].

With regard to modulation of the arrhythmic trigger, early or delayed afterdepolarizations are promoted by sympathetic-induced changes in ion handling, mainly calcium. As mentioned above, sympathetic stimulation increases the systolic calcium concentration and simultaneously augments calcium loading in the sarcoplasmic reticulum.[34] The former can induce early afterdepolarizations through the reactivation of the L-type calcium channels during the prolonged phase 2 of the action potential.[60] The latter can predispose the myocyte to spontaneous calcium release from the sarcoplasmic reticulum and subsequent activation of the sodium-calcium exchanger, thereby triggering an early or delayed afterdepolarization (Figure 2).[61] In addition, stimulation of I_{Na} can prolong action potential duration and thereby predispose to the development of afterdepolarizations.[62] This risk for afterdepolarizations is especially increased during the initial phase of stimulation, as the slower increase in $I_{K,s}$ cannot completely counterbalance the faster effects on calcium handling. Hence, a biphasic effect of sympathetic stimulation can be observed, with an initial and temporary prolongation of action potential duration, which promotes the development of early afterdepolarizations.[63,64]

Second, sympathetic stimulation also promotes the development of re-entry. This effect becomes more pronounced during prolonged stimulation, when increases in $I_{K,s}$ cause the effective refractory period to become shortened. Moreover, it is not just

the cellular electrical instability that promotes re-entry. At the tissue level, nerve sprouting and its heterogeneous nature might increase (transmural) dispersion of repolarization.[65] Especially in regions of hyperinnervation, overt release of NE can regionally exacerbate the aforementioned sympathetic-induced cellular instability.[59,66] Moreover, in these regions of hyperinnervation, chronic overt sympathetic innervation can result in the downregulation of potassium channels and prolong action potential duration,[67] which results in increased spatial dispersion of repolarization. On the contrary, local sympathetic hypo-innervation can promote spatial dispersion of repolarization and also result in super-sensitivity of the local β-adrenergic receptors, causing pro-arrhythmic conditions when exposed to catecholamines.[68] Correspondingly, following a myocardial infarction and associated neural remodeling, the myocardium has been reported to become more sensitive to circulating catecholamines, whereas the effects of direct nerve stimulation were decreased.[69] This was in contrast to healthy situations wherein direct nerve stimulation, rather than circulating catecholamines, increased spatial dispersion of repolarization.[70]

Hence, sympathetic stimulation destabilizes cardiac electrophysiology at the cellular level and thereby predisposes the heart to the development of arrhythmic triggers, whilst simultaneously increasing the arrhythmic susceptibility of the myocardial substrate.[59] As such, cardiac autonomic imbalance strongly promotes the initiation and perpetuation of ventricular arrhythmias.

INTERVENTIONS

As autonomic disbalance drives electrical instability of the myocardium and thereby predisposes to ventricular arrhythmias, antiarrhythmic neuromodulatory therapies aim to restore this balance. These interventions are primarily designed to *decrease* sympathetic efferent signaling and/or *increase* parasympathetic activity. This review has divided such interventions into three groups, based on their primary modulatory target. Therefore, neuromodulatory strategies are classified as modulating (i) the ICNS or myocytes, (ii) cardiac efferents or (iii) cardiac afferent signaling (and thus also affecting the integration of autonomic stimuli) (Figure 3; Table 1).

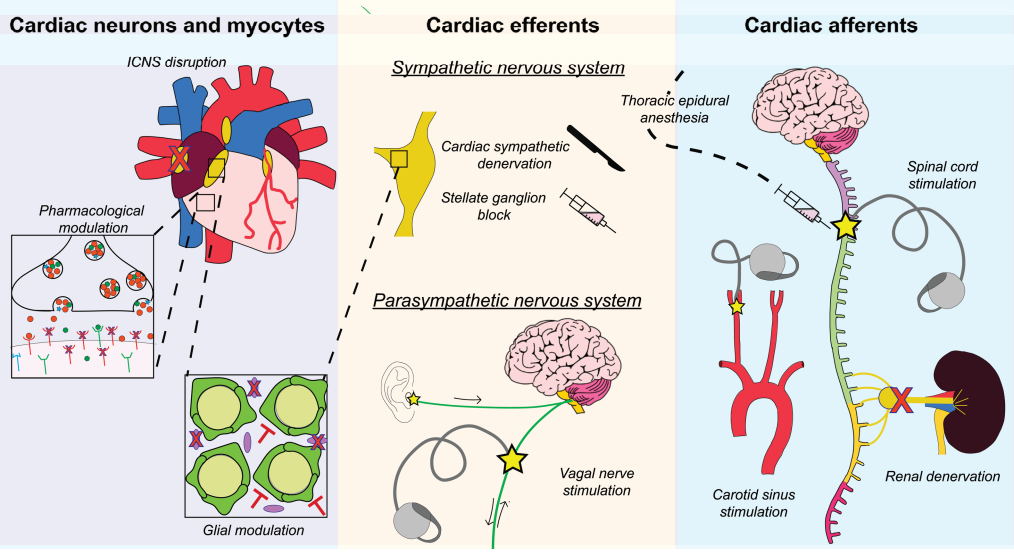

Figure 3. Schematic overview of neuromodulatory interventions that are currently being developed or are already clinically implemented. Interventions are divided into three groups based on their respective primary target for modulation. The first group of interventions modulates the intrinsic cardiac nervous system (ICNS) or the myocytes and includes pharmacological inhibition of sympathetic overdrive, ICNS disruption or glial modulation. Glial modulation has been studied in the ICNS and in the stellate ganglia and is therefore connected to both. The second group (consisting of cardiac sympathetic denervation, stellate ganglia block, thoracic epidural anesthesia and (auricular) vagal nerve stimulation) directly modulate cardiac efferent and thereby either decrease sympathetic outflow or increase parasympathetic tone. The arrows next to the (auricular branch of the) vagal nerve depict the presence of afferent and/or efferent nerves. Thoracic epidural anesthesia affects cardiac efferents and afferents to a comparable extent and is therefore placed at the border of the second and the third group. Lastly, the third group (including spinal cord stimulation, carotid sinus stimulation and renal denervation) primarily modulates cardiac autonomic balance indirectly by changing cardiac afferent activity and thereby influencing the efferent outflow that is established in integration centers across the cardiac neuraxis.

Modulation of cardiac neurons and myocytes

Pharmacological inhibition of the sympathetic nervous system

Ever since James Black introduced β-blockers as an antianginal drug in the 1950s, this group of sympathetic blocking drugs have revolutionized the pharmacological treatment of a plethora of cardiovascular diseases. Moreover, in the setting of ventricular arrhythmias, β-blockers are the only drugs that improve survival when used for either primary or secondary prevention of SCD,[9] and are thus not surprisingly the cornerstone of anti-arrhythmic treatment.[7] In addition, various inherited channelopathies (*e.g.* long QT syndrome, catecholaminergic polymorphic ventricular tachycardia) also rely on β-blockers as the first line of therapy in SCD prevention.

568622-L-bw-Weperen
Processed on: 3-11-2021

β-blockers are generally classified as either nonselective (with both β-1- and β-2- blocking properties, *e.g.* propranolol), or β-1-selective (*i.e.* bisoprolol).[7] Even though β-2 and β-3 receptors can also be selectively targeted, such drugs are not currently used as an adjuvant therapy.[9] Nevertheless, it is important to note that β-blocking properties are not solely limited to the category of β-blockers (class II of the Vaughan-Williams classification), but are also (to a lesser extent) shared by class I and class III antiarrhythmic drugs, such as propafenone and amiodarone, respectively.

However, even at maximally tolerated doses, β-blocker therapy can be insufficient to suppress recurrent VAs.[8] As such, novel pharmacological strategies have been developed that impede the sympathetic effects on the heart by targeting neurotransmitters or neuropeptides other than NE. NPY in particular has emerged as a promising target for next-generation neuromodulatory pharmacological therapies. This sympathetic co-transmitter is released during high-level sympathetic stimulation and has various (cardiovascular) effects including vasoconstriction,[71] parasympathetic inhibition[72] and cardiac electrical modulation[73] by increasing myocyte calcium loading.[74] Ajijola *et al.* (2020)[75] highlighted the possibly detrimental role of NPY in congestive heart failure, as they showed that elevated coronary sinus NPY levels (NPY ≥ 130 pg/mL) were significantly associated with a significantly increased risk in the composite endpoint of death, heart transplantation or implantation of a ventricular assist device.[75] Correspondingly, Kalla *et al.* (2020)[76] studied NPY (serum) levels in patients who underwent percutaneous coronary intervention. Their study showed that patients who suffered from recurrent VAs following the intervention had significantly higher levels of NPY.[76] Hence, even in the presence of β-blockade, NPY appears to destabilize cardiac electrical properties. These findings were corroborated by the observation that in isolated Langendorff perfused rat hearts, high-level stellate stimulation resulted in NPY release and calcium mishandling. The selective β_1-blocker metoprolol could not reverse these effects, but adjuvant therapy with BIBO 3304, a NPY Y1-receptor antagonist, did effectively nullify these pro-arrhythmic conditions.[76] Similarly, Hoang *et al.* (2020),[73] used their *in vivo* porcine model to decipher the differing effects of the nonselective β-blocker propranolol and BIBO 3304. They showed that under conditions of high frequency stimulation, propranolol could not reverse stimulation-induced changes in electrophysiological parameters. However, adjuvant therapy with BIBO 3304 resulted

in stabilization of cardiac electrophysiology and positively augmented cardiac inotropy. Hence, blocking the effects of NPY on the heart and cardiac nervous system represents an interesting and novel (adjuvant) therapeutic target. Similarly, studies have looked into the possibility of blocking other sympathetic nervous system co-transmitters, including galanin[77] and dopamine;[78] however, these avenues await further studies.

ICNS disruption

As the ICNS represents both a relay station of higher centers within the cardiac neuraxis and an independent nervous system located on the heart (Figure 1), it has a complex interaction with cardiac electrophysiology. Consequently, much of the relation between the ICNS, cardiac electrophysiology and arrhythmogenesis remain incompletely understood. Thus far, interventions directed to the ICNS have mainly been studied in the setting of atrial fibrillation (AF). For example, impeding ganglionated plexi activity through ablation[79] or botulinum toxin A injection[80,81] was demonstrated to suppress or prevent AF occurrence, respectively. However, the opposite has also been reported.[82] Moreover, the involvement of the ICNS in the development and maintenance of ventricular arrhythmias has been even less explored. Interestingly, He *et al.* (2013)[83] subjected canines in the setting of an acute myocardial infarction to either ganglionated plexus ablation, or combined ganglionated plexus and stellate ganglion ablation. They showed that the incidence of ventricular fibrillation was significantly higher in animals with isolated ganglionated plexus ablation, suggesting a protective role of ganglionated plexi.[83] Hence, although ganglionated plexi affect cardiac electrophysiology and could theoretically potentiate ventricular arrhythmogenesis, their exact role of this process and their potential as a therapeutic target remain to be elucidated.

Glial cell modulation

Glia are non-neuronal cells that are found throughout the central and peripheral nervous system. These cells fulfill a plethora of functions to both support and modulate neuronal function. However, it has become increasingly clear that derangement of the reciprocal interaction between glia and neurons often contributes to the initiation, promotion and maintenance of (neurological) diseases.[84]

Satellite glial cells

Satellite glial cells (SGCs), the peripheral counterparts of astrocytes, are increasingly of interest in the field of cardiac autonomics. They are found throughout the cardiac neuraxis where they envelope neurons,[85,86] and most likely, dynamically influence synaptic activity.[87,88] Moreover, in patients with recurrent ventricular arrhythmia, SGCs have been demonstrated to be significantly enlarged and to have upregulated *Gfap,* a molecular marker of satellite glial cell reactivity. Hence, SGCs could be involved in the maintenance, or potentially even progression, of sympathetic overdrive. Correspondingly, *Agulhon et al.* (2013)[89] expressed a designer receptor exclusively activated by designer drug (DREADD) on SGCs, which allowed for artificial and selective SGC activation upon administration of clozapine-N-oxide (CNO). They demonstrated that SGC activation increased heart rate and blood pressure, which was later demonstrated to specifically result from SGC activation in the stellate ganglia.[90] Hence, SGC activation in stellate ganglia modulates local neuronal activity which translates to an increased sympathetic outflow to the heart. Therefore, impeding pathological glial activity might represent a promising future target of sympathetic modulation. Such targeted approaches appear feasible as they are already implemented in the central nervous system. Riluzole for example, a drug that inhibits glutamate neurotransmission by decreasing its presynaptic release and facilitating its uptake by glial cells, is already being used in the treatment of amyotrophic lateral sclerosis[91] and has been demonstrated to be effective in the treatment of Alzheimer's disease[92] and various psychiatric disorders in which glia (including astrocytes) are fundamental players in the pathophysiology.[93] Hence, translating such glial modulatory treatments to the peripheral nervous system might expand the boundaries of current cardiovascular treatment options.

In addition, satellite glial cells are also abundantly present within the intrinsic cardiac nervous system,[94] and have been demonstrated to become injured upon catheter ablation of atrial fibrillation.[95] Interestingly, higher serum concentrations of S100B after catheter ablation of atrial fibrillation were associated with a lower recurrence rate.[95] As S100B can induce dendrite outgrowth of myocardial nerves and can also decrease neuronal activity,[96] ablation might induce glial-modulated neural remodeling.[95] It remains unknown if and how ablation of ventricular substrates affects

glia. Hence, more research is warranted into the mechanism by which glial cells of the ICNS influence neural remodeling and how their role in neural modulation might translate to anti-arrhythmic therapies.

Microglia

Lastly, microglia are also emerging as possible participants in various cardiovascular diseases. Also in the setting of recurrent ventricular arrhythmias, inflammatory processes were active in stellate ganglia, which might imply that microglia and other inflammatory cells contribute to this pathological phenotype. Though the role of microglia in ventricular arrhythmogenesis has been scarcely studied, Wang *et al.* (2019)[97] used a post-infarct murine model to demonstrate their involvement in ventricular arrhythmogenesis. In their study, microglial activation was inhibited through light-emitting diode (LED) illumination, a fairly new non-thermal method that modulates cellular activity through photons that are absorbed by mitochondrial chromophores.[98] In their study, they compared the arrhythmic outcome between control mice and mice in which microglia had been kept inactivated following myocardial infarction. They demonstrated that LED illumination resulted in significant decreases in neural activity in the left stellate ganglion and associated this effect with the observed reduction in microglial activity and reduced expression of pro-inflammatory cytokines.[97] Moreover, these effects decreased incidence of VAs significantly, which further highlighted the potential role and therapeutic potential of microglia in ventricular arrhythmias.[97]

Modulation of cardiac efferents

Cardiac sympathetic denervation

Even though increasing antiarrhythmic drugs to their maximally tolerated dose and catheter substrate ablation comprise the central steps in treatment of ventricular arrhythmias, a subset of patients suffer from recurrent ventricular tachycardia despite these treatment modalities.[99,100] Cardiac sympathetic denervation (CSD), the surgical disruption of neural transmission within the left stellate ganglion or bilateral stellate ganglia, has emerged as an effective procedure for this patient population. Even though this strategy is still restricted to a few "expertise centers", the number and size of clinical studies is ever expanding. The success of this treatment modality was reconfirmed in a meta-analysis by Murtaza *et al.* (2020),[101] which combined the results of 14 retrospective clinical studies that included a total of 311 patients with recurrent

ventricular tachycardia or electrical storm. Their analyses showed that CSD resulted in complete abolishment of ventricular tachycardia in approximately 60% of treated patients (average follow-up time: 15 ± 10.7 months) and a significant decrease of 3.01 in mean implantable cardioverter-defibrillator (ICD) shocks.[101] Importantly, these results of CSD efficacy are similar between patients with and without an ischemic substrate underlying their ventricular arrhythmias.[102,103] In addition, a recent study by Assis *et al.* (2021),[104] which represents the longest follow-up study on bilateral CSD thus far, reported a ventricular tachycardia-free survival in 54.5% of the patients at 4 years. Importantly, this study also demonstrated that early recurrence (≤12 weeks) of ventricular tachycardia after bilateral CSD, does not correlate with the long-term antiarrhythmic outcome of this intervention.

CSD has also been demonstrated to be an appropriate and effective antiarrhythmic strategy in the setting of long QT syndrome and catecholaminergic polymorphic ventricular tachycardia.[105]

Nevertheless, not all patients treated with CSD benefit from this intervention. There are various reasons for this undesirable outcome. For example, arrhythmic episodes might not be modulated by the sympathetic nervous system, and therefore CSD will not abolish the pro-arrhythmic factor. In addition, procedural differences in CSD might yield different outcomes. For example, bilateral CSD appears more effective in patients with either an ischemic substrate,[106] or a non-ischemic (including cardiac sarcoidosis) cardiomyopathy,[107] whereas isolated left-sided CSD is effective and even preferred in the setting of the long QT syndrome (type 1, 2 or 3)[108,109] or catecholaminergic polymorphic ventricular tachycardia.[110] Moreover, the extent to which the sympathetic chain needs to be resected is also under much discussion. Whereas the initial reports and CSD went as low as level T7 and T8,[111,112] current practice commonly resects the lower half of the stellate ganglia, down to the level of T4. Though not studied in the clinical setting yet, evidence from animal studies suggests that selected CSD to the level of T2 might be sufficient to be antiarrhythmic.[113] Nevertheless, interindividual variation in origin of cardiac sympathetic innervation might cause this approach to be less effective in the clinical setting.[114]

Hence, even though CSD is a great alternative to current antiarrhythmic therapies and has already been successfully used to treat many patients with recurrent

VAs, there are still possibilities for improvement. For example, as CSD has only been a clinical modality for recurrent VAs for a limited period, long-term results are yet to be published. As such, it is largely unknown yet whether reinnervation of postganglionic nerves, as for example observed following heart transplantation, might induce arrhythmic or other cardiac side effects after the passage of time.[115] Moreover, all trials thus far haven been prospective in character; hence, randomized controlled trials would greatly add to the evidence of CSD's success and could further elucidate the difference between left or bilateral cardiac denervation.

Stellate ganglion blockade

Whereas CSD is permanent and rather invasive, sympathetic outflow from stellate ganglia to the heart can also be interrupted via local pharmacological stellate ganglion blockade (SGB). Through a percutaneous approach in conscious patients, sodium channel blockers (*i.e.* bupivacaine, lidocaine) can be injected into the stellate ganglia to temporarily suppress nerve transmission in that restricted area. This temporarily block can suppress arrhythmias and thus serve as a bridge to longer lasting therapies, such as substrate ablation, CSD or heart transplantation.[116] Injection with these drugs effectively suppress drug-refractory electrical storm in over half of the patients treated (regardless of the intervention being directed to both stellate ganglia or only the left stellate ganglion).[117] However, in order to become a more widespread implemented strategy, SGB still has to overcome several difficulties. For one, though SGB is commonly accepted as a successful and safe procedure, SGB can cause various complications. Neck hematomas and transient hoarseness (caused by the accidental block of the recurrent laryngeal nerve or a large neck hematoma) are the most common complications of SGB.[118] However, also local anesthetic systemic toxicity, a rare but life-threatening adverse event that is caused by too high plasma levels of local anesthetics, can occur.[118] Nevertheless, these complications are rare as SGB is most often guided by ultrasound or performed under fluoroscopic guidance. Moreover, it remains difficult to determine successful SGB block. Various markers of successful blockade have been proposed, such as a temperature rise in the ipsilateral arm, presence of Horner's syndrome (ipsilateral ptosis, myosis and anhidrosis resulting from impeded sympathetic innervation to the eye and ocular adnexae) and the perfusion index.[118–121] Although out of these three parameters the perfusion index has been

established to be best, none of these three modalities is sufficiently sensitive in reflecting successful SGB. [118–121] Hence, for SGB to become a more customary strategy in the acute treatment of refractory VAs, more reliable and robust technical parameters will have to be developed that adequately confirm SGB.

Thoracic epidural anesthesia (TEA)

The injection of anesthetics in the high thoracic epidural space causes temporal and local nerve block, which has been repeatedly demonstrated to be an effective approach in acutely reducing the incidence of ventricular tachycardia and bridging to more permanent antiarrhythmic interventions.[116,117,122,123] The efficacy of this approach has been attributed to multiple factors, including complete and bilateral blockade of all cardiac afferents and sympathetic efferents, as it blocks all nerves in segments C8–T4. With regard to ventricular electrical activity, this complete nerve block impedes arrhythmogenesis by lengthening repolarization duration and prolonging the effective refractory period.[124,125] Moreover, since SGB impedes efferent sympathetic signaling more proximal than β-blockers, this strategy might be especially beneficial in patients with structural heart disease in which the myocardial substrate can be less receptive to pharmacological modulation.[116]

Even though TEA can robustly suppress VA in the acute setting, this technique still requires some refinement. For one, reliable parameters indicative of effective TEA are needed. Moreover, many clinicians remain reluctant to perform TEA, as high thoracic anesthesia could theoretically impede cardiac pump function. Nevertheless, the opposite was demonstrated by Wink *et al.* (2021),[126] who subjected patients with right and/or left ventricular dysfunction to ergometric testing before and after TEA, and showed that TEA did not significantly affect or diminish their exercise-induced increases in pump function.[126] Similarly, clinical case series reported minimal effects of TEA on hemodynamic function.[116,122,123] However, Wink *et al.* (2016)[127] also demonstrated that high thoracic anesthesia diminished right ventricular systolic function. Hence, additional studies into the mechanical and hemodynamic consequences of TEA are warranted, as this technique might represent a highly effective antiarrhythmic strategy that is currently undervalued.

Vagal nerve stimulation

Vagal nerve stimulation (VNS) was primarily developed as a treatment modality for heart failure, but can also be applied in other conditions that are similarly characterized by sympathetic overdrive. Through the continuous stimulation of the parasympathetic nervous system, sympathetic overdrive is mitigated. This strategy has also been effective in the setting of preclinical models of ventricular arrhythmias, as it stabilizes cardiac electrophysiology. For instance, recruitment of $I_{K,Ach}$ and the subsequent shortening of repolarization duration might impede the development of early afterdepolarizations, and VNS has been demonstrated to increase the ventricular fibrillation threshold.[128,129] Moreover, preclinical studies have highlighted the efficacy of VNS in reducing arrhythmic episodes and SCD in the setting of acute and chronic ischemia,[130–132] and in mitigating pro-arrhythmic effects of left stellate ganglion stimulation.[133]

Hence, even though VNS exerts multiple beneficial effects on the myocardium in preclinical studies, it has proven to be rather difficult to corroborate these findings in clinical studies. Especially since clinical studies for VNS were primarily designed to study its effects on heart failure progression, few clinical data are available on the effects of VNS on ventricular arrhythmias. Moreover, conflicting results of these clinical trials on the efficacy of VNS in heart failure patients[134] has constrained efforts towards further studies exploring the clinical applicability of VNS for other cardiovascular diseases. Nevertheless, these conflicting and confusing outcomes of the clinical studies were most likely not a result of VNS *inefficacy*, but rather a methodological problem caused by inappropriate stimulation protocols. In particular, the unsolicited stimulation of afferent vagal nerves and subsequent activation of sympathetic efferents could have induced the disappointing results. The differences in stimulation parameters and their possible effects on clinical outcome have been extensively reviewed elsewhere.[135]

Nevertheless, the ANTHEM II trial, which reported a beneficial effect of VNS on heart failure, also studied electrical effects of VNS during a 3-year follow-up and observed a reduction in the incidence of arrhythmic episodes in their cohort of patients.[136,137] Hence, though rudimentary and still insufficiently refined, VNS remains a promising candidate for future heart failure and antiarrhythmic purposes.

In addition to the inexperience with VNS, its invasive character is also a drawback of this therapy. Therefore, the possibility of transcutaneous VNS through stimulation of the auricular branch of the vagus nerve is currently being explored. Stimulation of this branch results in centrally mediated increases in vagal efferent activity.[138,139] This modality has already proven to be effective in suppressing ventricular arrhythmias in canine models of myocardial infarction[140,141] and has exerted antiarrhythmic effects in the setting of acute myocardial infarctions in humans.[142] In addition, auricular VNS could possibly be more effective than conventional VNS as the aforementioned adverse activation of vagal afferent is circumvented by this approach.

Future preclinical and clinical studies should therefore aim to optimize the stimulation parameters, to identify markers reflective of optimal stimulation and gear their therapeutic approach towards less invasive modalities.

Modulation of cardiac afferents and integration centers of the cardiac neuraxis

Spinal cord stimulation

As with many other neuromodulatory therapies, spinal cord stimulation (SCS) was initially developed to treat angina pectoris.[143,144] Though not completely understood, local stimulation of the spinal cord affects various central and local neural circuits, which collectively impede the process of arrhythmogenesis.[145–153] For instance, SCS impedes the ability of afferent cardiac nerves in transferring their signal to second order spinal cord neurons, thereby hampering the initiation of a sympathetic reflex and the development of sympathetically driven remodeling processes that are induced by myocardial ischemia.[146,147] In addition, SCS stabilizes the ICNS and decreases left stellate ganglion activity, all of which could contribute to its antiarrhythmic effects.[148, 151,154]

Another benefit of SCS is that it is a relatively fast-acting antiarrhythmic therapy, as it has been demonstrated to be effective within 1 hour in animal models of acute myocardial ischemia.[152,155] However, even though the preclinical success of SCS in animal studies was corroborated by an initial case series, which reported a significant reduction in arrhythmic burden in the two included patients,[156] 2 consecutive larger clinical trials observed contrasting effects on reduction of arrhythmic episodes in patients treated with SCS.[157,158] This inconsistency in results could be attributable to a variety of causes, including differences in SCS parameters (either "continuous and

optimally programmed as determined by the physician" or with a frequency of 50Hz, a pulse width of 200 μs and continuously paced at 90% of maximum tolerated voltage) and anatomical location of pacing (C6 *vs.* T2-T4).[157,158] Hence, SCS shows promise as an antiarrhythmic strategy in the setting of both acute and chronic cardiac injury, but insufficient knowledge on the physiology and interplay between neural centers and optimal location and stimulation parameters of SCS are impeding its advances into clinical applicability.

Carotid sinus stimulation

Carotid sinus stimulation aims to modulate the baroreflex. Normally, afferent nerves in the carotid sinus and aortic arch transmit mechanical information on arterial blood pressure to the central nervous system from where negative feedback is exerted by adapting the relative activity of the cardiac sympathetic and parasympathetic branch. However, chronically increased sympathetic tone causes this reflex to become depressed, resulting in inadequate coordination of sympatho-vagal balance. Therefore, carotid sinus stimulation aims to restore baroreflex sensitivity through artificial activation of baroreceptor afferents, which should cause central stimulation of parasympathetic efferents and inhibition of sympathetic efferents. This elegant tactic to indirectly restore cardiac autonomic tone has been performed in multiple preclinical studies and has been demonstrated to effectively reduce ventricular arrhythmias.[159–161] However, no clinical trials have studied the antiarrhythmic efficacy of this approach in humans. Nevertheless, case series have demonstrated that carotid sinus stimulation can effectively decrease blood pressure in patients suffering from hypertension, an outcome that was attributed to its mitigating effect on the sympathetic nervous system.[162–164] Hence, even though this approach seems effective, feasible and safe, more studies are warranted to expand (clinical) experience on its applicability in the setting of (recurrent) ventricular arrhythmias and to promote its clinical implementation.

Renal denervation

Disrupting renal nerves impedes sympathetic overactivation on a more systemic level. Even though it was first performed in 1953 as a treatment for primary hypertension,[165] sympathetic overdrive contributes to various other cardiovascular diseases and could thus be an adequate approach for a wider range of indications, including ventricular

arrhythmias. Multiple preclinical studies have demonstrated the antiarrhythmic effects of renal denervation. For example, in pigs subjected to 20 minutes of left anterior descending artery (LAD) occlusion, renal denervation exerted acute antiarrhythmic effects,[166] and in animal models of both ischemic and non-ischemic cardiac injury, disruption of renal autonomic nerves prevented pro-arrhythmic neurohumoral cardiac remodeling.[167–169] Unfortunately, the disappointing results of the SYMPLICITY HTN-3 trial,[170] the first sham-controlled clinical trial on the efficacy of renal nerve denervation for hypertension, greatly diminished clinical interest in this strategy. The additional critiques on the trial's experimental design and incomplete execution of renal denervation, have further discredited this strategy and greatly impeded its progression.[171–173] Consequently, clinical data on antiarrhythmic effects of renal denervation are also scarce. Nevertheless, the clinical results that have been published thus far seem promising.[174–180] For example, Remo *et al.* (2014)[175] showed that renal denervation effectively decreased ventricular tachycardia episodes in patients with ischemic and non-ischemic cardiomyopathies who were suffering from refractory ventricular tachycardia. Similarly, Ukena *et al.* (2016)[177] combined 13 cases of patients suffering from chronic heart failure who had undergone renal denervation and showed that this intervention was associated with a significant reduction in arrhythmic burden. Correspondingly, Tsioufis *et al.* (2014)[176] showed the beneficial effect of renal denervation on reducing the occurrence of premature ventricular contractions in patients with drug-resistant and uncontrolled hypertension. Hence, renal denervation positively affects cardiac electrophysiology and exerts an antiarrhythmic effect in a wide range of cardiovascular patients. Future preclinical studies should aim to expand our understanding of the physiology underlying the antiarrhythmic efficacy of renal denervation and to establish the long-term outcome of this approach. Moreover, the ability of renal denervation to *reverse* pro-arrhythmic remodeling remains to be elucidated and further investigations *validating and strengthening* the applicability of this treatment are warranted.

Table 1. Overview of the neuromodulatory interventions. Neuromodulatory interventions, their respective mechanism of action and stage of implementation.

Intervention	Modulatory mechanism	Stage of implementation
Pharmacological modulation		
Beta-blockers	Inhibition of sympathetic effectuation through blockade of beta-adrenergic receptors	Clinically used
NPY-receptor blockers	Blockade of neuropeptide Y (NPY) receptors inhibits the effects of sympathetic co-transmitter NPY	Preclinical
ICNS disruption	Mechanical interruption of neuronal activity within the intrinsic cardiac nervous system (ICNS) impedes pathological neural input	Preclinical
Glial modulation		
Satellite glial cells	Indirect modulation of neuronal behavior by manipulating satellite glial cell activity	Experimental
Microglia	Impediment of pathological inflammation in the stellate ganglia through suppression of microglial activity to modulate neuronal activity	
Cardiac sympathetic denervation	Elimination of cardiac sympathetic input through the mechanical disruption of all neural transmission through left or bilateral stellate ganglia	Clinically used*
Stellate ganglion blockade	Temporal inhibition of stellate ganglia nerve transmission to the myocardium through the administration of local anesthetics	Clinically used*
Thoracic epidural anesthesia	Pharmacological inhibition of all spinal cardiac afferents and sympathetic efferents at levels C8-T4 temporarily blocks sympathetic outflow	Clinically used*
Vagal nerve stimulation		
Vagal nerve stimulation	Direct stimulation of the vagal nerve increases cardiac parasympathetic tone	Clinical trials (Indication: heart failure)
Tragus stimulation	Indirect stimulation of the cardiac parasympathetic nerve fibers by transcutaneous stimulation of the vagal auricular branch	
Spinal cord stimulation	Local stimulation of spinal nerves modulates various central and local neural circuits, and, amongst other effects, impedes the initiation of a sympathetic reflex, the development of sympathetically-driven remodeling processes, stellate ganglion activity and stabilizes the ICNS	Clinical trials (Indication: ventricular arrhythmias)
Carotid sinus stimulation	Stimulation of baroreceptor afferents initiates centrally-driven activation of parasympathetic efferents and inhibition of sympathetic efferents	Preclinical
Renal denervation	Disruption of renal nerves impedes sympathetic overactivation on a more systemic level	Clinical trials (Indication: hypertension)

* The clinical application of these interventions remains limited to a number of specialty centers.

Emerging modalities of neural modulation

Thus far, this review has discussed neuromodulatory interventions that are already clinically implemented or currently progressing towards clinical application. However, novel methods of neuromodulation are continuously being developed as knowledge on the neural-cardiac interplay rapidly grows in parallel with technological advances. Therefore, this last section will briefly elaborate on interesting, novel avenues of neuromodulatory interventions that modify neural activity through the employment of magnetic or ultrasound stimulation.

Transcranial magnetic stimulation is a neuromodulatory technique that is already clinically used for pain and depression, and has much clinical potential for various other (neurological) disorders.[181] Moreover, this intervention has been observed to affect cardiac rhythm[182] and heart rate variability,[183] which indicates its ability to modulate cardiac autonomic tone. Though therapeutically appealing, this technique has thus far not been studied as an antiarrhythmic therapeutic option. Nevertheless, such refinement is made difficult by various confounding factors in clinical neuromodulatory research. For example, aging, comorbidities and interindividual variation in nervous system anatomy and/or functionality result in considerable variations in neuromodulatory response. Although these confounding variables are challenging, current research on modulatory therapies is progressing rapidly.

Electromagnetic stimulation of the ICNS or vagosympathetic nerve trunks were previously demonstrated to effectively suppress atrial fibrillation through modulation of cardiac autonomic balance.[184,185] Wang *et al.* (2016)[186] extrapolated this strategy to suppressing ventricular arrhythmias through low-frequency electromagnetic stimulation of the left stellate ganglia in canines with acute myocardial infarction. They showed that this strategy significantly decreased left stellate ganglion activity and reduced myocardial infarction-induced ventricular arrhythmia burden. Markman *et al.* (2020)[187] published a case series on five patients suffering from ventricular tachycardia storm (≥3 episodes of sustained ventricular tachycardia in 24 hours), which were all treated with transcutaneous magnetic stimulation of the left stellate ganglion. This strategy successfully lowered arrhythmia burden and was not associated with any adverse events, further highlighting the potential of this modality to serve as a bridge to more

permanent interventions. However, further (pre)clinical studies are warranted to further optimize the understanding of this approach.

Lastly, Wang *et al.* (2019)[188] recently reported on the possibility of using low-level ultrasound stimulation of the left stellate ganglion to reduce arrhythmic burden. In their study, dogs were exposed to 10 minutes of low-level ultrasound stimulation prior to the establishment of a myocardial infarction. This pretreatment was shown to possibly inhibit neural activity in the left stellate ganglion and to thereby reduce myocardial infarction-induced ventricular arrhythmias.[188] Though promising, this abstract is the first publication on the efficacy and applicability of this strategy.

It is clear that much more research is needed to advance these modalities to the clinical setting. Nevertheless, with the current pace of device development and progression, the implementation of these stimulatory techniques comparable to that of pacemakers is conceivable. Therefore, the subcutaneous implantation of a stimulatory device could be an excellent treatment option in the outpatient setting.

CONCLUSION

Much research has elucidated the elegance of the cardiac neuraxis and its intricate involvement in cardiac physiology. Moreover, its detrimental role in cardiovascular diseases and ventricular arrhythmogenesis is becoming increasingly clear, which has already resulted in targeted therapies for most levels of the cardiac neuraxis. Even though all these strategies appear very promising, there is still much room to gain in the treatment of these possibly fatal VAs. For example, there is much to learn about how central integration centers and the ICNS control sympatho-vagal balance and how antiarrhythmic therapies can target these structures more specifically. Additionally, even though many neuromodulatory interventions have been developed, most of these interventions would greatly benefit from additional refinement (e.g. identification of robust and reliable parameters of successful neuromodulation and/or optimal stimulatory parameters). Nevertheless, such refinement is made difficult by various confounding factors in clinical neuromodulatory research. For example, aging, comorbidities and interindividual variation in nervous system anatomy and/or functionality result in much variation in neuromodulatory response. Although these confounding variables are challenging, current research on modulatory therapies is progressing at a fast pace.

Lastly, the relatively young age of this research field has not allowed for long-term follow-up studies. Therefore, chronic effects of these therapies are yet to be elucidated. Nevertheless, current research is well on its way to fill these gaps and to further install neuromodulation as a widely implemented antiarrhythmic strategy.

REFERENCES

1. Goldberger JJ, Arora R, Buckley U & Shivkumar K. Autonomic Nervous System Dysfunction: JACC Focus Seminar. *J. Am. Coll. Cardiol.* **73,** 1189–1206 (2019).
2. Ardell JL & Armour JA. Neurocardiology: Structure-Based Function. in *Comprehensive Physiology* **6,** 1635–1653 (John Wiley & Sons, Inc., 2016).
3. Jänig W. Sympathetic nervous system and inflammation: A conceptual view. *Auton. Neurosci. Basic Clin.* **182,** 4–14 (2014).
4. Fukuda K, Kanazawa H, Aizawa Y, Ardell JL & Shivkumar K. Cardiac Innervation and Sudden Cardiac Death. *Circ. Res.* **116,** 2005–2019 (2015).
5. Ardell JL, Andresen MC, Armour JA, Billman GE, Chen PS, Foreman RD, Herring N, O'Leary DS, Sabbah HN, Schultz HD, Sunagawa K & Zucker IH. Translational neurocardiology: preclinical models and cardioneural integrative aspects. *J. Physiol.* **594,** 3877–3909 (2016).
6. Shivkumar K & Ardell JL. Cardiac autonomic control in health and disease. *J. Physiol.* **594,** 3851–3852 (2016).
7. Grandi E & Ripplinger CM. Antiarrhythmic mechanisms of beta blocker therapy. *Pharmacol. Res.* **146,** 104274 (2019).
8. Chatzidou S, Kontogiannis C, Tsilimigras DI, Georgiopoulos G, Kosmopoulos M, Papadopoulou E, Vasilopoulos G & Rokas S. Propranolol Versus Metoprolol for Treatment of Electrical Storm in Patients With Implantable Cardioverter-Defibrillator. *J. Am. Coll. Cardiol.* **71,** 1897–1906 (2018).
9. Al-Khatib SM, Stevenson WG, Ackerman MJ, Bryant WJ, Callans DJ, Curtis AB, Deal BJ, Dickfeld T, Field ME, Fonarow GC, Gillis AM, Granger CB, Hammill SC, Hlatky MA, Joglar JA, Kay GN, Matlock DD, Myerburg RJ & Page RL. 2017 AHA/ACC/HRS Guideline for Management of Patients With Ventricular Arrhythmias and the Prevention of Sudden Cardiac Death: Executive Summary: A Report of the American College of Cardiology/American Heart Association Task Force on Clinical Practice Gui. *Circulation* **138,** e210–e271 (2018).
10. Shivkumar K, Ajijola OA, Anand I, Armour JA, Chen P-S, Esler M, Ferrari GM De, Fishbein MC, Goldberger JJ, Harper RM, Joyner MJ, Khalsa SS, Kumar R, Lane R, Mahajan A, Po S, Schwartz PJ, Somers VK, Valderrabano M, Vaseghi M & Zipes DP. Clinical neurocardiology defining the value of neuroscience-

based cardiovascular therapeutics. *J. Physiol.* **594,** 3911–3954 (2016).

11. Kapa S, DeSimone C & Asirvatham SJ. Innervation of the Heart: An Invisible Grid within a Black Box. *Trends Cardiovasc. Med.* **26,** 245 (2016).
12. Chatterjee NA & Singh JP. Novel Interventional Therapies to Modulate the Autonomic Tone in Heart Failure. *JACC Hear. Fail.* **3,** 786–802 (2015).
13. Waldron NH, Fudim M, Mathew JP & Piccini JP. Neuromodulation for the Treatment of Heart Rhythm Disorders. *JACC Basic to Transl. Sci.* **4,** 546 (2019).
14. Choy L, Yeo JM, Tse V, Chan SP & Tse G. Cardiac disease and arrhythmogenesis: Mechanistic insights from mouse models. *IJC Heart and Vasculature* **12,** 1–10 (2016).
15. Mitchell GF, Jeron A & Koren G. Measurement of heart rate and Q-T interval in the conscious mouse. *Am. J. Physiol. - Heart Circ. Physiol.* **274,** 747–751 (1998).
16. Boukens BJ, Rivaud MR, Rentschler S & Coronel R. Misinterpretation of the mouse ECG: 'musing the waves of *Mus musculus* '. *J. Physiol.* **592,** 4613–4626 (2014).
17. Janssen BJA & Smits JFM. Autonomic control of blood pressure in mice: Basic physiology and effects of genetic modification. *American Journal of Physiology - Regulatory Integrative and Comparative Physiology* **282,** (2002).
18. London B. Cardiac arrhythmias: From (transgenic) mice to men. *Journal of Cardiovascular Electrophysiology* **12,** 1089–1091 (2001).
19. Kaese S, Frommeyer G, Verheule S, Van Loon G, Gehrmann J, Breithardt G & Eckardt L. The ECG in cardiovascular-relevant animal models of electrophysiology. *Herzschrittmachertherapie und Elektrophysiologie* **24,** 84–91 (2013).
20. Loen V, Vos MA & Heyden MAG. The canine chronic atrio-ventricular block model in cardiovascular preclinical drug research. *Br. J. Pharmacol.* bph.15436 (2021). doi:10.1111/bph.15436
21. Billman GE. A comprehensive review and analysis of 25 years of data from an in vivo canine model of sudden cardiac death: Implications for future anti-arrhythmic drug development. *Pharmacology and Therapeutics* **111,** 808–835 (2006).

22. Moïse NS, Flanders WH & Pariaut R. Beat-to-Beat Patterning of Sinus Rhythm Reveals Non-linear Rhythm in the Dog Compared to the Human. *Front. Physiol.* **10,** 1548 (2020).
23. Hamlin RL. Animal models of ventricular arrhythmias. *Pharmacology and Therapeutics* **113,** 276–295 (2007).
24. Tohyama S & Kobayashi E. Age-Appropriateness of Porcine Models Used for Cell Transplantation. *Cell Transplantation* **28,** 224–228 (2019).
25. Hadaya J & Ardell JL. Autonomic Modulation for Cardiovascular Disease. *Frontiers in Physiology* **11,** 617459 (2020).
26. Randall WC. *Efferent sympathetic innervation of the heart* in Neurocardiology. Oxford University Press, New York, 1994.
27. Armour JA & Ardell JL. *Basic and Clinical Neurocardiology*. Oxford University Press, 2004.
28. Jänig W. *The integrative action of the autonomic nervous system: Neurobiology of homeostasis*. *The Integrative Action of the Autonomic Nervous System: Neurobiology of Homeostasis.* Cambridge University Press, 2006. doi:10.1017/CBO9780511541667
29. Hopkins DA, Bieger D, De Vente J & Steinbusch HWM. Vagal efferent projections: Viscerotopy, neurochemistry and effects of vagotomy. *Prog. Brain Res.* **107,** 79–96 (1996).
30. Pauza DH, Rysevaite-Kyguoliene K, Vismantaite J, Brack KE, Inokaitis H, Pauza AG, Rimasauskaite-Petraitiene V, Pauzaite JI & Pauziene N. A combined acetylcholinesterase and immunohistochemical method for precise anatomical analysis of intrinsic cardiac neural structures. *Ann. Anat.* **196,** 430–440 (2014).
31. Armour JA, Collier K, Kember G & Ardell JL. Differential selectivity of cardiac neurons in separate intrathoracic autonomic ganglia. *Am. J. Physiol. Integr. Comp. Physiol.* **274,** R939–R949 (1998).
32. Wink J, van Delft R, Notenboom RGE, Wouters PF, DeRuiter MC, Plevier JWM & Jongbloed MRM. Human adult cardiac autonomic innervation: Controversies in anatomical knowledge and relevance for cardiac neuromodulation. *Autonomic Neuroscience: Basic and Clinical* **227,** 102674 (2020).

33. Herring N. Autonomic control of the heart: Going beyond the classical neurotransmitters. *Exp. Physiol.* **100,** 354–358 (2015).
34. Bers DM. Cardiac excitation-contraction coupling. *Nature* **415,** 198–205 (2002).
35. Walsh KB & Kass RS. Distinct voltage-dependent regulation of a heart-delayed I(K) by protein kinases A and C. *Am. J. Physiol. - Cell Physiol.* **261,** (1991).
36. Walsh KB & Kass RS. Regulation of a heart potassium channel by protein kinase A and C. *Science.* **242,** 67–69 (1988).
37. Bartos DC, Grandi E & Ripplinger CM. Ion channels in the heart. *Compr. Physiol.* **5,** 1423–1464 (2015).
38. Grandi E, Sanguinetti MC, Bartos DC, Bers DM, Chen-Izu Y, Chiamvimonvat N, Colecraft HM, Delisle BP, Heijman J, Navedo MF, Noskov S, Proenza C, Vandenberg JI & Yarov-Yarovoy V. Potassium channels in the heart: structure, function and regulation. *J. Physiol.* **595,** 2209–2228 (2017).
39. Herren AW, Bers DM & Grandi E. Post-translational modifications of the cardiac Na channel: Contribution of CaMKII-dependent phosphorylation to acquired arrhythmias. *American Journal of Physiology - Heart and Circulatory Physiology* **305,** (2013).
40. Ng GA, Brack KE, Patel VH & Coote JH. Autonomic modulation of electrical restitution, alternans and ventricular fibrillation initiation in the isolated heart. *Cardiovasc. Res.* **73,** 750–760 (2007).
41. Ajijola OA, Lux RL, Khahera A, Kwon O, Aliotta E, Ennis DB, Fishbein MC, Ardell JL & Shivkumar K. Sympathetic modulation of electrical activation in normal and infracted myocardium: Implications for arrhythmogenesis. *Am. J. Physiol. - Heart Circ. Physiol.* **312,** H608–H621 (2017).
42. Tomson TT & Arora R. Modulation of Cardiac Potassium Current by Neural Tone and Ischemia. *Cardiac Electrophysiology Clinics* **8,** 349–360 (2016).
43. Ajijola OA, Hoover DB, Simerly TM, Brown TC, Yanagawa J, Biniwale RM, Lee JM, Sadeghi A, Khanlou N, Ardell JL & Shivkumar K. Inflammation, oxidative stress, and glial cell activation characterize stellate ganglia from humans with electrical storm. *JCI insight* **2,** e94715 (2017).
44. Olivas A, Gardner RT, Wang L, Ripplinger CM, Woodward WR & Habecker BA. Myocardial infarction causes transient cholinergic transdifferentiation of cardiac

sympathetic nerves via gp130. *J. Neurosci.* **36,** 479–488 (2016).

45. Wang L, Olivas A, Francis Stuart SD, Tapa S, Blake MR, Woodward WR, Habecker BA & Ripplinger CM. Cardiac sympathetic nerve transdifferentiation reduces action potential heterogeneity after myocardial infarction. *Am. J. Physiol. Heart Circ. Physiol.* **318,** H558–H565 (2020).
46. Hopkins DA, Macdonald SE, Murphy DA & Armour JA. Pathology of intrinsic cardiac neurons from ischemic human hearts. *Anat. Rec.* **259,** 424–436 (2000).
47. Rajendran PS, Nakamura K, Ajijola OA, Vaseghi M, Armour JA, Ardell JL & Shivkumar K. Myocardial infarction induces structural and functional remodelling of the intrinsic cardiac nervous system. *J. Physiol.* **594,** 321–341 (2016).
48. Salavatian S, Yamaguchi N, Hamon D, Fishbein MC, Ardell JL, Shivkumar K & Vaseghi M. Myocardial Infarction Causes Both Structural and Functional Remodeling in Cardiac Neurons of the Inferior Vagal (Nodose) Ganglia: Implications for Mechanisms Behind Parasympathetic Withdrawal in Heart Disease. *Circulation* **136,** A17355 (2017).
49. Vaseghi M, Salavatian S, Rajendran PS, Yagishita D, Woodward WR, Hamon D, Yamakawa K, Irie T, Habecker BA & Shivkumar K. Parasympathetic dysfunction and antiarrhythmic effect of vagal nerve stimulation following myocardial infarction. *JCI insight* **2,** e86715 (2017).
50. Yokoyama T, Lee JK, Miwa K, Opthof T, Tomoyama S, Nakanishi H, Yoshida A, Yasui H, Iida T, Miyagawa S, Okabe S, Sawa Y, Sakata Y & Komuro I. Quantification of sympathetic hyperinnervation and denervation after myocardial infarction by three-dimensional assessment of the cardiac sympathetic network in cleared transparent murine hearts. *PLoS One* **12,** (2017).
51. Cao JM, Chen LS, KenKnight BH, Ohara T, Lee MH, Tsai J, Lai WW, Karagueuzian HS, Wolf PL, Fishbein MC & Chen PS. Nerve sprouting and sudden cardiac death. *Circ. Res.* **86,** 816–821 (2000).
52. Li W, Knowlton D, Van Winkle DM & Habecker BA. Infarction alters both the distribution and noradrenergic properties of cardiac sympathetic neurons. *Am. J. Physiol. Circ. Physiol.* **286,** H2229–H2236 (2004).

53. Lorentz CU, Parrish DC, Alston EN, Pellegrino MJ, Woodward WR, Hempstead BL & Habecker BA. Sympathetic denervation of peri-infarct myocardium requires the p75 neurotrophin receptor. *Exp. Neurol.* **249,** 111–119 (2013).
54. Armour JA, Richer L-P, Pagé P, Vinet A, Kus T, Vermeulen M, Nadeau R & Cardinal R. Origin and pharmacological response of atrial tachyarrhythmias induced by activation of mediastinal nerves in canines. *Auton. Neurosci.* **118,** 68–78 (2005).
55. Beaumont E, Salavatian S, Southerland EM, Vinet A, Jacquemet V, Armour JA & Ardell JL. Network interactions within the canine intrinsic cardiac nervous system: Implications for reflex control of regional cardiac function. *J. Physiol.* **591,** 4515–4533 (2013).
56. Richer L-P, Vinet A, Kus T, Cardinal R, Ardell JL & Armour JA. α-Adrenoceptor blockade modifies neurally induced atrial arrhythmias. *Am. J. Physiol. Integr. Comp. Physiol.* **295,** R1175–R1180 (2008).
57. Gibbons DD, Southerland EM, Hoover DB, Beaumont E, Armour JA & Ardell JL. Neuromodulation targets intrinsic cardiac neurons to attenuate neuronally mediated atrial arrhythmias. *Am. J. Physiol. Integr. Comp. Physiol.* **302,** R357–R364 (2012).
58. Ardell JL, Cardinal R, Beaumont E, Vermeulen M, Smith FM & Andrew Armour J. Chronic spinal cord stimulation modifies intrinsic cardiac synaptic efficacy in the suppression of atrial fibrillation. *Auton. Neurosci. Basic Clin.* **186,** 38–44 (2014).
59. Shen MJ & Zipes DP. Role of the Autonomic Nervous System in Modulating Cardiac Arrhythmias. *Circ. Res.* **114,** 1004–1021 (2014).
60. Weiss JN, Garfinkel A, Karagueuzian HS, Chen PS & Qu Z. Early afterdepolarizations and cardiac arrhythmias. *Heart Rhythm* **7,** 1891–1899 (2010).
61. Bers DM. Calcium cycling and signaling in cardiac myocytes. *Annu. Rev. Physiol.* **70,** 23–49 (2008).
62. Clancy CE & Rudy Y. Linking a genetic defect to its cellular phenotype in a cardiac arrhythmia. *Nature* **400,** 566–569 (1999).
63. Meijborg VMF, Boukens BJD, Janse MJ, Salavatian S, Dacey MJ, Yoshie K,

Opthof T, Swid MA, Hoang JD, Hanna P, Ardell J, Shivkumar K & Coronel R. Stellate ganglion stimulation causes spatiotemporal changes in ventricular repolarization in pig. *Heart Rhythm* **17,** 795–803 (2020).

64. Xie Y, Grandi E, Puglisi JL, Sato D & Bers DM. β-adrenergic stimulation activates early afterdepolarizations transiently via kinetic mismatch of PKA targets. *J. Mol. Cell. Cardiol.* **58,** 153–161 (2013).
65. Jiang H, Lu Z, Yu Y, Zhao D, Yang B & Huang C. Relationship between sympathetic nerve sprouting and repolarization dispersion at peri-infarct zone after myocardial infarction. *Auton. Neurosci. Basic Clin.* **134,** 18–25 (2007).
66. Myles RC, Wang L, Kang C, Bers DM & Ripplinger CM. Local β-adrenergic stimulation overcomes source-sink mismatch to generate focal arrhythmia. *Circ. Res.* **110,** 1454–1464 (2012).
67. Aflaki M, Qi XY, Xiao L, Ordog B, Tadevosyan A, Luo X, Maguy A, Shi Y, Tardif JC & Nattel S. Exchange protein directly activated by cAMP mediates slow delayed-rectifier current remodeling by sustained β-adrenergic activation in guinea pig hearts. *Circ. Res.* **114,** 993–1003 (2014).
68. Gardner RT, Wang L, Lang BT, Cregg JM, Dunbar CL, Woodward WR, Silver J, Ripplinger CM & Habecker BA. Targeting protein tyrosine phosphatase σ after myocardial infarction restores cardiac sympathetic innervation and prevents arrhythmias. *Nat. Commun.* **6,** (2015).
69. Tapa S, Wang L, Francis Stuart SD, Wang Z, Jiang Y, Habecker BA & Ripplinger CM. Adrenergic supersensitivity and impaired neural control of cardiac electrophysiology following regional cardiac sympathetic nerve loss. *Sci. Rep.* **10,** (2020).
70. Yagishita D, Chui RW, Yamakawa K, Rajendran PS, Ajijola OA, Nakamura K, So EL, Mahajan A, Shivkumar K & Vaseghi M. Sympathetic Nerve Stimulation, Not Circulating Norepinephrine, Modulates T-Peak to T-End Interval by Increasing Global Dispersion of Repolarization. *Circ. Arrhythmia Electrophysiol.* **8,** 174–185 (2015).
71. Malmström RE. Pharmacology of neuropeptide Y receptor antagonists: Focus on cardiovascular functions. *European Journal of Pharmacology* **447,** 11–30 (2002).

72. Herring N, Lokale MN, Danson EJ, Heaton DA & Paterson DJ. Neuropeptide Y reduces acetylcholine release and vagal bradycardia via a Y2 receptor-mediated, protein kinase C-dependent pathway. *J. Mol. Cell. Cardiol.* **44,** 477–485 (2008).

73. Hoang JD, Salavatian S, Yamaguchi N, Swid MA & Vaseghi M. Cardiac sympathetic activation circumvents high-dose beta blocker therapy in part through release of neuropeptide Y. *JCI Insight* **5,** e135519 (2020).

74. Heredia MDP, Delgado C, Pereira L, Perrier R, Richard S, Vassort G, Bénitah JP & Gómez AM. Neuropeptide Y rapidly enhances [Ca 2+] i transients and Ca 2+ sparks in adult rat ventricular myocytes through Y 1 receptor and PLC activation. *J. Mol. Cell. Cardiol.* **38,** 205–212 (2005).

75. Ajijola OA, Chatterjee NA, Gonzales MJ, Gornbein J, Liu K, Li D, Paterson DJ, Shivkumar K, Singh JP & Herring N. Coronary Sinus Neuropeptide y Levels and Adverse Outcomes in Patients with Stable Chronic Heart Failure. *JAMA Cardiol.* **5,** 318–325 (2020).

76. Kalla M, Hao G, Tapoulal N, Tomek J, Liu K, Woodward L, Dall'Armellina E, Banning AP, Choudhury RP, Neubauer S, Kharbanda RK, Channon KM, Ajijola OA, Shivkumar K, Paterson DJ & Herring N. The cardiac sympathetic co-transmitter neuropeptide Y is pro-arrhythmic following ST-elevation myocardial infarction despite beta-blockade. *Eur. Heart J.* **41,** 2168–2179 (2020).

77. Herring N, Cranley J, Lokale MN, Li D, Shanks J, Alston EN, Girard BM, Carter E, Parsons RL, Habecker BA & Paterson DJ. The cardiac sympathetic co-transmitter galanin reduces acetylcholine release and vagal bradycardia: Implications for neural control of cardiac excitability. *J. Mol. Cell. Cardiol.* **52,** 667–676 (2012).

78. Yamaguchi T, Sumida TS, Nomura S, Satoh M, Higo T, Ito M, Ko T, Fujita K, Sweet ME, Sanbe A, Yoshimi K, Manabe I, Sasaoka T, Taylor MRG, Toko H, Takimoto E, Naito AT & Komuro I. Cardiac dopamine D1 receptor triggers ventricular arrhythmia in chronic heart failure. *Nat. Commun.* **11,** 1–8 (2020).

79. Katritsis DG, Pokushalov E, Romanov A, Giazitzoglou E, Siontis GCM, Po SS, Camm AJ & Ioannidis JPA. Autonomic denervation added to pulmonary vein isolation for paroxysmal atrial fibrillation: A randomized clinical trial. *J. Am. Coll.*

Cardiol. **62,** 2318–2325 (2013).

80. Romanov A, Pokushalov E, Ponomarev D, Bayramova S, Shabanov V, Losik D, Stenin I, Elesin D, Mikheenko I, Strelnikov A, Sergeevichev D, Kozlov B, Po SS & Steinberg JS. Long-term suppression of atrial fibrillation by botulinum toxin injection into epicardial fat pads in patients undergoing cardiac surgery: Three-year follow-up of a randomized study. *Heart Rhythm* **16,** 172–177 (2019).
81. Waldron NH, Cooter M, Haney JC, Schroder JN, Gaca JG, Lin SS, Sigurdsson MI, Fudim M, Podgoreanu M V., Stafford-Smith M, Milano CA, Piccini JP & Mathew JP. Temporary autonomic modulation with botulinum toxin type A to reduce atrial fibrillation after cardiac surgery. *Heart Rhythm* **16,** 178–184 (2019).
82. Lo LW, Scherlag BJ, Chang HY, Lin YJ, Chen SA & Po SS. Paradoxical long-term proarrhythmic effects after ablating the head station ganglionated plexi of the vagal innervation to the heart. *Heart Rhythm* **10,** 751–757 (2013).
83. He B, Lu Z, He W, Wu L, Cui B, Hu X, Yu L, Huang C & Jiang H. Effects of ganglionated plexi ablation on ventricular electrophysiological properties in normal hearts and after acute myocardial ischemia. *Int. J. Cardiol.* **168,** 86–93 (2013).
84. Valles SL, Iradi A, Aldasoro M, Vila JM, Aldasoro C, de la Torre J, Campos-Campos J & Jorda A. Function of glia in aging and the brain diseases. *International Journal of Medical Sciences* **16,** 1473–1479 (2019).
85. Hanani M. Satellite glial cells: More than just rings around the neuron. *Neuron Glia Biol.* **6,** 1–2 (2010).
86. Hanani M & Spray DC. Emerging importance of satellite glia in nervous system function and dysfunction. *Nature Reviews Neuroscience* **21,** 485–498 (2020).
87. Feldman-Goriachnik R, Wu B & Hanani M. Cholinergic responses of satellite glial cells in the superior cervical ganglia. *Neurosci. Lett.* **671,** 19–24 (2018).
88. Enes J, Haburčák M, Sona S, Gerard N, Mitchell AC, Fu W & Birren SJ. Satellite glial cells modulate cholinergic transmission between sympathetic neurons. *PLoS One* **15,** e0218643 (2020).
89. Agulhon C, Boyt KM, Xie AX, Friocourt F, Roth BL & McCarthy KD. Modulation of the autonomic nervous system and behaviour by acute glial cell G_q protein-coupled receptor activation *in vivo*. *J. Physiol.* **591,** 5599–5609 (2013).

90. Xie AX, Lee JJ & McCarthy KD. Ganglionic GFAP+ glial Gq-GPCR signaling enhances heart functions in vivo. *JCI Insight* **2,** e90565 (2017).
91. Bensimon G, Lacomblez L & Meininger V. A Controlled Trial of Riluzole in Amyotrophic Lateral Sclerosis. *N. Engl. J. Med.* **330,** 585–591 (1994).
92. Vallée A, Vallée JN, Guillevin R & Lecarpentier Y. Riluzole: a therapeutic strategy in Alzheimer's disease by targeting the WNT/β-catenin pathway. *Aging.* **12,** 3095–3113 (2020).
93. Pittenger C, Vladimir C, Banasr M, Bloch M, Krystal JH & Sanacora G. Riluzole in the treatment of mood and anxiety disorders. *CNS Drugs* **22,** 761–786 (2008).
94. Hanna P, Dacey MJ, Brennan J, Moss A, Robbins S, Achanta S, Biscola NP, Swid MA, Pradeep ;, Rajendran S, Mori S, Hadaya JE, Smith EH, Peirce SG, Chen J, Havton LA, Zixi ;, Jack (, Cheng), Rajanikanth Vadigepalli ;, Schwaber J, Lux RL, Efimov I, Tompkins JD, Hoover DB, Ardell JL & Shivkumar K. Innervation and neuronal control of the mammalian sinoatrial node: a comprehensive atlas. *bioRxiv* 2020.10.28.359109 (2020). doi:10.1101/2020.10.28.359109
95. Scherschel K, Hedenus K, Jungen C, Lemoine MD, Rübsamen N, Veldkamp MW, Klatt N, Lindner D, Westermann D, Casini S, Kuklik P, Eickholt C, Klöcker N, Shivkumar K, Christ T, Zeller T, Willems S & Meyer C. Cardiac glial cells release neurotrophic S100B upon catheter-based treatment of atrial fibrillation. *Sci. Transl. Med.* **11,** 7770 (2019).
96. Sahoo N, Tröger J, Heinemann SH & Schönherr R. Current inhibition of human EAG1 potassium channels by the Ca2+ binding protein S100B. *FEBS Lett.* **584,** 3896–3900 (2010).
97. Wang S, Wu L, Li X, Li B, Zhai Y, Zhao D & Jiang H. Light-emitting diode therapy protects against ventricular arrhythmias by neuro-immune modulation in myocardial ischemia and reperfusion rat model. *J. Neuroinflammation* **16,** 1–10 (2019).
98. Li N, Oida S, Tulevski GS, Han SJ, Hannon JB, Sadana DK & Chen TC. Efficient and bright organic light-emitting diodes on single-layer graphene electrodes. *Nat. Commun.* **4,** 1–7 (2013).
99. Tung R, Vaseghi M, Frankel DS, Vergara P, Di Biase L, Nagashima K, Yu R,

Vangala S, Tseng CH, Choi EK, Khurshid S, Patel M, Mathuria N, Nakahara S, Tzou WS, Sauer WH, Vakil K, Tedrow U, Burkhardt JD, Tholakanahalli VN, Saliaris A, Dickfeld T, Weiss JP, Bunch TJ, Reddy M, Kanmanthareddy A, Callans DJ, Lakkireddy D, Natale A, Marchlinski F, Stevenson WG, Della Bella P & Shivkumar K. Freedom from recurrent ventricular tachycardia after catheter ablation is associated with improved survival in patients with structural heart disease: An International VT Ablation Center Collaborative Group study. *Heart Rhythm* **12,** 1997–2007 (2015).

100. Borne RT, Varosy PD & Masoudi FA. Implantable cardioverter-defibrillator shocks: Epidemiology, outcomes, and therapeutic approaches. *JAMA Internal Medicine* **173,** 859–865 (2013).
101. Murtaza G, Sharma SP, Akella K, Turagam MK, Rocca DG Della, Lakkireddy D & Gopinathannair R. Role of cardiac sympathetic denervation in ventricular tachycardia: A meta-analysis. *Pacing Clin. Electrophysiol.* **43,** 828–837 (2020).
102. Dusi V, Gornbein J, Do DH, Sorg JM, Khakpour H, Krokhaleva Y, Ajijola OA, Macias C, Bradfield JS, Buch E, Fujimura OA, Boyle NG, Yanagawa J, Lee JM, Shivkumar K & Vaseghi M. Arrhythmic Risk Profile and Outcomes of Patients Undergoing Cardiac Sympathetic Denervation for Recurrent Monomorphic Ventricular Tachycardia After Ablation. *J. Am. Heart Assoc.* **10,** e018371 (2021).
103. Vaseghi M, Barwad P, Malavassi Corrales FJ, Tandri H, Mathuria N, Shah R, Sorg JM, Gima J, Mandal K, Sàenz Morales LC, Lokhandwala Y & Shivkumar K. Cardiac Sympathetic Denervation for Refractory Ventricular Arrhythmias. *J. Am. Coll. Cardiol.* **69,** 3070–3080 (2017).
104. Assis FR, Sharma A, Shah R, Akhtar T, Adari S, Calkins H, Ha JS, Mandal K & Tandri H. Long-Term Outcomes of Bilateral Cardiac Sympathetic Denervation for Refractory Ventricular Tachycardia. *JACC Clin. Electrophysiol.* (2021). doi:10.1016/j.jacep.2021.02.003
105. Hong JC, Crawford T, Tandri H & Mandal K. What Is the Role of Cardiac Sympathetic Denervation for Recurrent Ventricular Tachycardia? *Current Treatment Options in Cardiovascular Medicine* **19,** (2017).
106. Vaseghi M, Gima J, Kanaan C, Ajijola OA, Marmureanu A, Mahajan A &

Shivkumar K. Cardiac sympathetic denervation in patients with refractory ventricular arrhythmias or electrical storm: Intermediate and long-term follow-up. *Heart Rhythm* **11,** 360–366 (2014).

107. Ajijola OA, Lellouche N, Bourke T, Tung R, Ahn S, Mahajan A & Shivkumar K. Bilateral cardiac sympathetic denervation for the management of electrical storm. *J. Am. Coll. Cardiol.* **59,** 91–92 (2012).
108. Schwartz PJ, Priori SG, Cerrone M, Spazzolini C, Odero A, Napolitano C, Bloise R, De Ferrari G, Klersy C, Moss AJ, Zareba W, Robinson J, Hall WJ, Brink P, Toivonen L, Epstein AE, Li C & Hu D. Left cardiac sympathetic denervation in the management of high-risk patients affected by the long-QT syndrome. *Circulation* **109,** 1826–1833 (2004).
109. Dusi V, De Ferrari GM, Pugliese L & Schwartz PJ. Cardiac Sympathetic Denervation in Channelopathies. *Front. Cardiovasc. Med.* **6,** 27 (2019).
110. Wilde AAM, Bhuiyan ZA, Crotti L, Facchini M, De Ferrari GM, Paul T, Ferrandi C, Koolbergen DR, Odero A & Schwartz PJ. Left Cardiac Sympathetic Denervation for Catecholaminergic Polymorphic Ventricular Tachycardia. *N. Engl. J. Med.* **358,** 2024–2029 (2008).
111. Estes EH & Izlar HL. Recurrent ventricular tachycardia. A case successfully treated by bilateral cardiac sympathectomy. *Am. J. Med.* **31,** 493–497 (1961).
112. Zipes D, Festoff B, Schaal S, Cox C, Sealy W & Wallace A. Treatment of ventricular arrhythmia by permanent atrial pacemaker and cardiac sympathectomy. *Ann. Intern. Med.* **68,** 591–597 (1968).
113. Buckley U, Yamakawa K, Takamiya T, Armour JA, Shivkumar K & Ardell JL. Targeted stellate decentralization: Implications for sympathetic control of ventricular electrophysiology. *Heart Rhythm* **13,** 282–288 (2016).
114. Ajijola O, Vaseghi M, Mahajan A & Shivkumar K. Bilateral cardiac sympathetic denervation: why, who and when? *Expert Rev. Cardiovasc. Ther.* **10,** 947–949 (2012).
115. Schwartz PJ. Cardiac sympathetic denervation to prevent life-threatening arrhythmias. *Nature Reviews Cardiology* **11,** 346–353 (2014).
116. Bourke T, Vaseghi M, Michowitz Y, Sankhla V, Shah M, Swapna N, Boyle NG, Mahajan A, Narasimhan C, Lokhandwala Y & Shivkumar K. Neuraxial

modulation for refractory ventricular arrhythmias: Value of thoracic epidural anesthesia and surgical left cardiac sympathetic denervation. *Circulation* **121,** 2255–2262 (2010).

117. Tian Y, Wittwer ED, Kapa S, McLeod CJ, Xiao P, Noseworthy PA, Mulpuru SK, Deshmukh AJ, Lee HC, Ackerman MJ, Asirvatham SJ, Munger TM, Liu XP, Friedman PA & Cha YM. Effective Use of Percutaneous Stellate Ganglion Blockade in Patients with Electrical Storm. *Circ. Arrhythmia Electrophysiol.* **12,** (2019).
118. Ganesh A, Qadri YJ, Boortz-Marx RL, Al-Khatib SM, Harpole DH, Katz JN, Koontz JI, Mathew JP, Ray ND, Sun AY, Tong BC, Ulloa L, Piccini JP & Fudim M. Stellate Ganglion Blockade: an Intervention for the Management of Ventricular Arrhythmias. *Current Hypertension Reports* **22,** 100 (2020).
119. Ginosar Y, Weiniger CF, Meroz Y, Kurz V, Bdolah-Abram T, Babchenko A, Nitzan M & Davidson EM. Pulse oximeter perfusion index as an early indicator of sympathectomy after epidural anesthesia. *Acta Anaesthesiol. Scand.* **53,** 1018–1026 (2009).
120. Aleanakian R, Chung BY, Feldmann RE & Benrath J. Effectiveness, Safety, and Predictive Potential in Ultrasound-Guided Stellate Ganglion Blockades for the Treatment of Sympathetically Maintained Pain. *Pain Pract.* **20,** 626–638 (2020).
121. Şahin ÖF, Tarıkçı Kılıç E, Aksoy Y, Kaydu A & Gökçek E. The importance of perfusion index monitoring in evaluating the efficacy of stellate ganglion blockage treatment in Raynaud's disease. *Libyan J. Med.* **13,** (2018).
122. Mahajan A, Moore J, Cesario DA & Shivkumar K. Use of thoracic epidural anesthesia for management of electrical storm: A case report. *Heart Rhythm* **2,** 1359–1362 (2005).
123. Do DH, Bradfield J, Ajijola OA, Vaseghi M, Le J, Rahman S, Mahajan A, Nogami A, Boyle NG & Shivkumar K. Thoracic epidural anesthesia can be effective for the short-term management of ventricular tachycardia storm. *J. Am. Heart Assoc.* **6,** (2017).
124. Meissner A, Eckardt L, Kirchhof P, Weber T, Rolf N, Breithardt G, Van Aken H & Haverkamp W. Effects of thoracic epidural anesthesia with and without autonomic nervous system blockade on cardiac monophasic action potentials

and effective refractoriness in awake dogs. *Anesthesiology* **95,** 132–138 (2001).

125. Blomberg S & Ricksten SE. Thoracic epidural anaesthesia decreases the incidence of ventricular arrhythmias during acute myocardial ischaemia in the anaesthetized rat. *Acta Anaesthesiol. Scand.* **32,** 173–178 (1988).
126. Wink J, Steendijk P, Tsonaka R, de Wilde RBP, Friedericy HJ, Braun J, Veering BT, Aarts LPHJ & Wouters PF. Biventricular function in exercise during autonomic (thoracic epidural) block. *Eur. J. Appl. Physiol.* 1–14 (2021). doi:10.1007/s00421-021-04631-6
127. Wink J, De Wilde RBP, Wouters PF, Van Dorp ELA, Veering BT, Versteegh MIM, Aarts LPHJ & Steendijk P. Thoracic Epidural Anesthesia Reduces Right Ventricular Systolic Function with Maintained Ventricular-Pulmonary Coupling. *Circulation* **134,** 1163–1175 (2016).
128. Ng GA. Vagal modulation of cardiac ventricular arrhythmia. *Exp. Physiol.* **99,** 295–299 (2014).
129. Brack KE, Winter J & Ng GA. Mechanisms underlying the autonomic modulation of ventricular fibrillation initiation - Tentative prophylactic properties of vagus nerve stimulation on malignant arrhythmias in heart failure. *Heart Failure Reviews* **18,** 389–408 (2013).
130. Shinlapawittayatorn K, Chinda K, Palee S, Surinkaew S, Thunsiri K, Weerateerangkul P, Chattipakorn S, Kenknight BH & Chattipakorn N. Low-amplitude, left vagus nerve stimulation significantly attenuates ventricular dysfunction and infarct size through prevention of mitochondrial dysfunction during acute ischemia-reperfusion injury. *Heart Rhythm* **10,** 1700–1707 (2013).
131. Vanoli E, De Ferrari GM, Stramba-Badiale M, Hull SS, Foreman RD & Schwartz PJ. Vagal stimulation and prevention of sudden death in conscious dogs with a healed myocardial infarction. *Circ. Res.* **68,** 1471–1481 (1991).
132. Vaseghi M, Salavatian S, Rajendran PS, Yagishita D, Woodward WR, Hamon D, Yamakawa K, Irie T, Habecker BA & Shivkumar K. Parasympathetic dysfunction and antiarrhythmic effect of vagal nerve stimulation following myocardial infarction. *JCI insight* **2,** e86715 (2017).
133. Huang J, Qian J, Yao W, Wang N, Zhang Z, Cao C, Song B & Zhang Z. Vagus nerve stimulation reverses ventricular electrophysiological changes induced by

hypersympathetic nerve activity. *Exp. Physiol.* **100,** 239–248 (2015).

134. Schwartz PJ, De Ferrari GM, Sanzo A, Landolina M, Rordorf R, Raineri C, Campana C, Revera M, Ajmone-Marsan N, Tavazzi L & Odero A. Long term vagal stimulation in patients with advanced heart failure. First experience in man. *Eur. J. Heart Fail.* **10,** 884–891 (2008).
135. Anand IS, Konstam MA, Klein HU, Mann DL, Ardell JL, Gregory DD, Massaro JM, Libbus I, DiCarlo LA, Udelson JJE, Butler J, Parker JD & Teerlink JR. Comparison of symptomatic and functional responses to vagus nerve stimulation in ANTHEM-HF, INOVATE-HF, and NECTAR-HF. *ESC Heart Fail.* **7,** 75–83 (2020).
136. Libbus I, Nearing BD, Amurthur B, KenKnight BH & Verrier RL. Autonomic regulation therapy suppresses quantitative T-wave alternans and improves baroreflex sensitivity in patients with heart failure enrolled in the ANTHEM-HF study. *Heart Rhythm* **13,** 721–728 (2016).
137. Nearing BD, Anand IS, Libbus I, Dicarlo LA, Kenknight BH & Verrier RL. Vagus Nerve Stimulation Provides Multiyear Improvements in Autonomic Function and Cardiac Electrical Stability in the ANTHEM-HF Study. *J. Card. Fail.* **27,** 208–216 (2021).
138. Kaniusas E, Kampusch S, Tittgemeyer M, Panetsos F, Gines RF, Papa M, Kiss A, Podesser B, Cassara AM, Tanghe E, Samoudi AM, Tarnaud T, Joseph W, Marozas V, Lukosevicius A, Ištuk N, Lechner S, Klonowski W, Varoneckas G, Széles JC & Šarolić A. Current directions in the auricular vagus nerve stimulation II - An engineering perspective. *Frontiers in Neuroscience* **13,** (2019).
139. Kaniusas E, Kampusch S, Tittgemeyer M, Panetsos F, Gines RF, Papa M, Kiss A, Podesser B, Cassara AM, Tanghe E, Samoudi AM, Tarnaud T, Joseph W, Marozas V, Lukosevicius A, Ištuk N, Šarolić A, Lechner S, Klonowski W, Varoneckas G & Széles JC. Current directions in the auricular vagus nerve stimulation I – A physiological perspective. *Frontiers in Neuroscience* **13,** (2019).
140. Buajieer-guli N, Wenhui Z, HuaXin S, Xianhui Z, Yaodong L, Yanmei L, Hongli W, ZuKe-la T, Qina Z & BaoPeng T. Vagus nerve stimulation reduces

ventricular arrhythmias and increases ventricular electrical stability. *Pacing Clin. Electrophysiol.* **42,** pace.13585 (2018).

141. Yu L, Wang S, Zhou X, Wang Z, Huang B, Liao K, Saren G, Chen M, Po SS & Jiang H. Chronic Intermittent Low-Level Stimulation of Tragus Reduces Cardiac Autonomic Remodeling and Ventricular Arrhythmia Inducibility in a Post-Infarction Canine Model. *JACC Clin. Electrophysiol.* **2,** 330–339 (2016).
142. Yu L, Huang B, Po SS, Tan T, Wang M, Zhou L, Meng G, Yuan S, Zhou X, Li X, Wang Z, Wang S & Jiang H. Low-Level Tragus Stimulation for the Treatment of Ischemia and Reperfusion Injury in Patients With ST-Segment Elevation Myocardial Infarction: A Proof-of-Concept Study. *JACC Cardiovasc. Interv.* **10,** 1511–1520 (2017).
143. Mannheimer C, Camici P, Chester MR, Collins A, DeJongste M, Eliasson T, Follath F, Hellemans I, Herlitz J, Lüscher T, Pasic M & Thelle D. The problem of chronic refractory angina: Report from the ESC Joint Study Group on the treatment of refractory angina. *European Heart Journal* **23,** 355–370 (2002).
144. Zhang TC, Janik JJ & Grill WM. Mechanisms and models of spinal cord stimulation for the treatment of neuropathic pain. *Brain Research* **1569,** 19–31 (2014).
145. Ardell JL. Heart failure: Mechanisms of spinal cord neuromodulation for heart disease. *Nature Reviews Cardiology* **13,** 122–123 (2016).
146. Ardell JL, Cardinal R, Vermeulen M & Armour JA. Dorsal spinal cord stimulation obtunds the capacity of intrathoracic extracardiac neurons to transduce myocardial ischemia. *Am. J. Physiol. Integr. Comp. Physiol.* **297,** R470–R477 (2009).
147. Salavatian S, Ardell SM, Hammer M, Gibbons D, Armour JA & Ardell JL. Thoracic spinal cord neuromodulation obtunds dorsal root ganglion afferent neuronal transduction of the ischemic ventricle. *Am. J. Physiol. Circ. Physiol.* **317,** H1134–H1141 (2019).
148. Cardinal R, Ardell JL, Linderoth B, Vermeulen M, Foreman RD & Armour JA. Spinal cord activation differentially modulates ischaemic electrical responses to different stressors in canine ventricles. *Auton. Neurosci. Basic Clin.* **111,** 37–47

(2004).

149. Cardinal R, Pagé P, Vermeulen M, Bouchard C, Ardell JL, Foreman RD & Armour JA. Spinal cord stimulation suppresses bradycardias and atrial tachyarrhythmias induced by mediastinal nerve stimulation in dogs. *Am. J. Physiol. - Regul. Integr. Comp. Physiol.* **291,** (2006).
150. Issa ZF, Zhou X, Ujhelyi MR, Rosenberger J, Bhakta D, Groh WJ, Miller JM & Zipes DP. Thoracic spinal cord stimulation reduces the risk of ischemic ventricular arrhythmias in a postinfarction heart failure canine model. *Circulation* **111,** 3217–3220 (2005).
151. Foreman RD, Linderoth B, Ardell JL, Barron KW, Chandler MJ, Hull SS, Terhorst GJ, Dejongste MJL & Armour JA. Modulation of intrinsic cardiac neurons by spinal cord stimulation: Implications for its therapeutic use in angina pectoris. *Cardiovasc. Res.* **47,** 367–375 (2000).
152. Wang S, Zhou X, Huang B, Wang Z, Liao K, Saren G, Lu Z, Chen M, Yu L & Jiang H. Spinal cord stimulation protects against ventricular arrhythmias by suppressing left stellate ganglion neural activity in an acute myocardial infarction canine model. *Heart Rhythm* **12,** 1628–1635 (2015).
153. Howard-Quijano K, Takamiya T, Dale EA, Kipke J, Kubo Y, Grogan T, Afyouni A, Shivkumar K & Mahajan A. Spinal cord stimulation reduces ventricular arrhythmias during acute ischemia by attenuation of regional myocardial excitability. *Am. J. Physiol. Circ. Physiol.* **313,** H421–H431 (2017).
154. Cardinal R, Pagé P, Vermeulen M, Bouchard C, Ardell JL, Foreman RD & Armour JA. Spinal cord stimulation suppresses bradycardias and atrial tachyarrhythmias induced by mediastinal nerve stimulation in dogs. *Am. J. Physiol. Integr. Comp. Physiol.* **291,** R1369–R1375 (2006).
155. Odenstedt J, Linderoth B, Bergfeldt L, Ekre O, Grip L, Mannheimer C & Andréll P. Spinal cord stimulation effects on myocardial ischemia, infarct size, ventricular arrhythmia, and noninvasive electrophysiology in a porcine ischemia-reperfusion model. *Heart Rhythm* **8,** 892–898 (2011).
156. Grimaldi R, De Luca A, Kornet L, Castagno D & Gaita F. Can spinal cord stimulation reduce ventricular arrhythmias? *Heart Rhythm* **9,** 1884–1887 (2012).

157. Tse HF, Turner S, Sanders P, Okuyama Y, Fujiu K, Cheung CW, Russo M, Green MDS, Yiu KH, Chen P, Shuto C, Lau EOY & Siu CW. Thoracic spinal cord stimulation for heart failure as a restorative treatment (SCS HEART study): First-in-man experience. *Heart Rhythm* **12,** 588–595 (2015).

158. Zipes DP, Neuzil P, Theres H, Caraway D, Mann DL, Mannheimer C, Van Buren P, Linde C, Linderoth B, Kueffer F, Sarazin SA & DeJongste MJL. Determining the Feasibility of Spinal Cord Neuromodulation for the Treatment of Chronic Systolic Heart Failure: The DEFEAT-HF Study. *JACC Hear. Fail.* **4,** 129–136 (2016).

159. Liao K, Yu L, Yang K, Saren G, Wang S, Huang B & Jiang H. Low-Level Carotid Baroreceptor Stimulation Suppresses Ventricular Arrhythmias during Acute Ischemia. *PLoS One* **9,** e109313 (2014).

160. Liao K, Yu L, He B, Huang B, Yang K, Saren G, Wang S, Zhou X & Jiang H. Carotid baroreceptor stimulation prevents arrhythmias induced by acute myocardial infarction through autonomic modulation. *J. Cardiovasc. Pharmacol.* **64,** 431–437 (2014).

161. Zhou X, Chen M, Wang S, Yu L, Bao M & Jiang H. Low-level carotid baroreceptor stimulation: A promising feasible modulator for ventricular and atrial arrhythmias. *Int. J. Cardiol.* **199,** 430–431 (2015).

162. Scheffers IJM, Kroon AA, Schmidli J, Jordan J, Tordoir JJM, Mohaupt MG, Luft FC, Haller H, Menne J, Engeli S, Ceral J, Eckert S, Erglis A, Narkiewicz K, Philipp T & De Leeuw PW. Novel baroreflex activation therapy in resistant hypertension: Results of a European multi-center feasibility study. *J. Am. Coll. Cardiol.* **56,** 1254–1258 (2010).

163. Bisognano JD, Bakris G, Nadim MK, Sanchez L, Kroon AA, Schafer J, De Leeuw PW & Sica DA. Baroreflex activation therapy lowers blood pressure in patients with resistant hypertension: Results from the double-blind, randomized, placebo-controlled rheos pivotal trial. *J. Am. Coll. Cardiol.* **58,** 765–773 (2011).

164. Hoppe UC, Brandt MC, Wachter R, Beige J, Rump LC, Kroon AA, Cates AW, Lovett EG & Haller H. Minimally invasive system for baroreflex activation therapy chronically lowers blood pressure with pacemaker-like safety profile: Results from the Barostim neo trial. *J. Am. Soc. Hypertens.* **6,** 270–276 (2012).

165. Smithwick RH & Thompson JE. Splanchnicectomy for essential hypertension: Results in 1,266 cases. *J. Am. Med. Assoc.* **152,** 1501–1504 (1953).
166. Linz D, Wirth K, Ukena C, Mahfoud F, Pöss J, Linz B, Böhm M & Neuberger HR. Renal denervation suppresses ventricular arrhythmias during acute ventricular ischemia in pigs. *Heart Rhythm* **10,** 1525–1530 (2013).
167. Dai Z, Yu S, Zhao Q, Meng Y, He H, Tang Y, Wang X, Xiao J, Wang X & Huang C. Renal sympathetic denervation suppresses ventricular substrate remodelling in a canine high-rate pacing model. *EuroIntervention* **10,** 392–399 (2014).
168. Zhang WH, Zhou QN, Lu YM, Li YD, Zhang L, Zhang JH, Xing Q, Lv WK, Cheng XC, Zhang GG, Wang XS, Gu Q, Lou X, Guli B, Tang BP & Zhou XH. Renal denervation reduced ventricular arrhythmia after myocardial infarction by inhibiting sympathetic activity and remodeling. *J. Am. Heart Assoc.* **7,** (2018).
169. Yamada S, Lo LW, Chou YH, Lin WL, Chang SL, Lin YJ, Liu SH, Cheng WH, Tsai TY & Chen SA. Beneficial effect of renal denervation on ventricular premature complex induced cardiomyopathy. *J. Am. Heart Assoc.* **6,** (2017).
170. Bhatt DL, Kandzari DE, O'Neill WW, D'Agostino R, Flack JM, Katzen BT, Leon MB, Liu M, Mauri L, Negoita M, Cohen SA, Oparil S, Rocha-Singh K, Townsend RR & Bakris GL. A Controlled Trial of Renal Denervation for Resistant Hypertension. *N. Engl. J. Med.* **370,** 1393–1401 (2014).
171. Kandzari DE, Bhatt DL, Brar S, Devireddy CM, Esler M, Fahy M, Flack JM, Katzen BT, Lea J, Lee DP, Leon MB, Ma A, Massaro J, Mauri L, Oparil S, O'Neill WW, Patel MR, Rocha-Singh K, Sobotka PA, Svetkey L, Townsend RR & Bakris GL. Predictors of blood pressure response in the SYMPLICITY HTN-3 trial. *Eur. Heart J.* **36,** 219–227 (2015).
172. Papademetriou V, Tsioufis C & Doumas M. Renal denervation and symplicity HTN-3: 'dubium sapientiae initium' (doubt is the beginning of wisdom). *Circulation Research* **115,** 211–214 (2014).
173. Epstein M & De Marchena E. Is the failure of SYMPLICITY HTN-3 trial to meet its efficacy endpoint the 'end of the road' for renal denervation? *Journal of the American Society of Hypertension* **9,** 140–149 (2015).
174. Ukena C, Bauer A, Mahfoud F, Schreieck J, Neuberger H-R, Eick C, Sobotka PA, Gawaz M & Böhm M. Renal sympathetic denervation for treatment of

electrical storm: first-in-man experience. *Clin. Res. Cardiol.* **101,** 63–67 (2012).

175. Remo BF, Preminger M, Bradfield J, Mittal S, Boyle N, Gupta A, Shivkumar K, Steinberg JS & Dickfeld T. Safety and efficacy of renal denervation as a novel treatment of ventricular tachycardia storm in patients with cardiomyopathy. *Heart Rhythm* **11,** 541–546 (2014).
176. Tsioufis C, Papademetriou V, Tsiachris D, Dimitriadis K, Kasiakogias A, Kordalis A, Antonakis V, Kefala A, Thomopoulos C, Kallikazaros I, Lau EOY & Stefanadis C. Drug-resistant hypertensive patients responding to multielectrode renal denervation exhibit improved heart rate dynamics and reduced arrhythmia burden. *J. Hum. Hypertens.* **28,** 587–593 (2014).
177. Ukena C, Mahfoud F, Ewen S, Bollmann A, Hindricks G, Hoffmann BA, Linz D, Musat D, Pavlicek V, Scholz E, Thomas D, Willems S, Böhm M & Steinberg JS. Renal denervation for treatment of ventricular arrhythmias: data from an International Multicenter Registry. *Clin. Res. Cardiol.* **105,** 873–879 (2016).
178. Scholz EP, Raake P, Thomas D, Vogel B, Katus HA & Blessing E. Rescue renal sympathetic denervation in a patient with ventricular electrical storm refractory to endo- and epicardial catheter ablation. *Clinical Research in Cardiology* **104,** 79–84 (2015).
179. Hoffmann BA, Steven D, Willems S & Sydow K. Renal sympathetic denervation as an adjunct to catheter ablation for the treatment of ventricular electrical storm in the setting of acute myocardial infarction. *Journal of Cardiovascular Electrophysiology* **24,** (2013).
180. Pokushalov E, Romanov A, Corbucci G, Artyomenko S, Baranova V, Turov A, Shirokova N, Karaskov A, Mittal S & Steinberg JS. A randomized comparison of pulmonary vein isolation with versus without concomitant renal artery denervation in patients with refractory symptomatic atrial fibrillation and resistant hypertension. *J. Am. Coll. Cardiol.* **60,** 1163–1170 (2012).
181. Lefaucheur JP, André-Obadia N, Antal A, Ayache SS, Baeken C, Benninger DH, Cantello RM, Cincotta M, de Carvalho M, De Ridder D, Devanne H, Di Lazzaro V, Filipović SR, Hummel FC, Jääskeläinen SK, Kimiskidis VK, Koch G, Langguth B, Nyffeler T, Oliviero A, Padberg F, Poulet E, Rossi S, Rossini PM, Rothwell JC, Schönfeldt-Lecuona C, Siebner HR, Slotema CW, Stagg CJ, Valls-

Sole J, Ziemann U, Paulus W & Garcia-Larrea L. Evidence-based guidelines on the therapeutic use of repetitive transcranial magnetic stimulation (rTMS). *Clinical Neurophysiology* **125,** 2150–2206 (2014).

182. Cabrerizo M, Cabrera A, Perez JO, De La Rua J, Rojas N, Zhou Q, Pinzon-Ardila A, Gonzalez-Arias SM & Adjouadi M. Induced Effects of Transcranial Magnetic Stimulation on the Autonomic Nervous System and the Cardiac Rhythm. *Sci. World J.* **2014,** 12 (2014).
183. Yoshida T, Yoshino A, Kobayashi Y, Inoue M, Kamakura K & Nomura S. Effects of slow repetitive transcranial magnetic stimulation on heart rate variability according to power spectrum analysis. *J. Neurol. Sci.* **184,** 77–80 (2001).
184. Scherlag BJ, Yamanashi WS, Hou Y, Jacobson JI, Jackman WM & Lazzara R. Magnetism and Cardiac Arrhythmias. *Cardiol. Rev.* **12,** 85–96 (2004).
185. Yu L, Dyer JW, Scherlag BJ, Stavrakis S, Sha Y, Sheng X, Garabelli P, Jacobson J & Po SS. The use of low-level electromagnetic fields to suppress atrial fibrillation. *Heart Rhythm* **12,** 809–817 (2015).
186. Wang S, Zhou X, Huang B, Wang Z, Zhou L, Wang M, Yu L & Jiang H. Noninvasive low-frequency electromagnetic stimulation of the left stellate ganglion reduces myocardial infarction-induced ventricular arrhythmia. *Sci. Reports 2016 61* **6,** 1–9 (2016).
187. Markman TM, Hamilton RH, Marchlinski FE & Nazarian S. Case Series of Transcutaneous Magnetic Stimulation for Ventricular Tachycardia Storm. *JAMA - Journal of the American Medical Association* **323,** 2200–2202 (2020).
188. Wang S, Li B, Li X, Wu L & Jiang H. Abstract: Low intensity ultrasound stimulation might reduce ventricular arrhythmia by modulating sympathetic neural activity in myocardial infarction canine model. *J. Am. Coll. Cardiol.* **73,** 531 (2019).

Valerie Y.H. van Weperen

CHAPTER 9

General discussion

GENERAL DISCUSSION

Ventricular arrhythmogenesis is an intriguingly complex and intricate phenomenon. The orchestrated interplay between electrical currents at the cellular level safeguards normal cardiac rhythm, but becomes dysregulated in arrhythmogenesis. This disruption of cardiac electrical stability endangers cardiac output.

Numerous conditions can predispose to ventricular arrhythmogenesis through various mechanisms. This thesis studied the regulation of cardiac electrical stability by several intra- and extracardiac factors, and related their effects to ventricular arrhythmogenesis.

MECHANISMS OF VENTRICULAR ARRHYTHMOGENESIS

Coumel reduced the process of arrhythmogenesis to the unison of a *trigger*, *substrate* and *modulator* (Figure 1A).[1,2]

In short, the *trigger* is the initial (local) derangement that sparks an arrhythmic episode.[3] Such triggers develop from electrical instability at the level of the myocyte. The ventricular action potential comprises an ordered set of phases that meticulously follow up on one another. In this manner, electromechanical coupling is established,[4] which allows for electrical signals to be translated into mechanical function. However, early or late afterdepolarizations disrupt the ventricular action potential, which can trigger arrhythmias.[5–7] In the CAVB dog model, arrhythmic events are also triggered by afterdepolarizations.[8–11] The augmented risk for afterdepolarizations results from electrical ($I_{K,r}$ and $I_{K,s}$ downregulation)[12–15] and contractile remodelling in combination with the administration of the specific $I_{K,r}$-inhibitor dofetilide.[14,15] All of these factors deplete the repolarization reserve and thereby cause ventricular electrophysiology to become increasingly vulnerable to electrical disturbances.[16] This instability is reflected by QT-prolongation, but is even better captured by the short-term variability in repolarization (STV).[16,17] This latter parameter measures beat-to-beat changes in repolarization duration and thereby quantifies the temporal dispersion of repolarization. Accordingly, a higher STV reflects greater beat-to-beat differences in repolarization duration, and thus a more volatile underlying electrophysiology and an increased susceptibility for afterdepolarizations.[16–18]

The *substrate* is the tissue that enables the cardiac spread of aberrant electrical waves.[19] The ability of cardiac tissue to perpetuate arrhythmic episodes relies

on spatial heterogeneity in ventricular electrical characteristics.[20–22] While these differences are also present under healthy conditions, they are generally too small to facilitate a ventricular arrhythmia. However, as a result of cardiac pathology, the substrate becomes diseased. This can increase the susceptibility for ventricular arrhythmias in many ways, for example through the presence of scar tissue,[23] and/or heterogeneous electrical characteristics of myocytes.[24,25] In the chronic AV-block (CAVB) dog model, remodelling occurs spatially heterogeneously, including a marked downregulation of potassium channels in the early activated regions.[26] Consequently, spatial dispersion of repolarization is increased. The specific $I_{K,r}$-blocker dofetilide further pronounces these spatial differences, thereby increasing arrhythmic susceptibility.[26,27]

Additionally, both *trigger* and *substrate* are under the influence of *modulators*, such as the autonomic nervous system.[28] Even in a background of low intrinsic propensity for ventricular arrhythmias (*e.g.* low trigger and low substrate conditions), modulators can enhance both trigger and substrate, thereby effectively lowering arrhythmia threshold and promoting arrhythmogenesis. Hence, while modulation promotes arrhythmogenesis *indirectly*, it is not a trigger or substrate itself. This concept is schematically depicted by the adapted triangle of Coumel, Figure 1A. Similarly, Figure 1B illustrates how changes in the respective presence and relative contributions of the different factors affect arrhythmogenic outcomes.

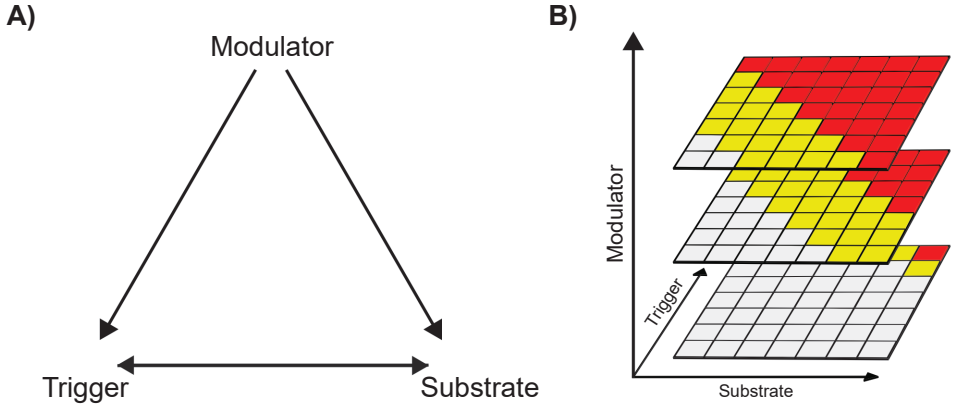

Figure 1: Schematic illustration of arrhythmogenesis. A) Arrhythmias result from an arrhythmic trigger in combination with an arrhythmic substrate, both of which can be modulated to promote or impede ventricular arrhythmogenesis. As such, the trigger and substrate are directly involved in arrhythmogenesis (double arrow), whereas modulators are indirectly involved in this process. **B)** The extent wherein an arrhythmic trigger, susceptible substrate and modulator are present determines the arrhythmic outcome. Whereas sufficiently high intrinsic predisposition for arrhythmias can cause arrhythmic events, the additional modulation of both elements facilitates arrhythmogenesis.

Chapter 2 demonstrated that electrical parameters indicative of the *trigger* and *substrate* for arrhythmias can accurately reflect the anti-arrhythmic effects of drugs. Assessment of either electrical index in isolation of the other is insufficient to evaluate the electrical stability of the myocardium. Therefore, estimation of the arrhythmogenic conditions and risk should preferably depend on one or multiple parameters that reflect both trigger and substrate. Modulators are not included in chapter two, but can additionally be assessed to explore the arrhythmic risk.[29,30] Although modulators affect arrhythmogenesis indirectly, they can be effective targets for anti-arrhythmic treatments (Figure 1B). This can also explain the anti-arrhythmic effects of tachypacing[31–33] and sympathetic denervation,[34–38] which mitigate trigger and substrate or even nullify the pro-arrhythmic modulator, respectively.

INTRACARDIAC REGULATION OF ELECTRICAL STABILITY

Whereas the arrhythmic trigger and substrate are intrinsic characteristics of the heart, modulatory factors can be both intra- and extracardiac. **Chapter 3** studied one of such intracardiac modulators, exploring the modulatory effects of bradycardia on the trigger and substrate. The results of this study confirmed the pro-arrhythmic effects of bradycardia and associated these effects with a primarily pro-arrhythmic effect on the substrate. Whereas temporal dispersion of repolarization appeared to be minimally affected by ventricular rate, high resolution *in vivo* mapping demonstrated significant increases in spatial heterogeneity in repolarization when rate was lowered. These effects were reflected in the persistence of ectopic activity at higher rates, though arrhythmias were significantly decreased. Hence, even though the *trigger* was still present, the decrease in spatial dispersion of repolarization limited the ability of the myocardium to sustain and perpetuate arrhythmic events, lowering the incidence of Torsade de Pointes arrhythmias (TdP).

Accordingly, tachypacing has been introduced as an effective anti-arrhythmic therapy. This strategy stimulates the heart at a higher frequency than the arrhythmic episode to render the tissue refractory before the arrhythmic wave front can depolarize it. The first publication on this strategy described its efficacy in terminating ventricular tachycardia in 22 patients that suffered from ischemic cardiac injury.[32] From there on, tachypacing was primarily thought to be an applicable strategy in the setting of macro-reentry arrhythmias, as is often the case with myocardial infarction-induced scar tissue.

However, a meta-analysis by Cheng *et al.* (2020)[33] showed that the efficacy of tachypacing is similar between ischemic and non-ischemic cardiomyopathy patients, as this approach terminated 76% and 75% of all episodes, respectively. Hence, under both circumstances, ventricular rate is a potent modulator of cardiac electrical instability. Although this modulator can adversely cause pro-arrhythmic conditions, it can also be leveraged clinically as an anti-arrhythmic strategy.

As illustrated in Figure 1B, arrhythmogenesis heavily depends on the intrinsic propensity for arrhythmogenesis. Ventricular remodelling affects electrical characteristics at the cellular and tissue level, increasing risk of an arrhythmic *trigger* and promoting the arrhythmic *substrate*. **Chapter 4** studied how different conditions of ventricular remodelling affect these factors and how this translates to TdP-inducibility. To this end, three groups of animals remodelled under different degrees of mechanical dyssynchrony. It was shown how the severity of electromechanical dyssynchrony, induced by altered ventricular activation, correlated with the development of TdP-susceptibility in the CAVB dog model. Moreover, these effects seemed to primarily result from differential substrate remodelling, rather than differences in cellular electrical instabilities. We showed that animals' persistent mechanical dyssynchrony was associated with more pro-arrhythmic electrical remodelling, which was reflected by a more spatially heterogeneous dofetilide-induced prolongation of repolarization (Figure 2). Interestingly, regardless of activation pattern, dofetilide-induced prolongation of repolarization was always longest in the early activated regions. Hence, intrinsic cardiac remodelling appears to be primarily driven by ventricular activation pattern and its associated mechanical effects.

These results are especially relevant to the clinical field of electrophysiology, as they underscore the potentially pro-arrhythmic consequences of electromechanical dyssynchrony induced by improper pacing lead placement. This could also explain the paradoxical pro-arrhythmic effects of cardiac resynchronization therapy (CRT) that has been reported in non-responders and/or heart failure patients with a narrow QRS complex.[39–42] Moreover, Behon et al. (2020)[43] performed a retrospective study in which they reported that lateral left ventricular lead placement was associated with better long-term mortality outcomes in comparison to anterior or posterior lead locations. Even though this study did not specify any measures of arrhythmic outcome, prior

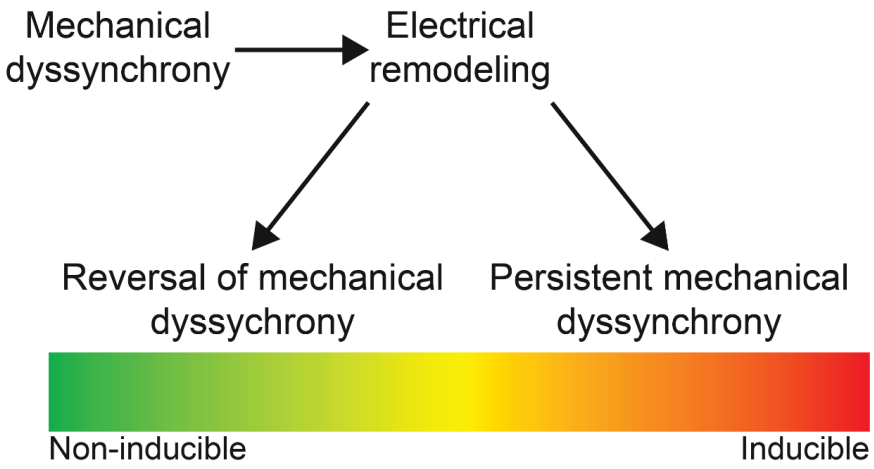

Figure 2: Schematic representation on how mechanical dyssynchrony can result in arrhythmic susceptibility. Acute mechanical dyssynchrony induces ventricular electrical remodelling. In response to electrical remodelling, mechanical dyssynchrony can be reversed or persistent. The extent wherein this dyssynchrony persist, correlates with the extent wherein the heart becomes susceptible for ventricular arrhythmias.

studies have similarly demonstrated that anterior and apical lead placements are associated with increased mortality and arrhythmic-susceptibility.[44–48]

Nevertheless, the most optimal placement of the left ventricular lead appears to depend on the patient-specific origin of the latest-activated region. Therefore, this placement should be tailored to the individual as much as possible to achieve the least possible mechanical dyssynchrony.[49]

EXTRACARDIAC REGULATION OF ELECTRICAL STABILITY

One of the best-known modulators of ventricular arrhythmias is the autonomic nervous system. In healthy conditions, the autonomic nervous system regulates cardiac function by finely controlling excitatory and inhibitory outputs from the sympathetic (SNS) and parasympathetic nervous systems (PNS), respectively.[50,51] Integration of afferent and efferent signals across the cardiac neuraxis achieves this complex, yet elegant, beat-to-beat regulation of sympathovagal balance and cardiac function.[50,52] At each level, cardiac sensory afferent information is processed and reflexively triggers efferent output to the heart.[50,52] Moreover, neurons of the intrinsic cardiac nervous system (ICNS) and stellate/thoracic sympathetic ganglia have their own local reflexes while integrating input from higher centers.[51]

Whereas this system relies on the careful titration of sympathetic to parasympathetic activity, cardiac injury causes pathological remodelling of cardiac autonomic neurons. Consequently, this fine balance is disrupted as remodelling culminates in sympatho-excitation.[50,51,53]

In **Chapter 5**, we established the role of the autonomic nervous system in modulating cardiac electrical stability in the CAVB dog model. We demonstrated that bilateral sympathetic denervation was a highly effective anti-arrhythmic strategy. As such, we showed that in most CAVB animals, sympathetic modulation was fundamental to the development of TdP. Hence, even though the myocardium itself was already highly susceptible to triggers and had a profoundly arrhythmic substrate, additional modulation was most often necessary to reach the arrhythmic threshold.

Interestingly, pharmacological modulation of cardiac autonomic innervation with the nicotinic acetylcholine-receptor blocker hexamethonium and the beta-blocker propranolol, lacked any anti-arrhythmic effects.

The clear discrepancy between mechanical and pharmacological blockade suggests that direct nerve stimulation could be a more potent pro-arrhythmic modulator than circulating catecholamines. Correspondingly, the study by Yagishita *et al.* (2015),[54] reported that bilateral stellate stimulation, but not norepinephrine infusion, increased ventricular dispersion of repolarization in pigs. Interestingly, Tanabe *et al.* (2001)[55] observed an increased spatial dispersion of repolarization upon norepinephrine infusion in patients with long QT syndrome (LQTS). Hence, even though circulating catecholamines might promote the arrhythmic substrate in LQTS patients, and thus also in the CAVB dog model, this pro-arrhythmic effect seems to be minimal as pharmacological suppression of these catecholamines could not suppress TdP.

As we became increasingly aware of the autonomic influence on ventricular arrhythmogenesis, we started to see more evidence of neural remodelling in the CAVB dog model. For example, we observed that the dofetilide-induced prolongation in PP-interval was different between inducible and non-inducible animals (Figure 3); the latter group showing a more pronounced prolongation (corresponding to a higher parasympathetic tone). Previous studies have demonstrated that dofetilide shifts cardiac autonomic tone to more parasympathetic-dominant conditions.[56] It could thus be hypothesized that inducible animals have a higher sympathetic tone which partially

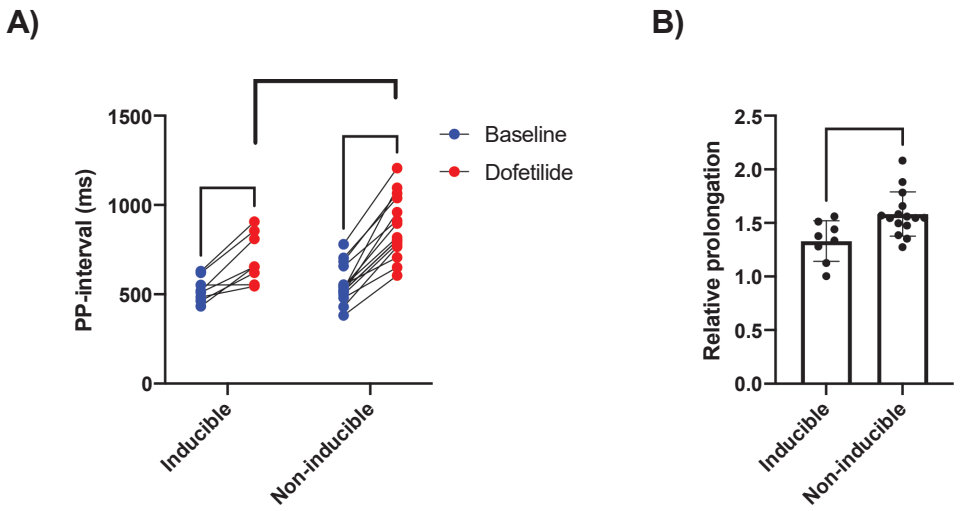

Figure 3: Dofetilide-induced prolongation in PP-interval in inducible and non-inducible animals. A) Individual PP-interval responses to dofetilide infusion. In both groups, dofetilide caused significant prolongations in PP-intervals. **B)** Relative increase in dofetilide-induced PP-interval was significantly greater in non-inducible animals. Included animals (n = 8 for inducible, n = 15 for non-inducible animals) overlap with animals used in chapter 3 and 4. To minimize confounding factors, all animals included in this sub-analysis were experimentally paced at 60 beats/minute from the right ventricular apex. * p<0.05; ** p<0.01; *** p<0.001; *** p<0.0001.

impedes the dofetilide-induced activation of the parasympathetic nervous system. The higher sympathetic tone in combination with dofetilide-infusion could cause more pro-arrhythmic conditions.

To further assess the role of autonomic modulation, we performed left stellate stimulation under acute AV-block conditions and followed-up with a dofetilide challenge after one hour (unpublished). Surprisingly, these animals were highly inducible to dofetilide-induced TdP, which were unresponsive to electrical cardioversion. Normally, a dofetilide-challenge under acute AV-block conditions does not cause any of the animals to become TdP-inducible.[13] However, when a similar experiment was performed under chronic AV-block conditions, but with a bilateral stellectomy after stellate stimulation, only 2 out of 17 animals remained inducible. This further suggests that it is the residual nerve activity that persists after stellate stimulation that caused TdP-inducibility, as circulating catecholamines should have been similar between the two conditions. Moreover, the highly pro-arrhythmic conditions that were observed in the setting of acute AV-block also demonstrate the powerful modulatory role of the autonomic nervous system; even in the absence of pro-arrhythmic remodelling of arrhythmic trigger and substrate, autonomic modulation could induce TdP.

As we had established the pro-arrhythmic character of the cardiac nervous system under CAVB conditions, **Chapter 6** explored the functional and cellular characteristics of neural remodelling in the CAVB dog model and its effects on cardiac electrophysiology. Previous human studies have shown that the phenotype of sympathetic overdrive may be initiated and propagated by neuronal hypertrophy, glial activation, and inflammation in stellate ganglia.[57] Unfortunately, most translational and clinical studies on autonomic remodelling have focused on ischemic cardiomyopathies, whilst functional and electrical consequences of neural remodelling in NICM are largely unknown. However, non-ischemic substrates differ markedly from ischemic substrates. Especially as it has been repeatedly shown that following myocardial infarction, chronic, excessive sympatho-excitation promotes arrhythmogenesis through inducing electrical instability and heterogeneity in scar-borderzones,[58] these findings are poorly translatable to the non-ischemic settings. Therefore, understanding both the presence and mechanisms of neural remodelling and how SNS-activation reciprocally affects non-ischemic substrates in this population is of great need.

A main finding of our study was that also in the setting of non-ischemic cardiac injury, cardiac autonomic tone progressively shifts towards sympathetic dominance. This increased sympathetic tone was associated with suppression of the arterial baroreceptor reflex, a consistent finding in ischemic cardiomyopathies.[59,60] Similar to the study by Notarius *et al.* (2007),[61] who studied cardiac autonomic tone in ischemic and non-ischemic cardiomyopathy patients, we also observed a decrease in both low frequency (LF; reflective of sympathetic activity) and high frequency (HF; reflective of parasympathetic activity) power. Their study also showed that the LF/HF ratio was higher in NICM patients than in ICM patients, suggesting a greater degree of autonomic imbalance. This could indicate that in contrast to the local neural remodelling processes which characterize ischemic cardiomyopathies, neural remodelling in the setting of non-ischemic cardiac injury is more extensive and results in a relatively higher sympathetic tone. Surprisingly, a meta-analysis reported that autonomic parameters indicative of cardiac autonomic disbalance could not predict the occurrence of ventricular arrhythmias in patients suffering from a non-ischemic dilated cardiomyopathy.[62] This seemingly paradoxical result could stem from multiple causes. For example, the review only included time-domain measurements of cardiac autonomic innervation (HRV, HRT and BRS). In contrast, Notarius *et al.* (2007)[61]

assessed frequency-domain measures of autonomic innervation (*e.g.* LF and HF). An advantage of these latter measurements is that they more specifically quantify the (relative) activity of the sympathetic and parasympathetic nervous systems and could thus be a more adequate assessment of cardiac autonomic tone. Secondly, the studies in this meta-analysis often only included a small number of patients (n < 100),[62] potentially biasing the outcome of their analysis.

In **Chapter 7**, we explored the transcriptomic heterogeneity of satellite glial cells in healthy murine stellate ganglia to study how these cells might modulate sympathetic activity and propagate autonomic imbalances. Satellite glial cells, the peripheral counterparts of astrocytes, ensheath neuronal soma and are capable of influencing neuronal activity.[63,64] Moreover, these cells become active in response to cardiac injury[57] and can promote activity of sympathetic neurons in the stellate ganglia.[65,66] Although these cells are fundamental to fully comprehend cardiac pathophysiology and might be potential targets for future modulatory strategies, little research has been conducted to understand their biology.

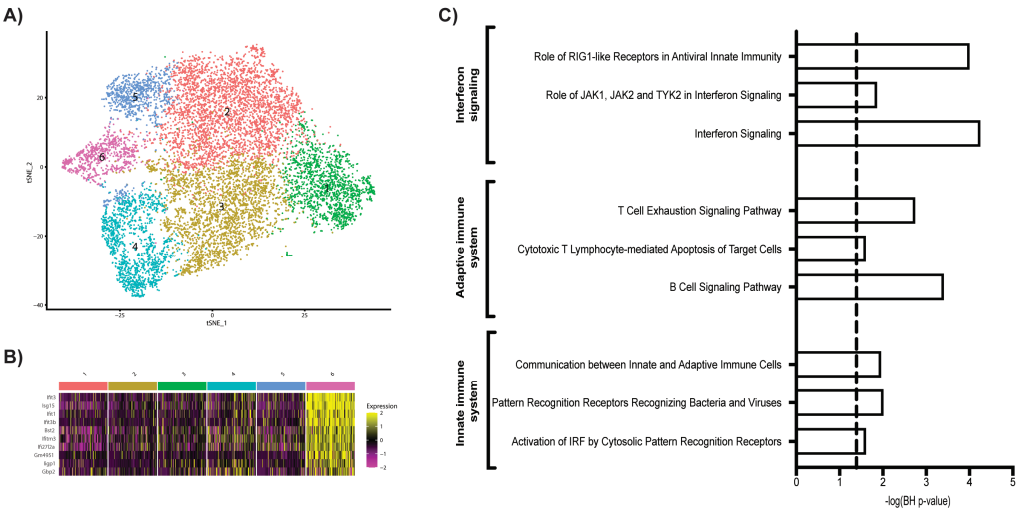

Figure 4: Characterization of the sixth population of satellite glial cells. A) t-SNE plot showing the co-existence of six satellite glial cell subtypes. **B)** Heatmap showing the expression of the differentially expressed genes of the sixth cluster across all populations. The sixth cluster was characterized by the upregulation of immune response related genes, including Ifit3, Ifit1 and Gbp2. **C)** Pathway analysis of the differentially expressed genes of the sixth cluster show that it is uniquely active in various defence mechanisms, which overlap with activity of the innate and adaptive immune system, as well as specific upregulation of various signalling pathways that are specific to anti-viral interferon signalling. Dotted line represents threshold of significance; -log(BH p-value) > 1.3 equals a p-value < 0.05.

Moreover, thus far most studies have focused on the physiology of murine satellite glial cells, resulting in very limited data availability on the behaviour of satellite glial cells in other animal models or humans. As such, we used the sympathetic ganglia of healthy mice to perform single cell RNA sequencing on. We observed five subtypes of satellite glial cells and classified them based on different functional and/or developmental stages. Though previously unspecified, a sixth population of satellite glial cells, characterized by its highly reactive phenotype, was found (Figure 4). Unfortunately, there was insufficient knowledge to interpret the function of this cluster in healthy mice and comparable single cell sequencing datasets to validate our findings were lacking. Therefore, this cluster was excluded from the manuscript. However, as knowledge on glial modulation of sympathetic activity is rapidly expanding and more research groups are performing comparable experiments, the existence of a reactive cluster of satellite glial cells has been validated.[67] The cells belonging to this cluster showed transcriptomic markers suggestive of a role in immune defence mechanisms. Interestingly, these cells appeared to possess both anti-bacterial and anti-viral properties (Figure 4C). Hence, within the stellate ganglia, a dedicated population of satellite glial cells appears to co-exist with immune cells to guard and preserve stellate ganglion homeostasis and health. Future research will have to elucidate the physiological role of this population in health and disease.

As has become evident by now, the cardiac autonomic nervous system is a powerful modulator of ventricular arrhythmogenesis. Unsurprisingly, neuromodulation has emerged as a promising therapeutic strategy against ventricular arrhythmias. These therapies aim to increase parasympathetic tone and/or suppress cardiac sympathetic tone. The present state of well-established, novel and upcoming neuromodulatory therapies for cardiac arrhythmias were reviewed in **Chapter 8.** This overview described the neuromodulatory mechanisms of the different strategies and highlighted the various (potential) targets of the cardiac neuraxis.

Another interesting avenue of neuromodulatory therapies that was not included in this chapter, are potential strategies to *prevent* pathological neural remodelling. As the biology of neural remodelling is becoming increasingly clear, novel therapies should aim to impede these processes from becoming detrimental. For example, one could think of using neural growth factor blockers, glial inhibitors or possibly even anti-inflammatory drugs, as all of these processes are involved in the development of acute

sympatho-excitation and its deterioration to chronic autonomic imbalance.[57,68–70] These burgeoning lines of investigation represent promising future therapies, all aimed at blunting progression of neural remodelling to lessen cardiovascular disease.

CONCLUSION

Philippe Coumel dissected arrhythmogenesis and formulated the three fundamental elements of ventricular arrhythmias: *a trigger, a substrate and a modulator.*[1,2] Reducing the complexity of ventricular arrhythmias to these three elements helps to understand why and how arrhythmias can develop in a certain situation. Moreover, establishing which intra- and extracardiac regulators of cardiac electrical stability are involved, can profoundly aid in identifying how these arrhythmic events could be suppressed or, even better, prevented.

REFERENCES

1. Coumel P. The management of clinical arrhythmias. An overview on invasive versus non-invasive electrophysiology. *Eur. Heart J.* **8,** 92–99 (1987).
2. Farré J & Wellens HJ. Philippe Coumel: a founding father of modern arrhythmology. *Europace* **6,** 464–465 (2004).
3. Antzelevitch C & Burashnikov A. Overview of Basic Mechanisms of Cardiac Arrhythmia. *Card. Electrophysiol. Clin.* **3,** 23–45 (2011).
4. Santana L, Cheng E & Lederer W. How does the shape of the cardiac action potential control calcium signaling and contraction in the heart? *J. Mol. Cell. Cardiol.* **49,** 901–903 (2010).
5. Priori SG & Corr PB. Mechanisms underlying early and delayed afterdepolarizations induced by catecholamines. *Am. J. Physiol. - Heart Circ. Physiol.* **258,** 1796–1805 (1990).
6. Weiss JN, Garfinkel A, Karagueuzian HS, Chen PS & Qu Z. Early afterdepolarizations and cardiac arrhythmias. *Heart Rhythm* **7,** 1891–1899 (2010).
7. Volders PGA, Kulcsár A, Vos MA, Sipido KR, Wellens HJJ, Lazzara R & Szabo B. Similarities between early and delayed afterdepolarizations induced by isoproterenol in canine ventricular myocytes. *Cardiovasc. Res.* **34,** 348–359 (1997).
8. Dunnink A, Stams TRG, Bossu A, Meijborg VMF, Beekman JDM, Wijers SC, De Bakker JMT & Vos MA. Torsade de pointes arrhythmias arise at the site of maximal heterogeneity of repolarization in the chronic complete atrioventricular block dog. *Europace* **19,** 858–865 (2017).
9. Kozhevnikov DO, Yamamoto K, Robotis D, Restivo M & El-Sherif N. Electrophysiological mechanism of enhanced susceptibility of hypertrophied heart to acquired Torsade de Pointes arrhythmias: Tridimensional mapping of activation and recovery patterns. *Circulation* **105,** 1128–1134 (2002).
10. Schreiner KD, Voss F, Senges JC, Becker R, Kraft P, Bauer A, Kelemen K, Kuebler W, Vos MA & Schoels W. Tridimensional activation patterns of acquired torsade-de-pointes-tachycardias in dogs with chronic AV-block. *Basic Res. Cardiol.* **99,** 288–298 (2004).

11. Boulaksil M, Jungschleger JG, Antoons G, Houtman MJC, de Boer TP, Wilders R, Beekman JD, Maessen JG, van der Hulst FF, van der Heyden MAG, van Veen TAB, van Rijen HVM, de Bakker JMT & Vos MA. Drug-Induced Torsade de Pointes Arrhythmias in the Chronic AV Block Dog Are Perpetuated by Focal Activity. *Circ. Arrhythmia Electrophysiol.* **4,** 566–576 (2011).
12. Volders PGA, Sipido KR, Vos MA, Spätjens RL, Leunissen JDM, Carmeliet E & Wellens HJJ. Downregulation of Delayed Rectifier K+ Currents in Dogs With Chronic Complete Atrioventricular Block and Acquired Torsades de Pointes. *Circulation* **100,** 2455–2461 (1999).
13. Dunnink A, van Opstal JM, Oosterhoff P, Winckels SKG, Beekman JDM, van der Nagel R, Cora Verduyn S & Vos MA. Ventricular remodelling is a prerequisite for the induction of dofetilide-induced torsade de pointes arrhythmias in the anaesthetized, complete atrio-ventricular-block dog. *Europace* **14,** 431–436 (2012).
14. Oros A, Beekman JDM & Vos MA. The canine model with chronic, complete atrio-ventricular block. *Pharmacol. Ther.* **119,** 168–178 (2008).
15. Loen V, Vos MA & Heyden MAG. The canine chronic atrio-ventricular block model in cardiovascular preclinical drug research. *Br. J. Pharmacol.* bph.15436 (2021). doi:10.1111/bph.15436
16. Thomsen MB, Volders PGA, Beekman JDM, Matz J & Vos MA. Beat-to-Beat Variability of Repolarization Determines Proarrhythmic Outcome in Dogs Susceptible to Drug-Induced Torsades de Pointes. *J. Am. Coll. Cardiol.* **48,** 1268–1276 (2006).
17. Bossu A, Varkevisser R, Beekman HDM, Houtman MJC, van der Heyden MAG & Vos MA. Short-term Variability of Repolarization Is Superior to Other Repolarization Parameters in the Evaluation of Diverse Antiarrhythmic Interventions in the Chronic Atrioventricular Block Dog. *J. Cardiovasc. Pharmacol.* **69,** 398–407 (2017).
18. van Weperen VYH, Bossu A & Vos MA. Point of View: Electrophysiological Endpoints Differ When Comparing the Mode of Action of Highly Successful Anti-arrhythmic Drugs in the CAVB Dog Model With TdP. *J. Cardiovasc. Pharmacol.* **74,** 499–507 (2019).
19. Janse MJ & De Bakker JMT. Arrhythmia substrate and management in

hypertrophic cardiomyopathy: from molecules to implantable cardioverter-defibrillators. *Eur. Hear. J. Suppl.* **3,** L15–L20 (2001).

20. Antzelevitch C, Shimizu W, Yan G, Sicouri S, Weissenburger J, Nesterenko V, Burashnikov A, Di Diego J, Saffitz J & Thomas G. The M cell: its contribution to the ECG and to normal and abnormal electrical function of the heart. *J. Cardiovasc. Electrophysiol.* **10,** 1124–1152 (1999).
21. Näbauer M, Beuckelmann D, Uberfuhr P & Steinbeck G. Regional differences in current density and rate-dependent properties of the transient outward current in subepicardial and subendocardial myocytes of human left ventricle. *Circulation* **93,** 168–177 (1996).
22. Antzelevitch C, Sicouri S, Litovsky S, Lukas A, Krishnan S, Di Diego J, Gintant G & Liu D. Heterogeneity within the ventricular wall. Electrophysiology and pharmacology of epicardial, endocardial, and M cells. *Circ. Res.* **69,** 1427–1449 (1991).
23. Stevenson WG. Ventricular Scars and Ventricular Tachycardia. *Trans. Am. Clin. Climatol. Assoc.* **120,** 403 (2009).
24. Antzelevitch C. Role of spatial dispersion of repolarization in inherited and acquired sudden cardiac death syndromes. *Am. J. Physiol. - Heart Circ. Physiol.* **293,** 2024–2038 (2007).
25. Antzelevitch C. Heterogeneity and cardiac arrhythmias: an overview. *Heart Rhythm* **4,** 964–972 (2007).
26. Stams TRG, Dunnink A, van Everdingen WM, Beekman HDM, van der Nagel R, Kok B, Bierhuizen MFA, Cramer MJ, Meine M & Vos MA. Deleterious acute and chronic effects of bradycardic right ventricular apex pacing: consequences for arrhythmic outcome. *Basic Res. Cardiol.* **112,** 46 (2017).
27. Vandersickel N, Bossu A, De Neve J, Dunnink A, Meijborg VMF, van der Heyden MAG, Beekman JDM, De Bakker JMT, Vos MA & Panfilov A V. Short-Lasting Episodes of Torsade de Pointes in the Chronic Atrioventricular Block Dog Model Have a Focal Mechanism, While Longer-Lasting Episodes Are Maintained by Re-Entry. *JACC Clin. Electrophysiol.* **3,** 1565–1576 (2017).
28. Coumel P. Cardiac Arrhythmias and the Autonomic Nervous System. *J. Cardiovasc. Electrophysiol.* **4,** 338–355 (1993).
29. Stavrakis S, Kulkarni K, Singh J, Katritsis D & Armoundas A. Autonomic

Modulation of Cardiac Arrhythmias: Methods to Assess Treatment and Outcomes. *JACC. Clin. Electrophysiol.* **6,** 467–483 (2020).

30. Vaseghi M & Shivkumar K. The Role of the Autonomic Nervous System in Sudden Cardiac Death. *Prog. Cardiovasc. Dis.* **50,** 404 (2008).
31. Wathen MS, Sweeney MO, DeGroot PJ, Stark AJ, Koehler JL, Chisner MB, Machado C, Adkisson WO & Investigators for the PR. Shock Reduction Using Antitachycardia Pacing for Spontaneous Rapid Ventricular Tachycardia in Patients With Coronary Artery Disease. *Circulation* **104,** 796–801 (2001).
32. Lindsay BD, Saksena S, Rothbart ST, Wasty N & Pantopoulos D. Prospective evaluation of a sequential pacing and high-energy bidirectional shock algorithm for transvenous cardioversion in patients with ventricular tachycardia. *Circulation* **76,** 601–609 (1987).
33. Cheng A, Joung B, Brown ML, Koehler J, Lexcen DR, Sanders P & Ellenbogen KA. Characteristics of ventricular tachyarrhythmias and their susceptibility to antitachycardia pacing termination in patients with ischemic and nonischemic cardiomyopathy: A patient-level meta-analysis of three large clinical trials. *J. Cardiovasc. Electrophysiol.* **31,** 2720–2726 (2020).
34. Assis FR, Krishnan A, Zhou X, James CA, Murray B, Tichnell C, Berger R, Calkins H, Tandri H & Mandal K. Cardiac sympathectomy for refractory ventricular tachycardia in arrhythmogenic right ventricular cardiomyopathy. *Heart Rhythm* **16,** 1003–1010 (2019).
35. Kopecky K, Afzal A, Felius J, Hall SA, Mendez JC, Assar M, Mason DP & Bindra AS. Bilateral sympathectomy for treatment of refractory ventricular tachycardia. *Pacing Clin. Electrophysiol.* **41,** 93–95 (2018).
36. Schwartz PJ. Cardiac sympathetic denervation to prevent life-threatening arrhythmias. *Nature Reviews Cardiology* **11,** 346–353 (2014).
37. Okada DR, Assis FR, Gilotra NA, Ha JS, Berger RD, Calkins H, Chrispin J, Mandal K & Tandri H. Cardiac sympathectomy for refractory ventricular arrhythmias in cardiac sarcoidosis. *Heart Rhythm* **16,** 1408–1413 (2019).
38. Vaseghi M, Gima J, Kanaan C, Ajijola OA, Marmureanu A, Mahajan A & Shivkumar K. Cardiac sympathetic denervation in patients with refractory ventricular arrhythmias or electrical storm: Intermediate and long-term follow-

up. *Heart Rhythm* **11,** 360–366 (2014).

39. Deif B, Ballantyne B, Almehmadi F, Mikhail M, McIntyre WF, Manlucu J, Yee R, Sapp JL, Roberts JD, Healey JS, Leong-Sit P & Tang AS. Cardiac resynchronization is pro-arrhythmic in the absence of reverse ventricular remodelling: a systematic review and meta-analysis. *Cardiovasc. Res.* **114,** 1435–1444 (2018).
40. Ruschitzka F, Abraham WT, Singh JP, Bax JJ, Borer JS, Brugada J, Dickstein K, Ford I, Gorcsan J, Gras D, Krum H, Sogaard P & Holzmeister J. Cardiac-Resynchronization Therapy in Heart Failure with a Narrow QRS Complex. *N. Engl. J. Med.* **369,** 1395–1405 (2013).
41. Eickholt C, Siekiera M, Kirmanoglou K, Rodenbeck A, Heussen N, Schauerte P, Lichtenberg A, Balzer J, Rassaf T, Perings S, Kelm M, Shin DI & Meyer C. Improvement of Left Ventricular Function under Cardiac Resynchronization Therapy Goes along with a Reduced Incidence of Ventricular Arrhythmia. *PLoS One* **7,** e48926 (2012).
42. Guerra F, Palmisano P, Dell'Era G, Ziacchi M, Ammendola E, Pongetti G, Bonelli P, Patani F, Devecchi C, Accogli M, Occhetta E, Nigro G, Biffi M, Boriani G & Capucci A. Cardiac resynchronization therapy and electrical storm: Results of the OBSERVational registry on long-term outcome of ICD patients (OBSERVO-ICD). *Europace* **20,** 979–985 (2018).
43. Behon A, Schwertner WR, Merkel ED, Kovács A, Lakatos BK, Zima E, Gellér L, Kutyifa V, Kosztin A & Merkely B. Lateral left ventricular lead position is superior to posterior position in long-term outcome of patients who underwent cardiac resynchronization therapy. *ESC Heart Fail.* **7,** 3374–3382 (2020).
44. Singh JP, Klein HU, Huang DT, Reek S, Kuniss M, Quesada A, Barsheshet A, Cannom D, Goldenberg I, McNitt S, Daubert JP, Zareba W & Moss AJ. Left ventricular lead position and clinical outcome in the multicenter automatic defibrillator implantation trial-cardiac resynchronization therapy (MADIT-CRT) trial. *Circulation* **123,** 1159–1166 (2011).
45. Kronborg MB, Johansen JB, Riahi S, Petersen HH, Haarbo J, Jørgensen OD & Nielsen JC. An anterior left ventricular lead position is associated with increased mortality and non-response in cardiac resynchronization therapy. *Int. J. Cardiol.* **222,** 157–162 (2016).

46. Kronborg MB, Johansen JB, Haarbo J, Riahi S, Philbert BT, Jørgensen OD & Nielsen JC. Association between implantable cardioverter-defibrillator therapy and different lead positions in patients with cardiac resynchronization therapy. *Europace* **20,** E133–E139 (2018).
47. Friedman DJ, Upadhyay GA, Altman RK, Orencole M, Barrett CD, Mela T, Kevin Heist E & Singh JP. The anatomic and electrical location of the left ventricular lead predicts ventricular arrhythmia in cardiac resynchronization therapy. *Heart Rhythm* **10,** 668–675 (2013).
48. Kutyifa V, Zareba W, McNitt S, Singh J, Hall WJ, Polonsky S, Goldenberg I, Huang DT, Merkely B, Wang PJ, Moss AJ & Klein H. Left ventricular lead location and the risk of ventricular arrhythmias in the MADIT-CRT trial. *Eur. Heart J.* **34,** 184–190 (2013).
49. Khan FZ, Virdee MS, Palmer CR, Pugh PJ, O'Halloran D, Elsik M, Read PA, Begley D, Fynn SP & Dutka DP. Targeted left ventricular lead placement to guide cardiac resynchronization therapy: The TARGET study: A randomized, controlled trial. *J. Am. Coll. Cardiol.* **59,** 1509–1518 (2012).
50. Fukuda K, Kanazawa H, Aizawa Y, Ardell JL & Shivkumar K. Cardiac Innervation and Sudden Cardiac Death. *Circ. Res.* **116,** 2005–2019 (2015).
51. Goldberger JJ, Arora R, Buckley U & Shivkumar K. Autonomic Nervous System Dysfunction: JACC Focus Seminar. *J. Am. Coll. Cardiol.* **73,** 1189–1206 (2019).
52. Ardell JL & Armour JA. Neurocardiology: Structure-Based Function. in *Comprehensive Physiology* **6,** 1635–1653 (John Wiley & Sons, Inc., 2016).
53. Randall WC. *Efferent sympathetic innervation of the heart* in Neurocardiology. Oxford University Press, New York, 1994.
54. Yagishita D, Chui RW, Yamakawa K, Rajendran PS, Ajijola OA, Nakamura K, So EL, Mahajan A, Shivkumar K & Vaseghi M. Sympathetic Nerve Stimulation, Not Circulating Norepinephrine, Modulates T-Peak to T-End Interval by Increasing Global Dispersion of Repolarization. *Circ. Arrhythmia Electrophysiol.* **8,** 174–185 (2015).
55. Tanabe Y, Inagaki M, Kurita T, Nagaya N, Taguchi A, Suyama K, Aihara N, Kamakura S, Sunagawa K, Nakamura K, Ohe T, Towbin JA, Priori SG & Shimizu W. Sympathetic stimulation produces a greater increase in both transmural and spatial dispersion of repolarization in LQT1 than LQT2 forms of

congenital long QT syndrome. *J. Am. Coll. Cardiol.* **37,** 911–919 (2001).

56. Champeroux P, Thireau J, Judé S, Laigot-Barbé C, Maurin A, Sola ML, Fowler JSL, Richard S & Le Guennec JY. Short-term variability in QT interval and ventricular arrhythmias induced by dofetilide are dependent on high-frequency autonomic oscillations. *Br. J. Pharmacol.* **172,** 2878–2891 (2015).
57. Ajijola OA, Hoover DB, Simerly TM, Brown TC, Yanagawa J, Biniwale RM, Lee JM, Sadeghi A, Khanlou N, Ardell JL & Shivkumar K. Inflammation, oxidative stress, and glial cell activation characterize stellate ganglia from humans with electrical storm. *JCI insight* **2,** e94715 (2017).
58. Vaseghi M, Lux RL, Mahajan A & Shivkumar K. Sympathetic stimulation increases dispersion of repolarization in humans with myocardial infarction. *Am. J. Physiol. - Heart Circ. Physiol.* **302,** H1838-1846 (2012).
59. La Rovere M, Bigger J, Marcus F, Mortara A & Schwartz P. Baroreflex sensitivity and heart-rate variability in prediction of total cardiac mortality after myocardial infarction. ATRAMI (Autonomic Tone and Reflexes After Myocardial Infarction) Investigators. *Lancet* **351,** 478–484 (1998).
60. Wu P & Vaseghi M. The Autonomic Nervous System and Ventricular Arrhythmias in Myocardial Infarction and Heart Failure. *Pacing Clin. Electrophysiol.* **43,** 172 (2020).
61. Notarius CF, Spaak J, Morris BL & Floras JS. Comparison of Muscle Sympathetic Activity in Ischemic and Nonischemic Heart Failure. *J. Card. Fail.* **13,** 470–475 (2007).
62. Goldberger JJ, Subačius H, Patel T, Cunnane R & Kadish AH. Sudden cardiac death risk stratification in patients with nonischemic dilated cardiomyopathy. *J. Am. Coll. Cardiol.* **63,** 1879–1889 (2014).
63. Hanani M. Satellite glial cells in sympathetic and parasympathetic ganglia: In search of function. *Brain Research Reviews* **64,** 304–327 (2010).
64. Hanani M. Satellite glial cells: More than just rings around the neuron. *Neuron Glia Biol.* **6,** 1–2 (2010).
65. Agulhon C, Boyt KM, Xie AX, Friocourt F, Roth BL & McCarthy KD. Modulation of the autonomic nervous system and behaviour by acute glial cell G_q protein-coupled receptor activation *in vivo*. *J. Physiol.* **591,** 5599–5609 (2013).
66. Xie AX, Lee JJ & McCarthy KD. Ganglionic GFAP+ glial Gq-GPCR signaling

enhances heart functions in vivo. *JCI Insight* **2,** e90565 (2017).

67. Mapps AA, Thomsen MB, Boehm E, Zhao H, Hattar S & Kuruvilla R. Diversity of satellite glia in sympathetic and sensory ganglia. *bioRxiv* 2021.05.25.445647 (2021). doi:10.1101/2021.05.25.445647
68. Zhou S, Chen LS, Miyauchi Y, Miyauchi M, Kar S, Kangavari S, Fishbein MC, Sharifi B & Chen P-S. Mechanisms of Cardiac Nerve Sprouting After Myocardial Infarction in Dogs. *Circ. Res.* **95,** 76–83 (2004).
69. Wernli G, Hasan W, Bhattacherjee A, Rooijen N van & Smith PG. Macrophage depletion suppresses sympathetic hyperinnervation following myocardial infarction. *Basic Res. Cardiol.* **104,** 681 (2009).
70. Hasan W, Jama A, Donohue T, Wernli G, Onyszchuk G, Al-Hafez B, Bilgen M & Smith P. Sympathetic hyperinnervation and inflammatory cell NGF synthesis following myocardial infarction in rats. *Brain Res.* **1124,** 142–154 (2006).

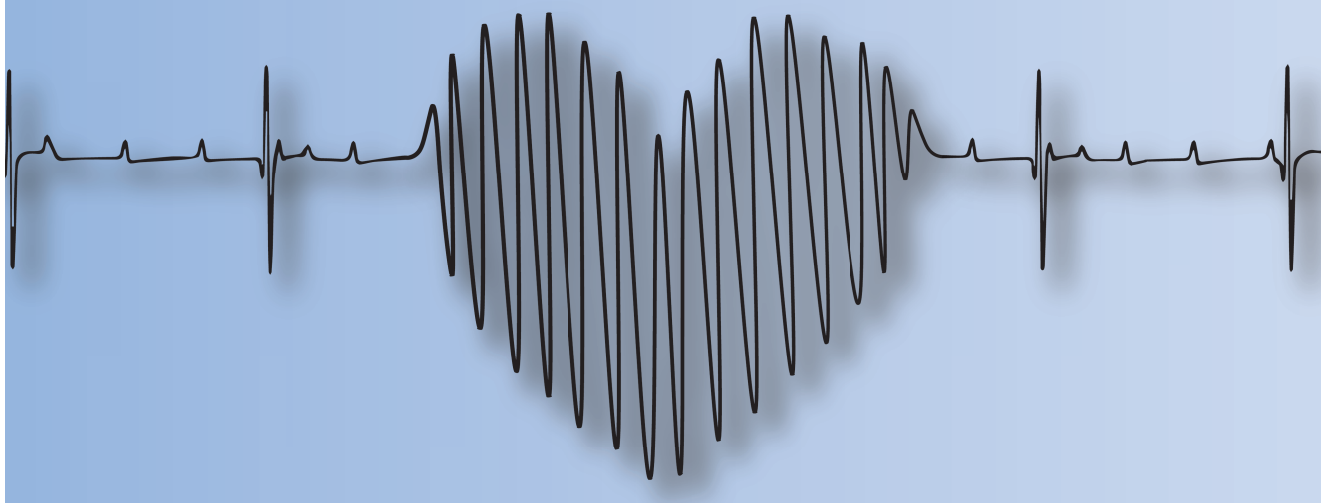

Valerie Y. H. van Weperen

568622-L-bw-Weperen
Processed on: 3-11-2021

Addendum

English summary
Nederlandse samenvatting
Acknowledgements
List of publications
Curriculum vitae

SUMMARY

With every beat, the heart pumps blood into the body. This way, organs and tissues are provided with the necessary nutrients and oxygen while simultaneously waste is carried away. It is the electrical conduction system of the heart, which regulates this rhythmic and continuous activity. This system *initiates* an electrical impulse, which then *conducts* across the heart. Finally, this electrical signal is transformed into a mechanical function: a contraction.

Normally, an electrical stimulus is generated in the sinoatrial node, located in the right upper chamber (atrium) of the heart. From here, electrical impulses travel down the conduction pathway, through the atrioventricular node (AV-node) to the lower chambers (the ventricles). Normally, the conduction of this electrical stimulus occurs in a predetermined, coordinated manner, which results in the coordinated contraction of the heart. This results in the blood to be pumped out as effectively as possible. After contraction, the repolarization phase follows, during which the cells recover and get ready for the next heartbeat.

In addition, the heart is also under the influence of the brain. We experience this interaction when our hearts start to beat faster in response to strong emotions such as happiness or stress. The brain influences and modulates the heart through the autonomic nervous system. This system comprises a network of nerves that travel between the brain and the heart. This network can be grossly divided into two parallel systems, the sympathetic and parasympathetic nervous system. These two divisions function like the gas and brake of a car; whilst the sympathetic nervous system stimulates the heart, the parasympathetic nervous system does the opposite. Hence, normal cardiac rhythm is regulated by its own electrical system and by signals coming from within the heart (intra-cardiac), as well as factors originating from outside of it (extra-cardiac).

However, in the case of a ventricular arrhythmia, the electrical system of the heart as described above becomes unstable. This instability can be caused by various intra- and extra-cardiac factors, which are collectively called pro-arrhythmic factors. Outside of normal functioning, the electrical stimulus originates from the ventricles (instead of

568622-L-bw-Weperen
Processed on: 3-11-2021

from the sinoatrial node), which results in abnormal activation of the ventricles. Often, this signal goes too fast (ventricular tachycardia), but it can also cause the heart to beat chaotically (ventricular fibrillation). The consequential rapid and chaotic beating of the heart hampers the adequate extrusion of blood. When ventricular fibrillation does not stop in time, it can lead to sudden cardiac death.

Anti-arrhythmic strategies are being developed to prevent and/or to treat ventricular arrhythmias. These therapies are commonly aimed at impeding one or more pro-arrhythmic factors from promoting the development of arrhythmias (arrhythmogenesis). Unfortunately, ventricular arrhythmias remain difficult to prevent or treat because 1) many pro-arrhythmic factors remain to be identified, and 2) for many pro-arrhythmic factors it remains insufficiently clear how they promote arrhythmogenesis. **Therefore, this thesis aimed to identify predisposing factors and elucidate the mechanism through which they destabilize the cardiac electrical system.**

Most of the work in this dissertation was performed in the chronic atrioventricular block (CAVB) dog model. In this model, ablation of the AV-node blocks the electrical signals from the sinoatrial node from reaching the ventricles. As a consequence, the ventricles have to initiate their own electrical stimulus. The resulting heart rhythm is called idioventricular rhythm. This rhythm is much slower than under normal circumstances, and also causes the activation pattern of the ventricles to become inefficient. Consequently, the heart will try to adapt to these changed conditions through a process called *remodelling*. Cardiac remodelling induces various adaptations including an increased force of contraction, an increase in heart size (hypertrophy), and a prolongation of the repolarization phase. In addition, the acute drop in heart rate also activates the sympathetic nervous system. Collectively, these adaptations ensure that the body is provided with enough blood flow despite the slow heart rate and altered ventricular activation. However, they simultaneously cause the animals to become prone for a specific type of ventricular arrhythmia: Torsade de Pointes arrhythmias (TdP). Their susceptibility for this arrhythmia can be tested through the administration of the pro-arrhythmic drug dofetilide. Hence, by exposing animals to other pro-arrhythmic factors – or by adding an anti-arrhythmic factor before or after administration of dofetilide – the extent to which these factors promote or inhibit arrhythmias can be

studied. For that reason, the CAVB dog model is an excellent model to use in studies regarding (pro- and anti-arrhythmic factors of) ventricular arrhythmogenesis.

As ventricular arrhythmias result from instability of the electrical system of the heart, the risk for ventricular arrhythmias can be estimated by quantifying the electrical instability. Important parameters that reflect cardiac electrical instability include repolarization duration, and *temporal* and *spatial* dispersion of repolarization. The temporal dispersion of repolarization quantifies the beat-to-beat variability in repolarization duration, whereas the spatial dispersion of repolarization assesses the extent of local differences in repolarization duration. We reviewed the applicability and accuracy of these parameters in **chapter two.** In this study, we demonstrated that repolarization duration inaccurately reflects cardiac electrical (in)stability. Temporal and spatial dispersion of repolarization were better parameters, even more so when combined. In those circumstances, these measures adequately reflected the efficacy of anti-arrhythmic drugs. This suggests that arrhythmogenesis is driven by both temporal and spatial dispersion of repolarization, and that it is therefore important to assess both factors when studying the consequences of pro- or anti-arrhythmic effects or conditions.

In **chapter three**, we looked into the mechanism by which a severely lowered heart rate (bradycardia) promotes arrhythmogenesis. Whereas bradycardia was already known to promote arrhythmogenesis, the mechanism that underlies this phenomenon remained largely unknown. In our study, we showed that severe bradycardia did not increase *temporal* dispersion of repolarization, but that *spatial* dispersion of repolarization was significantly larger under bradycardic conditions. We therefore demonstrated that when heart rate is severely lowered, spatial heterogeneities in electrical characteristics of the heart are augmented. This augmentation and the consequential instability of the heart's electrical system promotes the development of arrhythmias.

Under normal circumstances, both ventricles are activated at more or less the same time. As such, contraction of the ventricles occurs in a coordinated and synchronized manner. In **chapter four** we explored to what extent the pattern of ventricular activation

could affect cardiac remodelling and thereby determine arrhythmic outcome. For that purpose, we exposed three groups of animals to different extents of ventricular dyssynchrony and examined their arrhythmic susceptibility after remodelling. We showed that the more dyssynchronous the ventricular contraction occurred, the more animals became susceptible for arrhythmias. Thereby, we showed that more dyssynchronous conditions require more extensive cardiac adaptation, which causes the heart to become more susceptible for arrhythmias. This shows the importance of adequate implantation of pacemaker leads and devices, as pacing induced ventricular dyssynchrony can cause adverse pro-arrhythmic effects.

Next, we explored the role of an extra-cardiac factor that influences the cardiac electrical system: the autonomic nervous system. It was already known that the autonomic nervous system remodels in response to a heart attack. This then causes the sympathetic nervous systems to become overactive, whilst the parasympathetic nervous becomes progressively more inactivated. These changes and the resulting autonomic imbalance promote arrhythmogenesis.

However, all of these changes in autonomic balance have mainly been studied in the setting of a heart attack in which the heart remodels in response to oxygen deprivation. The involvement of the autonomic nervous system in arrhythmogenesis in hearts that have remodelled due to *another* cause than a heart attack, has however only been studied very scarcely. Therefore, we explored the role of the autonomic nervous system in the development of ventricular arrhythmias in the CAVB dog model. In **chapter five**, we aimed to establish *if* and *how* the sympathetic nervous system promoted ventricular arrhythmogenesis in the CAVB dog model. Therefore, we exposed CAVB dogs to three different manners of autonomic or sympathetic blockade and evaluated the anti-arrhythmic effects of these strategies. We showed that all drugs tested were ineffective anti-arrhythmic strategies. However, cutting the sympathetic nerves traveling to the heart (sympathetic denervation) was a highly effective anti-arrhythmic strategy. Interestingly, this antiarrhythmic effect was not reflected in temporal *nor* spatial dispersion of repolarization, but was rather associated with changes in parameters that reflect the force of contraction.

568622-L-bw-Weperen
Processed on: 3-11-2021

In **chapter six** we studied whether this pro-arrhythmic effect of the sympathetic nervous system was associated with remodelling of the autonomic nervous system. We showed how following AV-block, autonomic tone progressively shifts towards increased sympathetic and decreased parasympathetic tone. Moreover, we correlated these adaptations to an increased susceptibility for ventricular arrhythmias as we showed how sympathetic stimulation caused increasingly more spatial dispersion of repolarization. Interestingly, we also showed that parasympathetic stimulation appeared to stabilize the cardiac electrical system. Hence, also in hearts that have remodelled due to *another* cause than a heart attack, restoring autonomic balance might be an interesting approach for future anti-arrhythmic strategies.

Many of the therapies that are aimed at restoring autonomic balance target the sympathetic ganglia (stellate ganglia). These ganglia are networks of nerves and comprise the main origin of sympathetic input to the heart. There is however little known about the biology of these ganglia, especially as these ganglia are comprised of many different cell types. Most studies have only looked into the neurons that reside in the ganglia, leaving the function and biology of the other cell types to be severely overlooked. For that purpose, **chapter seven** specifically focused on satellite glial cells. Satellite glial cells both support, but also modulate the behaviour and activity of neurons. To get a better understanding of the biology of these cells, we performed single-cell RNA sequencing. This technique specifies and quantifies what part of the DNA of these cells is active at a certain moment in time. It essentially offers a snapshot into the activity of a certain cell type. By using this method, we found that six different types of satellite glial cells exist in the stellate ganglia of healthy mice and that these subtypes are either in different developmental stages and/or have different functions. Thereby, we offered new insights on the function of satellite glial cells, suggested various mechanisms through which they might adjust neuronal behaviour, and prompted future studies into the specific role of these cells in the setting of sympathetic overactivity and ventricular arrhythmias.

It has become clear that autonomic activity is often involved in the development of ventricular arrhythmias. Strategies that modulate the sympathetic or parasympathetic nervous system have become increasingly interesting and are currently subject to

much research. **Chapter eight** summarizes current and future neuromodulatory methods that can or may effectively impede ventricular arrhythmogenesis.

CONCLUSION

Ventricular arrhythmias result from a complex interplay between various proarrhythmic factors. This thesis highlighted the role of several of such factors, including bradycardia, altered ventricular activation and the autonomic nervous system. Preventing or impeding these factors can be an effective treatment for ventricular arrhythmias.

SAMENVATTING

Het hart pompt met iedere hartslag bloed het lichaam in. Alle organen en weefsels worden zo voorzien van zuurstof en de benodigde voedingsstoffen en tegelijkertijd worden afvalstoffen afgevoerd. Dit ritmische samenknijpen van het hart wordt mogelijk gemaakt door het interne elektrische systeem van het hart. Dit systeem *initieert* in eerste instantie een elektrische stimulus, die hierna over het hart wordt *geleid*. De elektrische stimulatie wordt vervolgens omgezet in een mechanische functie: de samentrekking van het hart (een contractie).

Normaal gesproken ontstaat het elektrische signaal in de sinusknoop, die zich in de rechterboezem (het atrium) bevindt. Vanaf hier wordt het via de atrioventriculaire knoop naar de kamers van het hart (de ventrikels) geleid. Dit elektrische signaal volgt in principe altijd hetzelfde, vaste patroon. Zo verloopt de contractie gecoördineerd en gesynchroniseerd, waardoor het bloed zo efficiënt mogelijk uit het hart wordt gepompt. Na de contractie volgt de repolarisatiefase. In deze periode herstellen de cellen zich en zorgen ze ervoor dat ze klaar zijn voor de volgende hartslag.

Het hart wordt daarnaast ook beïnvloed door de hersenen. Dit ervaren we bijvoorbeeld als (heftige) emoties, zoals stress en blijdschap, ons hart sneller laten kloppen. De werking van het hart wordt zo dus niet alleen beïnvloed door signalen die uit het hart zelf komen en eigen zijn aan het hart (intra-cardiaal), maar ook van signalen die hun oorsprong vinden buiten het hart (extra-cardiaal). De hersenen beïnvloeden het hart via het autonome zenuwstelsel. Dit stelsel bestaat uit een netwerk van zenuwen die informatie tussen de hersenen en het hart uitwisselen. Het autonome zenuwstelsel bestaat uit twee delen: het sympathische zenuwstelsel en het parasympatische zenuwstelsel. De werking hiervan is vergelijkbaar met het gas- en remsysteem van een auto; waar het sympathische zenuwstelsel het hart stimuleert, heeft het parasympatische zenuwstelsel juist een remmende werking.

In het geval van een ventriculaire ritmestoornis is het hierboven beschreven elektrische systeem van het hart instabiel geraakt. Deze instabiliteit kan worden veroorzaakt door verschillende intra- en extra-cardiale factoren, die ook wel aritmogene factoren worden genoemd. Anders dan bij normaal functioneren, ontstaat bij een ventriculaire

ritmestoornis de elektrische stimulatie van de kamers in de kamers zelf (in plaats van de sinusknoop), wat voor een abnormale activatie zorgt. Bij een dergelijke activatie gaat het ritme vaak te snel (ventriculaire tachycardie) en worden de hartkamers doorgaans op een chaotische wijze geactiveerd (ventrikel fibrilleren). In dat geval gaat het hart ook te snel en chaotisch samentrekken, waardoor het bloed niet meer goed het lichaam kan worden ingepompt. Als ventrikel fibrilleren niet tijdig stopt, kan dit tot plotselinge hartdood leiden.

Om ventriculaire ritmestoornissen te behandelen en/of te voorkomen, worden anti-aritmische therapieën ontwikkeld. Deze therapieën onderdrukken veelal één of meerdere aritmogene factoren. Voorkoming en behandeling van ventriculaire ritmestoornissen blijft echter lastig, omdat: (1) nog niet alle aritmogene factoren als zodanig zijn geïdentificeerd en (2) het vaak nog onvoldoende duidelijk is op welke manier aritmogene factoren het ontstaan van een ventriculaire ritmestoornis stimuleren. **Het doel van deze thesis was om additionele aritmogene factoren te identificeren en uit te zoeken via welke mechanismen zij het elektrische systeem van het hart instabiel maken.**

De meeste onderzoeken in deze thesis zijn uitgevoerd in het chronisch atrioventriculaire blok (CAVB) hondenmodel. In dit dierenmodel wordt de atrioventriculaire knoop doorgebrand, waarna de elektrische signalen van de sinusknoop niet meer naar de kamers van het hart kunnen worden geleid. Hierdoor worden de kamers geactiveerd door een elektrische signaal wat uit de kamers zelf komt. Dit ritme waarbij de kamers door hun eigen signaal geactiveerd worden, wordt het idioventriculair ritme genoemd. Aangezien dit ritme trager is en de kamers via een ander patroon geactiveerd worden, zal het hart zich proberen aan te passen aan deze veranderde omstandigheden. Dit noemen we *remodelleren.* Het remodelleringsproces heeft diverse gevolgen: het hart kan harder samenknijpen, het hart wordt groter en de repolarisatiefase duurt langer. Als reactie op dit vertraagde ritme wordt bovendien het sympathische zenuwstelsel geactiveerd. Al deze aanpassingen zijn erop gericht dat ondanks het trage ritme en de abnormale activatie, voldoende bloed het lichaam in wordt gepompt. Tegelijkertijd wordt het hart echter ook gevoeliger voor een specifiek type ventriculaire ritmestoornissen: Torsade de Pointes-ritmestoornissen (TdP). In het

CAVB-hondenmodel, kan de gevoeligheid hiervoor geobjectiveerd worden door het aritmogene medicijn dofetilide toe te dienen. Door CAVB-honden bloot te stellen aan een andere aritmogene factor en de uitkomst met het effect van dofetilide te vergelijken – of door ze voor of na toediening van dofetilide aan een anti-aritmische factor bloot te stellen – kan bestudeerd worden in welke mate deze factoren ritmestoornissen stimuleren of onderdrukken. Daarom is het CAVB-hondenmodel een geschikt model om te gebruiken in onderzoeken naar (bijdragende factoren aan) het ontstaan van ritmestoornissen.

Omdat ventriculaire ritmestoornissen ontstaan door een instabiel elektrisch systeem van het hart, wordt de kans op een ventriculaire ritmestoornis beoordeeld door de elektrische instabiliteit te meten. Belangrijke parameters van elektrische instabiliteit zijn de repolarisatieduur, de *temporele* en de *spatiële* dispersie in repolarisatie. De temporele dispersie in repolarisatie meet de variatie in repolarisatieduur slag op slag. De spatiële dispersie daarentegen kwantificeert de mate van plaatselijke verschillen in repolarisatieduur. De betrouwbaarheid en toepasbaarheid van deze parameters werd in **hoofdstuk twee** onderzocht. Hierin toonden wij aan dat de duur van repolarisatie geen goede maat was voor elektrische (in)stabiliteit. Temporele en spatiële dispersie van repolarisatie waren betere parameters, maar vooral wanneer zij samen werden gebruikt. In die gevallen kon met een hoge mate van precisie de effectiviteit van verscheidene antiaritmische medicijnen worden voorspeld. Hieruit volgt dat in onderzoeken naar aritmogene of antiaritmische factoren beide parameters moeten worden onderzocht . Daarnaast suggereert het ook dat het ontstaan van ventriculaire ritmestoornissen gedreven wordt door elektrische instabiliteit in beide dimensies.

In **hoofdstuk drie** onderzochten we het mechanisme waarmee een sterk vertraagde hartslag (bradycardie) ventriculaire ritmestoornissen stimuleert. Hoewel al bekend was dat bradycardie het ontstaan van ventriculaire ritmestoornissen stimuleert, was het mechanisme dat hierachter zit nog niet in kaart gebracht. In deze studie lieten wij zien dat een vertraagde hartslag niet zozeer de elektrische stabiliteit in de temporele dimensie, maar juist in de spatiële dimensie doet toenemen. Hiermee hebben wij aangetoond dat een trage hartslag spatiële verschillen in elektrische eigenschappen

uitvergroot en dat daardoor het hart zodanig instabiel kan worden dat ventriculaire ritmestoornissen kunnen ontstaan.

Normaal gesproken worden de kamers ongeveer tegelijkertijd geactiveerd, waardoor zij gecoördineerd en synchroon samenknijpen. In **hoofdstuk vier** onderzochten we hoe een ongecoördineerde en dyssynchrone activatie van de kamers het proces van remodelleren en de vatbaarheid voor ventriculaire ritmestoornissen beïnvloedt. Hiervoor werden drie groepen CAVB-honden aan verschillende maten van dyssynchrone elektrische activatie blootgesteld. In dit onderzoek toonden wij aan dat de mate waarin de kamers ongecoördineerd geactiveerd worden en samentrekken, direct verband houdt met de gevoeligheid voor ventriculaire ritmestoornissen: hoe dyssynchoner de contractie, hoe meer het hart moet remodelleren en hoe gevoeliger het wordt voor ventriculaire ritmestoornissen. Dit is een belangrijk inzicht voor - onder andere - het implanteren van pacemakers. Het suggereert namelijk dat suboptimale implantatie, die dyssynchrone activatie en samentrekking van de kamers veroorzaakt, tot een toegenomen gevoeligheid voor ventriculaire ritmestoornissen kan leiden.

Vervolgens richtte ons onderzoek zich op een extra-cardiale factor die de hartfunctie beïnvloedt: het autonome zenuwstelsel. Het was al bekend dat na een hartaanval het autonome zenuwstelsel remodelleert. Als gevolg daarvan wordt het sympathische zenuwstelsel overactief, terwijl het parasympatische zenuwstelsel juist steeds meer geïnactiveerd wordt. Deze veranderingen en autonome disbalans stimuleren het ontstaan van ventriculaire ritmestoornissen.

Dit alles is echter vooral onderzocht in harten die geremodelleerd zijn na een hartaanval waarbij er sprake is geweest van zuurstofgebrek van het hart. Hoe het autonome zenuwstelsel bij ventriculaire ritmestoornissen betrokken is als het hart geremodelleerd is door een *andere* oorzaak, is nog maar weinig onderzocht. Daarom onderzochten wij de rol van het autonome zenuwstelsel in de ontwikkeling van ventriculaire ritmestoornissen in het CAVB-hondenmodel. In **hoofdstuk vijf** wilden wij allereerst vaststellen of en hoe het sympathische zenuwstelsel betrokken is bij de ontwikkeling van ventriculaire ritmestoornissen in het CAVB hondenmodel. Daarvoor hebben we CAVB-honden aan drie verschillende wijzen van autonome of

sympathische blokkade blootgesteld, om te onderzoeken of deze therapieën antiaritmische effecten hadden. Wij concludeerden dat alle medicamenteuze therapieën de ventriculaire ritmestoornissen niet konden onderdrukken of voorkomen, maar dat het doorsnijden van de sympathische zenuwen van het hart wel een hele effectieve antiaritmische werking had. Dit effect werd weerspiegeld door een afname in de kracht waarmee de kamers zich samentrokken.

In **hoofdstuk zes** hebben we vervolgens onderzocht of dit aritmogene effect van het sympathische zenuwstelsel een gevolg was van aanpassingen in de autonome balans. In dit onderzoek toonden wij aan dat na het maken van AV-blok, het sympathische zenuwstelsel steeds actiever wordt, terwijl het parasympatische zenuwstelsel steeds inactiever wordt. We correleerden deze veranderingen aan een toegenomen vatbaarheid voor TdP door aan te tonen dat met de tijd sympathische stimulatie voor steeds meer elektrische instabiliteit zorgde. Parasympatische stimulatie daarentegen leek het elektrische systeem van het hart juist te stabiliseren. Herstellen van de autonome balans is dus een effectieve antiaritmische behandeling tegen ventriculaire ritmestoornissen, ook wanneer het hart geremodelleerd is door een andere oorzaak dan een hartaanval.

Veel van de huidige behandelingen die erop gericht zijn om de autonome balans te herstellen, pogen dit te bewerkstelligen door de sympathische activiteit te remmen. De meeste behandelingen richten zich daarvoor op de sympathische ganglia. Deze ganglia zijn netwerken van zenuwen waarvandaan de zenuwen die naar het hart lopen ontspringen. Er is echter nog maar beperkte kennis over de biologie van deze ganglia. In ganglia bevinden zich veel verschillende soorten cellen. De meeste studies hebben zich tot nu voornamelijk op de zenuwcellen gericht. Hierdoor is weinig bekend over de functie en biologie van andere cellen die zich in deze ganglia bevinden. **Hoofdstuk zeven** richtte zich daarom specifiek op de satellietcellen in de sympathische ganglia. Satellietcellen ondersteunen de zenuwen, maar kunnen hun activiteit ook beïnvloeden. Om hun functie en biologie beter te begrijpen, hebben we '*single cell RNA sequencing*' uitgevoerd. Deze techniek specificeert en kwantificeert welk gedeelte van het DNA van deze cellen op een bepaald moment actief is. Deze methode biedt daarmee een momentopname van de activiteit van een specifiek type cel. Met behulp van deze

methode hebben we aangetoond dat onderscheid kan worden gemaakt tussen zes verschillende typen satellietcellen in de sympathische ganglia. Deze subgroepen bevinden zich elk in een ander stadium van ontwikkeling en/of oefenen een andere functie uit. Hiermee hebben we nieuwe inzichten in de biologie en functie van deze cellen verkregen en hebben we ook aangetoond op welke manieren deze cellen de activiteit van zenuwen kunnen beïnvloeden. Deze inzichten stimuleren toekomstige onderzoeken naar de rol en activiteit van satellietcellen in het kader van autonome disbalans en ventriculaire ritmestoornissen.

Het is duidelijk dat het autonome zenuwstelsel een grote rol speelt in het ontstaan van ventriculaire ritmestoornissen. Therapieën die de activiteit van het sympathische en/of parasympatische zenuwstelsel beïnvloeden, worden op dit moment veel onderzocht en ontwikkeld. **Hoofdstuk acht** vat de behandelingen die al gebruikt worden om het autonome zenuwstelsel te beïnvloeden en daarmee ventriculaire ritmestoornissen te onderdrukken samen. Het geeft daarnaast een overzicht van vergelijkbare toekomstige behandelopties die op dit moment nog nader onderzocht worden.

CONCLUSIE

Ventriculaire ritmestoornissen zijn het resultaat van een complexe interactie tussen verschillende aritmogene factoren. In deze thesis werden verschillende factoren onderzocht, waaronder bradycardie, veranderde ventriculaire activatie en het autonome zenuwstelsel. Ventriculaire ritmestoornissen kunnen effectief worden voorkomen of behandeld door de aritmogene effecten van deze factoren te identificeren en te behandelen.

ACKNOWLEDGEMENTS

Dear reader, you have reached the final chapter of this dissertation: the acknowledgements. As this is also always my favorite chapter to turn to, I don't blame you if this is the first (but hopefully not last) chapter of my thesis that you will read. In this chapter, I'd like to thank the many, many people that have supported or improved this thesis or made the journey towards it more enjoyable.

Aan het hoofd van dit proefschrift staat **Professor Vos,** Marc. De mogelijkheid die jij me geboden hebt om tijdens mijn studie al het gros van mijn proefschrift te schrijven is een kans waar ik ontzettend dankbaar voor ben. Het was een risico en het was zeker niet altijd even makkelijk, maar ik had het niet anders (en ook zeker niet met iemand anders) willen doen. Jij hebt mij de vrijheid gegeven om al redelijk vroeg zelfstandig de wereld van de wetenschap verkennen, met knikkende knietjes op congressen staan en ongenadig afgewezen manuscripten terug te krijgen. Ik heb ervan genoten (behalve de afwijzingen dan). Ook die keer dat jij en Alex mij met de auto van LAX oppikten, onze ietwat verschillende interesses tijdens de ijshockeywedstrijd (ik was meer onder de indruk van het huwelijksaanzoek, jij meer van de wedstrijd) of natuurlijk de dagen dat jij mij bezocht aan UCLA zijn herinneringen die mij nog lang bij zullen blijven. HRS 2020 en AHA 2021 konden we helaas niet fysiek bijwonen, maar dat betekent alleen maar dat we wat in te halen hebben bij de volgende paar congressen! Ik hoop dat je me ook nog eens komt opzoeken, ik zal je dan zeker (op de fiets) meenemen naar een echte sportwedstrijd (in plaats van een sportcafé)!

Aan de wieg van mijn avontuur bij de MedFys stond **dr. van der Heyden. Marcel,** jij nam mij 7 jaar geleden als student aan op het lab en hebt sindsdien zowel mijn schrijfstijl als mij als persoon zien veranderen. Ik kon altijd bij jou binnen lopen als ik het even niet meer begreep of overzag, als ik even wilde sparren of juist je onverbloemde mening over een plaatje of een stuk wilde hebben. Ik heb enorm genoten van de ‘zoek de overeenkomsten’ intermezzo’s wanneer jij weer fraude had ontdekt of de examenvragen van geneeskunde die jij bij ons kwam testen. Jouw kritische blik en oog voor detail, gecombineerd met een oprechte interesse in onderzoek hebben mij enorm gedreven en geholpen in het schrijven van de verschillende stukken. Ik ben enorm blij en trots om jou als copromotor te hebben.

Dr. Ajijola, Olu, you have turned my time at UCLA, which was intended as a six-month internship, into something incredible and more than I had ever hoped for. I remember going to your talk at AHA in 2018 and was fascinated by your research, unbeknownst to me that you would soon become my mentor. I am deeply grateful for your generosity and hospitality, for showing me all the different corners of neurocardiology, allowing me to engage in scientific discussions as a member of the 'Olu group' and having me join your weekly (online) lab meetings. You pushed me out of my comfort zone and elevated me to levels that were beyond my imagination. Thank you for all your help and guidance, you did not only spark my interest for neurocardiology, you ignited a fire.

Dear **Prof. van der Harst**, **Prof. Hauer, Dr. Meine**, **Prof. Rinkel**, **Prof. van Rooij, Prof. Shivkumar**, and **Dr. van Veen,** it is an honour to have you in my assessment committee and/or to defend my thesis with you as my opposition.

Jet Beekman, lieve Jet, wat heb ik ontzettend genoten van de ontelbare uren waarin wij samen experimenten hebben gedraaid! Ik weet nog goed hoe na een hele uitleg defibrilleren ik helemaal geen induceerbare honden had, hoe jij met een koplamp op zoek ging naar de stellate of hoe ik in het begin anderhalve meter afstand van de honden hield. Elk experiment was weer uniek op zijn eigen manier, maar zelfs als ze wat minder goed verliepen kon jij er altijd nog een positieve draai aan geven. Werken met jou was niet alleen plezierig door deze momenten in de OK, de grappen en de uiteenlopende gesprekken op het lab. Het was vooral het gevoel dat jij mij, en alle anderen op het lab geeft: dat jij ons in al onze keuzes steunt en het allerbeste met ons voor hebt. Op de hoogte- en de dieptepunten kunnen wij altijd op je rekenen. Ik ben ontzettend blij voor jou en Esther met jullie nieuwe huis en nieuwe camper, ik weet zeker dat jullie er enorm van zullen genieten. Tot snel!

Alexandre Bossu, Alex, I vividly remember the numerous times we stood in the OR together (especially the time that we actually performed the experiment together!!), the various discussions that we have had and of course the trip to Anaheim (including Apple Store and amazing direction skills on our way back to the hotel). I am profoundly grateful to have had you as my supervisor when I initially started at the lab. Although I have come across many mentors that have *shaped* my scientific career, you created

the scientist in me. From the very first day, your enthusiasm and eye for research have continued to inspire me. If had not been for you, I probably would have canceled my internship at UCLA. Thank you for pushing me to choose courage over comfort and to pursue my dreams, even if it doesn't always fit others' perspectives.

During my years at the Medical Physiology, I have had the privilege to work with many different people that each have inspired me in their own unique ways. **Tonny,** om jou als eerste te zien bij binnenkomst van het lab was iedere keer weer als een warme knuffel. Ik ben blij dat je nu vol kunt genieten van je pensioen! **Linda**, jouw opgewekte stemming kan een ieders dag weer helemaal opfleuren! Bedankt voor al je hulp met het afronden van mijn promotie! **Toon**, je bent altijd in voor een praatje en denkt actief mee met alle onderzoeken. Hoewel onze samenwerking pas bij mijn laatste onderzoek begon, heeft dit veel indruk op mij gemaakt. Bedankt voor al je inzicht en begeleiding met de immunochemie, jouw aanwijzingen hebben het absoluut verbeterd. **Marti**, **Sanne en Maria,** ik vind het jammer dat ik niet meer van jullie cursussen heb kunnen volgen, ze waren altijd erg leuk. **Teun**, jouw prikkelende vragen bij de werkbespreking waren niet alleen uitdagend om te beantwoorden, maar zetten mij altijd weer aan het denken. Dit heeft zeker bijgedragen aan mijn onderzoeken - dank je wel hiervoor! **Marien**, ik kreeg pas echt waardering voor jouw patch-clamp kunsten toen ik het zelf probeerde en met een petrischaal vol krampende, ontplofte myocyten eindigde. **Joanne**, jij laat iedereen altijd meteen op haar / zijn gemak voelen. Voor mij persoonlijk was je zeker de laatste paar maanden een enorme steun samen op de kamer. Ik bewonder je doorzettingsvermogen en authenticiteit, ik ben benieuwd naar jouw volgende stappen! **Vera**, jouw eerlijkheid en openheid sieren je enorm. Als ik even wilde lachen of ontspannen kon ik altijd op je rekenen! Gefeliciteerd met je huisje, ik wacht nog op onze gedeelde housewarming. **Agnieszka**, met een lach denk ik terug aan onze avonturen tijdens de Dutch Physiology Days. Leuk om je nu zo af en toe in de wandelgangen van het Diak tegen te komen! **Willem**, ook al heb ik niet lang tegenover je gezeten, jouw droge humor en baby yoda bobblehead maakten iedere dag beter. Ik vind het bewonderenswaardig hoe jij binnen tien seconden van academisch hoogstaande gesprekken kon switchen naar het bespreken van een meme. Bedankt dat je van mijn bescheiden afscheidsborreltje een echte borrel hebt gemaakt. **Meye, Stephanie,** we hebben niet veel samengewerkt maar de praatjes op

de kamer en de borrels waren altijd gezellig met jullie! **Encan**, 雖然我們沒有很多一起工作過,但你開朗的心情讓我們每一天都很開心! **Kubra**, goodluck with your PhD back in Turkey! **David, Helen**, Chicago was fantastisch, ik kan nog lachen om onze vlogs en koffie-uurtjes bij REPATHA. **Albert**, we hebben nooit direct samengewerkt, maar jouw commentaren op manuscripten waren altijd van grote toegevoegde waarde. **Muge, Yuan,** 我真的很喜歡和你們一起工作.我們一起去維也納的時候也非常好玩! 歡迎你們再來荷蘭玩! **Alan,** you and your Italian spirit brought much joy and laughter to the lab. I truly miss your great tiramisu. I wish you all the best back in Italy! **Odette,** bedankt voor al jouw echo lessen, ik heb er nog vaak plezier van! **Veronique,** bedankt voor al je hulp bij de mapping experimenten. Jouw inzicht en ideeën tijdens de experimenten waren altijd erg behulpzaam. **Marcel** bedankt voor al je hulp met de immunochemie en kleuringen. Ik heb veel geleerd van onze samenwerking!

I had the amazing opportunity to conduct research at the University of California, Los Angeles Cardiac Arrhythmia Center as part of my medical curriculum from October 2019 to March 2020.

Professor Shivkumar, Shiv, I vividly remember how I nervously sent you an email, asking to do a scientific rotation at your institute. To my surprise, you answered within an hour (I believe it was 04:00 AM in Los Angeles), offered me a research project and even invited me to visit your center prior to my rotation. I felt petrified, vicious, vulnerable and excited all at once. I remain grateful for the opportunities that you have created for me. I am deeply honored and humbled to have you as part of my opposition.

Dr. Vaseghi, dear Marmar, I am beyond grateful and incredibly happy for the opportunity to return to the Cardiac Arrhythmia Center. I am excited to embark on this journey with you and to broaden my knowledge on neurocardiology. As I aspire to combine clinical practice with scientific research, I am grateful to be directly mentored by one of the leading (female) physician scientists in this field. It's inspiring.

Dr. Tompkins, thank you for the small talk every time you entered the room. The conversations about licorice and Dutch cookies made me feel a bit more home.

Also in our student room, I was welcomed with open arms. **Amit**, you gave me my daily dose of girl talk about dating shows on Netflix and Taylor Swift lyrics, whilst you, **Chris,** always provided me with 'authentic' Taiwanese foods and endless matcha-flavoured sweets. **Ali,** I envy your ability to make perfectly inappropriate jokes at the wrong time and still make it funny and get away with it. **Al-Hassan,** you made me feel like a real 'Californian' when you started calling me dude, and in you, **Lucian,** I saw a younger version of myself that would actually get excited over my explanation of an ECG or PV-loop. Although you introduced me as Veronica on my first day, I found another lasting friend in you, **Jaime.** The trip to Big Bear that you and Van organized remains one of the highlights of my stay. Your passion for medicine is evident and I wish you all the best in your journey to medical school. **ZhiWei** thank you for your patience and all your help with the experiments. **Russell,** thank you for your patience when I had yet another question about R or Seurat. **Jonathan,** you taught me a lot about science, but mostly with you I discovered not just the beauties of LA or California, but also myself. Also many thanks to **Amer, Amiksha, Ching, Yuichi, Chris, Christian, Joe, Maria, Michael, Peter, and Sachin,** you all made my stay unforgettable.

Ook in het Diak ben ik met open armen ontvangen. **Lieve iedereen,** bedankt voor het geduld waarmee jullie mij alles hebben uitgelegd, de ruimte die jullie creëren voor vragen, en jullie begeleiding in mijn eerste stappen als (echte) dokter. Ik hoop dat we elkaar zo nu en dan nog zullen tegenkomen, misschien op een borrel? :))

Ilana, wat kan ik genieten van jouw nuchterheid en doortastendheid tijdens onze koffietjes, taartjes en natuurlijk het weekje Griekenland. De manier waarop jij van het leven geniet en kan relativeren is inspirerend! Laten we snel weer samen een paar daagjes weggaan! **Koen** en **Rik,** of moet ik zeggen mede-oprichters van het ‘Vragenvuur Uur’?! Bedankt voor al het gelach, de gezelligheid en niet te vergeten de leerzame uurtjes. We hebben elkaar de laatste jaren wat minder gezien, maar ik hoop dat we nu weer vaker met een biertje en een bitterbal samen kunnen lachen! **Roel**, jij maakt mijn zus blij en dat maakt mij blij. Fijn dat je een talent hebt voor Nederlands en mijn stukken wilde controleren, dat maakt mij ook blij.

Ook ben ik erg dankbaar voor **Albert-Kees, Christelle** en **Corno.** Als jong meisje van 17 dacht ik dat de wereld zou instorten toen ik niet werd ingeloot voor geneeskunde. Jullie hadden vertrouwen in mij en durfden dat ook uit te spreken op de momenten waarop ik dat zelf minder had. Dit betekende toen erg veel voor mij, en nu nog steeds!

表哥表姐，謝謝你們常常帶我們出去玩, 出去吃東西。我還記得爸爸怎麼把我們在夜市贏到的獎品塞在皮箱裡, 讓我們回來還可以繼續回應我們在台灣快樂的生活。可惜撈到的魚不可以帶回家! **大阿姨**，謝謝妳讓我們了解什麼是真正客家的生活習慣也教了我們煮很多客家餐。下次我一定要再跟你一起做粿和年年糕! 真可惜妳今天沒辦法參加!
舅舅，小心心長大了！希望你們有空來荷蘭玩！**小阿姨,** 謝謝妳常常相信我,也是第一個叫我謝醫生的人。不管妳在哪裡我相信妳天天讓阿公和芳孜大笑。妳大聲的哈笑和妳教了我和姐姐的生活課我永遠不會忘記！
阿公和**阿媽**，我們從小時候就粘在一起。一起出去玩, 去市場買魚, 喝養樂多, 看電視, 到晚上的時候睡在同一張床說 Goodnight。雖然我們住那麼遠，我從來沒有感覺我們有分開過。阿媽**,**我非常期待畢業後打電話給你, 告訴你我過關了。阿公**,** 我相信你今天會站在我身邊, 陪我一起慶祝這個特別的一天。

Vivian, lieve Viv. Jij bent de vliegende kiep van deze PhD, van spellingscheck tot BBQ-date tot coach of oppositie-lid, je hebt alle mogelijke rollen wel op je genomen. Met niemand kan ik ook zo lachen als met jou, je bent mijn beste maatje, ik kan me geen betere zus wensen. Het is geen geheim dat ik niet zonder jou kan. Ik ben ook super super super blij dat we zelfs na al 25 jaar samen te hebben gewoond er toch nog voor kozen om samen een huisje te kopen. Je weet dat ik ontzettend naar je opkijk en meer dan van wie dan ook jouw goedkeuring en bevestiging zoek (behalve wanneer we als buurman & buurman IKEA kasten in elkaar proberen te knutselen). Ik denk dat niemand dan ook verrast is dat jij vandaag naast mij staat, maar ik had deze promotie en deze dag niet zonder jou kunnen voltooien. 我愛妳!!

Lieve **mama en papa**, jullie hebben Vivian en mij altijd gesteund, gedreven en gemotiveerd om groots te dromen. Jullie hebben ons van jongs af aan geleerd hard te werken voor onze dromen en ik ben dankbaar dat jullie bij iedere stap, lach en traan onze handen hebben vastgehouden.

568622-L-bw-Weperen
Processed on: 3-11-2021

媽媽, 從我小時候到今天, 不管有什麼事情我馬上會找妳。跟妳一起笑,哭或是發脾氣, 妳抱我的時候，我知道一切都會好起來的。謝謝妳, 不管發生了什麼事, 常常幫我點亮一盞燈, 牽著我的手一步一步的往前走。妳真的是世界上最好的媽媽! 我愛妳!!

Lieve **papa**, dankjewel dat jij mijn paranimf wilde zijn. Ik had op deze dag niemand liever naast me willen hebben. Ik kijk ernaar uit om na het verkrijgen van het diploma opzij te kijken en jou vol trots te zien lachen. Ik weet dat ik vaak schuw lach wanneer iemand zegt dat ik veel op je lijk, maar van binnen ben ik dan heel trots. Het is een van de grootste complimenten die ik kan krijgen.

LIST OF PUBLICATIONS

Van Weperen VYH, Vos MA, Ajijola OA. Autonomic modulation of ventricular electrical activity: recent developments and clinical implications. *Clinical Autonomic Research.* 2021. doi: 10.1007/s10286-021-00823-4.

Van Weperen VYH*, Dunnink A*, Bossu A, Beekman HDM, van der Heyden MAG & Vos MA. Severe bradycardia increases the incidence and severity of Torsade de Pointes arrhythmias by augmenting pre-existent dispersion of repolarization in the CAVB dog model. *Front. Physiol.* 2021. doi: 10.3389/fphys.2021.642083.

van Weperen VYH, Littman RJ, Arneson DV, Contreras J, Yang X & Ajijola OA. Single-cell transcriptomic profiling of satellite glial cells in stellate ganglia reveals developmental and functional axial dynamics. *Glia*. 69: 1281-1291. 2021. doi: 10.1002/glia.23965.

Smoczyńska A, Aarnink EW, Dunnink A, Bossu A, van Weperen VYH, Meijborg VMF, Beekman HDM, Coronel R, Vos MA. Interplay between temporal and spatial dispersion of repolarization in the initiation and perpetuation of Torsades de Pointes in the chronic atrioventricular block dog. *Am J Physiol Heart Circ Physiol.* 321: 569 - 576. 2021. doi: 10.1152/ajpheart.00945.2020.

van Weperen VYH, Bossu A & Vos MA. Point of View: Electrophysiological Endpoints Differ When Comparing the Mode of Action of Highly Successful Anti-arrhythmic Drugs in the CAVB Dog Model With TdP. *J Cardiovasc Pharmacol.* 74:499-507. 2019. doi: 10.1097/FJC.0000000000000748.

Te Dorsthorst RPM, Hendrikse J, Vervoorn MT, van Weperen VYH, van der Heyden MAG. Review of case reports on hyperkalemia induced by dietary intake: not restricted to chronic kidney disease patients. *Eur J Clin Nutr,* 73: 38 - 45. 2019. doi: 10.1038/s41430-018-0154-6.

van Weperen VYH, Vos MA & van der Heyden MAG. Commentary: Autonomic modulation in patients with heart failure increases beat-to-beat variability of ventricular action potential duration. *Frontiers in Physiology*. 8: 459. 2017. doi: 10.3389/fphys.2017.00459.

van Weperen VYH, Vos MA & van der Heyden MAG. A Role of Preload Variability in Quantifying Cardiac Repolarization Reserve in Baseline. *Adaptive Medicine.* 8: 107 - 111. 2016. doi: 10.4247/AM.2016.ABG151

LIST OF PRESENTATIONS

van Weperen VYH, Bossu A, Dunnink A, ter Horst I, Salden OAE, Beekman HDM, van der Heyden MAG, Vos MA. Proarrhythmic remodeling in the chronic AV block dog model is controlled by the degree of intraventricular dyssynchrony caused by altered ventricular activation. *Heart Rhythm Scientific Sessions 2020 - Online*

van Weperen VYH, Littman RJ, Arneson DV, Contreras J, Yang X, Ajijola OA. Single-cell RNA sequencing reveals molecular heterogeneity of glia within mouse sympathetic ganglia. *Experimental Biology 2020 - Online*

van Weperen VYH, Bossu A, Bourgonje VJA, Thomsen MB, Beekman HDM & Vos MA. Electrophysiological endpoints differ when comparing the mode of action of highly successful anti-arrhythmic drugs in the CAVB dog model with TdP. *Dutch Physiology Days 2018 - Wolfheze (The Netherlands)*

van Weperen VYH, Bossu A, Bourgonje VJA, Thomsen MB, Beekman HDM & Vos MA. Electrophysiological endpoints differ when comparing the mode of action of highly successful anti-arrhythmic drugs in the CAVB dog model with TdP. *AHA Scientific Sessions 2018 - Chicago (United States of America)*

van Weperen VYH*, Bossu A*, Beekman HDM, van der Heyden MAG & Vos MA Local, but not systemic, blockade of autonomic nervous activity is antiarrhythmic against dofetilide-induced Torsade de Pointes arrhythmias in the anesthetized chronic atrioventricular block dog model. *AHA Scientific Sessions 2017 - Anaheim (United States of America)*

van Weperen VYH*, Dunnink A*, Bossu A, Beekman HDM, van der Heyden MAG & Vos MA. Eliminating acute bradycardia by pacing decreases the incidence and severity of Torsade de Pointes arrhythmia in the anaesthetized chronic AV-block dog. *EHRA europace-cardiostim 2017 - Vienna (Austria)*

CURRICULUM VITAE

Valerie Yeh-Shing Hsieh van Weperen was born on the 5th of May 1996 in Riyadh, Saudi-Arabia. She attended secondary education at the Christelijk Gymnasium Utrecht. In 2013 she started her Bachelor's degree in Biology at Utrecht University with an emphasis on molecular and cellular biology, which she completed in 2016. Given her dream to become a physician, she started her Bachelor program in medicine in 2014 at Utrecht University. During the final year of her Biology Bachelor, she merged her interests in molecular & cellular biology with cardiology by joining the Utrecht University department of Medical Physiology as a student researcher under the guidance of Professor Marc Vos, Dr. Marcel van der Heyden and Dr. Alexandre Bossu.

Also during her entire studies in Medicine, Valerie stayed with the department of Medical Physiology. During the final year of her medical studies, Valerie had the opportunity to do an internship abroad. For six months, she conducted research with the Cardiac Arrhythmia Center at the University of California, Los Angeles, where she developed increasingly more insight into neurocardiology under the supervision of Dr. Olujimi Ajijola. Upon her return, she completed her medical degree with a final rotation in cardiology at the Gelre Hospital in Zutphen. Only nine months after this, she completed her PhD dissertation entitled '*Regulation of Cardiac Electrical Stability by Intra- and Extra-Cardiac Factors: Implications for Ventricular Arrhythmogenesis in the Chronic AV-block Dog Model*', which she will defend on the 7th of December 2021. Meanwhile, Valerie returned to the clinic and has since been working as a resident at the cardiology and pulmonology department of the Diakonessenhuis Utrecht. Valerie was awarded the NWO Rubicon grant 2021, which she will use to continue her academic career as a postdoctoral researcher in the field of neurocardiology at the UCLA Cardiac Arrhythmia Center. Hereafter, she has the ambition to start her training in cardiology. Her dream is to translate her preclinical knowledge on neurocardiology to the clinical setting.

A